CRANFIELD UNIVERSITY

BRIANNA FITZMAURICE

THE SHOCK RESPONSE OF BIOMATERIALS

CRANFIELD DEFENCE AND SECURITY

PhD
Academic Year: 2017 - 2018

Supervisor: Dr Gareth Appleby-Thomas
Dr Jonathan Painter

June 2018

CRANFIELD UNIVERSITY

CRANFIELD DEFENCE AND SECURITY

PhD

Academic Year 2017 - 2018

BRIANNA FITZMAURICE

The Shock Response of Biomaterials

Supervisor: Dr Gareth Appleby-Thomas
Dr Jonathan Painter
June 2018

This thesis is submitted in partial fulfilment of the requirements for the degree of PhD

ABSTRACT

The shock response of microorganisms is of particular interest to many different areas of research including, but not limited to: asteroid and meteoritic impacts and origins of life; food sterilisation; and deep-sea organisms. The primary interest behind the investigation presented in this thesis is the origins of life and how, if life began elsewhere in the universe, it could survive transfer from one planetary body to the next. This ties in with the theory of panspermia and suggests that life on Earth, or its building blocks, may have originated elsewhere in the universe and was transferred here via an asteroid or meteor. Aside from the many other caveats that travel through space would present to an organism, such as extreme temperatures and ionising radiation, to survive a meteoritic impact onto a planetary body would be to survive extreme shock pressures as well. The purpose of this investigation, therefore, was to examine a number of organisms under quasi-one-dimensional shock loading conditions in order to assess the organisms' response to shock pressure.

The microorganisms chosen were *Escherichia coli* NCTC 10538 and *Saccharomyces cerevisiae* ATCC 18824, two model organisms, a prokaryote and a eukaryote, respectively, whose biochemistry is well characterised. The shock loading experiments were carried out in a 50 mm bore single stage gas gun using the plate-impact technique. The bio-samples were contained within a capsule system that allowed them to be safely contained and retrieved after the shock so that their growth rates could be assessed. *E. coli* was subjected to shock pressures ranging from 0.55 to 10 GPa under various different shock conditions, yielding growth rates of 6% to 0.09%, respectively. *S. cerevisiae* was shock loaded to from 0.49 to 2.33 GPa with resulting growth rates ranging from 1.8% to zero growth. Additionally, to probe further into how life forms of varying complexity might respond to these shock pressures, the multicellular organism, *Artemia salina*, was shock loaded under the same conditions, but only up to a maximum pressure of 1.5 GPa. It was noted that *Artemi*a cysts showed hatching rates of up to 18% at this pressure, but this was not always without residual damage to the shell and the embryo within.

Since pressure gauges could not be attached to the target capsule due to the complexity of the set-up, validated numerical models had to be employed to interrogate

the pressures occurring within the sample. This also gave an indication as to the type of loading occurring within the sample. It was also desired to measure temperatures occurring during shock loading and to explore methods to better control this so that samples could be shocked to a particular pressure, while still controlling temperature. This was achieved using a novel type of flyer plate called Surfi-Sculpt® while validated numerical models were again used to estimate peak temperatures inside the capsule containing the biological sample. From the findings of a variety of shock experiments carried out throughout this project, a number of mechanisms were proposed to explain some of the results seen, providing insight into how microorganisms in particular might survive high shock pressures.

Keywords:

Shock loading; ramp loading; plate-impact; Surfi-Sculpt®; asteroid impact; Panspermia; *Escherichia coli*; *Saccharomyces cerevisiae*; *Artemia salina*.

ACKNOWLEDGEMENTS

There are many people I would like to thank for helping me through this project and sticking by me through the stress of it all – I hope I don't leave anyone out.

First of all, I want to thank my friends and family who have supported me my whole life, but particularly during these last few years. I want to especially thank my parents for always believing in me and being there for me no matter what. This is for you.

Next, I must thank my supervisors Gareth and Jon for being so supportive over the last three and a half years; always offering me advice and boosting my confidence when I needed it most.

I would also like to thank everyone outside of the university who helped with my project, especially Prof. Paul McMillan and Prof. Fumihisa Ono for the collaborations.

Finally, I want to thank everyone in Building 18 who has supported me in so many ways:

- Dave, for helping me with the science, doing most of my shots with me in the lab and listening to me complain about things… your pep talks have gotten me through this, not to mention all the chocolate!
- Andy, for also helping me in the lab and being supportive all these years - and for all the chats and lifts home!
- Rachael, for being a great sounding board to talk about bio stuff and for taking your time out to help me, even before you started working here. I'm sorry we didn't have time to do fun bio experiments together!
- Cait, for your support too and all our chats in the office. It's been great sharing an office with you!
- And Mike – even though you finished your PhD soon after I started – thanks for the help with the computer modelling!

I want to finish by thanking you all for being a family-away-from-family to me over the last four years.

TABLE OF CONTENTS

LIST OF FIGURES

LIST OF TABLES

LIST OF ABBREVIATIONS

AFM	Atomic force microscopy
CFL	Courant Friedrich Levy
EOS	Equation-of-state
ESWL	Extracorporeal shock wave lithotripsy
GDF	Graded density flyer
Het-V	Heterodyne velocimetry
HHP	High hydrostatic pressure
PBS	Phosphate buffered saline
PG	Peptidoglycan
SEM	Scanning electron microscopy
SPH	Smoothed particle dynamics
TEM	Transmission electron microscopy

LIST OF SYMBOLS

Symbol	**Units**	**Meaning**
C_0	mm μs^{-1}	Hugoniot intercept
E	J (Joules)	Internal energy
P	GPa	Pressure
ρ	g cm^{-3}	Density
R	Ω (ohms)	Resistance
T	K (Kelvin)	Temperature
u_p	mm μs^{-1}	Particle velocity
U_s	mm μs^{-1}	Shock velocity
V	V (Volts)	Voltage

1 Introduction

The theory of life being distributed throughout the Universe is a controversial one, but for decades there has been evidence of organic materials existing on extra-terrestrial bodies. Recent discoveries include potential hydration in equatorial regions of the planet [1] while estimations have been made as to when life first evolved on Earth (0.5-0.7 Ga) [2]. For a number of years, the panspermia theory has been outlined as a possible route for life to permeate the Universe and has been considered a possible explanation for the existence of life and its resilience on this planet. Panspermia is the theory that life may be transferred and distributed through space, suggesting that life may have settled on this planet after having originated elsewhere. Panspermia relies on the exchange of materials between planets, while lithopanspermia, specifically, is the transfer of life through space via rocky material expelled from a planet's surface, often due to meteoritic impact. This transfer of rocky materials between planetary bodies has been well documented with meteorites of lunar origin, such as Allan Hills A81005, and Martian meteorites including Allan Hills 84001, both of which were discovered in Allan Hills, Antarctica [3].

Transit time is a vital parameter regarding the survival of biological materials that may live within meteorites and other planetary ejecta [4]. As would be expected, meteorites travelling from Mars take longer to arrive on Earth than those derived from the Moon, which would result in longer exposure to conditions such as radiation. Survivability may therefore depend on the mode of panspermia, of which two were suggested by Gladman *et al.*; direct impact of an interstellar object on a planet or temporary capture of an interstellar object in the solar system and transfer of life due to [5].

Transit of meteoritic bodies is more likely to occur from Mars to Earth than from Earth to Mars, due to the pull of the sun's gravity. While transfer from Earth to

Mars is possible, there is a much lower probability of this occurring compared to Mars-to-Earth transit [4]. Flight times of meteorites from Mars to Earth, through semiempirical calculations, were found to range from 1 year to 20 million years, although only those in transit for less than 1 million years were determined capable of delivering viable microbial life, particularly in the case of *Deinococcus radiodurans* and *Bacillus subtilis* [4]. In the case of meteoritic bodies with vacuated ejecta pores, however, life would only remain viable for a few hundred years due to DNA decay [4]. This evidence suggests that panspermia delivering life to Earth may be very likely, especially in the case of Martian meteorites.

In considering whether or not life on Earth, or its building blocks, might have occurred extrinsically, there are a number of caveats that must also be examined: excess temperature, over-pressure, radiation and DNA decay [2]. In this expanding field of research, great consideration has been given to the pressure levels at which organisms can survive. Experiments in the application of up to thousands of atmospheres of pressure to a variety of organisms have been carried out, all while atmospheric pressure just above sea level is 0.1 MPa. Temperature is, of course, another significant factor for biological systems and depending on the nature of the pressure applied, whether it is hydrostatic or hydrodynamic, this may change considerably. However, the focus of this thesis will be the effects of shock pressures on organisms to interrogate the likelihood of life surviving a meteoritic impact.

1.1 Aims and Objectives

The aims and objectives of this thesis included the following:

- To investigate the effects of one-dimensional, or quasi-one-dimensional, shock pressure on microorganisms in order to further the work in the area of research

on panspermia. By investigating the growth of cells post-shock loading, it could be determined that cells were being affected only by shock pressure and no other caveats (under particular shock conditions); i.e. temperature or multi-dimensional wave fronts.

- To utilise varying methods of the plate-impact technique for pressure loading these organisms, i.e. extend the shock wave pulse to investigate what difference, if any, this has on these organisms.
- To investigate a novel method for controlling temperature during these experiments and to use this to interrogate the effects of raising and lowering temperature during shock loading.

1.2 Scientific background

The shock pressures induced by meteoritic impact and resulting release of ejecta into space has long been considered. These studies began with Melosh (1988) who postulated, among others, that primitive forms of life can withstand the shock pressures produced during planetary impacts and remain viable. Meteorites may also have resulted from ejection of rocks and debris from planets and non-planetary bodies [6]. The use of shock waves for experimental purposes began in the 19th century with the design of weaponry [7-9], but since then it has become an appropriate manner for analysing materials at high-strain rates.

The soundspeed of a material is the speed at which an acoustic wave can propagate through the material; this varies depending on the nature of the material, be it crystalline, amorphous or polymeric. A shock wave is created when a high stress is applied rapidly across a material and the moving wave exceeds the sound speed of that material.

Along the shock front, a discontinuity in the material properties of the medium is induced and these properties include pressure, temperature, density and internal energy. Upon shock loading a particular material, the material that is propagated by the shock wave is changed into a multiaxial state. This is defined by the boundary conditions of the loading and may be constrained so that the wave moves through the material uniaxially. The strain along that axis will be constant and the strain along all other axes will equal zero. The material will compress down the impact axis and expand laterally [10].

Acoustic impedance Z (Equation 1.1) is the product of material density, ρ_0, and the bulk modulus, C_B, is the bulk modulus or resistance of a material to change in volume; acoustic impedance is calculated according to Equation 1.1. As shown in Figure 1.1, material behind the discontinuity is of greater density than that ahead of the wave. The particle velocity, u_p, is identical to the velocity of the projectile. In most cases the sound speed of a material increases with pressure so that as a compressive wave moves into the material, the sound speed at higher pressures is higher than the sound speed at lower pressures. The higher pressure regions of the wave-front will catch the lower pressure regions. Eventually, this leads to a discontinuous wave that moves at a single velocity, denoted as U_s, and produces a single particle velocity, u_p. For a release wave, the same process is applied; higher pressure regions travel faster due to a quicker sound speed than lower pressure regions, which lag behind. This results in the release waves spreading into a ‘release fan’.

$$Z = \rho_0 C_B \tag{1.1}$$

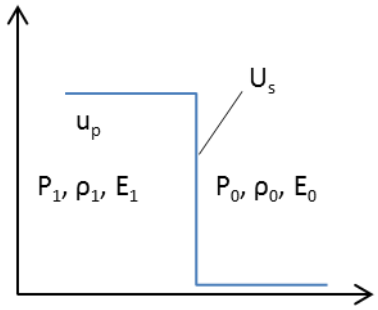

Figure 1.1 Progression of a shock wave through a material at velocity U_s. The particle velocity of the impactor is given by particle velocity, u_p. Pressure P, density ρ and internal energy E are elevated behind the shock front, denoted by 1. In front of the shock wave, the unshocked material is still in its ground state, denoted by 0.

A material experiencing a shock state will eventually return to its stable state and this may be depicted as in Figure 1.2. The shock rises as a square pulse and from this a release, or rarefaction, wave will form. The rear peak shock pulse will travel through the material that has already been shocked and the velocity will increase as it moves through this material. The base of the rear pulse, however, will lag behind due to a loss of energy. This will eventually result in the wave collapsing and the material returning to its stable state.

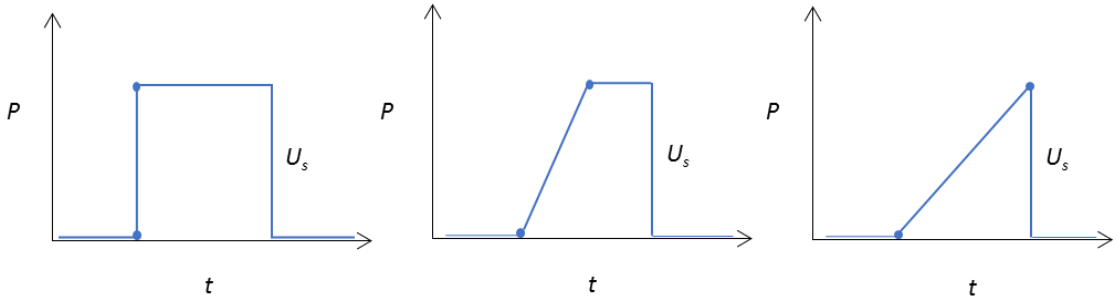

Figure 1.2 A square pulse rises as the shock moves through the material at velocity U_s. Eventually the wave transforms into a rarefaction as the rear peak shock pulse travels through shock material and catches up with the shock front. At the same time, the rear base of the pulse lags behind resulting in wave collapse.

The key variables to consider when describing the Hugoniot state of a shock loaded material are the pressure P, density ρ, internal energy ε, shock velocity U_s and particle velocity u_p. Particles which constitute the material propagate the wave through the material and thus particle velocity is always lower than the shock velocity. Only two of these five parameters are needed to define the response of a material to shock. Others can be determined using the Rankine-Hugoniot equations which relate the conservation of mass, momentum and energy (Equations 1.2 -1.4).

$$\rho_1 = \frac{\rho_0(U - u_0)}{(U - u_1)} \tag{1.2}$$

$$P_1 - P_0 = \rho_0(u_1 - u_0)(U - u_0) \tag{1.3}$$

$$E_1 - E_0 = \tfrac{1}{2}(P_1 + P_0)\left(\tfrac{1}{\rho_0} - \tfrac{1}{\rho_1}\right) = \tfrac{1}{2}(u_1 - u_0)^2 \tag{1.4}$$

where ρ, U, u, P and E are density, shock wave velocity, particle velocity, pressure and internal energy, respectively. Compression in a shocked material occurs at a velocity of U_s-u_p, therefore the mass of the shocked material over the shock front is then defined as Equation 1.2. The material is said to be in a steady state both before and after the shock wave. Momentum is also conserved throughout the shock (Equation 1.3), although this is dependent on the difference in momentum across the shock front being equal to the impulse. The impulse is the force required to change the momentum. The conservation

of energy may be calculated by Equation 1.4, after determining the work done before and after shock front.

From these equations, a shock wave equation-of-state (EOS) can be formulated to describe the state of a material under shock pressure conditions, much like the ideal gas equation $PV = nRT$ describes a material in its stable state. In order for these equations to be valid, the rise-time of the shock must be relatively short compared to the length of time for which the shock pressure is sustained.

The Hugoniot shock state is achieved by a material jumping from its ground state (same pressure-volume-temperature state) to the shock state via a thermodynamic path known as the Rayleigh line (Figure 1.3). This is represented on the graph as a straight line. In other words, the Hugoniot curve shows the locus of the final shock state and not the individual states that reach that point. The Hugoniot allows us to form equations-of-state to describe the behaviour of materials under shock pressures. The advantage of obtaining Hugoniot equations-of-state is that it allows materials to be modelled thermodynamically in a reliable way, since the end state for materials under shock compression would already be known from the Hugoniot curve. The EOS can be explored depending on whether the compression is along the Hugoniot, isentrope or isotherm.

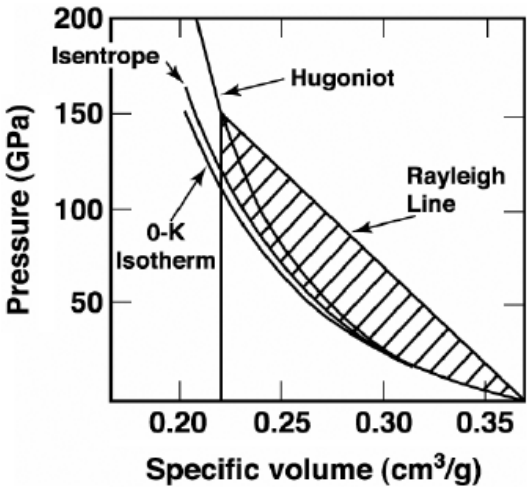

Figure 1.3 P-V plot of Hugoniot, Isentrope and Isotherm curves. The Rayleigh line represents where a material jumps from its ground state to a shocked state along the Hugoniot [11].

The impedance match technique [12] can be used to calculate the value for u_p. This is achieved by finding the intersect of the EOS of the flyer material and the EOS of the target material for particular experimental conditions. The Hugoniot for a target material can be calculated using at least two of the variables previously mentioned; U_s and u_p, for example. For the U_s-u_p plane, pressure may be calculated according to Equation 1.5. When plotting U_s-u_p, Equations 1.6 and 1.7 may be followed for linear and non-linear Hugoniots, respectively.

$$P_H = \rho_0 U_s u_p \tag{1.5}$$

$$U_s = C_0 + S u_p \tag{1.6}$$

$$U_s = C_0 + S_1 u_p + S_2 u_p^2 \quad (1.7)$$

The use of one-dimensional shock waves not only allows for the effects of pressure (and temperature) to be elucidated, but it does so without a need to consider how the nature of the shock front affects the target, whereas a multi-dimensional wave may cause structural damage to the material in question [13]. Hence the use of quasi-one-dimensional shock loading has been applied throughout this thesis.

1.3 Prokaryotic and eukaryotic organisms

Life takes many different forms. The three kingdoms of life include prokaryotes, eukaryotes and eubacteria (Figure 1.4). Prokaryotes, the most primitive forms of life, which include all types of bacteria, are considered to be the precursors to more evolved eukaryotic cells. One largely accepted theory is that prokaryotic cells engulfed each other to gradually develop into more complex eukaryotic cells. Eukaryotes are the kingdom to which all plants and animals belong. Primordial environmental conditions are thought to have played an important role in the origination of life on Earth, which was first suggested by the ground-breaking Miller-Urey experiment [14]. This experiment led to the unprecedented discovery of amino acid formation under a relatively simple laboratory mixture of gases – including nitrogen, methane – all subjected to a spark of electricity to incite nucleic acid production. This discovery sparked a litany of investigations into the origins of life and the type of environments required to facilitate this occurrence.

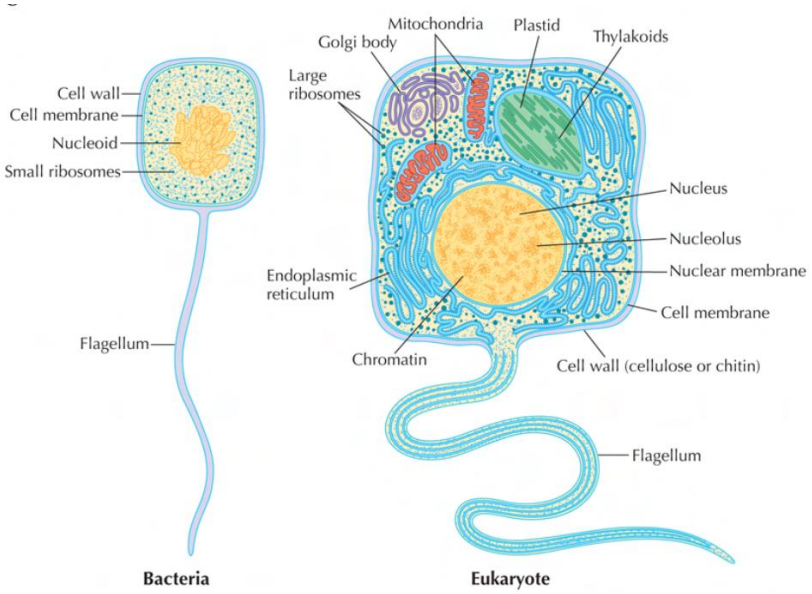

Figure 1.4 Diagrams of typical eukaryotic and prokaryotic cells. Eukaryotic cells represent all fungi, plants and animals. All bacteria are prokaryotes. Bacterial cells contain cell walls surrounding a cell membrane, while many eukaryotes, such as yeast, only have cell membranes for protection [15].

Bacterial species are typically characterised by the presence or absence of the protein peptidoglycan (PG) within their cell walls; they are considered to be either gram-positive or gram-negative, respectively, due to the application of the Gram staining technique when characterising them. With this technique an insoluble complex of crystal violet-iodine forms within the cell wall and can be removed with alcohol if PG is not present. Hence, gram-positive cells will remain visibly stained while gram-negative cells do not [15].

Bacteria also demonstrate a large variance in cell size from 0.2 to 750 μm [12, p. 78]. As a general rule, cells that are smaller undergo more cell divisions. This is due to the surface-to-volume (S/V) ratio increasing as a cell decreases in size. Prokaryotic and eukaryotic cells have cell membranes; thin barriers that separate the cell cytoplasm from the external environment. When the integrity of the cell membrane is damaged, the

contents of the cell may leak out and result in cell death. The cell membrane consists of a phospholipid bilayer (containing fatty acids and glycerol-phosphates) with hydrophilic and hydrophobic regions. These are arranged as shown in Figure 1.5. Small cells with high surface-to-volume ratios allow them to increase their nutrient exchange, thus speeding up their growth time in comparison to larger cells.

Escherichia coli are a gram-negative rod-shaped bacterium and are chemoorganotrophs approximately 2 μm in length [15]. Chemoorganotrophs are organisms that use the oxidation of chemical bonds in organic compounds as a source of energy. Since this is a model organism and well characterised genetically, *E. coli* has been selected as the prokaryotic model for this thesis.

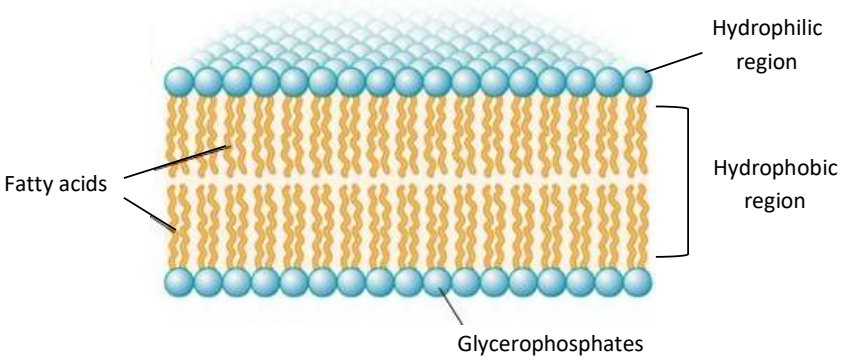

Figure 1.5 The lipid bilayer in a cell membrane consists of hydrophilic areas which include glycerol and phosphate groups. The hydrophobic regions in the centre consist of fatty acids [15].

Eukaryotic cells are generally more complex than prokaryotes. The primary defining feature of eukaryotes, from which they get their name, is a nuclear membrane which surrounds the nuclear material. Other organelles which are common among eukaryotes, though not present in all of these cells, include mitochondria and lysosomes; the centres for respiration and hydrolytic enzymes, respectively. *Saccharomyces cerevisiae* is a standard model eukaryotic organism. It belongs to a family of fungi called ascomycetes and it can reproduce sexually or asexually. In unfavourable conditions, such as a lack of

nutrients, UV exposure or high pressure conditions, diploid cells can form. These fungi reproduce by the fusion of two haploid nuclei from different mating types to form a diploid nucleus, which then undergoes meiosis to produce a haploid ascospore [16]. A single cell is approximately 6 μm in diameter. It reproduces by a process known as budding; when a daughter cell splits away from a parent cell as shown in Figure 1.6.

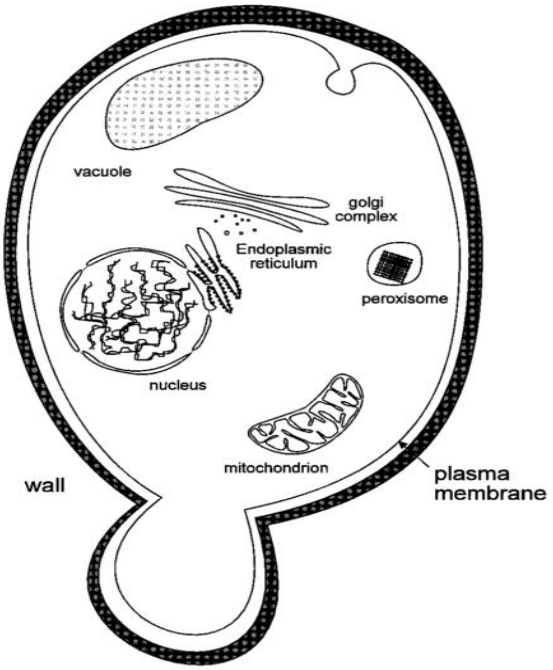

Figure 1.6 Diagram of a budding yeast cell including intercellular components [15].

High pressure studies are important to many different fields; not only panspermia, but also to deep subsurface biology, deep sea biology and Pascalisation in food preservation [17, 18], although the focus of this thesis is on panspermia. Evidence for panspermia lies in a number of experiments that have revealed certain microorganisms can survive several atmospheres of pressure. In order for an organism to withstand delivery and impact onto another planet, it would have to survive pressures of around 10 GPa [19]. Sizes of organisms may also be a contributing factor as to whether or not they can survive. It was proposed by Price *et al.* that organisms up to 10 μm in size can survive

pressures of at least 1 GPa, while those that are millimetres in length are usually broken apart at this pressure [19]. This demonstrates the importance of nature of the shock wave front being used on organisms, i.e. one-dimensional or multi-dimensional (expanding radially outwards).

Deep sea organisms, in contrast, offer an opportunity to study beings well-adapted to constant high pressures. These pressures reach up to 110 MPa at the deepest level of the ocean [20]. In recent years, biotechnology has improved based on the growing understanding of the adaptive mechanisms of such microorganisms achieved by techniques such as DNA recombination. Although gene expression has been studied in a number of cases, it is important to decipher which proteins become deactivated under extreme conditions and which ones may subsequently become activated.

2 Literature Review

2.1 Introduction

In this chapter, techniques for inducing shock waves and other forms of pressure loading will be discussed, as well as the different analytical techniques associated with them when investigating materials under pressure. Additionally, recent discoveries into pressurisation of biological materials are also presented and these will include discussions of preliminary studies on intercellular pressure response mechanisms for both unicellular and multicellular organisms.

2.2 Pressure loading techniques

2.2.1 Dynamic pressure loading

Ramp loading

Shock pressure loading was discussed in the last chapter, but also of importance to this thesis is ramp loading, which follows a thermodynamic path in contrast to shock loading that follows the Rayleigh line between two Hugoniot states. Isentropic compression, rather than shock compression, is seen since loading rates are slower. Shock and ramp loading are depicted in Figure 2.1. Ramp loading produces continuous loading curves (as opposed to a Hugoniot shock which is nearly discontinuous). This means that the stress-strain response and wave profiles are very sensitive to small changes in wave response. A ramp wave can be seen where the compression is broken up into a series of weak shocks that isentropically compress the material to the final pressure. The amount of heating in ramp waves is less than with a shock wave, which is one advantage for dynamic loading of temperature-sensitive materials. Large amplitude

pressure waves can steepen into shocks [21]. Ramp waves can steepen into shocks also; the wave elongation being governed by the local elastic modulus of the material.

Figure 2.1 An example of shock wave (a) and a ramp wave (b).

The generation of ramp waves has been applied to areas of research including explosive detonation, EOS and quasi-isentropic processes. A number of techniques have been used to apply these ramp waves across various media, including lasers and magnetic flux, but gas guns are also frequently used in ramp wave production [22-25]. Ramp waves of this nature can be produced through a number of different avenues, from layered impactors with shock impedance gradients to contemporary graded areal density flyer plates, or functionally graded material (FGM) impactors. These impactors have a varying density across the structure; a low density at the initial point of contact with the target material, gradually increasing with the depth of the impactor. Methods to produce these impactors have recently included the 3D printing of metallic and ceramic flyer plates with graded areal densities [24, 25]. Various additive manufacturing techniques have been used to produce such flyer plates, including Selective Laser Melting (SLM) and Toll Ceramic Stereolithography (CSL) [24, 25].

The use of ramp waves in explosives has led to numerous studies on their generation in various target materials, including granular explosives [26] and Kel-F 81 (PCTFE) [27]. Markedly, this approach also offers insight into equations-of-state, particularly, as shown by Ray and Menon, thermal EOS and the reversible adiabat [28, 29], of materials

in shock pressure magnitudes but with relatively low temperatures. It facilitates observation of each stage of compression of a material, as opposed to a 'jump' to shock states that are observed with shock loading paths. These low temperature regimes may prove useful for other types of temperature-sensitive targets, such as biological materials and the use of this isentropic approach to pressure loading has been applied to aspects of this thesis.

2.2.2 Hydrostatic pressure loading

Piston cylinder

Although the focus of this thesis is on the effects of shock compression of biological materials, it is necessary to provide comparison between these techniques and hydrostatic pressurisation methods. One device commonly used for hydrostatic testing is the piston cylinder (Figure 2.2) which was originally used in geological studies [30] but has more recently been applied to high pressure biology [31-33]. This device allows a controlled pressurisation of a sample through compression and cooling using tap water. Some operate with hydraulic rams and hand pumps. A piston cylinder often consists of a tungsten carbide pressure plate, or pressure vessel, which contains the sample assembly. The sample is held within a cylinder and is compressed at two ends by pistons made of very hard material, usually tungsten carbide [21]. To allow for truly hydrostatic pressures up to ~ 3 GPa, the sample is surrounded by a fluid pressure medium; often a pentane-isopentane mixture or argon [21].

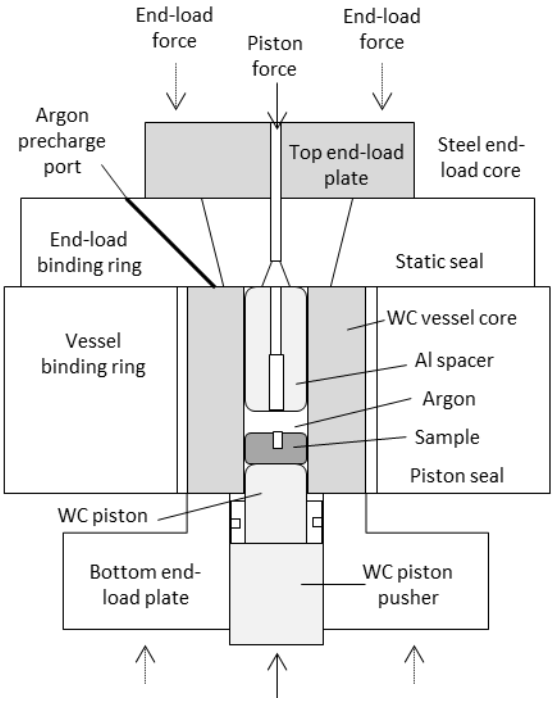

Figure 2.2 Internal schematic of the piston cylinder at University College London.

Diamond anvil cell

The first use of diamonds for high pressure studies was used by Lawson and Tang in 1950 [34]. One of the most common pieces of apparatus for producing and analysing hydrostatic pressures on ~ 10-100 μm size samples is the diamond anvil cell (DAC), often in conjunction with varying types of spectroscopy. The DAC consists of a metal gasket which holds the sample and two opposing diamond anvils upon which flat surfaces are ground where they come into contact with the sample [35]. It operates by using two diamonds as the pressure-inducing material and also as the spectroscopic windows. Tiny ruby grains are often used for pressure calibration of a DAC [35].

Pressure is not the only parameter that can be measured with this instrument. The volume of a sample can also be measured using X-ray diffraction methods to determine the distance *d* between the lattice planes using Bragg's law (Equation 2.1) where λ is the wavelength of the rays and θ is the angle between the incident beam and

the surface of the sample [35]. Additionally, laser heating is often incorporated into this device. DACs can generally achieve pressures of up to ~ 300 GPa, equivalent to pressures found at the centre of the Earth [36], making it ideal for geological and microbiological studies [37].

$$n\lambda = 2d\sin\theta \tag{2.1}$$

2.2.3 Hydrodynamic pressure loading

Explosives

Shock waves produced by explosives have been studied in the interest of defence, but also to simulate the effects of meteor impact and explosive crater formation. That leads to the ejection of rocks, the fundamentals of which are based in spall [38]. An explosion is the exothermal reaction of two or more chemicals with the emergence of a gaseous product. The main difference between the plate-impact experiment and an explosive loading experiment is that a plate impact produces a planar compression pulse into a target, whereas explosive loading produces a pulse in which compression rises rapidly and immediately begins a gradual fall after reaching a peak. This peak is usually in excess of the spall strength [39]. Detonating an explosive charge on the surface of a target is the simplest method to induce shockwaves through that material. A triangular pulse is indicative of spall occurrence and this feature is regularly seen in explosive wave profiles. The reason for its occurrence in explosive wave profiles is that due to detonation products, the pressure begins to fall immediately after the shock. In contrast, a rectangular pulse which would normally be required for a non-energetic study with a constant amplitude [39].

Explosively driven flyer plates can also be used. This set-up involves detonation of an explosive that is retained on guard rings above the target (Figure 2.3). These guard

rings compensate for a pressure gradient that appears as the detonation products move radially away from the centre of the explosive charge. The reflection of the waves at the guard rings causes pressure to build around the perimeter of the flyer plate and a higher inflow of detonation debris into the gap to reach the flyer plate. This prevents fracturing of the flyer plate. Velocities tend to reach ~ 1 km s^{-1} using this experimental configuration [39]. In order to reach lower pressures, an attenuation plate is placed between the explosive and a flyer plate of lower shock impedance than the attenuator.

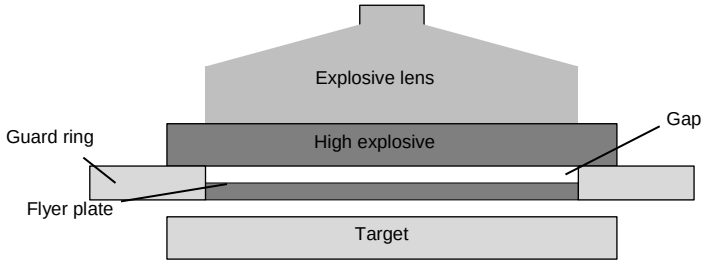

Figure 2.3 Set-up of an explosively driven flyer plate.

Underwater detonations

In order to demonstrate the importance of the nature of the wave front and one-dimensionality of a shock, one must also observe the effects of a multidimensional wave front on a target. Underwater detonations have been used to test multidimensional wave fronts on biological materials. Imploding gas detonations have also been used to test small crustaceans under water in their own environment [40, 41]. Detonating volatile mixtures of oxygen and methane gas have led to the production of shock waves ranging from 50-100 MPa using very sophisticated equipment to induce and monitor resulting pressures [42]. The nature of this experiment will be discussed later in this chapter.

Extracorporeal shock wave lithotripsy (ESWL)

The type of shock waves used in extracorporeal shock wave lithotripsy has been traditionally used in medicine for the treatment of urinary calculi, or kidney stones. As the name suggests, it is a non-invasive therapy but one whose technique has been applied to other fields in recent years. Shock waves are generated from a lithotripter outside the body and then focused onto a stone using a variety of techniques. Energy is released into the kidney stone as the shock wave passes through the body and into the stone. Pressure generated through ESWL is often between 50 and 80 MPa [43]. In this method, it is assumed that human tissues have the same acoustic impedance as water, therefore the shock waves are generated in water in each technique. The waves are then transferred to human tissue via a coupling gel. In this way, it is ensured that the energy will be concentrated on the area of interest.

High-energy shock waves from lithotripters have also been incorporated into studies of human bladder cancer cells through increasing permeability of the cell membrane so that drugs may be introduced more efficiently [44]. However, the effect of these transient shock waves in this study was also found to cause damage to cell organelles [44]. The three main techniques for producing shock waves through ESWL are the electrohydraulic (EH), piezoelectric (PE) and electromagnetic (EM) principles [45].

L**aser ablation**

Laser ablation is the coupling of laser energy to a target in order to remove surface material. High amplitude pressure loadings with very short durations caused by high power pulse lasers (> 1 GW/cm^2) of short duration (nano- to femtoseconds) can result in strong but short shock waves in solid materials [46]. Laser ablation works by creating a

plasma on the surface of the target material via this high intensity laser pulse and is often a means of removing a layer of the target material. The plasma rapidly expands and pressure builds, inducing a shock wave through the target. Induced plasmas near the ablation front also affect the sharpness of the laser. Penetration depth and spot diameter contribute to the volume of ablation [47]. Two varieties of laser ablation include direct and confined ablation [46]. Direct ablation is when a laser pulse of high power density and short duration is focussed directly on the surface of a target. Confined ablation involves covering the target with a transparent medium to slow plasma expansion.

Laser ablation is useful for brittle and thermal-sensitive materials, unlike more traditional methods of micro processing. This is because only small volumes of material are subjected to defects beyond the removed material. Laser ablation is also good for non-planar work surfaces given the non-contact nature [47]. The expansion of this plasma induces a shock wave. This occurs if the laser pulse is of short duration and high intensity ($> 10^9$ W/cm^2) [46]. Recovery of shocked samples is a big advantage of this method of shock generation.

This method has been used by a number of labs to launch flyer plates [48] and also as a dynamic loading technique that produces shockless loading paths which allow for the maintenance of low temperatures throughout the impact [49]. It has been useful for chemically analysing materials, cleaning layers of contamination and biomedical sciences. The use of laser ablation has been reported to reach a range of pressure regimes (mega-, giga- and terapascals) [49]. Lorenz *et al.* have reached pressures in the MPa range, with initial loading in aluminium samples being shockless, developing into a shock at depths of 20-25 μm. Ramped compression led to peak pressures of up to 200 GPa in some cases [49].

Gas guns

There are a number of different methods used in dynamic pressure loading: lasers, magnetic flux and gas guns [50]. Lasers have been used in a number of experiments and have become increasingly common due to their practicality, efficiency and precision. However, this thesis will focus on the gas gun as this was used to carry out plate-impact on the targets throughout this project. The gun used for this thesis was a 50 mm bore single-stage gun [50] (Figure 2.4).

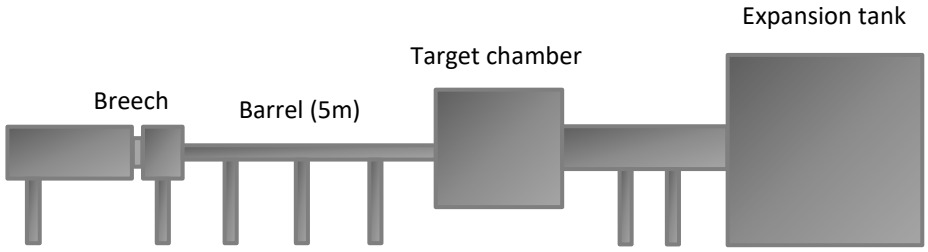

Figure 2.4 The 50 mm bore gas gun based at Cranfield University, Shrivenham, UK. This gun is a single-stage with a 5 m barrel.

Light gas guns have been the most common means of shock wave production for many decades. This initially began during WWII with ballistic work and was mainly used to investigate tolerances of metals. Since then, gas gun techniques have expanded to examine a wide range of materials, including those biological in nature. The first two-stage gas gun was developed in 1948 [51]. Equally, the development of the plate-impact technique has allowed material properties to be examined under high strain-rate, one-dimensional loading, leading to a better understanding of material behaviours and equations-of-state of solid metals, polymers and even liquids.

Coil guns and electromagnetic rail guns are other types of hypervelocity launchers [52], as are explosively driven gas guns; they can therefore be split into two broad categories: gun accelerators and explosive accelerators [53]. Single-stage guns

can also be split into those that function under inert compressed gas and powder propellant guns [27]. Single-stage gas guns operate more efficiently with driving gases including Helium and Hydrogen; i.e. gases of low molecular weight since this factor is what determines the kinetic energy that can be gained by a gas [51]. With minimal kinetic energy in the gas, the kinetic energy input to the projectile is increased, therefore increasing the velocity of the projectile. Velocities for these guns normally do not exceed 3 km s^{-1} for low weight projectiles.

A further development of these is the aforementioned two-stage gas gun [51], generally capable of achieving higher velocities and often involving larger projectiles and targets. This involves both a powder propellant and compressed gas. Propellant may be used to drive the piston forward in order to compress the gas. When the gas reaches a high enough pressure, a diaphragm ruptures and the gas rushes forward to the rear of the projectile. This drives the piston down the barrel, although sometimes this is achieved by the creation of a shock wave [50]. The operation of light gas guns will be discussed further in the next chapter.

2.3 Diagnostic techniques

2.3.1 Interferometry

Interferometry is a technique that involves observing the interference of waves (light, sound, radio). In the case of the experiments referred to in this thesis, interference of light waves (from a laser) is used to measure displacements of particles on the rear surface of a target during impact. Velocimetry has long been used in dynamic impact experiments as a method of measuring fluid velocities and surface velocities. In many cases, laser velocimetry involves the use of a Doppler radar which measures the change in wavelength of emitted light, or radiation, due to the movement of the source of that

radiation. This system allows for the measurement of surface velocities directly and has played a role in finding EOS of materials with lustrous surfaces.

2.3.2 Fabry-Perot and VISAR

There are different versions of this technique which are applicable to different scenarios; such as, for velocities reaching km s^{-1}, the Fabry-Perot method and velocimetry interferometer system for any reflector (VISAR). The latter system is insensitive to tilting [54] and is cheaper than the Fabry-Perot system [52]. The main advantage of the Fabry-Perot system is the capability it has to measure a number of discrete velocities simultaneously as well as velocity dispersion [55]; VISAR cannot do this. Instead, VISAR works by laser measurements of the Doppler shift in light frequency that is reflected from a moving target surface. The Doppler shift of light produce fringes in the interferometer. The number of fringes observed is proportional to the change in surface velocity [55].

2.3.3 Heterodyne velocimetry

Another such method is Heterodyne velocimetry (Het-V), or Photon Doppler velocimetry (PDV). Het-V is a combination of some advantages belonging to both VISAR and Fabry-Perot systems, while also excluding many of their disadvantages. In this technique, a laser detects displacement on the surface to be measured rather than measuring surface velocity, which is how it differs from the latter systems. The number of fringes produced during a Het-V experiment up to a time, *t*, is proportional to the displacement of the surface on which the laser is focused [56].

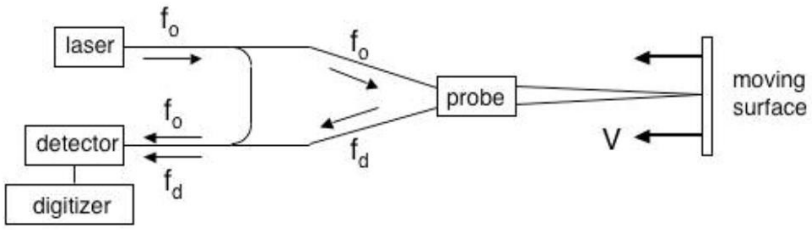

Figure 2.5 Diagram of an interferometer setup. The incident beam (laser light) and reference beam (Doppler-shifted light) combine at the detector to form the beat frequency.

A Het-V system consists of an interferometer with a probe, laser and detector (Figure 2.5) [57]. Optical fibres are used to transport light from the laser to the probe which then focuses the light onto the rear surface of the target via a special lens. A reference beam is reflected back from this surface and guided back through the probe to be collected by the detector. This reference beam has a Doppler-shifted frequency (due to the movement of the target surface and the ensuing change in frequency of the light) and at the detector, it crosses over with the incident beam so that a beat frequency can be measured [58], which is calculated by Equation 2.2. Here, f_0 is the frequency of the incident beam, f_b is the beat frequency and is the frequency f_d of the Doppler-shifted light. Following from this, the speed of light is denoted by $c = \lambda_0 f_0$, where λ_0 is the wavelength of the light emitted by the laser. Particle velocity can then be denoted by Equation 2.3.

$$f_b = f_d - f_0 = 2(v/c)\, f_0 \tag{2.2}$$

$$v = \left(\frac{\lambda_0}{2}\right) f_b \tag{2.3}$$

The beat frequency is the difference in frequency between the incident and reference beam, or the rate of signal cycles, and is proportional to the velocity of the target [12] [54]. Light that has not been Doppler-shifted must also be sent to the detector because this is where the two beams of light will be superposed and the beat signal generated from the different frequencies. The fringe is the difference in the paths of the two beams once they intersect again. This creates a phase difference which produces a fringe pattern from which surface displacements can be measured.

Limitations include media with matt surfaces and uneven exteriors, such as porous materials. Equally, the number of signals recorded, the length of time to perform the analysis and the noise associated with the signal can affect the resolution, meaning a visible or clear trace may not always be obtainable using the Het-V system [59].

2.3.4 Hydrocode modelling

Hydrocodes are computer codes specifically used to simulate hydrodynamic events. They are a useful tool to supplement experimental data and operate by way of meshes that consist of discretised cells which behave hydrodynamically. Hydrocode modelling has also provided a more efficient and inexpensive route for measuring pressures produced by multi-dimensional dynamic loading e.g. as in the study by Martins *et al*. [60] and has been used to model craters [61].

In order to determine the forces at each time step that will act on the mesh, hydrocodes must incorporate Newtonian Laws of Motion, the EOS for a given material and the constitutive model. The Laws of Motion determine the governing equations for all numerical simulations and incorporate the conservation of mass, momentum and energy [62]. This implies that if a cell decreases in size during a simulation, there will be an increase in density, but the mass remains constant. The EOS, as discussed previously, relates the density with internal energy of the materials in the model, detecting the changes in these factors and observing the effects of compression. The

constitutive model describes the result of the deformation by relating the damage incurred, the strain rate effects, and the internal energy of the materials.

There are different approaches to building hydrocode models and these include the Lagrangian, Eulerian, Arbitrary Lagrangian-Eulerian (ALE) and Smoothed Particle hydrodynamics (SPH) methods [62]. SPH is a mesh-free system and consists of particles that are interpolation functions. This allows the conservation equations to be solved at various points. Each of these particles also has material properties and a finite number of discrete particles may be used to simulate one physical object in the system [62].

Lagrangian, Eulerian and ALE are grid-based methods [62]. The mesh consists of cells defined by nodal points to which velocities are assigned. The Lagrangian method describes the geometry of the material, while the Eulerian method describes the framework of space surrounding that material. In the Lagrangian method, the surrounding mesh moves with the material. Boundary conditions are automatically imposed due to the placement of grid nodes along free surfaces and material interfaces. Connecting nodes may expand and contract during the process which may result in deformation of the mesh [62]. If the mesh deforms too much, the results will be adversely affected. Conversely, no grid is required beyond the problem domain, making the overall process more efficient in comparison to other grid-based methods [62].

In the Eulerian method, space surrounding the model is fixed and does not flow with the material; the material moves through the mesh on its own. The mesh volume and shape remain unchanged and so while the material will deform, the mesh will not [63]. This ultimately avoids the numerical problems one would encounter with large deformations in a Lagrangian mesh. Eulerian arrangements hence work well with fluid and gaseous flow problems, not purely solid materials. In contrast to Lagrangian meshes, free surface positions and boundaries which must deform are more complex to determine accurately because the energy, mass and momentum fluctuations are measured at cell boundaries. In addition, for computational efficiency, it is often

necessary to use coarse meshes which will affect the resolution and accuracy of the simulation.

ALE is a method which utilises advantages from both Lagrangian and Eulerian codes by rezoning meshes. Rezoning takes results from a deformed mesh and remaps them onto a new mesh. The Euler components allows for large distortions in small subdomains of the mesh by applying more calculations per times step [64]. As with the Eulerian method, ALE allows the material to flow through the mesh [62] and in this way, distortion of the mesh can be minimised. However, larger grids are involved here which makes them less efficient than Lagrangian methods. Due to its relative efficiency, Lagrangian models have been used for the numerical simulations in this thesis and will be the primary focus of each of the hydrocode methods.

2.4 Planetary impact

A number of different models regarding planetary impact by extraterrestrial bodies have been proposed by Melosh; from models of resulting shock waves and fragments to models for crater formation [65]. The 1984 article by Melosh [65] focussed mainly on the ejection of material from an impact crater. Understanding the pressures and stress waves involved in such an occurrence offers the chance to properly examine how potential biological materials or whole organisms, particularly prokaryotic or single-celled organisms, may thrive under these conditions. The reason for focussing more consistently on these more primitive life-forms relates to the fact that this may be how life was first introduced to our planet.

The aforementioned models were discussed in detail, explaining the different types of stress waves and the overall process of meteorite impact on a planetary body. The main type of shock loading discussed by Melosh here was so-called ‘detached shock’; this is the initial stress wave that occurs after impact and is the area of high

stress and particle velocity. This stress wave dissipates and weakens as it moves away from the site of impact. This is due to the decrease in energy density as the stress wave expands and inelastic processes within the wave occurring. A different kind of stress wave arises after the detached shock passes a point in the target and rarefaction waves from the free surface, and the momentum from the meteorite, force the target material into an almost incompressible, subsonic movement. This is known as excavation flow and it is this wave that removes most of the material from the crater [65].

The detached shock peak particle velocity can be up to five times greater than the velocity for excavation flow, so in that sense, the detached shock was of more importance for this study. This was determined using computer models. The rise time for the detached shock is also shorter than the decay of the shock and the shape of this shock pulse determines the size of fragments that are ejected from the impact site [65].

The primary stress wave also reaches the impactor. When the wave touches the rear of the impactor, it is reflected as a tensile wave that moves back to the impactor-target interface and reduces the high pressures that are initiated there during impact. This wave acts alongside other rarefaction waves from the rear surface to move back down to the target, moving downward and outward behind the stress wave. The decay time of this pulse is the time taken for the rarefaction to traverse the impactor. Other rarefaction waves form when the impactor gets buried in the ground, so the decay of the pulse is rather complex [65].

Previous models suggested a simple model for the shape of the pulse with a spherical wave front. It propagates from some point below the surface and underneath the impact site. It maintains its shape but weakens over distance from the impact. There are also “free-field zones” in which the stress wave can propagate without interruption by rarefaction waves. However, near the free surface (on the back of the projectile), the waves are reflected back as tensile waves; therefore, the point just beneath the surface of the target sees a stress wave from the impactor as well as the reflected tensile wave.

The free-field zone has a stress level different to that of these two overlapping waves. When the reflected tensile wave arrives before the primary stress wave reaches its peak stress this is referred to as the "near-surface zone". Material in this zone is subject to less stress than material lying deeper at the same radius. This explains the results from Ahrens and O'Keefe (1978) in which it was found that lightly shocked ejecta originate close to the impact site [66]. Ahrens and O'Keefe determined the energy and mass distributions of ejecta from both Mercury and the Moon [66]. This was achieved by measuring the mass and energy distributions after impact of gabbroic anorthosite rock on similar material to describe impact onto planetary bodies having a similar mass and radius of the moon and Mercury.

2.5 Pressure loading of biological materials

The food industry has also provided major incentive to study new, and more efficient, applications for sterilisation through temperature increase as well as pressure induction. The latter technique is known as high-pressure processing (HPP) and has become especially popular in the last three decades, although work initially began in this field in the 19th century [18]. The main advantage of this method of sterilisation is circumventing damage to food that may occur due to temperature increase. This type of sterilisation treatment also allows food to maintain its nutritional content and to be processed evenly throughout, regardless of shape or size of the food product [18].

However, as with sterilising food via applying high temperatures, some disadvantages arise when using HPP on certain types of food: some animal products, a number of dairy products and low acid food [18]. Sterilisation is also not an option in cases of bacterial spores which are heavily resilient under such conditions. These spores are known to survive pressures greater than 1 GPa. Another challenge that arises during HPP treatment is that spores can be induced to germinate – a similar problem sometimes seen with elevated temperatures. Other issues to consider in this process are

the adiabatic heating that may take place in the packaging of some food during HPP. This can be between 5 – 15 °C which is mostly inconsequential as long as heat is applied to, or removed, from the system during the pressure hold. Food colouring can also be altered, particularly in gas-containing foods, when pressure is released, which may be a disadvantage in the consumer market since sensory quality of food may be as important as nutrition. The application of static high pressure loading has also been attributed to determining survival rates of certain organisms under long term pressurisation.

2.5.1 Protein structure and biochemistry

The study of pressure effects on biological materials began a century ago, with the observation of pressure-induced coagulation of albumen (egg white) [67]. This pressure has been determined to affect protein folding and enzymatic reactions, causing coagulation. Induction of pressure slows down the reactions and folding rates of proteins, which is the opposite of the effects of temperature on the biochemistry of an organism. Elevated temperatures tend to speed up reactions, but only to a certain point [68]. The study of the effects of pressure loading on both prokaryotic and eukaryotic organisms may be applied to a number of different fields, including the food industry, numerical modelling, medical science, marine biology and planetary science/panspermia.

Proteins could be considered the most vital macromolecular components of the cell. Consisting of individual amino acids linked together by peptide bonds to form polypeptide chains, they play a number of different roles in the cell, be it structural or enzymatic. They also have their own specific folding structures that determine whether or not they are active, or whether or not they can be acted upon by enzymes (Figure 2.6).

Figure 2.6 An example of a folded protein structure (left). Proteins unfolded in response to the application of static pressure (right) [69].

Proteins are most stable when they are in their native folding states; the level of their stability is dependent on the difference in free energy (ΔG_{stab}) between the native and unfolded states in optimum conditions [70]. When these proteins are unfolded, the ΔG_{stab} value is negative, which is in keeping with the Gibbs free energy equation and implies a positive entropy (ΔS) value, indicative of an increase in disorder of the protein structure. Equation 2.4 is a modified Gibbs free energy equation to include the volume change ΔV between the folded and unfolded structures as well as pressure P (MPa) [69]:

$$\Delta G_{stab} = -\Delta S dT + \Delta V dP \tag{2.4}$$

A number of factors are known to change the folding of proteins and cause their denaturation. Stretching protein disulphide bonds, for example, under high pressure conditions damages them irreversibly so they are no longer active [71]. The presence of urea also causes denaturation; the same effect that high temperature has on a protein, which has an optimum temperature of 37°C in humans. Whether urea is present or temperatures reach 75°C, similar results are seen at the denaturation midpoint (T_m); the

point where both folded and unfolded states of the protein simultaneously exist in equal amounts at equilibrium [16].

The macromolecules that allow proteins to change their folding in order to carry out chemical reactions are the enzymes. Enzymes are catalytic proteins that carry out all chemical reactions in an organism and can act on a protein to make it go through a number of chain reactions before the final product is produced (Figure 2.7). The rate of these reactions varies according to the temperature and pressure applied to the system. There is also the possibility that the type of pressure may have a dramatic role in a living cell's biochemistry.

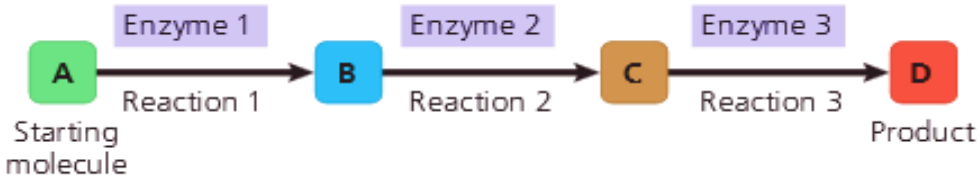

Figure 2.7 Process of protein formation through enzyme catalysis [72].

Many questions have arisen surrounding not only the origins of life itself, but also the energetic processes that were involved in it [73]. The main by-product of bioenergetic reactions is adenosine triphosphate (ATP) [73], but how did these reactions first evolve? What conditions facilitated cellular harnessing of energy to drive evolution itself? The answer possibly lies with understanding the progress of anaerobic organisms thriving in states with no oxygen. However, the main issue here is the fact that anaerobic environments are not as ripe with energy as aerobic environments are. In submarine hydrothermal vents, H_2 is generated and is the primary source of energy. Some bacteria and archaea are understood to use the ancient form of energy metabolism involving the reduction of CO_2 with H_2 to make acetate and methane with ATP. The chemical mechanism used is flavin-based electron bifurcations to generate iron-sulphur proteins.

2.5.2 Analytical techniques for cells and cellular components

Diagnostic techniques for studying microorganisms range from various forms of microscopy to the analyses of chemical structures and reactions in biological materials. Such methods include Raman spectroscopy, X-ray diffraction, synchrotron radiation and mass spectrometry (MS) among others.

Light and electron microscopy

Microscopy is a fundamental analytical method for the study of microbial systems. There are several different types of microscopy which fall under two main categories; light microscopy and electron microscopy. Generally, light microscopy enables lower resolution imaging while electron microscopy allows very high resolution images to be produced. This high resolution can even provide images from within the cell membrane in order to view cell organelles. The most basic form of light microscope is the bright field compound microscope which uses visible light to illuminate the specimen and consists of two lenses; the objective and ocular [15]. If the specimen is not very well pigmented, it will require staining in order to provide contrast. When greater magnification is desired to visualise specimens at the molecular level, electron microscopy is used. The effective wavelength of electrons is much shorter than that of visible light and wavelength negatively affects resolution, meaning that electron microscopes are capable of producing much higher resolution images than light microscopes [15]. The two main forms of electron microscopy include scanning electron microscopy and transmission electron microscopy.

Scanning electron microscopy

The scanning electron microscope (SEM), shown in Figure 2.8, is useful for observing the external features of whole and intact cells. The specimen is coated in a thin film of heavy metal, e.g. gold, so that the scanning electron beam will be scattered from the surface of the specimen [15]. The scattered electrons will then be collected by an anode known as the secondary electron detector. Depending on the texture and coarseness of the surface of the specimen, the electrons may be scattered at different angles, resulting in a final image that provide topological information. High-energy incident electrons may also be reflected back from the surface and collected by the backscattered electron detector. A computer is then used to compound the data to form an image of the specimen's surface. Although they are mainly suitable only for observing surface structures, SEMs can offer a wide range of magnifications, up to ~ 100,000 times [15].

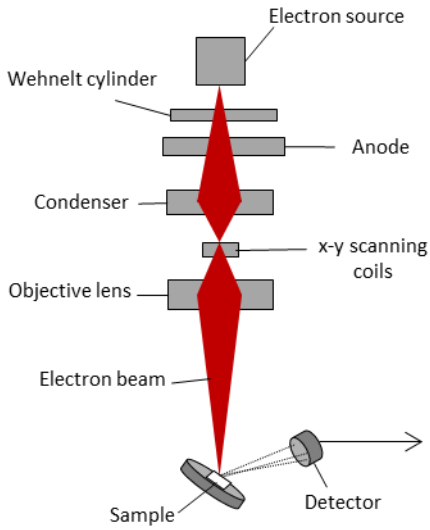

Figure 2.8 Diagram of a SEM set-up. The beam from the electron source passes through a Wehnelt cylinder which focuses the beam through the condenser and objective lenses and stabilises the beam current. The lenses in the SEM are electromagnetic which help to accelerate the beam towards the specimen. The scanning coils deflect the beam along the x-y axes so that it scans the specimen to create a raster image.

Transmission electron microscopy

A simpler form of electron microscopy is transmission electron microscopy (TEM). In TEM, electrons are thermoionically emitted using a high voltage power supply and cathode. Like in SEM, a number of electromagnetic lenses are placed throughout the microscope in order to drive and focus the beam onto the specimen. Once the beam passes through the specimen, the objective lens produces an image before the projector lens forms the true image onto an electron optical system (Figure 2.9). The main advantage of TEM is that it may be used to examine intercellular structures with a resolving power of ~ 2 nm [15]. The disadvantage is that electrons do not penetrate very well, and specimens must be specially prepared and cut into very thin slices. For contrast, stains such as lead salts, permanganate and uranium may be used [15].

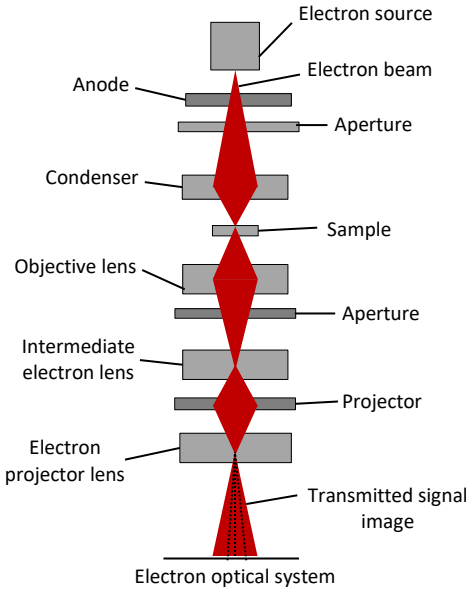

Figure 2.9 Diagram of a TEM set-up. The condenser and lenses are electromagnetic in order to drive the beam towards the specimen. A screen, also known as the electron optical system, produces the final image.

Mass spectrometry

Mass spectrometry (MS) is used to measure the mass/charge ratio (*m/z*) of analytes, describing the structure of the molecule and its molecular mass. This technique has been used for over a century for the chemical analysis of many types of samples, dating back to the early 1900s when it was primarily used to measure atomic masses and to detect isotopes [74, pp. 10-12]. The tandem mass spectrometer was later introduced in 1960 as researchers gained a better understanding of the fragmentation of molecules inside the instrument and found new applications for it [74, pp. 270-272].

MS has since been used for a number of different applications for chemistry and biochemistry, e.g. with gas chromatography-mass spectrometry (GC-MS) and liquid chromatography-mass spectrometry (LC-MS). The key components of a mass spectrometer include the ionisation chamber, the mass analyser and the detector. A substance is ionised in the ionisation chamber of a mass spectrometer, creating a positively charged molecular ion (radical cation). The mass analyser, which is the ion accelerating section, separates these molecules out according to their *m/z* through electric or magnetic fields inside the instrument [75, p. 85]. It has been considered a useful tool for the analysis of many chemicals. Relative abundance is plotted against *m/z* and this is known as a mass spectrum. The detector is used to detect only the cations after the radicals are released. It records the abundance of ions at each *m/z* to allow for the creation of a mass spectrum (ion abundance *vs* its *m/z*) [75, p. 2].

MS has been implemented in the analysis of peptides for decades, with newer methods regularly being developed, including gas chromatography/combustion/isotope ratio mass spectrometry (GC/C/IRMS) [76]. This method, outlined by Macko and Uhle (1997), was used to examine the nitrogen isotope composition of amino acids [76]. It was proven to be more efficient than previous chromatographic procedures designed for looking at more stable isotopes. Each stereoisomer of an amino acid could be analysed in nanomole quantities in this way, which was advantageous as it could measure smaller

samples and allowed for more detailed analyses and better understanding of isotope fractionations [76].

MS has evolved to examine not only simple compounds, but also complex molecules including proteins using soft-ionisation methods. Soft ionisation is the creation of droplets of bio-macromolecules rather than fragmentation of these macromolecules into ions [77]. A significant development of MS in protein analysis came with the technique to volatise biomolecules in electrospray ionisation (ESI) and matrix assisted laser desorption/ionisation (MALDI). ESI involves the solubilisation of a sample (before entering the mass spectrometer), the production of charged particles and then passing these through a high voltage needle. ESI normally induces a large range of charged states, so the resulting spectra may have a high number of ions for each analysis. In ESI, higher voltages result in lower charged forms and as such, larger peptides may not be within the mass range of the mass analyser and may exceed the mass limit. Lower voltages, in contrast, are better for smaller analytes [75, pp. 307-309]. Instrument and ionisation parameters are a compromise when looking at complex samples; in complex peptides where there is no separation, only some of the molecules will become ionised and detected, making a true analysis of the entire peptide impossible [77]. In contrast, only singly charged ions are primarily seen in MALDI. In this case, samples are cocrystallised with a particular organic matrix containing a conjugated aromatic ring structure which allows it to absorb the wavelength of the laser. In the case of MALDI, one strong limitation includes the ability of a peptide to cocrystallise with the organic matrix [77].

There are a number of other versions of MS; those with multiple analysers are especially useful in biology to determine structures of polymers. An important advancement in MS is the development of tandem MS that allows for much smaller fragments to be obtained for a more detailed analysis [75, p. 189]; it is used to analyse fragmentations of certain ions in mixtures of ions. More sensitive versions of MS and tandem mass spectrometry (MS/MS) are continually produced due to a growing desire

to analyse smaller and smaller quantities and higher resolution separation technologies [76]. Quadruple mass spectrometry may also be used alongside Raman spectroscopy for a non-invasive study of phase identification [77].

2.5.3 Pressurisation of prokaryotic organisms

Escherichia coli are capable of surviving a number of different stressors. A recent study found that *E. coli* cultured in space showed a 13-fold growth increase compared to Earth-cultured cells [78]. Changes noted were in cell envelope thickness, which increased by up to 43% in space, and cell aggregation which was greatly enhanced in space-cultured samples. In this case, the *E. coli* demonstrated an ability to adapt to microgravity. There are also a number of other pressure resistant strains of bacteria that have been found to resist protein inactivation up to relatively high magnitudes of pressure. However, expression of certain outer membrane proteins in *E. coli* and in *Photobacterium profundum*, for example, was found to be dependent on pressure [17]. These proteins are known as the SOS proteins and they are a response to counter DNA damage and prevent further adverse effects from the injurious source.

The SOS mechanism has been investigated using a number of methods; one being differential fluorescence induction (DFI). DFI is a technique that relies on the detection of the green fluorescent protein reporter gene, *gfp*, which is used to indicate promoter activity of genes which are of interest [79]. This method involves flow cytometry using a laser to excite cellular components containing the *gfp* gene. This has been used in a number of cases for the analysis of genes and proteins in bacteria, including *Streptococcus pneumoniae* and *E. coli*.

In *E. coli*, proteins involved in a bacterial genetic reaction to DNA damage known as the SOS response were analysed using DFI. The SOS response in bacteria is a mechanism designed to stall DNA replication by disassembling the protein structures involved in the replication process. This protection apparatus was first discovered in *E.*

coli. Normally, the damage acquired by the genetic material is a result of UV irradiation or exposure to the chemotherapy drug mytomycin C [17]. It is governed primarily by the *lexA* and *recA* genes, the repressor and inducer of the system, respectively, which regulate over 40 other genes involved in the SOS response [17]. Together, these genes work to return the cell to its original stable state. *lexA* induces the system by preventing error-prone replication and excision repair of DNA as well as cell division. It does this by expressing the LexA protein to bind to the SOS sites (thereby supressing SOS response) on the DNA strand that normally is bound by RNA-polymerase, which induces DNA replication. Once RNA-polymerase is repressed, the RecA protein, involved in maintenance of the DNA then binds to single stranded DNA (ssDNA) that results from the halted replication of the double helix. The binding of RecA to ssDNA leaves this protein in an active state to cleave LexA, which represses LexA and then allows SOS to be induced. This elegant system allows lesions in the DNA to either be repaired or bypassed by the replication mechanism. When this has occurred, RecA is no longer capable of binding ssDNA and the cell returns to its stable state with intact LexA suppressing the SOS response [80].

Other genes involved in this mechanism include the promotors, *uvrA*, *recA* and *sulA* which were also analysed using DFI by Aertsen *et al*. (2004) [17]. *uvrA* is involved in DNA repair after UV damage and *sulA* inhibits cell division. This group reported the first SOS response mechanism in a cell as a result of pressure induction instead of DNA damage. Evidence of this was seen through the aforementioned promotors being tagged with *gfp*. These promotors have been previously observed to be part of the heat shock regulon. The promotor for *recA* showed an 18-fold fluorescence induction after pressure loading at 100 MPa, while the *sulA* promotor showed a 20-fold fluorescence induction. Since these promotors are known to be activated during the SOS response, it was deduced that the *E. coli* cells were undergoing an SOS mechanism under pressure. Aertsen *et al.* (2004) suggested that, since DFI screening found induction of SOS genes

by pressure, LexA was denatured by pressurisation [17]. Pressure-induced SOS is different from that in classic SOS response due to DNA damage.

Furthermore, in a subsequent study, Aertsen *et al*. (2004) [81] found genes involved in the heat shock regulon (dnaK, lon and clpPX) being expressed as a result of pressure due to deformation of these structures. Heat shock led *E. coli* to be more resistant to high pressure under inactivation. Interestingly, this followed the same time course as induction of heat shock genes, further proving their theory [81, 82].

In 1997, Hauben *et al*. [83] observed *E. coli* mutants that were resistant to inactivation under high hydrostatic pressure. Cycles of exposure of the bacteria to high pressures were alternated and surviving populations were selected for continued pressure exposure. The pressure-resistant mutants were isolated by using outgrowth temperatures of 30, 37 and 42 °C. They were treated for 15 min and survival at ambient temperature was 40-85% at 220 MPa to 2 x 10^{-8}% at 700 MPa. Pressure sensitivity of the mutants increased from 10 to 50 °C, contrasting with the parent strain which showed a minimum sensitivity around 40 °C. The temperature-sensitive mutants showed a reduced ability to grow at slightly elevated pressures (50 MPa) over 37 °C. These results implied that the resistance to pressure inactivation is unrelated to barotolerant growth [83]. Microbial growth is usually inhibited at pressures in the range of 20-130 MPa. Cell death normally occurs in the range of 130-800 MPa. In these experiments the results suggest that *E. coli* can develop barotolerance, which has implications in other fields such as the food industry [83].

B. subtilis spores have also been rather extensively studied in line with the well-accepted concept that bacterial spores may survive space [84]. In one study by Horneck *et al*. [84], a number of permutations were used for *B. subtilis* spores being subjected to the vacuum of space for ~ 2 weeks and then analysed to see the number of colonies formed. The European Space Agency's BIOPAN facility was used to expose these

spores to space. Unprotected spores that were directly exposed to space in layers, or behind a quartz window, showed severely reduced survival rates ($\leq 10^{-6}$). The different mixtures of *B. subtilis* spores include clay, red sandstone, Martian analogue soil in dry layers, artificial meteorites and naked spores in naturally occurring concentrations [84].

Thin layers of clay acted as optical filters but were relatively ineffective as very low survival rates were also seen with this set-up. Spores mixed with a dry powder of clay saw a 5-order increase in survival, while those mixed with soil saw up to 100% survival. The evidence suggested that small rocks may be enough to protect bacterial spores from UV radiation (this is likely what killed the other spores). However, micron-sized particles, as suggested by panspermia, may not be sufficiently large enough to provide protection from UV radiation. Spores in direct contact with clay showed better survival (5 orders of magnitude) than those under a "filter" of clay. The different strains of *B. subtilis* spores used were those deficient in particular amino acids and spores with those same missing amino acids and deficient in DNA repair mechanisms.

Some spores survive the vacuum of space when mixed with glucose. It is speculated that glucose prevents damage to DNA and proteins by replacing water molecules in membranes and intracellularly helping to preserve three-dimensional structures of biomolecules. It was further confirmed by this study that the ejection process, long-term exposure to space and radiation, and the entering process must be survived by organisms re-entering a planetary body [84]. Microorganisms cannot undergo metabolism in space, but they can exist in a dormant state. Mileikowsky *et al*. [2] calculated that behind 1 m of meteorite a substantial spore population (10^{-6}) would survive exposure to cosmic radiation.

After one BIOPAN flight, 100% of the spores were recovered from the "artificial meteorite" mixture of clay or red sandstone (covered by a quartz window). For the first flight, all samples were kept in the dark, not sun-exposed, and survival rates were 12-15%. With thin clay filters (exposed to UV and visible light) very few of each

type of spore survived [84]. This investigation showed that certain bacteria, and especially their spores, may survive the most extreme of condition in space, including exposure to ionising radiation. Comparison of these prokaryotes to more complex organisms may provide answers as to how survival is maintained in severe environments.

2.5.4 Pressurisation of eukaryotic organisms

Both hydrostatic and hydrodynamic pressure tests have been employed on different types of organisms from bacteria to plants to multicellular animals. The Centre for Astrophysics and Planetary Science at the University of Kent has found some substantial robustness in a number of microorganisms using shock waves [19, 85]. Additionally, they have used shock waves to look at the macromolecular elements of a cell. Martins *et al*. induced shock waves upon ice targets as further proof that life can not only be sustained, but possibly created under these significant pressures. The result was amino acid synthesis carried out by using a light gas gun to impact ice mixtures - analogous to those found in comets - with steel projectiles [60]. Hydrolysis of these mixtures led to the formation of amino acids; alanine and two non-protein amino acids, as determined through mass spectrometry. An important point to be deduced from their work is that high pressures are not necessarily sterilising as one might expect: microorganisms and macromolecules can survive.

Other cases investigated by the same group have established these pressures as a substitute for cometary environments and meteor impacts on this planet, which have been survived by not only prokaryotic bacteria, but eukaryotes such as yeast. Yeast cells subjected to pressure testing were found to withstand impact velocities up to 7.4 km s^{-1}, corresponding to a peak shock pressure of ~43 GPa [19]. The yeast strains used in this case (BY 4743 *Saccharomyces cerevisiae*) had a deleted URA3 gene, which prevented

the production of an enzyme for breaking down uracil; in this way this strain could be easily selected for on a particular growth medium that ambient strains of yeast could not.

Other eukaryotic organisms that have been subjected to static and shock pressure loading include a variety of plant seeds [86, 87]. However, there has been controversy over the effects that various internal factors of an organism, such as water content, can have on its durability under high pressure loading. The influence of water content on fennel plant seeds (*Foeniculum vulgare*) was studied by Ahmadi *et al.* for the purposes of determining their mechanical properties and understanding their behaviour when undergoing harvesting and processing equipment. Seeds were soaked in water to apply different moisture contents and were then subjected to static pressure loading [87]. Those with the highest moisture content showed a generally greater level of deformation along the length of the seeds than those with lower moisture contents. The rupture force required to deform the seeds along the length and width axes was also much less for those with higher water content. For example, the moisture content on dry basis (d.b.) of 21.67 % d.b. had a rupture force of 186.44 N and deformation of 1.86 mm along the length of the seed. A seed of 7.78 % d.b. moisture content showed a rupture force of 600.25 N and a deformation of 1.71 mm along the length of the seed [87]. Deformation levels appeared to increase with moisture content.

A later study carried out by Herák *et al.*, however, contradicted these findings. In pressure loading a range of different seeds (jatropha, common sunflower, bean and garden pea), some of which were also soaked in water, the strain energy to deform the seeds was found to increase with water content, while the deformation volume decreased with moisture [88]. In this case, moisture was determined to provide a resistance to pressure deformation.

While the experimental techniques of both experiments could be revaluated, it is important to note that the findings presented in both cases are based on different types of seeds and that the internal structure of each seed would present different moisture levels in different parts of the structure. The contrast in these results could be indicative of a more fundamental mechanism that responds to pressure that is not yet properly understood. This question could then be applied not only to flora, but most other organisms as well. Differences have already been uncovered between varying *E. coli* strains with regards to pressure increase not allowing for temperature increase in one strain but tolerating it in the other strain [78]. The ultimate conclusion from such experiments is that there are a number of different factors that contribute to their reactions under hydrostatic pressure.

These cases are examples of the existence of discrepancies in the literature with regards to the true effects of pressure on organisms. Could there be an underlying mechanism in the deformation of all types of organisms exposed to high pressure that is not yet understood? This question of whether or not there is a shared fundamental behaviour across different biological systems could be vital in understanding more of how organisms react to high pressure environments, not least how they might survive asteroid impact and spallation.

2.5.5 Cytoplasm and cell wall dynamics

Intercellular mechanisms must be examined in order to better understand what takes place within a cell. Studies of piezophiles have provided information on an abundance of likely mechanisms governing an organism's response to pressurisation. These include the aforementioned *B. subtilis* spores, and of increasingly growing interest, *Shewanella*. This is a deep-sea gram-negative bacterium that is a model organism for studying life under several atmospheres of pressure [31]. *S. oneidensis* has also been found to be capable of being trained to withstand increasing pressures by Hazael *et al*., 2017 [89].

Important considerations for the survival of micro-organisms under pressures reaching the gigapascal range include how they bypass the crystallisation of the cytoplasm. This is a matter of timescales of intercellular reactions *vs* the timescales at which peak pressures are sustained across the samples [89]. Water is known to crystallise under certain pressures, and fluid within the cytoplasm of a cell may see similar effects under these conditions. In keeping with the dynamic pressures applied throughout this project, the dynamic compression of water will also be discussed.

If pure water is compressed isothermically, phase transitions from ice VI to ice VII may be detected (Figure 2.10). According to Nagayama *et al.*, potential ice phases were detected after dynamic compression of a pure water sample using the plate impact technique [90]. Behaviour of the water was observed during the shock using a high-speed streak camera. The shock particle velocity Hugoniot for water was also obtained during this experiment (Equation 2.5).

$$U_s = 1.45 + 1.99\, u_p \tag{2.5}$$

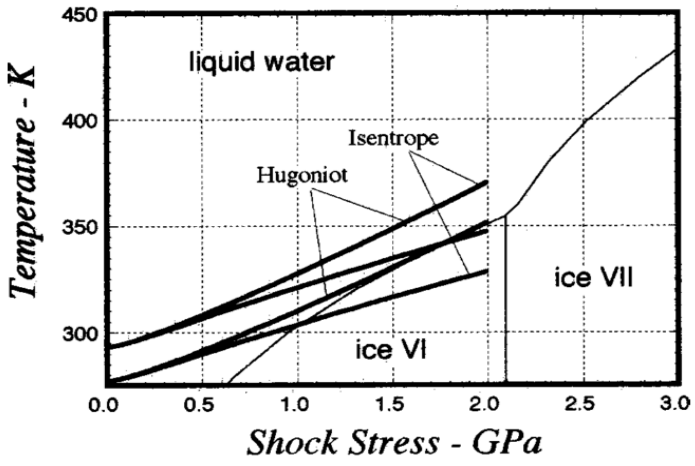

Figure 2.10 Hugoniot and Isentrope curves for water with starting temperatures of 277 and 297 K [90].

It was also deduced from their investigation that the Hugoniot for water crosses the phase line at the water-ice VII phase above 2 GPa [90]. However, a later study by Dolan and Gupta in 2003 presented a study in which water was investigated under dynamic quasi-isentropic compression on nanosecond timescales [91]. Their experiment involved the use of silica and sapphire plates to compress the samples to pressures ranging between 1.1–5.1 GPa. Freezing was detected through a loss of transparency from optical scattering due to a coexistence of liquid and solid phases. Collimated visible light was shone through the water sample. A photodiode detector was used to measure the average transmission of the light in the visible spectrum, while the light intensity was measured during the impact and compared to the measurements taken at ambient conditions. Under quasi-isentropic compression, time-dependent freezing of water was observed. Due to the presence of nucleation sites, freezing only occurred between the silica windows, not the sapphire windows. It was postulated that long relaxation times are generally required for freezing, and shock compression timescales may not be sufficient to allow ice formation, in conflict with Nagayama *et al.*'s report [90].

Dolan and Gupta discussed how the large specific heat of water in the liquid phase moderates the temperature rise during adiabatic compression. Quasi-isentropic compression was achieved during their study by the induction of multiple shock waves onto the target. Many liquids (> 15%) undergo large volume changes under shock pressures in the range of 1–2 GPa. All of these events cause an increase in temperature which can inhibit the pressure-temperature conditions needed for freezing. In the case of the quasi-isentropic loading used here, the isentropic curve passed through the Ice VII region at pressures above 2 GPa, suggesting that any freezing that occurred would likely be seen along the isentrope. This was noted in Nagayama *et al.*'s work also [90]. Freezing occurred when the liquid phase was metastable with respect to Ice VII, but this could not be confirmed as there were no details on the structure of the solid phase formed [91].

While the formation of pressure induced ice phases have also been interrogated at length in water within organisms under static pressure conditions, studies under dynamic conditions are still comparatively immature, particularly in terms of one-dimensional loading. Amid the controversial findings of Sharma *et al*., organisms were found to remain viable under high pressure conditions despite ice formation. Here, static compression at 1.5 GPa was carried out on *Escherichia coli* and *Shewanella oneidensis* and the aqueous suspension medium crystallized into ice VI but intact bacteria remained inside fluid inclusions and along grain boundaries [92].

These same principles apply to organisms under pressure; bacteria been examined inside various frozen matrices. In the case of *Listeria innocua* BG 3532, cell activation was still detected at temperatures of – 10 °C and static pressures of 300 MPa for up to 15 minutes, although their survival was greatly reduced compared to counterparts held at 0 °C and lower pressures [93]. Equally, individual minerals have been known to exist in the ice of certain comets [94-96] and have acted as amino acid precursors post shock pressure loading [61]. Investigation of the reaction of organisms and organic materials to ice formation is key to understanding their survival under high pressures.

Elongation and relaxation timings of cell walls are also particularly important for the overall structure being able to withstand a high-pressure environment, be it under long-term hydrostatic pressure or short-term hydrodynamic pressure. As mentioned earlier, bacterial cell walls may contain PG; a protein is made up of strands of glycan (polysaccharides) that are cross-linked by peptides. It is a dynamic layer to allow insertion of new material for growth and passage of molecules in and out of the cell, but also prevents lysis by turgor pressure.

The kinetics behind the elongation process of the cell wall has been studied for decades, with earlier tests producing conflicting results. An investigation by Baldwin

and Wegener (1986) found that the gram-negative bacterium *Lineola longa* elongates exponentially and produces “minicells” with an absence of DNA by cell division [97]. They postulated that the septum only needs to be regulated insofar as to allow the genetic material to be separated to facilitate growth and is not highly regulated genetically. The model of cell growth proposed by Baldwin and Wegener was that enzymes are likely added to the cell (wildtype) throughout the cell cycle and those that are added in a stepwise manner will not be rate limiting in exponential-growth conditions. It also states that cell division need only be regulated enough to allow separation of the nuclear material; placement of the septum is not critical given the numerous growth zones and enzymes. More minicells may be formed during septation than at other stages of the cell cycle [97].

Bacterial growth has been suspected to rely in part on turgor pressure within the cell, driving cell wall expansion [98]. This has been based on theories of plant cell growth and the phenomenon of bacterial growth decreasing in the presence of a high-osmolarity growth medium. However, the experiments carried out by Rojas *et al*. (2014) suggest that expansion of the cell wall in *E. coli* is not controlled by pressure [98]. They monitored the dynamics of MreB, a protein whose motion is dependent on PG synthesis in the cell wall. The second measurement carried out was that of the cell elongation rate ,and both of these parameters were used to determine that the growth of *E. coli* is not primarily dependent on turgor pressure. This was proven by demonstrating that increasing the osmolarity of the surrounding medium inhibits cell growth, but the elastic strain within the cell wall only decreases marginally with osmolarity. Second, the rates of elongation respond on slow timescales. Third, osmotic shock has little effect on MreB motion. Fourth, normal growth rates can be restored after plasmolysing the cell, even though this process can slow the expansion of the cell wall. Their model for the rate of cell wall synthesis was one that suggested the rate of synthesis was independent of turgor pressure and was the main determinant of the cell wall elongation rate [98].

They propose that nascent, unextended PG is inserted into the cell wall and positive turgor pressure is required for extension [98]. Hence, during plasmolysis, the PG makes little contribution to elongation than when the cell is turgid (swollen with high water content); this contribution can be restored. The model proposed here suggests a minimal role for turgor pressure in that only a positive value is required for elongation (extension of the unstretched PG). *E. coli* differs from plant cells in that its elongation is not directly controlled by turgor pressure. However, like plant cells, it is able to store its ability to grow upon depletion of turgor pressure. The cell wall of *E. coli* is ~ 3 nm – very thin when compared with plant cells, therefore requiring an extended PG protein for the cell wall for any growth be expected [98]. This suggests the dynamics of the cell wall in bacteria may play an important role in their response to static and dynamic compression.

2.6 Summary

A variety of techniques for hydrostatically and hydrodynamically loading materials have been discussed here. These techniques have been applied to both unicellular and multicellular organisms, leading to a number of general conclusions: multicellular organisms are more susceptible to high pressure than unicellular organisms; certain strains of bacteria have the ability to adapt to high pressure environments; biological samples in high pressure experiments are naturally complex given their different cell and tissue layers - each individual layer must be analysed separately in order to truly understand its behaviour under shock compression. While some genes and proteins have been linked to high pressure response, there is still much to be understood about these intercellular mechanisms and how survivability is at all feasible under such high pressure regimes. The pressure responses of whole organisms and subcellular components discussed in this chapter have shown the complexity behind survival and the ability of some organisms to adapt to unfavourable conditions. This thesis aims to

further elucidate this adaptability by concentrating on the effects of simplified and controlled shock pressures on a number of different life forms.

3 Experimental Procedure

3.1 Gas gun experiments

All shock experiments during this project were carried out using the single stage gas gun at Cranfield University [50], consisting of a gas reservoir, 5 m barrel, a 50 mm bore, a target chamber and an expansion tank designed to collect expanded propelling gasses from the reservoir (Figures 2.4 and 3.1). The target chamber was located at the end of the barrel, which in turn was sealed by an encasement surrounding the target. This barrel / encasement arrangement was evacuated to >2 mbar before an experiment to ensure alignment, while the surrounding inter-connected target and expansion chambers were evacuated to a vacuum of no greater than 400 mbar before the shock experiment with the aim of ensuring that no overpressure would result post-shot. Within the target encasement a barrel extension was attached to the end of the barrel in order to hold the test sample. The gun was operated by a rapid and controlled expansion of compressed gas. Air or helium gas was used, depending on the desired velocity, with He used for shots of a velocity > 500 m s^{-1} as it was capable of expanding at a faster rate due to its lower density and viscosity / higher inherent sound speed. The velocity of the projectile impact onto the target was measured immediately prior to impact by a set of light gates located within the target chamber. This will be discussed further in section 3.5.2. An example of a typical experimental set-up within the target chamber is shown schematically in Figure 3.2.

Figure 3.1 Image of the 50 mm bore single stage gas gun at Cranfield University.

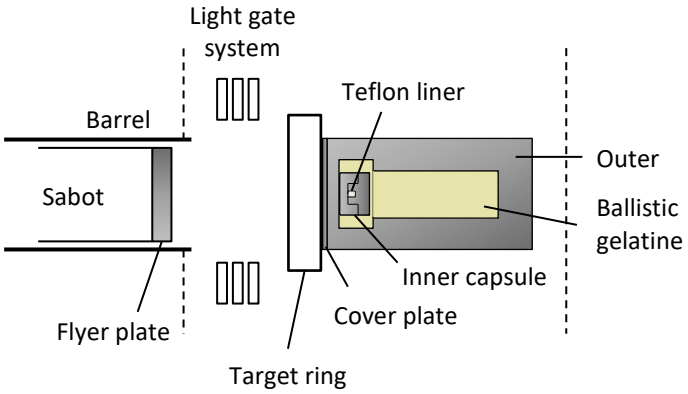

Figure 3.2 Typical experimental set-up inside the target chamber with an Al capsule target.

The mechanism by which this gun operated was a fast-acting valve design (Figure 3.3). In this design, pressure behind the piston was brought to ~10 bar using the inlet valve and the selected driving gas. This forced the piston forwards sealing the barrel – although, as indicated in Figure 3.3, a small ring of material was still exposed to any subsequent gas in the breech. The gun was then evacuated with this pressure holding the piston forward. Gas was then slowly bled into the main reservoir/ breech as well as

this chamber, with the pressure behind the piston kept at least 10 bar above that of the gas pressure in the main reservoir until it was time to fire. Once the breech was filled to the desired firing pressure a solenoid was used to rapidly evacuate the high pressure region behind the piston. The small ring of piston material exposed to this pressure then caused the piston to move rapidly backwards and the breech pressure, which was then the higher pressure region, accelerated forward to drive the projectile down the barrel. The advantages of the fast-acting valve system included efficiency and the capability to repeat experiments with relative ease and accuracy.

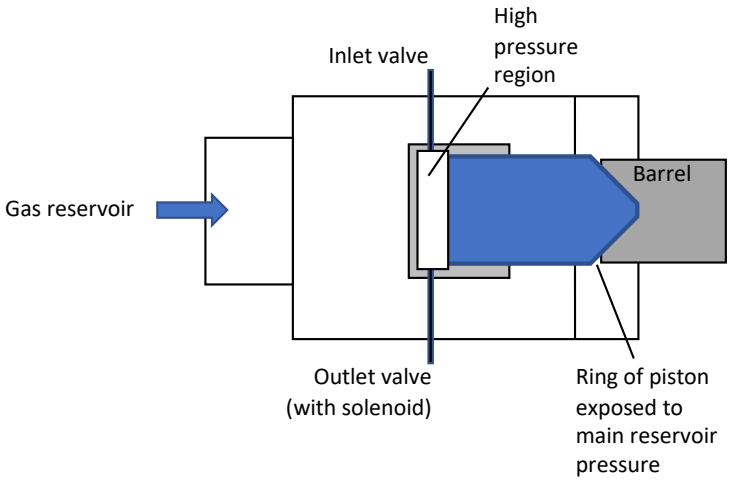

Figure 3.3 Fast acting valve system belonging to the 50 mm bore single stage gas gun at Cranfield University.

3.2 Plate impact technique

The plate impact technique used in each shock experiment was carried out with planar flyer plates (either Al or stainless steel) in order to create strain through one dimension of the material, thereby controlling and simplifying the experiments. During this process, the target becomes inertially confined due to the material in the centre of the target being prevented from flowing radially. This leads to the establishment of a shock rather than stress wave, allowing access to hydrodynamic states. Flyer plates were

generally of 5-mm thickness, but in one particular set of experiments, the effects of flyers of varying thickness (5, 15 and 20 mm) were examined (Figure 3.4). The reason behind this was to extend the pulse for as long as possible through the microbial samples to deduce whether colony growth rates were affected. By using flyer plates of varying thickness, pulse duration could be controlled and accurately measured by validated hydrocode models. As part of the experiments to create ramped waves through the biological samples, novel stainless steel 316 graded density flyers (GDF) called Surfi-Sculpt® were employed. These were produced by TWI® using electronic beam technology to displace material on the front side of the plate to create a spiked surface (Figure 3.4).

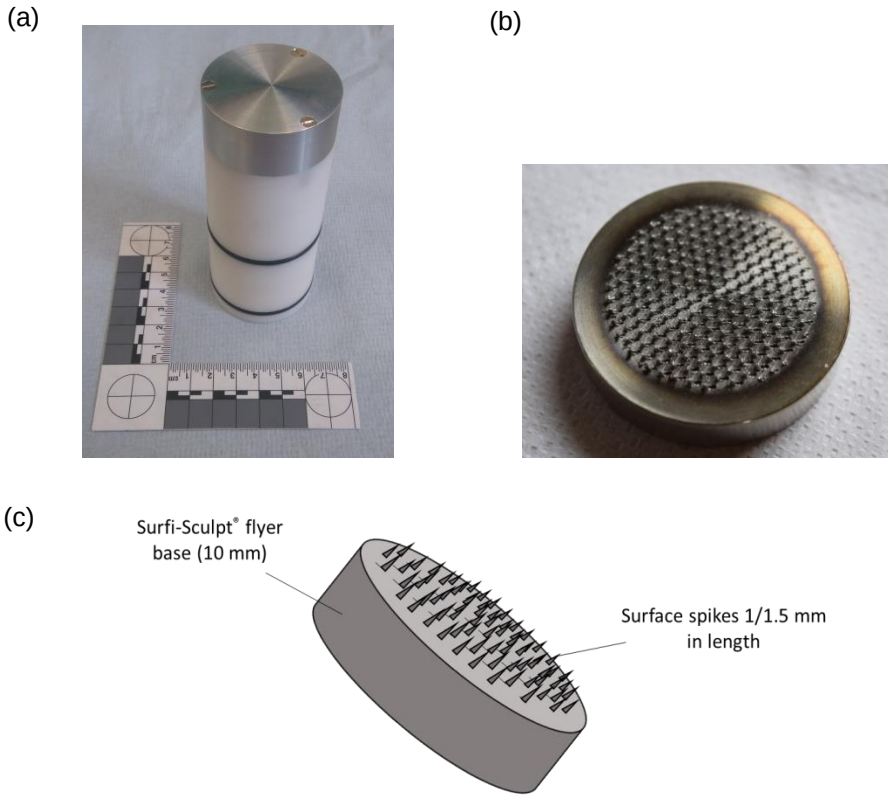

Figure 3.4 a) Example of a 20 mm Al flyer plate attached to a sabot with 'o' rings (designed to minimise gas-wash past the projectile which might affect the planarity of subsequent impact). b) Surfi-Sculpt® flyer plate with surface spikes of 1 mm. c) Diagram of the Surfi-Sculpt® flyer.

3.3 Impedance matching technique

In order to determine the shock Hugoniot of phosphate buffered saline (PBS) – the solution used to hydrate the microbial pellets for the experiments – it was necessary to determine the particle velocity (u_p). This was achieved by using the impedance matching technique [9, p. 126]. This technique enables the pressure resulting from an impact to be calculated and requires that the pressure and particle velocity be continuous across the interface of the impact. In this case, impedance matching was used to calculate the u_p of PBS and hence the shock Hugoniot for the liquid solution could be ascertained since the pressure and shock velocity (U_s) could be identified from the associated experimental shock trace. The impedance matching technique may be applied graphically, as shown in Figure 3.5 by taking the known Hugoniot of one of the materials, e.g. the flyer material, and inverting it along the pressure axis according to the impact velocity of the experiment. The intersect of the inverted flyer Hugoniot and the Hugoniot allows shock properties of the experiment, such as pressure and u_p, to be determined.

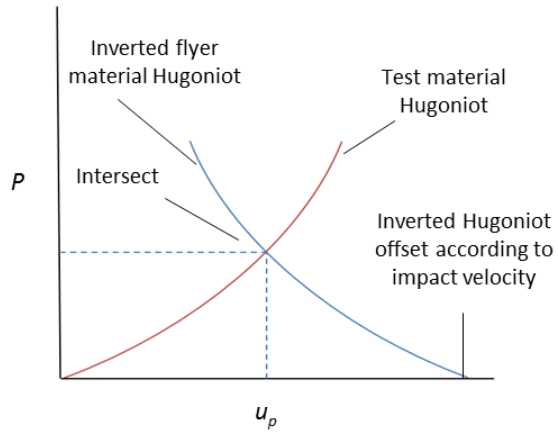

Figure 3.5 Example of the impedance matching technique on a *P*-u_p plot. The inverted Hugoniot of the flyer plate is shown in blue while the Hugoniot of the test material is shown in red. The intercept shows the pressure and particle velocity for the experiment.

3.4 Recovery capsule system

The capsule system used throughout this project was designed for the safe containment of the organisms during shock loading and the retrieval of the samples post-experiment. The original design [99] was modified slightly for different sets of experiments, including those intended to increase pressure and temperature. The original capsule system design included an outer 50 mm diameter Al capsule with an inner 25 mm diameter Al capsule [99]. A Teflon® (PTFE) liner (6 mm diameter) was also designed to sit inside the inner Al capsule. This capsule system is shown in Figures 3.6 and 3.7. A 1.5 mm diameter cavity sat in the Teflon® liner which could hold ~ 6 μl of a test solution. The larger capsule was intended to be filled with ballistic gelatine as a low impedance material to attenuate reflecting shock waves from the sides of the capsule.

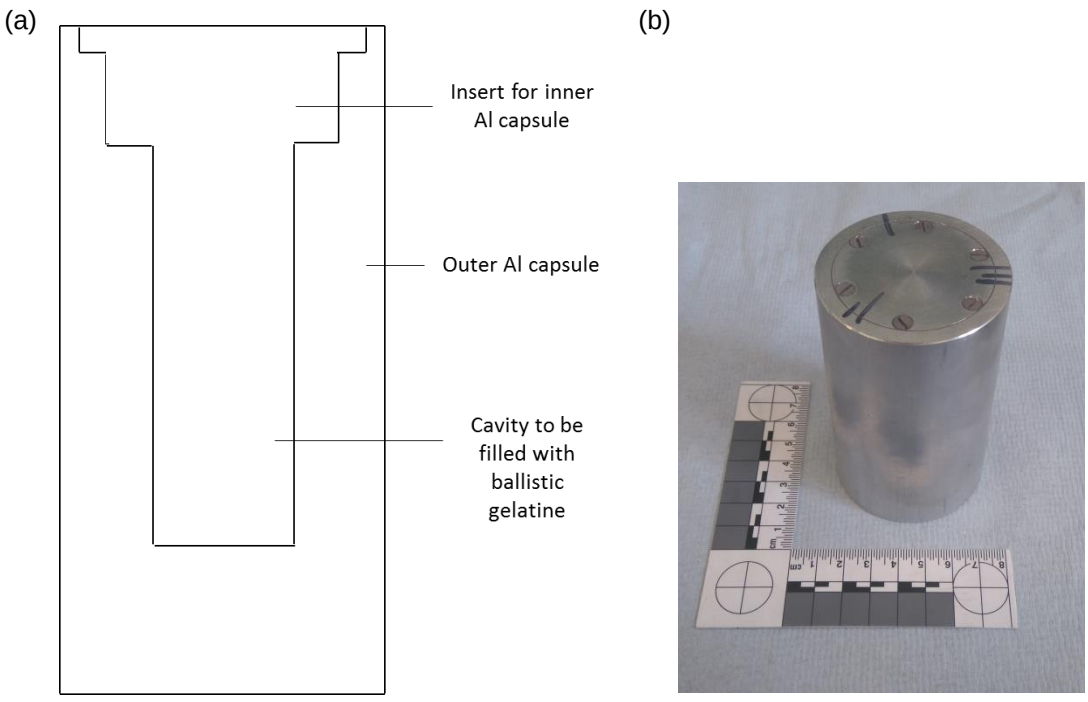

Figure 3.6 a) Diagram of the outer capsule. b) Image of the outer Al capsule and lid. Inside sits the smaller Al capsule containing the test sample surrounded and backed by 20% ballistic gelatine.

(a)

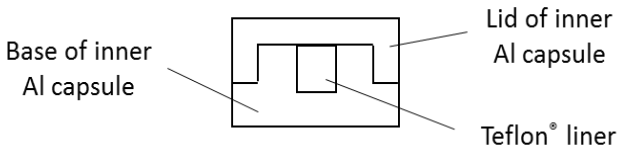

(b)

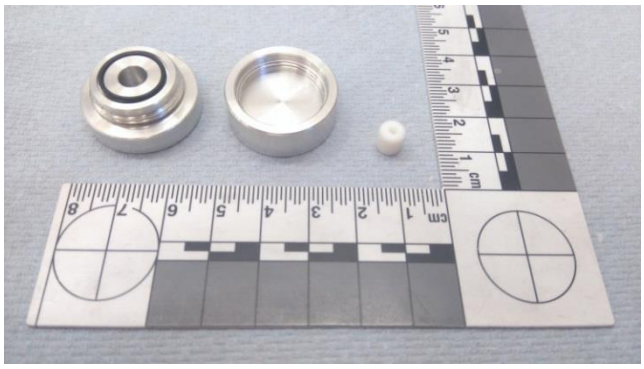

Figure 3.7 a) Diagram of the inner capsule. b) Image of the inner Al capsule with lid and 'o' ring. The Teflon capsule is also pictured with a cavity that holds liquid samples.

It was intended that a layer of fast-curing epoxy resin would sit at the very bottom of the capsule, below a layer of ballistic gelatine to aid with the attenuation of rarefaction waves from the rear surface of the outer capsule [99]. It has been determined here, however, that no meaningful difference in survival rates of the *Escherichia coli* NCTC 10538 was seen between experiments with and without the use of the epoxy resin. Therefore, further experiments have been carried out with only the use of 20% ballistic gelatine.

In order to examine the control of temperature at elevated pressures, and how this might affect microbial life, a higher density material for the capsule was required. A copper capsule was designed for these experiments, but with the addition of a layer of 50 μm Mylar® to cover the top of the Teflon® liner and separate it from the Cu lid of the inner capsule, as Cu is not a biocompatible material. This thickness of Mylar® was chosen so as to minimise attenuation of the shock, but also to remain intact upon dynamic loading.

3.5 Diagnostic techniques

In order to interrogate material behaviour during shock a number of different diagnostic approaches / techniques were employed – with the approach taken dependant on the nature of the experiment in question. To this end the following diagnostic techniques were used to retrieve shock profiles – to be later assessed and used to determine shock Hugoniots – as well as impact velocities.

3.5.1 Manganin stress gauges

The piezoresistive gauges used during this project consisted of manganin, an alloy of copper (84%), manganese (12%) and nickel (4%) [100]. The advantage of using manganin gauges is its large pressure tolerance, capable of withstanding pressures up to 100 GPa [12], as well as its constant resistance over a range of temperatures [100]. The brand of gauge used in this investigation was the Vishay Precision Group LM-SS-125CH-048 longitudinal manganin gauge (Figure 3.8) with a resistance of 48Ω.

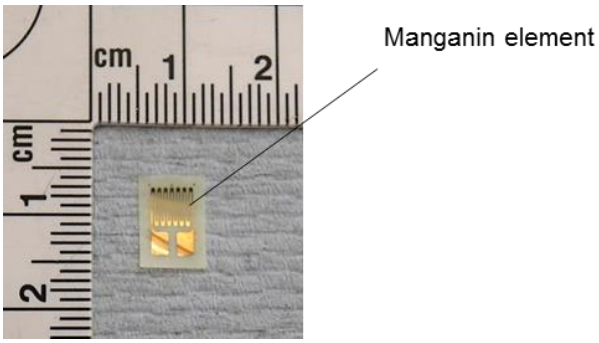

Figure 3.8 Image of a manganin gauge. Strips of brass shim were used as 'gauge legs' and soldered to the element with indium solder. This would eventually lead to the oscilloscopes measuring the shock profile during a shock experiment.

When interpreting these gauges, Equations 3.1 and 3.2 are considered, where P is pressure, R is resistance and A is the coefficient as outlined by Rosenberg *et al*. (1980) [101]. When the gauge responds in the plastic regime, Equation 3.1 is applied; whereas when the gauge is in the plastic regime, Equation 3.2 applies. Note that the value for R_0 is nominally 48Ω, although this may vary slightly between each experiment. The resistance of the gauge package was measured with a multimeter before each calibration. In order to carry out the calibration, the relative change in resistance, ΔR is calculated using Equation 3.3.

$$P = \frac{1}{A_0}\left(\frac{\Delta R}{R_0}\right) \tag{3.1}$$

$$P = A_0 + A_1\left(\frac{\Delta R}{R_0}\right) + A_2\left(\frac{\Delta R}{R_0}\right)^2 + A_3\left(\frac{\Delta R}{R_0}\right)^3 + A_4\left(\frac{\Delta R}{R_0}\right)^4 + A_5\left(\frac{\Delta R}{R_0}\right)^5 \tag{3.2}$$

The coefficients derived previously [100] are as follows:

A_0 = 0.0195, A_1 = 0.572, A_2 = 29.59, A_3 = 95.20, A_4 = -312.74 and A_5 = 331.77.

The calibration of the gauge involved simulating a shock wave across the gauge before observing the resulting changes in voltage using an oscilloscope, which is described in the next section. During calibration, different known resistances were applied across the gauges while the changes in voltage when a short duration high voltage power supply was discharged were noted (Table 3.1). This meant that during the experiment, recorded changes in voltage could be converted to changes in resistance, leading to the derivation of the coefficients for Equation 3.3, where V was the voltage. The coefficient C was set to 0, since at zero voltage, there is no change in resistance.

$$Theoretical\ \Delta R = aV^2 + bV + C \tag{3.3}$$

Once ΔR had been established, the ratio $\Delta R/R_0$ could be calculated by dividing the theoretical ΔR equation by R_0, according to Equation 3.4. Following this, $\Delta R/R_0$ could be substituted into the equation by Rosenberg *et al*. [101] to obtain the pressure values for each experiment. This then allowed the original voltage-time shock traces to be plotted and analysed in the pressure-time plane. Importantly, the current was kept constant so that changes in voltage corresponding to these different resistances could be recorded (Table 3.1).

$$\frac{\Delta R}{R_0} = \frac{aV^2 + bV + C}{R_0} \tag{3.4}$$

Table .3.1 Example of voltages (V) associated with applied resistances (Ω) to manganin gauges.

ΔR (Ω)	Voltage (V)
0.22	0.03
0.70	0.08
1.47	0.17
2.20	0.25
4.71	0.51
9.96	1.02

3.5.2 Nickel temperature gauges

Vishay Precision Group nickel temperature gauges were applied for a set of experiments for which the peak temperature in the capsule was under investigation. The results from these experiments were used to validate hydrocode models that were ultimately used to measure temperatures inside the Teflon® liner. Resistance of the nickel gauge is calculated using Equation 3.5. It is assumed that the resistance is 50 Ω at 24 °C.

$$R = A + BT + CT^2 + DT^3 + DT^4 + FT^5 + GT^6 \tag{3.5}$$

In order to determine temperature, Equation 3.5 can be rearranged to give Equation 3.6.

$$T = A' + B'R + C'R^2 + D'R^3 + E'R^4 + F'R^5 + G'R^6 \tag{3.6}$$

The coefficients given by the manufacturer [102] are:

A' = -2.329, *B'* = 7.984, *C'*=-1.147, *D'*=1.927, *E'*=-2.054, *F'*=1.144 and *G'*=-2.531.

For calibration, the gauges were subjected to heating at different temperatures and the resulting resistances were measured as outlined in Table 3.2.

Table 3.2 Example of resistances (Ω) associated with temperature of nickel gauges.

ΔR (Ω)	Temp (°C)
49.6	24
52	35
53.2	40
57	60
59.2	80
62.1	100

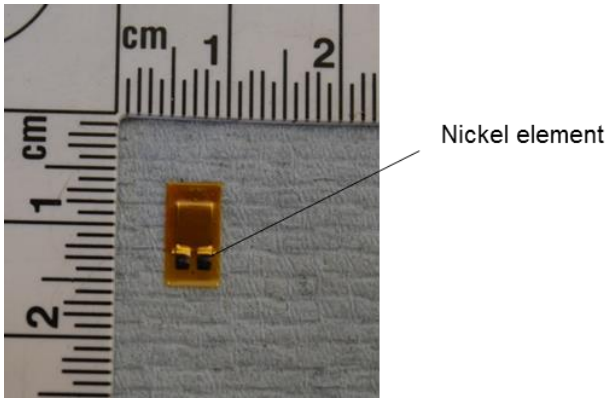

Figure 3.9 Image of a nickel gauge. As was the case for the manganin gauges, strips of brass shim were used as 'gauge legs' and soldered to the element with indium solder. This allowed the gauge to be connected to the oscilloscope.

3.5.3 Oscilloscopes

Two main oscilloscopes were used to record the data from the gauges; a 5 GS/s Tektronix DPO oscilloscope. Data was recorded by the oscilloscopes on the order of nanoseconds, with the corresponding voltage measured at each time interval. The voltage was converted to pressure using the calibration technique discussed in section 3.5.1. A Tektronix TDS 460A oscilloscope was also used to record velocity measurements. The experimental set-up included a set of three sequential light gates, with a gap of 25 mm between each. As the projectile passed between each light gate, the oscilloscope was triggered, recording the time each light gate was interrupted. These light gates had been previously calibrated against a series of shorting pins in-house and were shown to be accurate to ±2%. From this, the impact velocity could be calculated.

3.5.3 Heterodyne velocimetry

Heterodyne velocimetry (Het-V), as previously mentioned, is a technique that consists of an optical fibre-based laser interferometer to measure displacement of materials. It was used for the validation of the hydrocode models used throughout this thesis to determine the pressures reached for each shock loading experiment. The interferometer used here consisted of a single disposable probe (Laser Components Ltd.) as well as a collimated laser and a detector. The free-surface velocity of the rear surface of an inner Al capsule (Figure 3.10) was determined by measuring the Doppler shift frequency of a reflected reference light.

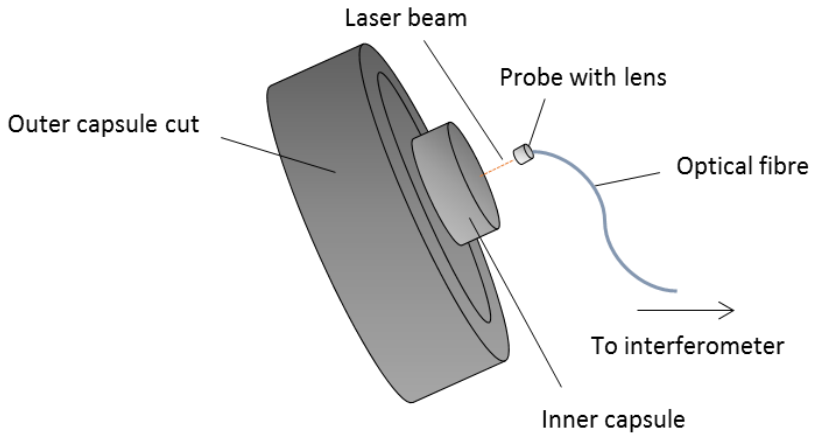

Figure 3.10 Set-up of Heterodyne velocimetry experiments to validate hydrocode models. A larger capsule was cut to allow the rear surface of the inner capsule to protrude so that it was exposed to the laser beam.

The incident beam (0.47 mm in diameter) from the lens at the end of the probe was reflected back from the illustrious surface of the aluminium. The probe was connected to an interferometer via a 5 m long single mode optical fibre. The interferometer to which the probe was connected consisted of a 20 mW Gen 0 light source (DFB-1550-BF-20-2.5-FA) with a wavelength of 1550 ± 30 nm. The light source was turned down to 17 mW for these experiments. The reflected beam, also known as the reference wavelength, changed in frequency as the material was shock loaded, resulting in a difference of frequency between this and the incident beam; this is known as the beat frequency. The beat frequencies were proportional to the rate at which the surface of the capsule moved at a distance of $\lambda/2$ along the probe beam, where λ is the wavelength. The optical fibre was used to feed this information back to a PDA8GS amplified photodetector where the reflected light was detected. The resulting signal was recorded using a 5 GS/s Tektronix DPO 7254C oscilloscope. The raw data were then converted into a velocity-time spectrogram using a MATLAB-based program called Het-V Tool (version 2.01). This program used a sliding Fourier Transform analysis to calculate the particle velocity from the recorded Doppler shift frequencies. Subsequently, the freely

available ImageJ software was used to manually produce a more visible velocity-time trace, which could then be compared to the corresponding data output by the hydrocode simulations. In this way, the numerical models could be validated and used to calculate pressures at different impact velocities recorded for each shock loading experiment.

3.6 Assessment of shock loaded organisms

3.1.1 Preparation of microorganisms

The microorganisms chosen for this project were *Escherichia coli* NCTC 10538 and *Saccharomyces cerevisiae* ATCC 18824 and were obtained from Technopath® in the form of lyophilised pellets. During preparation, both bacterial and yeast pellets were hydrated with 1 ml phosphate buffered saline (PBS). Hydrated bacterial pellets were subsequently pipetted into Sigma Aldrich® LB nutrient broth (10 ml), while hydrated yeast pellets were pipetted into Sigma Aldrich® YPD nutrient broth (10 ml). The microorganisms were then incubated for 18 hr at 37°C and 42 hr at 30°C, respectively according to the process described in section 3.7.

After 18 hr, which was the end of the exponential growth phase for the *E coli*, the sample was removed from incubation. An Eppendorf tube was filled with 1 ml of the sample and this was then centrifuged at 600 rpm for 4 min before removing the supernatant. This process was repeated twice in order to produce a pellet. The pellet was then rehydrated with PBS (1 ml), and 6 μl was pipetted into the Teflon® capsule for the shock experiment. This process was repeated for the *S. cerevisiae* after incubation for 42 hr.

3.1.2 Determination of microbial survival

Post shock loading, recovered samples were inoculated on a solid growth medium to allow colonies to grow and survival rates to be calculated. Before plating the samples on agar, the shocked samples were serially diluted in order to make the colonies visible enough to be individually counted (Figure 3.11). Dilutions up to 1 in 10 000 000 (10^{-7}) were carried out. This was achieved by taking 1 µl of the original sample and adding it to 9 µl of phosphate buffered saline (PBS) to form a 1 in 10 (10^{-1}) dilution. 1 µl from the 10^{-1} aliquot was then taken and added to a further 9 µl of PBS and so on. This was carried out for both shocked and control samples.

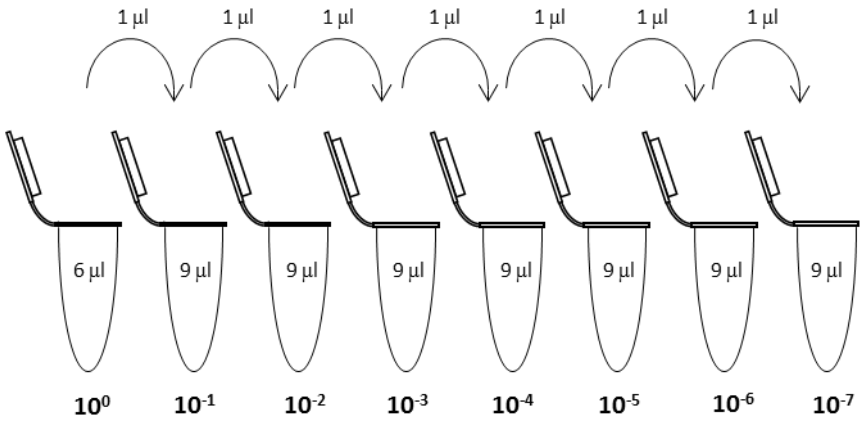

Figure 3.11 Serial dilutions were carried out on the shocked and control microbial samples in Eppendorf tubes. 1 µl of the original 6 µl sample (10^0) was added to 9 µl of PBS to produce a 1 in 10 (10^{-1}) dilution. This process was continued along consecutive Eppendorf tubes until a 1 in 10 000 000 (10^{-7}) dilution was achieved. The aliquots from each tube were plated on appropriate nutrient medium so that the growth of colonies could be counted visually.

The *E. coli* and *S. cerevisiae* were plated on nutrient agar medium; Sigma-Aldrich® LB Broth with agar (consisting of agar, NaCl, Tryptone and yeast extract) and YPD nutrient agar (consisting of glucose, bacteriological peptone, agar and yeast extract) respectively. The growth of colonies after incubation was measured in colony forming units (CFU) per millilitre and was calculated using Equation 3.7. A mean value was taken for the colonies formed in each serial dilution on the agar plate.

$$Population\ (CFU/ml) = \frac{CFU\ on\ plate}{Volume\ plated}\ \text{x}\ Dilution\ factor \tag{3.7}$$

3.1.3 *Artemia salina* preparation and assessment

Artemia salina was obtained from Sciento® in the form of frozen cysts. For the cyst shock loading experiments, the nauplius first emerges as an embryo from the hatching membrane. A total of 10 cysts were placed in the capsule in a 3% saline medium inside the Aluminium capsule. For the experiments regarding the shock loading of hatched nauplii (or larvae), the cysts had to be placed in a 3% saline solution in a water bath at 24 °C for 48 hr. This was to ensure that the maximum number of cysts was allowed to hatch.

Hatching rates of the cysts were measured after both 24 hr and 48 hr. The hatching process included the breaking of the cyst and the emergence of the embryo from a hatching membrane [103]. The motility of the *Artemia* larvae, or nauplii, was also observed in order to give a preliminary account of their activity once hatched post-shock loading.

3.2 Spectrophotometry

Spectrophotometry is a method by which the amount of light absorbed by a substance is quantified by measuring the intensity of a beam of light of a given wavelength as it passes through a sample. For the purposes of this project, this technique allowed measurements of the cell density of microbial populations to be made. A spectrophotometer is a combination of a spectrometer and a photometer. It consists of a light source, a collimator, monochromator, wavelength selector, photoelectric detector (or photocell) and galvanometer where the electrical output from the activated photocell may be converted into a transmittance value to be read by a digital display. The monochromatic grating separates the light into its component wavelengths. The rotation of this grating, along with a wavelength selector, allows the desired wavelength to be chosen by the operator. The transmitted light will be detected by a photocell. A schematic illustration of this arrangement is shown in Figure 3.12 The spectrophotometer used throughout this project was a Jenway Genova Plus with a variable wavelength of 198 to 1000 nm.

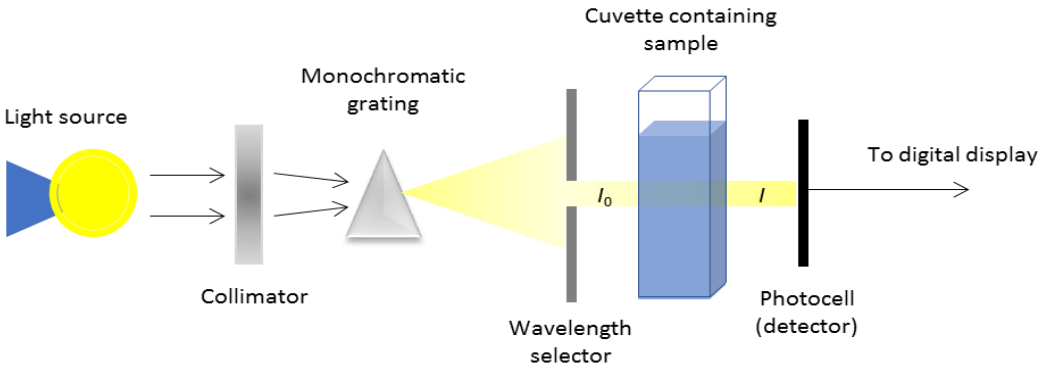

Figure 3.12 Set-up of a typical spectrophotometer with a specific wavelength of light chosen to shine on the sample so that the optical density (OD), or absorbance, may be measured.

Transmittance (T) may be described as the fraction of light that passes through the sample and is calculated according to Equation 3.8.

$$T = \left(\frac{I}{I_0}\right) \tag{3.8}$$

Where I_0 is the light intensity entering the sample and I is the light intensity emerging from it.

The transmittance may also be expressed in terms of absorbance A according to the Equation 3.9.

$$A = -\log(T) = -\log\left(\frac{I}{I_0}\right). \tag{3.9}$$

Given the known absorbance, the Beer-Lambert Law (Equation 3.10) may be used to find the unknown concentration of the sample;

$$A = \epsilon l c \tag{3.10}$$

Where ϵ is the absorption coefficient, l is the length of the path length of the light and c is the concentration of the sample.

Equation 3.9 can also be rearranged to Equation 3.11 to find the absorbance, or optical density (OD) of a sample:

$$OD = \log_{10}\left(\frac{I_0}{I}\right) \tag{3.11}$$

The spectrophotometer used in this project was calibrated using blank samples of water and uninoculated nutrient broth. Its original purpose was to calculate the growth curves of both *E. coli* and *S. cerevisiae* to determine their incubation time and maximum cell growth that could be achieved. Microorganism growth is divided into four phases; lag, log (or exponential), stationary and death.

1) The lag phase is the primary stage of growth where cells become acclimated to their environment of particular nutrients and temperature.
2) The log phase is where cell growth rapidly takes place as cells divide exponentially due to their favourable environment.
3) The stationary phase is the point at which nutrients begin to deplete and cells stop growing.
4) Finally, once all nutrients have been used, cells eventually die (death phase).

For the calculation of growth rates of *E. coli* (Figure 3.13) and *S. cerevisiae* (Figure 3.14), OD measurements were taken at hourly intervals during the lag phase. As soon as the organisms reached their respective log phases, the OD measurements were then taken every half hour until the stationary phase was reached. At this stage, the organisms were removed from incubation.

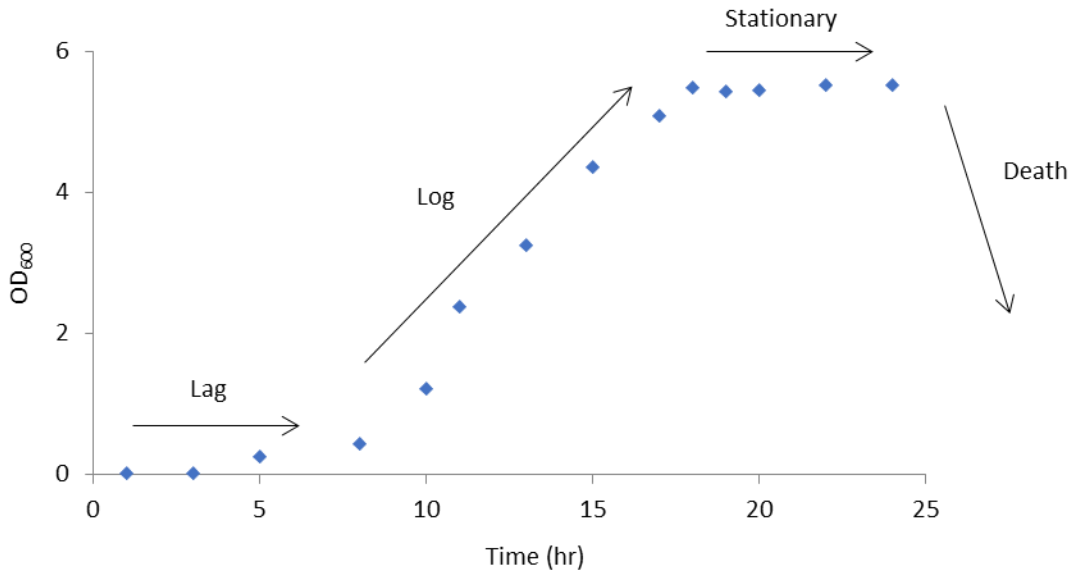

Figure 3.13 The growth curve of *E. coli* at 37°C given as transmittance with respect to time. This is according to absorbance measurements taken at different times during incubation. The end of the log phase (18 hr) indicates when the cells have stopped growing due to a depletion in nutrients in the growth medium.

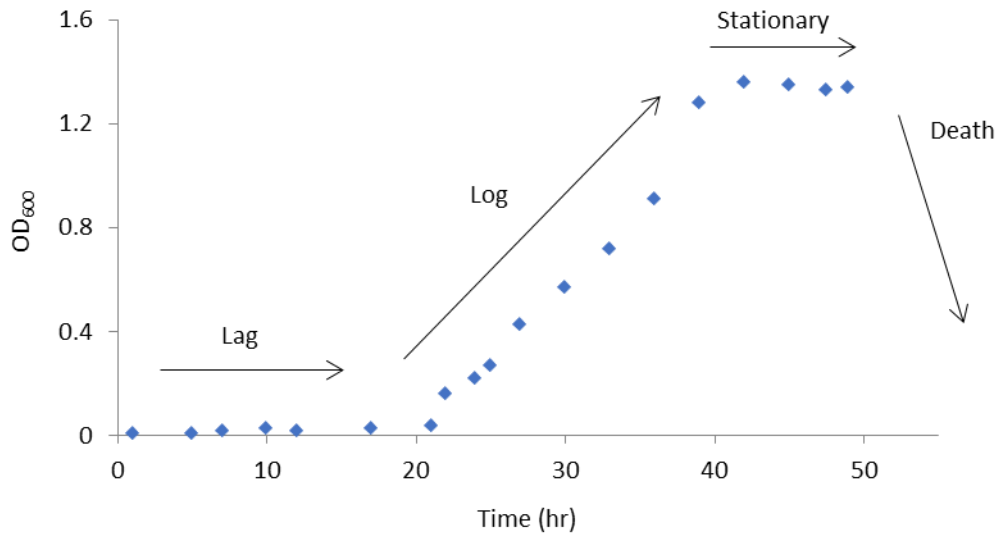

Figure 3.14 The growth curve of *S. cerevisiae* at 30°C. The log phase ends after (42 hr) of incubation, indicating maximum cell growth.

3.3 Light microscopy

For analysis of the biological samples after impact, light microscopy was carried out using an Olympus BX53 light microscope. Basic bright field microscopy was carried out with this microscope using an Olympus SC50 camera. It was primarily used for the *Artemia* cysts and larvae in order to count hatching rates and to determine the number of shocked larvae that were visibly alive after a period of about two days. The microscope enabled real-time assessment of the larvae behaviour pre- and post-shock. The camera also allowed video of the hatched larvae to be recorded.

3.4 Error Analysis

There were a number of areas throughout this project where errors were introduced. Although the occurrence of this was minimised through careful preparation of samples and repetition of experiments, there were still a number of potential sources for both random and systematic errors. Random errors were introduced when calculating the growth rates of microbial colonies, as these could only be counted by eye and also involved natural errors when pipetting microbial samples onto the agar plate. For an individual experiment, errors could be noted between the three separate aliquots at each dilution factor. However, the shock experiments at each pressure were performed at least three times each and errors in colony growth rates were calculated according to the highest and lowest growth rate from each experiment. In the case of the *Artemia salina* experiments, each experiment was carried out 5 times in order to gain a more reliable sample size to better evaluate trends.

There will also be errors in the actual preparation of the target; for instance, when gluing the cover plate to the front end of the capsule, as well as in the some of the components for the target build. For example, the machined components of the experimental set-up had a tolerance of ± 10 μm; this included the flyer plates used in each experiment (excluding the Surfi-Sculpt® flyer plates). Equation 3.12 was used to calculate the errors in machining tolerance in milliradians. For the capsules with a diameter of 50 mm, the maximum error in tolerance is ± 0.2 mrad, given the opposite value as 10 μm and the adjacent value as 50 mm.

$$\tan(\theta) = \frac{Opposite}{Adjacent} \tag{3.12}$$

Errors in the manganin gauge traces also had to be considered. When plotting a pressure profile, the pressure-time plane, the errors in shock, U_s, velocity could be calculated. U_s was calculated by measuring the time between the rise of the front gauge and the rise of the rear gauge. The errors were taken as the minimum and maximum times for the wave to travel. An example of this is shown in Figure 3.15. The maximum time was determined by measuring the time between the beginning of the rise (t_1) of the front gauge to the end of the rise (t_2) on the rear gauge. Conversely, the minimum time was calculated by the difference between the end of the rise (t_2) in the front gauge to the beginning of the rise on the rear gauge (t_1). It is also at this stage that issues with misalignment of the target in the gas gun will be apparent. From U_s and the impedance match technique, particle velocity, or u_p, can also be determined. Errors for this value are then based on the error values of U_s. While U_s and u_p were measurable for the experiments involving pressure gauges, it was not possible to do this for the shock experiments involving the capsule system. The errors calculated in the latter case will be discussed later in this section.

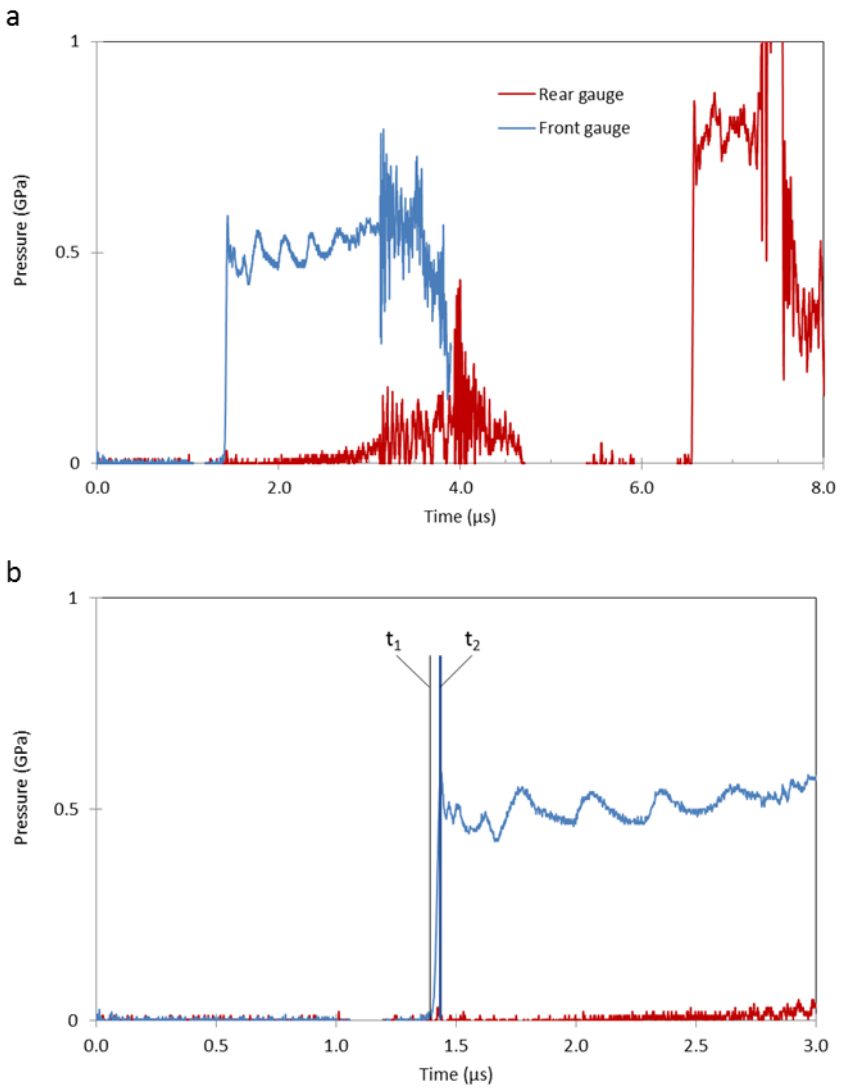

Figure 3.15 a) Shock profile for deionised water at an impact velocity of 362.32 m s^{-1} b) Zoomed in version of the front gauge trace to indicate the beginning (t_1) and end (t_2) of the rise time of the shock wave through the material.

Impact velocities were measured by a light gate system which consisted of three channels; errors were calculated from the differences in the time at which each light gate was triggered by the projectile passing between them. The velocities recorded were input to the numerical models used to measure pressure for each shot carried out in this project, which could have resulted in some systematic error. There could also be some

inherent errors in the materials used in the models, compared to the real materials used to collect empirical data.

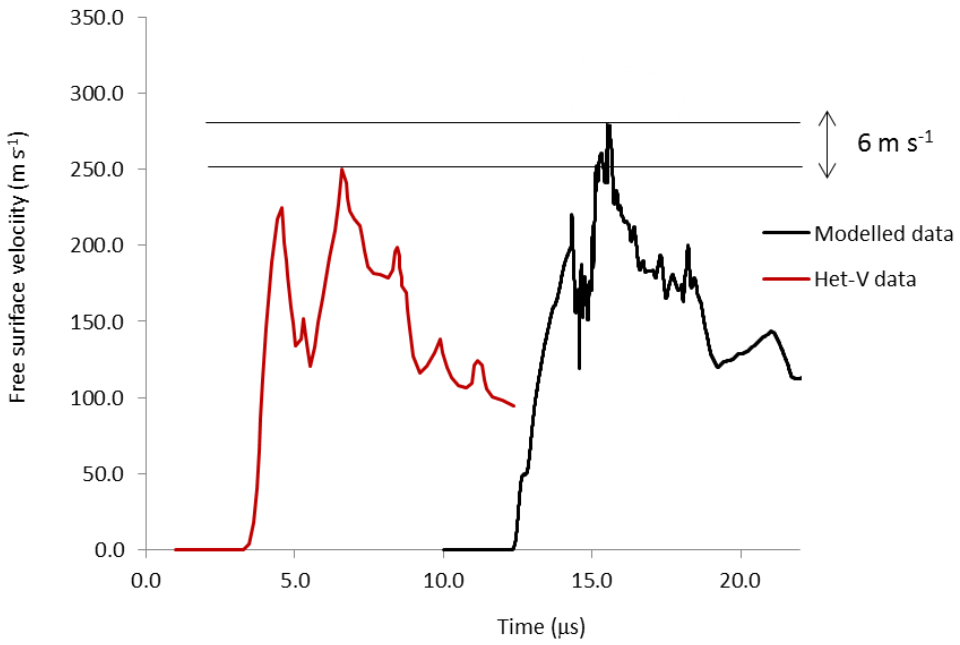

Figure 3.16 Het-V data compared with hydrocode model.

The errors for the numerical models used were measured in a number of ways. Firstly, Het-V was utilised to validate the models eventually to be used in this investigation. Het-V measured the free surface velocity on the rear of the inner capsule, while ANSYS® Autodyn – the modelling program used throughout this project – was used to measure this value using the same impact velocity. The difference in peak free surface velocity between the Het-V data and that of the numerical model is shown in Figure 3.16. At a velocity of 316 m s^{-1} the difference in free surface velocity according to Het-V and the numerical models is 6 m s^{-1}, equating to an error of ± 2.3%.

Errors in pressure for each simulated experiment were taken from the highest and lowest pressure values measured from the virtual gauge points in the simulated Teflon® liner. An example of pressure values from a simulated experiment is shown in Figure 3.17. Errors in temperature for each *E. coli* shock experiment (detailed further in Chapter 5, section 5.3) were also calculated from the virtual gauge points inside the Teflon® capsule, in the same manner as the pressure values. The gauge points in the simulations are explained further in the following chapter.

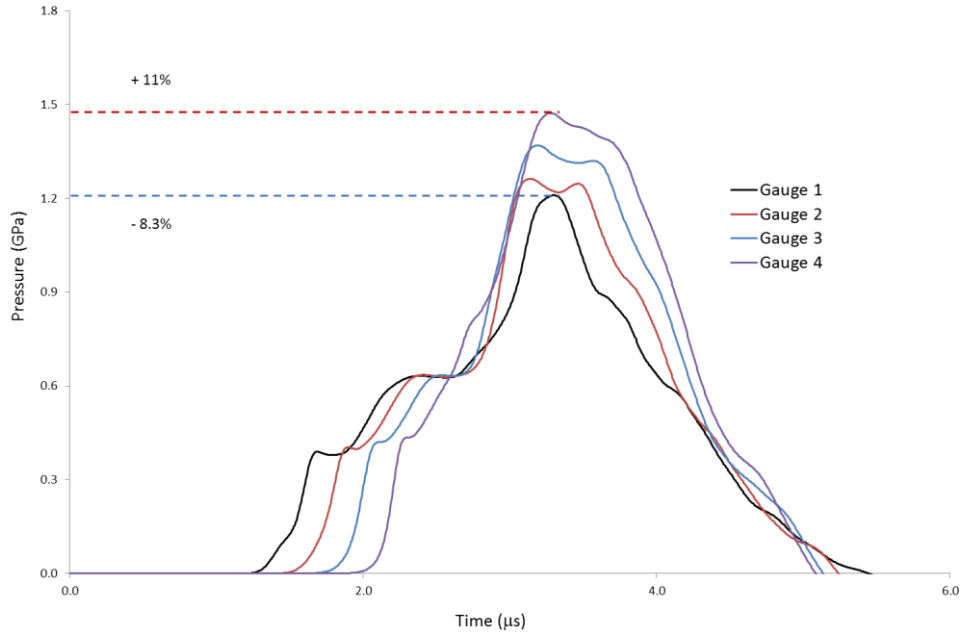

Figure 3.15 Modelled shock experiment with an impact velocity of 221 m s^{-1}. The average pressure here was 1.33 GPa with an error of +11/-8.3%.

4 Hydrocode modelling

4.1 Introduction

Hydrocode models were applied throughout this thesis primarily as a method for measuring peak pressure inside the Teflon® capsule in which the microbial samples were placed. As shown in Chapter 3, the experimental set-up did not allow for pressure gauges as there was nowhere to appropriately place the gauges and still seal the capsule during the shot. Gauges also could not be added to the outside of the capsule due to the existence of too many interfaces between the gauge and the target sample, leading to unreadable pressure profiles. As a consequence of this, numerical simulations had to be relied upon to determine pressures occurring inside the sample. While the models offered a better understanding of what was occurring inside the Teflon® liner, and acted as a way to validate the real capsule design, they a first had to be validated themselves; this was achieved by a number of different experiments that will be explained in this chapter. Firstly, since ANSYS® Autodyn, was not solely reliable for predicting temperatures in the target during shock loading, nickel temperature gauges were used to help validate the peak temperatures calculated by the model. Secondly, in order to validate the pressures predicted by the model, a Heterodyne velocimetry laser was applied to the inner capsule to determining the free surface velocity, or particle velocity, of the rear surface of the inner capsule. Thirdly, in an attempt to confirm the appropriateness of the materials used within the model, numerical simulations recorded in the literature were replicated using the same materials and material properties. Finally, the suitability of water to represent the microbial sample in the simulations was investigated experimentally.

4.2 Hydrocode models

In order to keep the model construction as simple as possible to aid with the run-time and to avoid issues of complex distortions, the majority of models built for this project were 2D Lagrangian. As mentioned previously, numerical models may be created in 2D or 3D mode, with 3D generally being the more accurate representation of real dynamic processes involving complex geometries. Models in 2D form are useful for more simplistic simulations, such as the quasi-one-dimensional experiments carried out in this thesis. 2D models can be built in either of two symmetries; planar and axial. While Eulerian systems are useful in a number of respects, i.e., measuring large distortions of solid materials or gas flow, they can be largely inefficient, whereas the Lagrangian method can be used to construct more efficient models. Often these complex distortions are incapable of being run with Lagrangian structures. Lagrangian models were chosen for use in this work given the overall simplicity of the experimental set-up.

As mentioned above, 2D models may be utilised in either planar or axial symmetry. Planar symmetry extends the model to infinity in either direction along the axis perpendicular to the axis of impact. Axial symmetry allows the construct to be repeated rotationally around the impact axis. An axial symmetry was used for each of the models since this method was more efficient and was found to match empirical data. In this way, it was also possible to note graphically, as well as visually, what pressures were occurring inside the Teflon® liner.

In ANSYS® Autodyn, numerical models are processed by solving a set of equations which describe how the material properties change in response to shock [104]. These equations are similar to the Rankine-Hugoniot equations discussed in Chapter 2, section 2.2, where mass, momentum and energy are conserved. This is shown by Equations 4.1, 4.2 and 4.3, respectively.

$$\frac{D\rho}{Dt} + \rho \frac{\delta v_i}{\delta x_i} = 0 \tag{4.1}$$

$$\rho \frac{Dv_i}{Dt} = -\frac{\delta P}{\delta x_i} + \frac{\delta S_{ji}}{\delta x_i} + \rho f_i \tag{4.2}$$

$$\rho \frac{De}{Dt} = \rho \dot{q} + \frac{\delta}{\delta x}\left(k \frac{\delta T}{\delta x}\right) - P \frac{\delta v_i}{\delta x_i} + S_{ji} \frac{\delta v_i}{\delta x_j} \tag{4.3}$$

Here, i, j, and k denote vector axes, δ = density v = velocity, x = displacement, S = stress, e = internal energy, q̇ = viscosity and T = temperature. Numerical models also require calculations to determine how materials behave under shock compression based on the density and energy of said material. This is given by Equation 4.4., where *P* = pressure. Additionally, stress distribution within the material is calculated according to Equation 4.5, where σ = traceless symmetric deviatoric stress. The simulation solves these equations at each time-step for each cell within the grid.

$$P = P(\rho, e) \tag{4.4}$$

$$\sigma_{ij} = S_{ij} - \delta_{ij} P \tag{4.5}$$

The time-step is controlled using the Courant-Friedrich-Levy (CFL) criterion, set out in Equation 4.6. This equation dictates that the time-step must be less than the time it takes for the sound wave to travel across the grid.

$$\Delta t < \frac{\Delta x}{c} \tag{4.6}$$

Equation 4.6 consists of Δt, the time-step; Δx, the grid spacing; and c, the sound speed for the target material. As mentioned previously in Chapter 2, numerical models cannot solve the mathematical discontinuity of a shockwave since the equations to do this would tend towards infinity. To solve this problem, viscosity is added to the solution so that the shock becomes spread out over several cells and the hydrocode can more readily calculate the solution [104]. Erosion models then become necessary to overcome the introduction of overly distorted cells to the model. Severely deformed cells can cause the simulation to stop running and fail; erosion models are used to remove these deformed cells; this will be discussed further in the next section.

4.3 Capsule and model design

The design of the Al capsule system allowed quasi-one-dimensional shock waves to propagate through the target, as described in the previous chapter; the application of the hydrocode models provided a method to validate this capsule and also allowed insight into the type of loading occurring within the target. Each simulation was used to assess the slightly more complex quasi-one-dimensionality of the loading, as opposed to the typical planar wave front produced from plate-impact experiments. The reason behind the development of this more complex wave front was due to the number of interfaces between components of the target, as well as the wave traversing materials of various impedance.

Whereas PV gauges are of a finite length, virtual gauge points are infinitesimal points which record the conditions at the corner of mesh cells (Lagrangian) or at the centre of

the mass particle (SPH). Since Lagrangian models were primarily applied throughout this thesis. Gauge points were plotted along the inside of the Teflon® capsule (Figure 4.1) to measure peak pressures at each point; an average of these values would then be taken as the overall pressure seen by the sample. ANSYS® Autodyn allows virtual gauge points to be added to the model to record a number of features, including pressure, temperature and free surface velocity, all of which have been used in this thesis. The virtual gauge points here were designed to flow with the target material, in keeping with a real-life set-up.

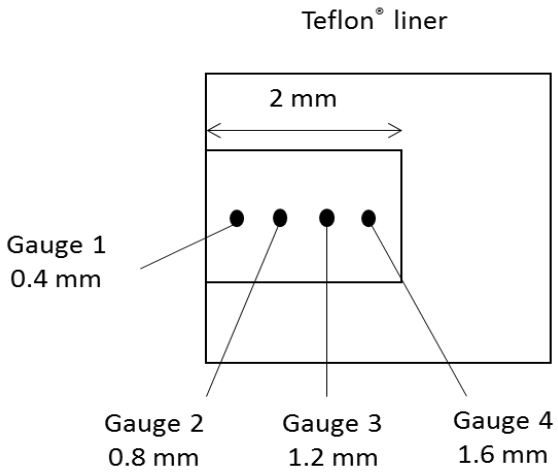

Figure 4.1 Location of virtual gauge points in relation to depth inside the modelled Teflon® liner.

An SPH hydrocode was employed initially to model the Surfi-Sculpt® flyer due to the complexity of the structure and the fact that SPH simulations negate the need for erosion models and avoid associated time-step issues, essentially simplifying the build of the model. However, the results from the SPH model was later compared to those from a Lagrangian model and while comparing both of these to experimental data, the Lagrangian model matched better with real shock profiles. A diagram and screenshot of the modelled capsule is shown in Figure 4.2. While the Surfi-Sculpt® flyers have a more complex structure, there were rather large errors – as stated in the previous chapter – in

the spikes protruding from the surface. Since the largest of these protrusions was only nominally 1.5 mm in length on a 10 mm solid base.

Table 4.1 Parameters of the materials used in each of the hydrocode models throughout this thesis. Note that the values labelled N/A indicate parameters that were not essential for the corresponding material in the numerical calculation.

Material	Strength model	Density ($g\ cm^{-3}$)	Gruneisen coefficient	Thermal conductivity ($J\ m^{-1}\ K^{-1}\ s^{-1}$)	Specific heat capacity ($J\ kg^{-1}\ K^{-1}$)	Reference EOS
S/steel 316	Piecewise Johnson-Cook	7.86	1.67	N/A	4.23×10^{2}	Matsuka, 1984
Copper	Piecewise Johnson-Cook	8.9	2.0	403	3.90×10^{2}	Matsuka, 1984
Al 6061-T6	Steinberg-Guinan	2.703	1.97	247	8.85×10^{2}	Steinberg, 1991
Teflon	von Mises	2.16	0.9	0.25	1.05×10^{3}	Matsuka, 1984
Water	N/A	1.0	0.28	0.609	4.18×10^{3}	Nagayama *et al*., 2002
PMMA	von Mises	1.186	0.97	0.2	1.26×10^{3}	LA-4167, 1969

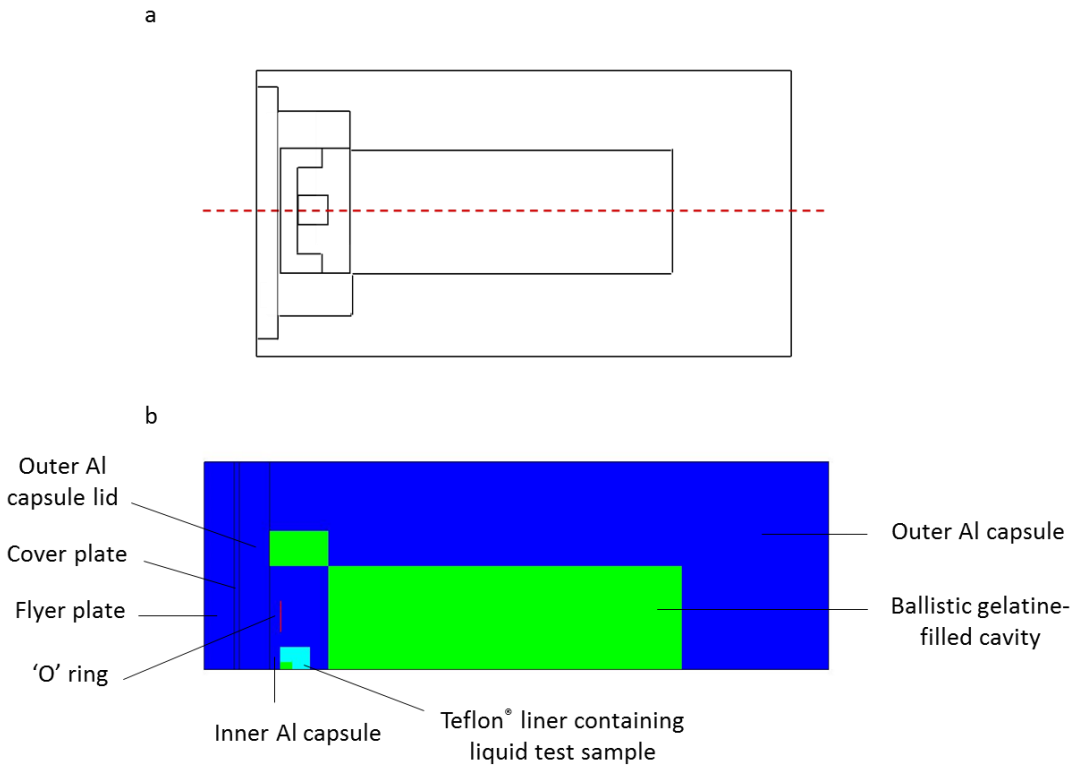

Figure 4.2 a) Diagram of the Al capsule with a section through the centre to demonstrate the geometry built in axial symmetry. b) Screen shot of capsule built in ANSYS® Autodyn.

The purpose of the capsule design was to reduce rarefaction waves within the Teflon® liner and to maintain a mostly one-dimensional wave for as long as possible through the target. Numerical models demonstrated this behaviour and gave an understanding as to the features of the shock profile in the Teflon® capsule. When designing the models, materials were taken from the Autodyn library (except in the case of stainless steel) with careful attention paid to the parameters listed in Table 4.1. For each model, the erosion model geometric strain with a value of 2 (or 200%) was used. The purpose of the erosion model is to remove cells before they deform to the point that the time-step of integration is degraded. While the disadvantage of this model is that is an unrealistic phenomenon in dynamic processes, it may not pose a problem if it occurs in a portion of the model not of interest to the user. The erosion model in this case was chosen to be a

geometric strain of 200%, which when reached, was the point where a cell would be deleted.

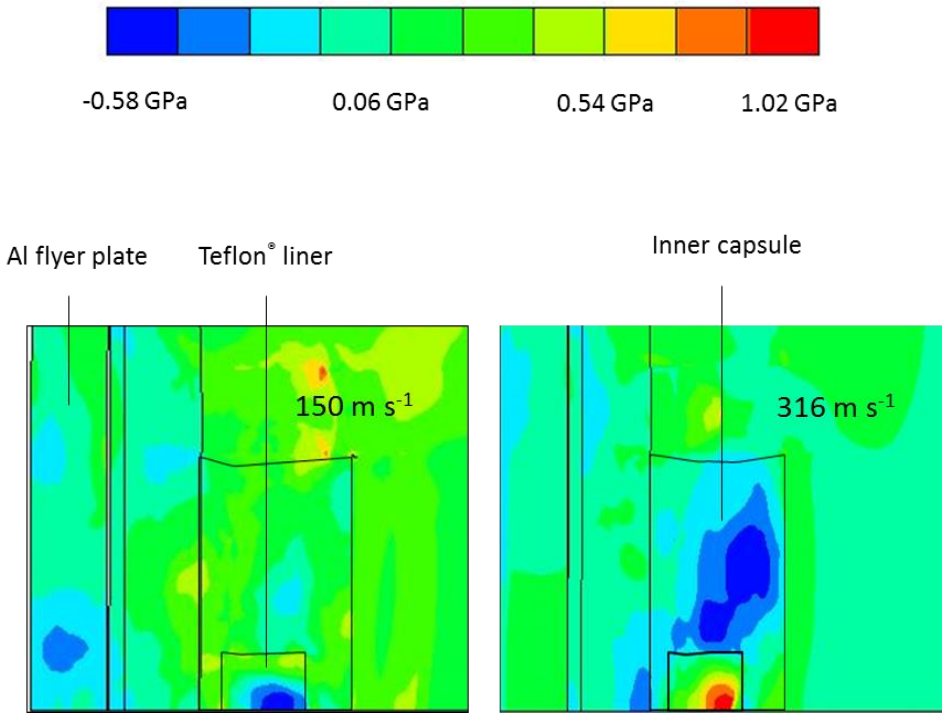

Figure 4.3 Zoomed-in screenshots taken at 4 μs from models of the Al capsule undergoing plate-impact at two different velocities: 150 m s^{-1} and 316 m s^{-1}.

Models were built for each type of experiment carried out: standard plate-impact, temperature experiments and extended pulse duration experiments. In section 4.4, other models were also used in combination with experimental results to verify those used for each experiment. These models were used for measuring the pressures occurring inside the Teflon® liner and also the nature of the shock wave front and the overall loading profile.

4.4 Validation of the hydrocode models

It was necessary for the pressures and temperatures predicted by the capsule system to be backed by empirical data, since these models were used to predict the pressure and temperature for every shock experiment involving the capsule system for the organisms. From the outset, each model with a particular material has to be validated experimentally so that they could be used to measure the pressure, temperature or free surface velocity.

4.4.1 Temperature measurement and Surfi-Sculpt® flyer plates

Firstly, in order to validate the simulations of the Surfi-Sculpt® flyer impact on the capsule system, experiments were carried out to investigate the ramp loading produced by these graded areal density flyers *vs* a traditional shock wave with a planar wave front produced by a planar stainless steel 316 flyer plate. Since the Surfi-Sculpt® flyers were available with two different spike lengths (~ 1 and 1.5 mm) one of each of these was tested along with the planar flyer. The experimental set-up involved a 10 mm stainless steel buffer plate as the target, with a single manganin gauge on the rear surface, backed by a PMMA plate (11 mm). Each flyer was used to impact these targets at 500 m s^{-1}. The results are shown in Figure 4.4. Although the ramping was very slight towards the plateau of the pressure traces for the Surfi-Sculpt® flyers, there was a clear distinction between these impactors and the planar flyer. Each shot resulted in a pressure of 9.7 GPa.

In order to simulate this ramp loading, both smoothed particle hydrodynamics (SPH) and Lagrangian models of the Surfi-Sculpt® flyers were built. Initially, the model

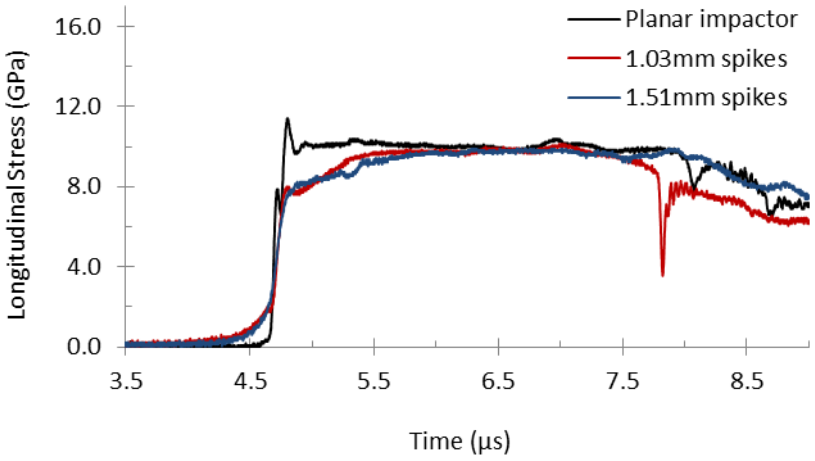

Figure 4.4 Shock profiles of Surfi-Sculpt® flyers at an impact velocity of 500 m s^{-1}. The Surfi-Sculpt® flyers had spikes of nominally two different lengths which, overall, showed very little difference in their shock traces. As a control, the shock profile of a planar flyer with a thickness of 10 mm was compared to the Surfi-Sculpt® profiles. While the same pressure was reached in each case, a lazier rise was noted in the case of the Surfi-Sculpt® flyers.

was built in SPH (Figure 4.5) as it offered a more realistic representation of the loading path created by the graded areal density. A 3D model allowed the structure of the Surfi-Sculpt® surface to be replicated more accurately. Figure 4.6 shows the shock profiles produced by the Lagrangian and SPH models. The SPH model demonstrates an obvious ramp towards the peak of the shock trace to more closely match those of the real Surfi-Sculpt® flyers than the Lagrangian model. However, when simulating the effect of the Surfi-Sculpt® flyers on the capsule system, a 2D Lagrangian model was more feasible

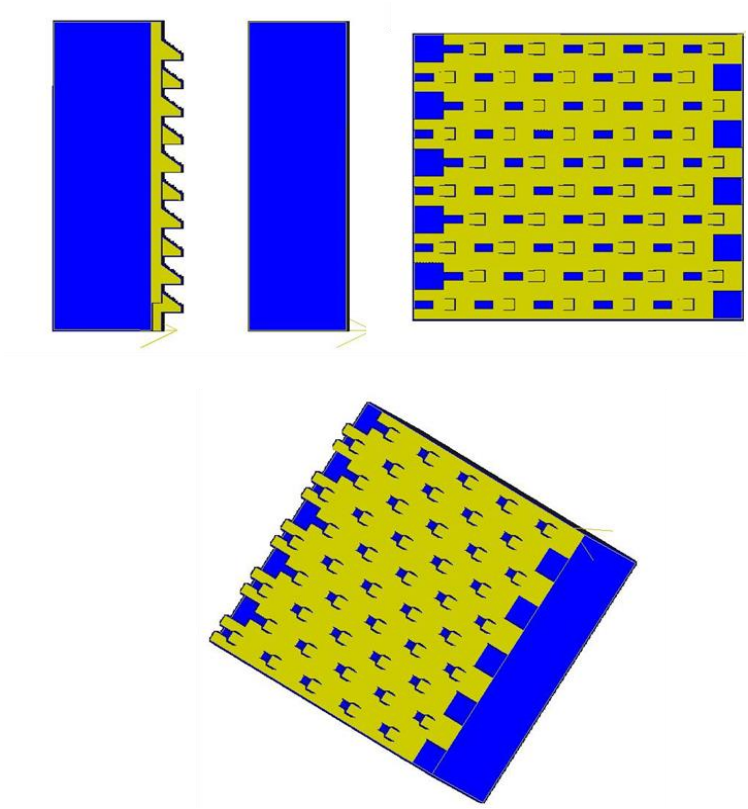

Figure 4.5 SPH model of the Surfi-Sculpt® flyer plate at different orientations.

since the capsule model was originally designed as a 2D Lagrangian model with axial symmetry and this greatly reduced the complexity and run-time of the model. With the appropriate erosion model – geometric strain – there was no issue of excessive cell deformation interrupting the simulation.

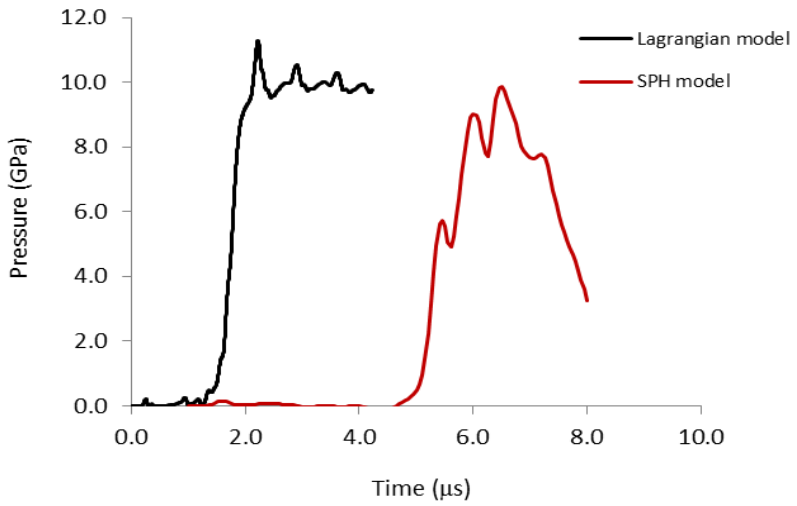

Figure 4.6 Shock profiles for the Surfi-Sculpt® flyer as produced by Lagrangian and SPH models. A more prominent ramp is seen with the SPH trace. The reason for the short duration of the SPH pulse was due to the location of the gauge which was very close to the front surface of the target buffer plate. The trace from the Lagrangian model showed a more prolonged plateau (up to ~ 10 μs) but was shortened here for clarity.

Since the purpose of the Surfi-Sculpt® flyers was to investigate the lower temperatures that would be associated with ramp loading, it was desired to predict the temperatures associated with certain shock pressures with the models. However, ANSYS® Autodyn is not designed to measure the time it takes for temperatures to reach equilibrium at a particular gauge point. In response to this, nickel temperature gauges were utilised to show real temperatures reached during validation experiments, and the peak temperatures were compared with those predicted by the models. These experiments were initially carried out using the set-up outlined by Rosenberg and Partom [105] as outlined in Chapter 3.

A number of shots were carried out with these gauges, including test shots in order to figure out the optimum target set-up to allow the temperature profiles to reach equilibrium. This is explained further in Appendix A. Once an appropriate backing thickness had been determined to prolong the gauge trace, the first shot was carried out

at a velocity of 205 m s^{-1}, the profile for which is shown in Figure 4.7. The temperature at the front gauge increased to 41.5 °C which equates to 314.61 K. The modelled shock profile, shown in Figure 4.8, predicted a peak temperature of 318 K giving the model an error of ± 1.1%. A higher velocity shot was also carried out at 625 m s^{-1} on a target representing the lids of the outer and inner Cu capsules. The temperature profile for this shot is shown in Figure 4.9. The peak temperature noted was 59.48 °C (332.63 K).

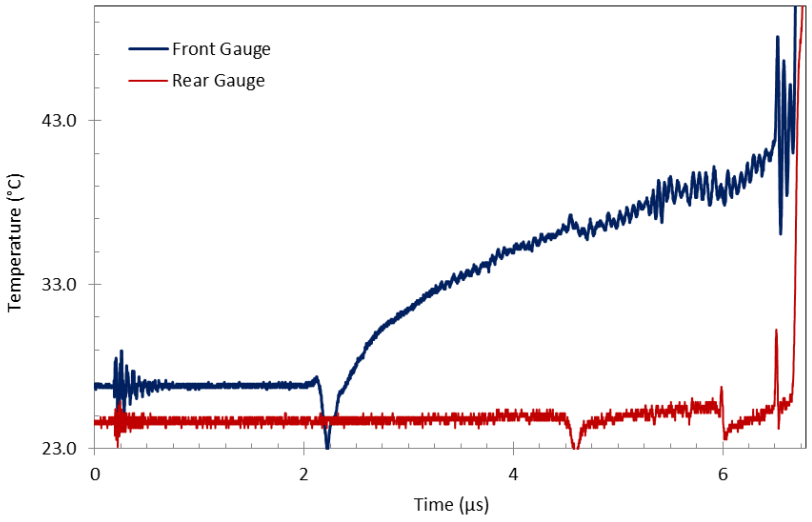

Figure 4.7 Temperature profile an impact velocity of 205 m s^{-1}. The front trace plateaus at 41.5 °C before gauge death.

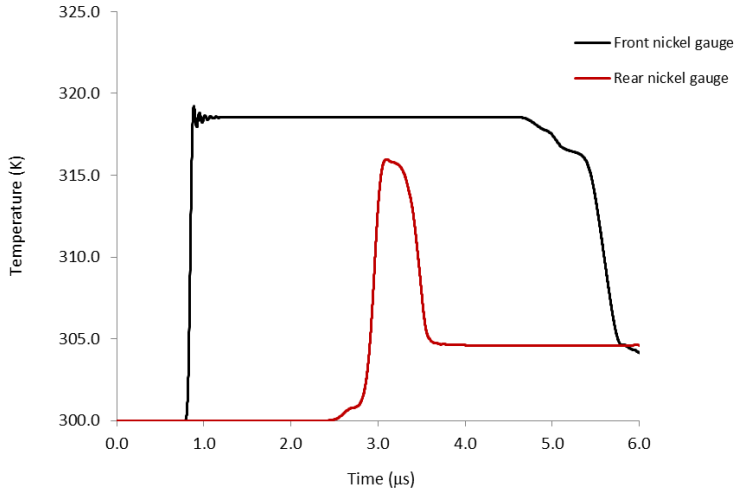

Figure 4.8 Modelled temperature profile for PMMA following an impact velocity of 205 m s^{-1}. The peak temperature measured at the front gauge was 318 K.

The modelled temperature profile for this experiment, shown in Figure 4.10, had a peak temperature of 337 K, making the error for this model ± 1.3%. A number of shock experiments were carried out with these experiments. An example of a low end shot with an impact velocity of 190 m s^{-1} for a nickel gauge is shown in Appendix A.

The disadvantage of the validation experiments is that the true temperature duration could not be accurately measured through use of nickel gauges. The reason for this was that targets would have to be sufficiently thick in order to allow time for the temperature to reach equilibrium in the material. However, peak temperatures could generally be determined once a plateau in the traces was noted and this temperature was then compared with the peak temperature in each model. However, during the shock experiments on the microbial samples, the cultures were not exposed to high residual temperatures in the capsule for long enough to affect viability. This will be discussed further in the Discussion chapter.

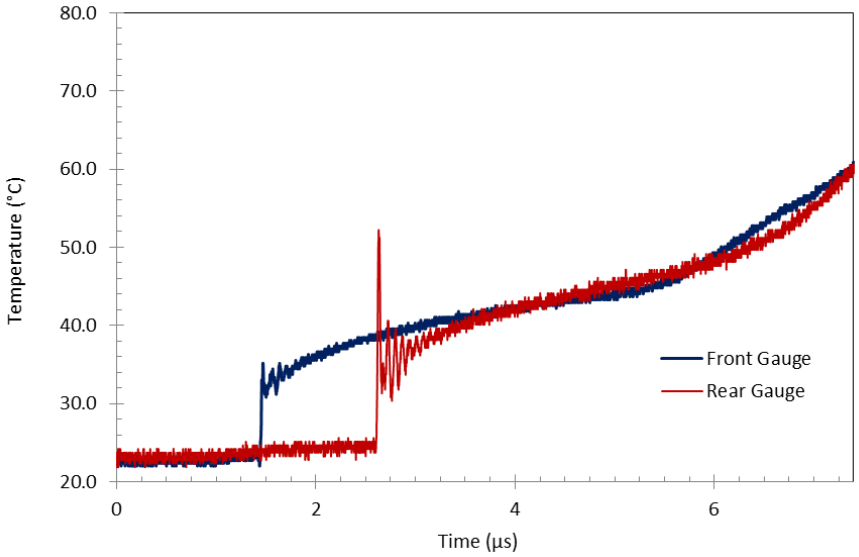

Figure 4.9 Measured temperature profile for Cu after an impact velocity of 625 m s^{-1}. The set-up of this experiment was meant to replicate the actual set-up of the capsule with both the outer and inner capsule lids. After 7.28 µs, both front and rear gauges failed, but the peak temperature measured for both gauges is 59.48 °C (332.63 K).

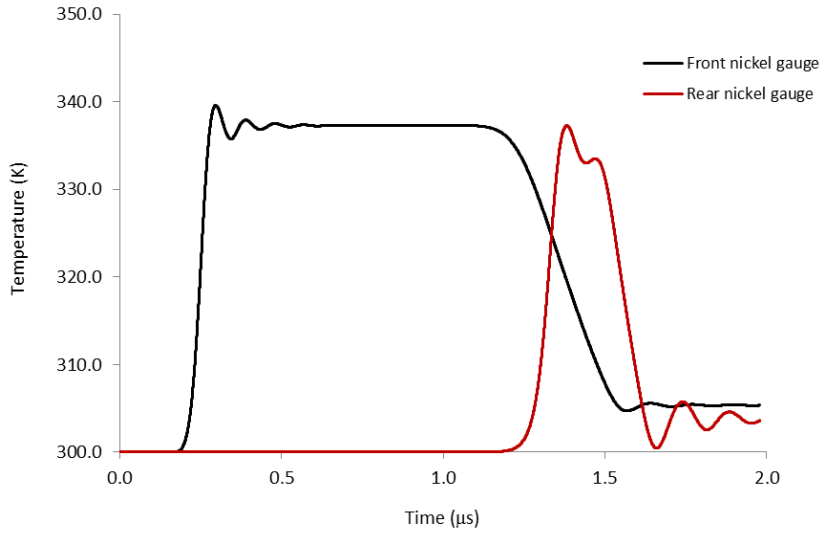

Figure 4.10 Modelled temperature profile for Cu after a velocity of 625 m s^{-1}. The peak temperature measured here is 337 K.

4.4.2 Heterodyne velocimetry

Heterodyne velocimetry, described in Chapter 3, was used to measure the free surface velocity of the rear of the inner capsule. The results were matched with the modelled data and found to be in good agreement with an error of 2.3%. The free surface velocity profile is presented in Figure 4.11. Since the free surface velocity values were in good agreement following the impact velocity of 376 m s^{-1}, the modelled pressures were also deemed to be reliable.

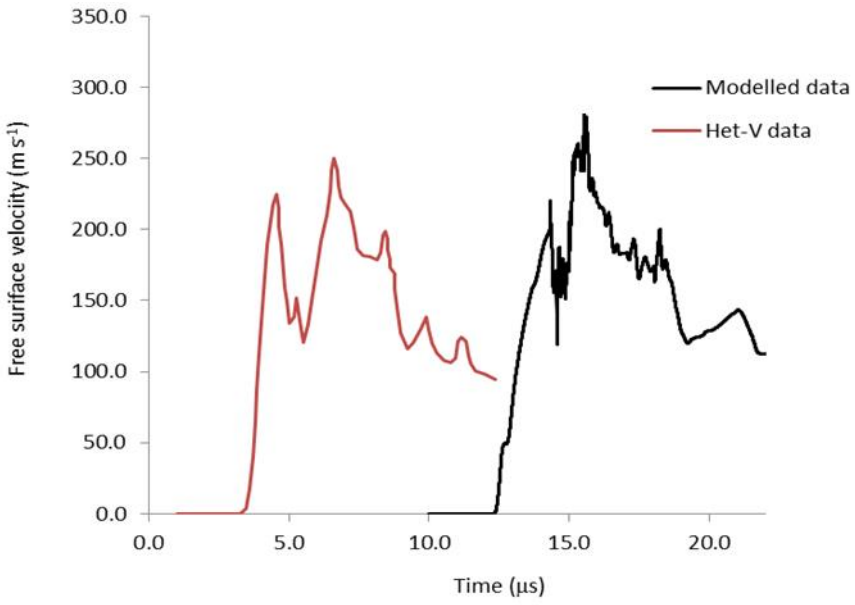

Figure 4.11 Free surface velocity profiles for the inner Al capsule as measured by Het-V and the hydrocode model. It was previously determined in Chapter 3 that the error in the models with respect to the Het-V trace was 2.3%. Profiles are offset for clarity.

4.4.3 Comparison of hydrocode models with results in the literature

In addition to the validation of the temperatures and pressures predicted by the models, the materials used in the models were compared with data in the literature. Taking the study by Nagayama *et al*. on the shock Hugoniot of water, the models used in that study were replicated here, using the materials pre-selected for this project. At 478 m s^{-1}, the shock pressure for water was found to be 0.6 GPa according to the simulation. This was in keeping with the data by Nagayama *et al.* [90] which recorded a pressure of 0.63 GPa for water at this velocity. This modelled shock profile is shown in Figure 4.12.

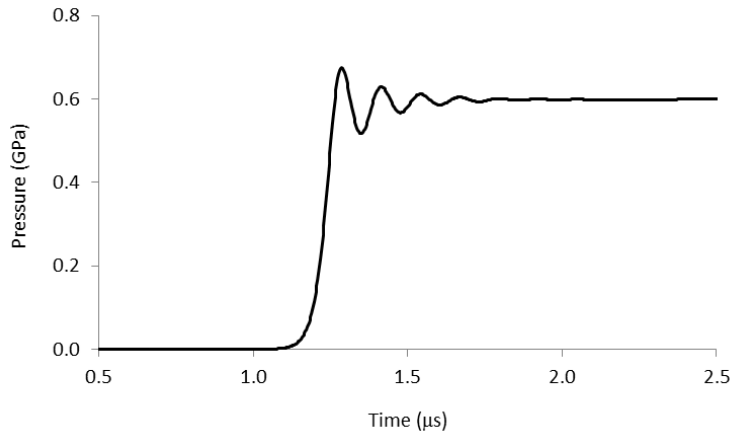

Figure 4.12 At 478 m s^{-1}, the shock pressure for water was found to be 0.6 GPa according to the simulation. This was in keeping with the data by Nagayama *et al.* [89] which recorded a pressure of 0.63 GPa.

4.4.4 Comparison of water and phosphate buffered saline equations-of-state

The EOS of water as determined by Nagayama *et al*. [90] was given previously by Equation 2.5. In order to validate the use of water as the test sample in place of PBS - PBS being used as the buffer solution for all microbial shock experiments as well as the control – the Hugoniot EOS for PBS (Equation 4.7) and deionised water (Equation 4.8)

was determined as part of this work through the plate-impact technique (Figure 4.13). The results were plotted in the U_s-u_p plane and both PBS and deionised water were found to be in good agreement with the data by Nagayama *et al*. This further justified the use of water as part of the numerical models.

$$U_s = 1.34 + 2.76\, u_p \tag{4.7}$$

$$U_s = 1.45 + 2.45\, u_p \tag{4.8}$$

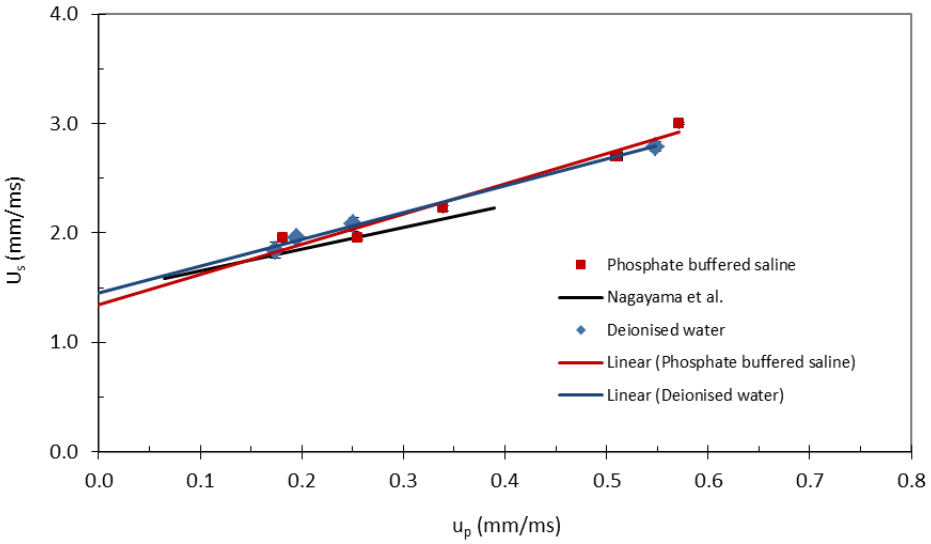

Figure 4.13 Shock Hugoniot of deionised water and PBS plotted in the U_s-u_p plane. These results were compared to the EOS found by Nagayama *et al*. [89] and were found to be in generally good agreement with each other.

4.5 Summary

The hydrocode models used in this thesis were used to confirm the suitability of the capsule design by confirming that rarefaction waves did not interfere with the microbial sample in the Teflon® liner. It also revealed the shape of the wave front and the duration of the pulse throughout the sample. Additionally, it aided the prediction of the maximum pressure the outer capsule could withstand while safely retrieving the sample from the inner capsule. The models also proved useful for predicting maximum temperatures inside the Teflon® liner. These models were validated by a number of methods, including nickel temperature gauges, Het-V, comparison of these models with data in the literature and determining the EOS of the PBS solution used for the microbial shock experiments. This reduced the errors that would be introduced to the results as well as the empirical results described in the following chapters.

5 Quasi-one-dimensional dynamic loading of *Escherichia coli* NCTC 10538

5.1 Introduction

The growth of the bacterium *E. coli* NCTC 10538 was assessed after carrying out four different iterations of shock loading experiments including:

- standard quasi-one-dimensional loading
- ramp loading to influence change in temperature
- shock loading of different concentrations of *E. coli*
- loading with extended shock pulse durations.

The results presented in this chapter show broad trends of decreasing survivability with increasing pressure, but this is influenced by factors such as the concentration of the test sample and the duration of the shock pulse. Each of these experiments was carried out on the aforementioned 50 mm bore single stage gas gun at Cranfield University and follows the standard set-up as outlined in Chapter 3 (Figure 3.2). In each case, the capsule recovery system, described in Chapter 3, section 3.4, was used with 6 µl of prepared *E. coli* inserted into the Teflon® liner. This ensured a quasi-one-dimensional shock wave for as long as possible through each target sample.

5.2 Standard quasi-one-dimensional loading of *E. coli*

For the standard quasi-1D experiments on *E. coli* NCTC 10538, 5-mm thick Al flyer plates were used. Peak pressures reached by the bacterial samples during the shock experiments were measured using Lagrangian models employed via ANSYS Autodyn® (discussed in detail in Chapter 4). As depicted in Figure 5.1, the ANSYS Autodyn® model employed to accompany these experiments consisted of four gauge points within

the fluid of the Teflon® liner. The average pressure across these four gauges was calculated for each experiment. These models were validated by the Heterodyne velocimetry experiments as described in Chapter 4.

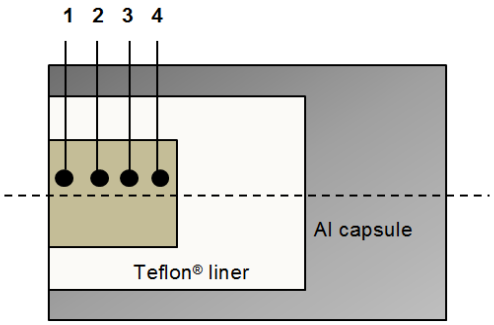

Figure 5.1 Teflon® liner filled with bacterial broth. Dashed line depicts the axial symmetry used in the hydrocode models. Gauges in the models are labelled 1-4.

After shock loading, sample analysis followed a number of key stages:

1) The capsule was opened carefully in a controlled environment with note taken to ensure that confinement had not been breached (i.e. that no fluid had escaped from the Teflon® liner).
2) Assuming confinement had not been breached, a pipette was employed to extract the bacterial broth.
3) The bacterial broth was plated on an agar nutrient medium and incubated for 18 hours.
4) The process was repeated for the control samples which consisted of unshocked *E. coli* from the original stock solution.
5) After incubation, the *E. coli* colonies were counted, and growth rates calculated by measuring colony forming units (CFU) per millilitre to according to Equation 3.5. Examples of *E. coli* colony growth on agar plates are shown in Figure 5.2.

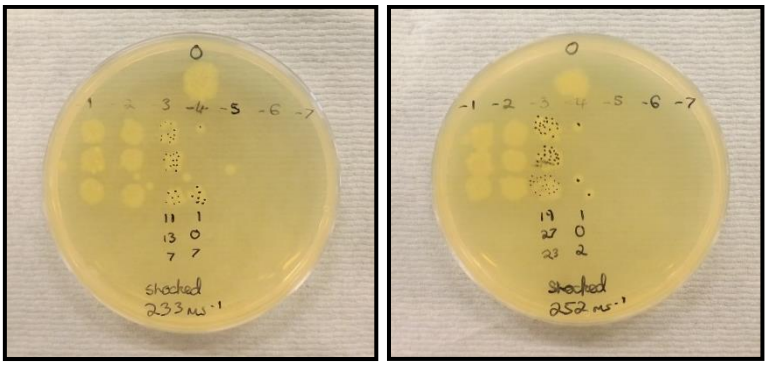

Figure 5.2 Example of the agar plating technique for microbial samples shock loaded at 233 and 252 m s^{-1}, respectively.

Pressures in this investigation ranged from 0.55 to 3.6 GPa, with an apparent associated exponential decline in survival rates from 6% to 0.01%. The experimental results are listed in Table 5.1. The lowest achievable pressure it proved possible to reliably reach using the plate impact technique was 0.55 GPa, as going below this pressure made experiments unrepeatable. In turn, 3.6 GPa was the highest pressure that could be reached while maintaining the structural integrity of the capsule system. The experiments plotted in Figure 5.3 were repeated three times to ensure reliability in the results.

Table 5.1 Growth of *E. coli* following shock loading experiments using standard capsule technique with planar Al flyers. *These results were appeared distorted due to unusually high survival rates in comparison to other experiments at similar pressures. This is likely due to effects of high concentration, which will be discussed in section 5.4.

Velocity (m s^{-1})	Pressure (GPa)	Growth rate (%)
152*	0.55 (+23.0/-14.0%)	6.00
188	0.8 (+18.5/-17.0%)	0.96 (+23.2/-15.8%)
234	1.2 (+11.3/-9.0%)	0.81(+14.1/-13.2%)
235*	1.2 (+10.7/-9.1%)	15.50
247	1.3 (±9.6%)	0.10 (+10.6/-13.1%)
252*	1.4 (+8.3/-8.1%)	10.00
316	3.6 (±3.2%)	0.01 (+6.4/-8.1%)

There was some variation of the data points at lower pressures but this decreased as loading pressure was increased. The gap in errors also closed as pressure increased. While large errors are still present for the lower pressure experiments, the data points presented in Figure 5.3 are a good indication of a general trend of the effects of quasi-1D shock pressure on growth and survivability of *E. coli*. This data is in keeping with results of other studies that observed exponential decreases in survival with increasing shock pressure.

There were also a number of experiments that did not yield expected results as they did not fit with the majority of data points. These data points were considered anomalies, although they are highlighted in Table 5.1 with an asterisk to provide the reader with an insight into the challenges associated with these experiments. Overall, the growth rate errors appear larger towards the lower end of the pressure scale, reflecting the lack of

repeatability of some of these experiments at these lower velocities and pressures – with values of at most ±2.1% for pressures between 1.3-3.6 GPa as opposed to up-to ±5.8% for lower pressures. The occurrence of large errors and lack of repeatability at this lower pressure end suggested that concentration may be an important element to consider in these experiments. This will be further explored and explained in section 5.5 and Chapter 8.

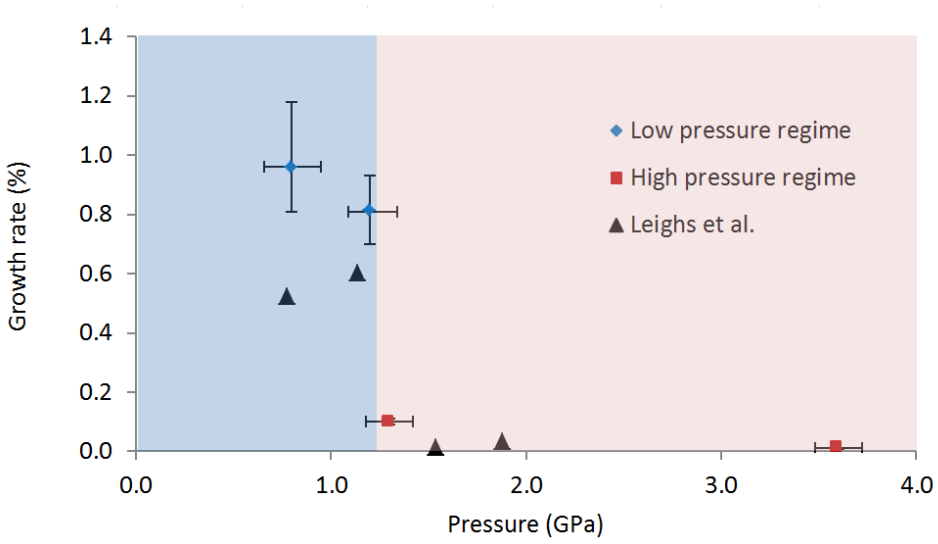

Figure 5.3 Plot of percentage growth of *E. coli* colonies following 1D shock loading experiments in this thesis. For comparison, results from the study by Leighs *et al.* [106] are also plotted.

As presented in Figure 5.3, there was a sudden drop in survival between 1.2 and 1.3 GPa. The reasoning behind this was deemed to be a result of the high concentration of the sample, which led to the following set of experiments described in section 5.5. The high concentrations could have led to overcrowding which may have offered protection to some cells and allowed for higher rates of survival. The potential mechanisms to describe these results will be discussed in Chapter 8.

5.3 Temperature control via ramp loading

E. coli were later examined under higher pressure conditions well into the GPa range (0.7–10.0 GPa). As a result, temperature in the target sample was increased. According to the data outlined in Table 5.2, again, the growth of *E. coli* colonies appeared to decay exponentially under increasing shock pressure. This was seen after use of both planar and Surfi-Sculpt® flyer plates discussed in Chapter 3. In particular, there was a noticeable difference between colony growth rates at lower pressures. This relationship is shown in more detail in Figure 5.4, with the nominally linear relationship between the logarithm of the growth rate and impact pressure demonstrating the aforementioned exponential relationship. Growth rates at the lowest pressure (0.7 GPa) were 2% for the planar flyer and 3% for the Surfi-Sculpt®, each with a temperature difference of 4 K. At pressures reaching up to 10 GPa, a survival rate of 0.09% was seen with each flyer type. There was less variation in temperature with increasing pressure for both flyer plates. In order to produce higher shock pressures, Al capsules were replaced with Cu capsules for use during higher velocity impacts. Essentially the higher impedance Cu led to more energy being coupled into the target for otherwise identical impact conditions, leading to higher pressures. Further, the ductile nature of the Cu allowed for recovery at higher pressures than was possible with the Al capsules. In particular, the outer Al capsule failed at 4.5 GPa with no sample was retrieved from the Teflon® liner; Cu flyers were then used for obtaining pressures above 4.5 up to 10 GPa.

Table 5.2 Growth rates of bacterial colonies post shock loading with both planar and Surfi-Sculpt® flyers. *The Al capsule failed at this pressure, preventing safe retrieval of the bacterial solution.

Flyer type	Capsule material	Flyer velocity (m s^{-1})	Average pressure (GPa)	Average temperature (41°C)	Growth rate (%)
Planar	Al	107 (±3%)	0.7 (±7%)	315 (+0.1/-0.2%)	2 (+25/-17.2%)
Surfi-Sculpt				311 (±0.2%)	3 (+24.5/-21.3%)
Planar	Al	173 (±1.2%)	1.2 (+4/-5%)	320 (±0.2%)	1 (+19.2/-21.9%)
Surfi-Sculpt				315 (+0.4/-0.3%)	0.9 (+20.1/18.7%)
Planar	Al	316 (±1%)	3.6 (±6%)	333 (±0.6%)	0.01 (+10.7/-12%)
Surfi-Sculpt				330 (+0.9/-0.5%)	0.1 (+15.2/-10.8%)
Planar	Al*	385 (±4.6%)	4.5 (+4/-9%)	340 (±1%)	-
Surfi-Sculpt				334 (+1.2/-1.1%)	-
Planar	Cu	175 (±1.4%)	6.6 (+5/-12%)	335 (+0.3/-0.5%)	0.06 (+9.6/-6.8%)
Surfi-Sculpt				332 (±0.6%)	0.1 (±4)
Planar	Cu	268 (±3.2%)	10.0 (+15/-16%)	341 (+1/-2%)	0.09 (+1.7/-0.5%)
Surfi-Sculpt				341 (+1.4/-1.2%)	0.09 (+2.6/-3.5%)

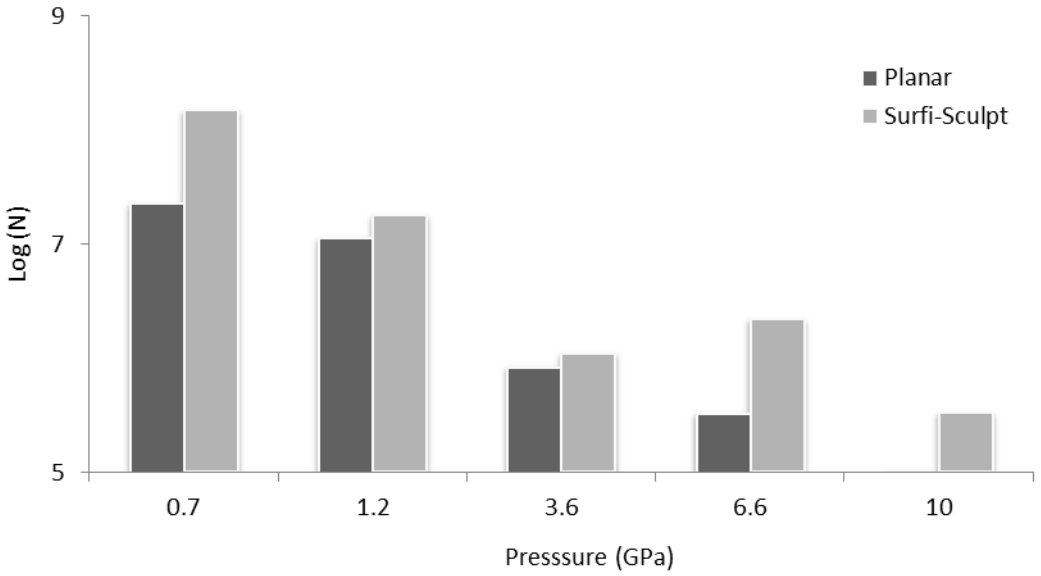

Figure 5.4 Log plot of the colony growth counts *vs* pressure. The differences in growth rates between those impacted by the planar and Surfi-Sculpt® flyers is evident (where peak temperatures were lower), although both sets of data show an approximately exponential decline with increasing pressure.

The use of Surfi-Sculpt® flyers created ramped waves through the target, which were more pronounced at lower impact velocities. As expected, the waves produced by Surfi-Sculpt® flyers at higher pressures gradually produced traces which were more 1D in nature than at lower pressures (due to faster shock rise times); this is illustrated in Figure 5.5. which compares modelled impact pressures and peak temperatures (based on the data presented in Table 5.2). As a result, the highest-pressure experiment at 10 GPa yielded the same temperature for both flyer types (341 K). However, there were noticeable changes in temperature at lower pressures, e.g. at 0.7 GPa there was a temperature difference of 4 K [Figure 5.5 (a) and Figure 5.5 (b)]. Peak pressures were found to be the same with a maximum error of 7% at the lowest pressure (0.7 GPa) and a maximum of 16% for the highest pressure reached (10 GPa).

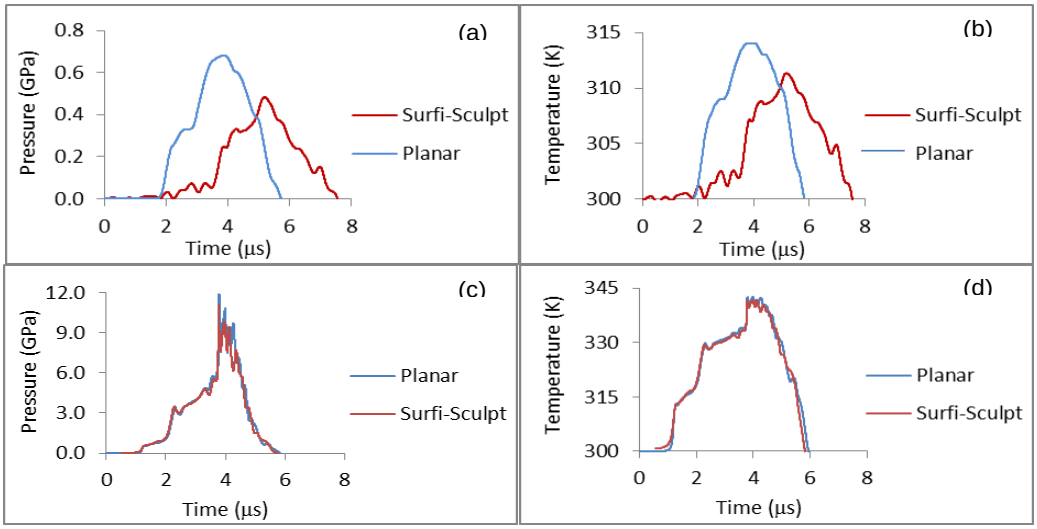

Figure 5.5 Sample pressure and temperature traces from within the Teflon liner using planar and Surfi-Sculpt® flyers at two different impact velocities. Pressure profile from Al capsule at 107 m s^{-1} (a); temperature profile from Al capsule at 107 m s^{-1} (b); pressure profile from Cu capsule at 268 m s^{-1} (c); temperature profile from Cu capsule at 268 m s^{-1} (d).

In each case in Figure 5.5, even at the lowest impact velocity of 107 m s^{-1}, ramped traces are visible for the Surfi-Sculpt® flyers. Although a modest ramp is also seen for the planar flyer at lower velocity impacts, there is a distinct difference between the overall rise times for both flyer types at the lower velocities. At the lowest impact velocity, the planar pulse had a duration of ~ 4 µs, while the Surfi-Sculpt® flyer produced a pulse lasting ~ 5.5 µs. At the 268 ms^{-1} impact velocity, the pulse length for the Surfi-Sculpt® and planar flyers was ~ 5 µs. The differences in temperature caused by each flyer type became smaller as the pressure increased for each experiment due to the aforementioned associated faster rise times.

The dynamic loading profiles from the Surfi-Sculpt® and planar flyers in each experiment described here resulted in different loading paths, but with similar (stress) pressure plateaus in each case. With the use of the Surfi-Sculpt® flyers, there was a greater time delay for the peak pressure to be achieved as the ramped waves traversed the target more slowly and this facilitated temperature control throughout the loading process. The lower velocity impacts for the Surfi-Sculpt® flyers have resulted in more exaggerated ramped traces as expected. In addition, at lower velocities the traces for the planar flyers indicated a slight ramped wave occurring (due to the complexity of the target capsule construction); although in these cases the associated temperatures inside the capsule were consistently higher.

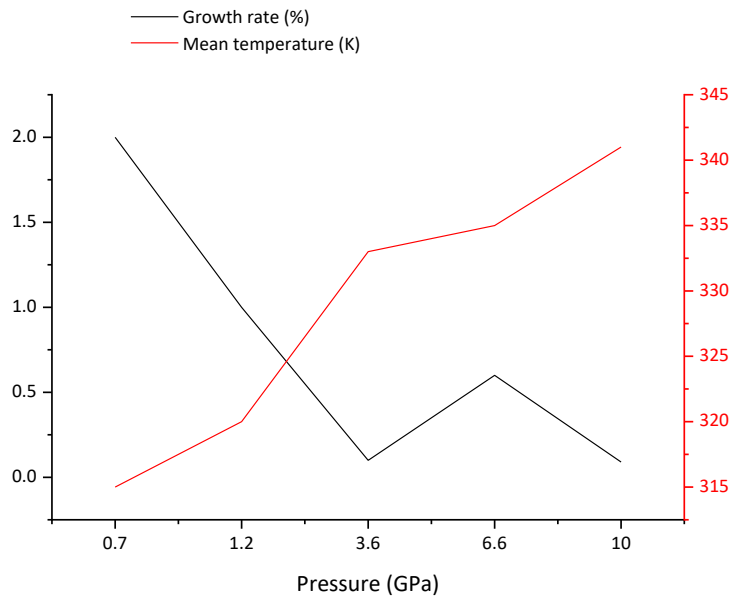

Figure 5.6 Temperature and growth rate plot *vs* pressure. There is a broadly linear decline in growth as pressure increases. Conversely, there is a near-linear increase in temperature with the use of the planar Stainless steel flyers.

The increase in temperature and decrease in growth rates with increasing pressure is presented in Figure 5.6. The survival of *E. coli* up to at least 10 GPa and 341 K in these experiments suggests that the quasi-one-dimensional shock waves produced during

these experiments are likely to invoke a protective response in the bacterium that may exist on a genetic level. This may result in a protective coating for the cell, or a temporary suspension of viability where cell activity will only be stimulated again in the presence of an appropriate nutrient medium. The relatively simplified loading path followed in this set of experiments by impact using the planar flyers generally resulted in lower growth rates for the *E. coli* than their Surfi-Sculpt® counterparts. Given the relative decrease in growth rates for the planar flyers, it may be inferred that elevated temperatures reached as a result of the planar shock wave affect the mechanisms governing cell growth. While these temperature changes were relatively small, the associated changes in growth rates seen between the planar and Surfi-Sculpt® flyers can clearly be seen in Figures 5.4 and 5.6. The timescales during which the bacteria were subjected to the shock pulse were on the microsecond scale, implying that certain internal mechanisms that control the cell's shock response may be triggered after < 1 ms. These mechanisms will be explored in more detail in Chapter 8. As an aside, it is also worth noting that these experiments confirm that the use of Surfi-Sculpt®, or similar flyers, have the potential to be a useful tool to precisely control loading temperatures under shock.

5.4 Effects of varied sample concentration on *E. coli* growth

Samples of the bacteria were also tested after being diluted to two different concentrations in order to examine any potential changes in growth rates of the colonies. This was carried out by diluting samples in the same manner as the serial dilutions were carried out post-shock loading (described in Chapter 3). The dilute concentrations tested in these cases were x 10^{-3} and x 10^{-5} of the original stock solution (3.1 x 10^{11} cells/ml). However, dilutions of up to 10^{-5} were found to yield little or no growth; consequently, only the 10^{-3} dilutions were considered. Shock pressures for these experiments ranged between 0.7 and 1.4 GPa, as outlined in Table 5.3. As with the previous sets of

experiments, colony growth from diluted samples was determined to generally decrease exponentially; this is shown more clearly in Figures 5.7 and 5.8. Since colony growth at 1.2 GPa was found to be inordinately higher than at 1.4 GPa, this was considered to be an anomalous point in the data.

The dilutions were found to have a strong effect on growth in the lower pressure range (0.7– 0.9 GPa). Excluding the data point at 1.2 GPa, the plotted data in Figure 5.7 are in general agreement with the previous sets of experiments that measured growth following quasi-1D shock loading (see Figures 5.3 and 5.6); there is an overall exponential decline in growth rates with increasing shock pressure.

Table 5.3 Growth rates of diluted and undiluted bacterial colonies post shock loading. *This data point is an example of an experimental result that could not be repeated and, hence, was excluded from the final cumulated data.

Velocity (m s^{-1})	Pressure (GPa)	Growth rate (%)	
		Diluted	Undiluted
170.00 (±1.6%)	0.7 (+1.9/-0.6%)	0.81 (+22.5/-21.2%)	6.00 (+25.7/-1%)
201.25 (±4%)	0.9 (+3/-2%)	0.53 (+16.6/-2.1%)	0.90 (+19.2/-16.4%)
235.00* (±2.7%)	1.2 (+1.3/-3%)	0.90 (+15.5/-17.2%)	0.10 (+20.6/-16.1%)
251.00 (±4.6%)	1.4 (+0.8/-0.2%)	0.06 (+6.3/-9.2%)	0.08 (+10.6/-8.3%)

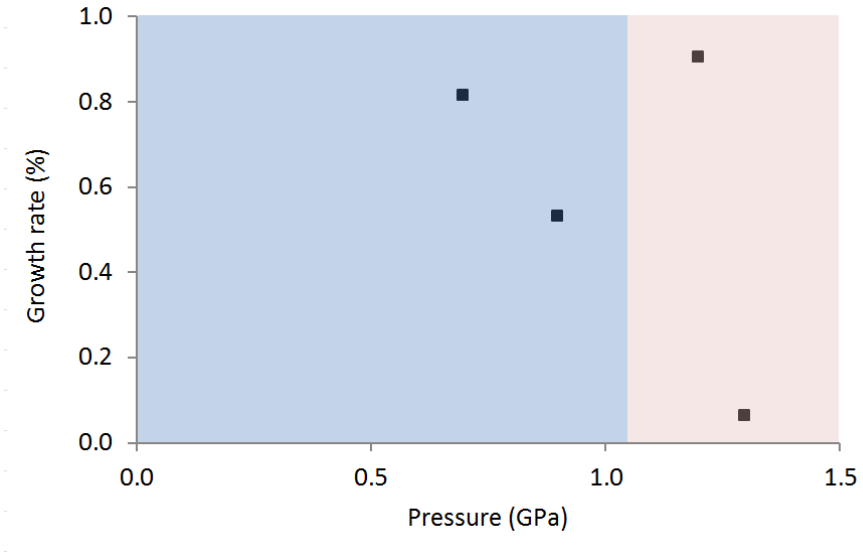

Figure 5.7 Growth rates of dilute *E. coli* samples over a pressure range of 0.7–1.4 GPa. While the growth rate of 0.9% at 1.2 GPa was conflicting with the other results, the remaining growth rates imply decline, with a rather sharp decline in growth at 1.4 GPa. The interface between the blue and pink shaded regions of the graph highlight a potential threshold where dilute samples of *E. coli* survival drops. In the pink higher pressure region, results begin to match those of the undiluted samples, according to Table 5.3.

According to these results, there may be a threshold between 0.9–1.4 GPa in which concentration no longer has an effect on growth or survival. This may explain some unusually high results noted in section 5.2 in the lower pressure regime, particularly in the MPa range. Beyond this threshold, growth from stock solutions of lower concentrations is more similar to those from higher concentrations post-shock. The contrast between diluted and undiluted samples is illustrated more clearly in Figure 5.8. The errors in the diluted samples are within the confines of those recorded in Table 5.3, excluding the anomalous data point at 1.2 GPa. The results here show a general trend that demonstrates the importance of concentration of the bacterial samples at lower pressures. The reason for this trend of lower growth at lower concentrations was deemed to be an effect of over-crowding and potential 'cushioning' of surviving cells by surrounding cells in the Teflon® capsule. This will be further discussed in Chapter 8.

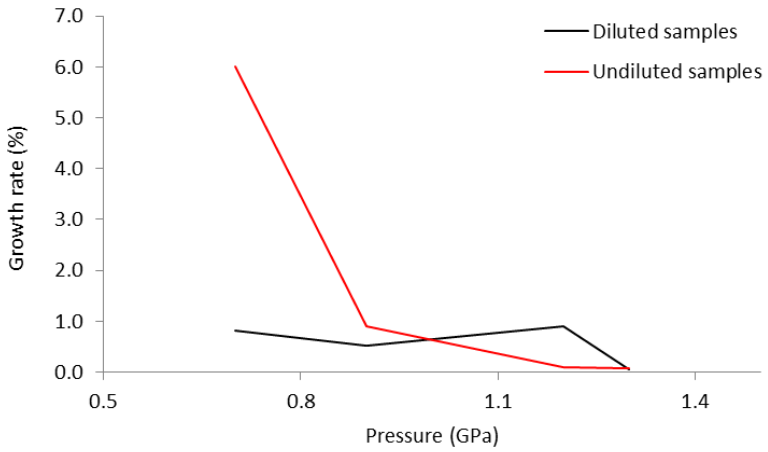

Figure 5.8 Growth rates of diluted *E. coli* samples *vs* undiluted *E. coli* samples. Results from both sets of experiments begin to converge as pressure increases.

5.5 Control of pulse duration on *E. coli* with 5 mm and 20 mm flyers

Since timescale is already known to play an important role in the pressure loading of bacteria, particularly in comparing static and dynamic pressure loading, it was deemed important to explore the outcomes of longer shock pulses through the bacterial sample. This was carried out using thicker flyer plates; the standard shock experiments were carried out using 5 mm flyers and the extended pulse experiments used 15 and 20 mm flyers. Modelled pressure profiles for these two thicknesses, presented in Figure 5.9, show very little variance in pulse duration

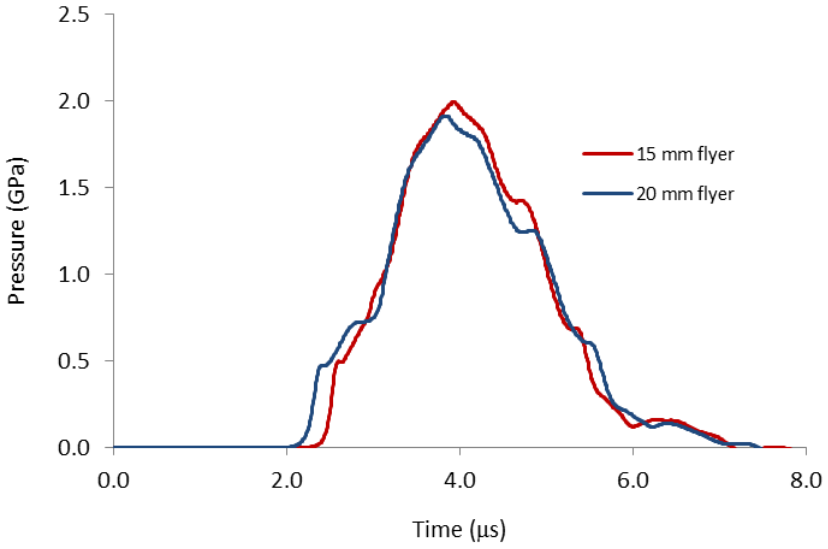

Figure 5.9 Modelled pressure profiles for 15 mm and 20 mm flyer plates at the highest impact velocity of 267 m s^{-1}, according to Table 5.4.

The conditions of these experiments for the 20 mm flyers are outlined in Table 5.4. The shock pressures used ranged from 0.75-1.9 GPa and yielded growth rates of 2.9% (at 1.3 GPa) to 1.52% (at 1.9 GPa) – much higher than the growth seen for the 5 mm flyer shots, shown in Table 5.1. The shock pulse duration for each experiment was determined through numerical modelling and at the highest impact velocity, 267 m s^{-1}, a pulse length of 5.22 µs was seen for the longest pulse trace with the 20 mm flyer; in comparison, the longest pulse for the 5 mm flyer at this velocity was 3.29 µs. The difference in pulse length has led to a significant difference in colony growth and this can be seen in Figure 5.10.

Table 5.4 Growth rates of bacterial colonies post shock loading with 20mm flyers. *The Al capsule failed at this pressure, preventing safe retrieval of the bacterial solution.

Velocity (m s^{-1})	Pressure (GPa)	Colony forming units (CFU/ml)	Growth rate (%)
176 (± 2.6%)	0.75 (+21.3/-17.1%)	5.6 x 10^6	2.50 (+21.3/25.4%)
240 (± 2.2%)	1.3 (±9.6%)	6.4 x 10^6	2.90 (+17.5/-20.1%)
253 (± 2.8%)	1.4 (+8.3/-8.1%)	4.7 x 10^6	2.10 (+18.3/-19.8%)
267 (± 3%)	1.9 (+6.2/-8.8%)	3.3 x 10^6	1.52 (+14.3/-12.5%)

The trend of decreasing colony growth with increasing pressure shown in Figure 5.10 is true for both flyer types, but 20 mm flyers resulted in significantly higher growth rates. The log plot of the colony forming units for the 20 mm flyer is displayed in Figure 5.11. The reasoning for why this has occurred may be due to the fact that a longer pulse length led to more cells being exposed to a shock pulse at a given time. Energy being dispersed across a high number of cells – especially in a concentrated sample – would allow an individual cell to overcome the overall shock, leading to higher survival and growth rates.

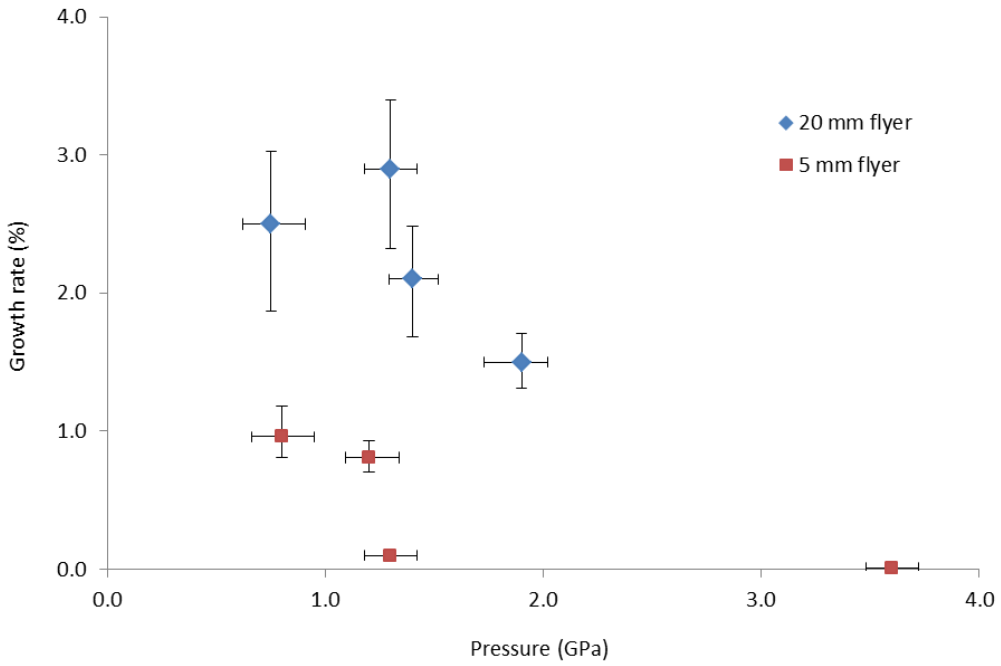

Figure 5.10 Growth rates of diluted *E. coli* samples *vs* undiluted *E. coli* samples. Results from both sets of experiments begin to converge as pressure increases.

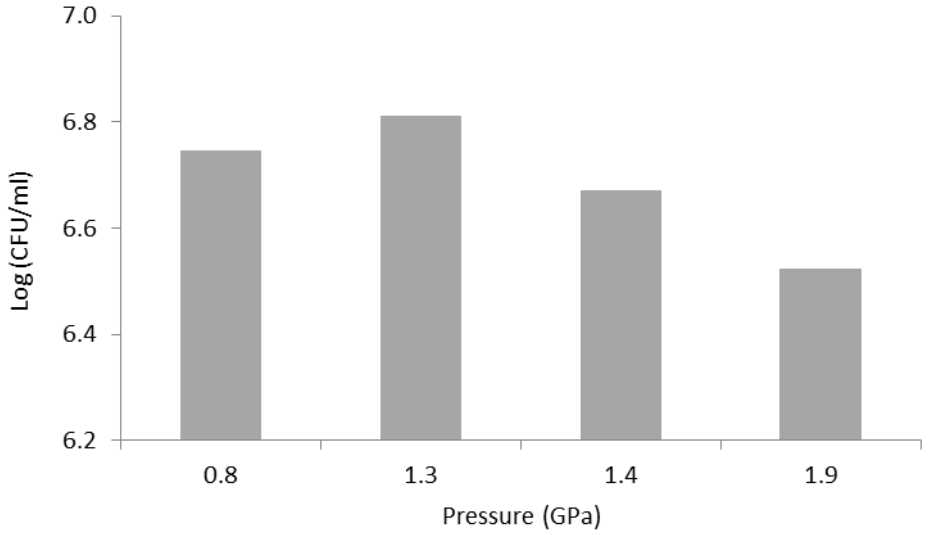

Figure 5.11 Log plot of colony forming units of *E. coli* post shock loading with a 20 mm flyer plate.

5.6 Summary

In each set of experiments presented in this chapter, there is a broadly exponential decrease in the growth of *E. coli* NCTC 10538 colonies with increasing shock pressure. Each experiment has also produced distinct results including:

- Within the pressure range 0.8-3.6 GPa, standard quasi-one-dimensional shock loading resulted in *E. coli* colony growth rates of 0.96-0.01%, respectively. There appeared to be a threshold between pressures 1.2 and 1.3 GPa across which growth rates drop dramatically.
- *E. coli* demonstrate sensitivity to minor temperature changes during shock experiments. There may be a threshold within the temperature range explored here (311 to 341 K) that has a notable effect on survival. The use of Surfi-Sculpt® flyers has also offered an alternative type of loading path to reach certain pressures – e.g. while very precisely controlling sample temperatures. The use of planar flyers ensured a mostly 1D shock wave front, while the Surfi-Sculpt® flyers created a ramped front which may be crucial for the conservation of the outer cell structure during pressure loading.
- The effects of a longer shock pulse duration on *E. coli* were much greater colony growth rates than those seen for the standard quasi-one-dimensional shots; however, growth rates decreased in a trend to what was seen in the aforementioned experiments.
- There is a strong indication that high concentrations of microbial samples encourage higher survival at low pressures, potentially by offering protection or inducing a ‘cushioning’ effect on cells within the centre of a cluster. This explains the higher growth rates noted by shock loading more dilute samples of cells.

The results indicate that quasi-1D shock waves may affect both internal and external mechanisms that govern survival and may influence the ‘cushioning’ effect. While the

mechanisms for this phenomenon and general survival under pressure have not yet been elucidated, potential models to explain this behaviour will be explored in Chapter 8.

6 Quasi-one-dimensional dynamic loading of Saccharomyces cerevisiae ATCC 18824

6.1 Introduction

The second organism to be analysed under hydrodynamic pressure conditions was *Saccharomyces cerevisiae* ATCC 18824 (Figure 6.1); a eukaryotic unicellular organism. By definition, it has a more complex structure than a prokaryote, but with a less complex outer coating; it lacks a cell wall and the polymer peptidoglycan (discussed in Chapter 2) are present in bacterial cells such as *E. coli*. It is postulated that this could likely influence a different mechanical response in *S. cerevisiae* to shock, since it contains only a cell membrane. In order to evaluate how *S. cerevisiae* responds to some of the shock loading conditions to which *E. coli* was subjected in the previous chapter, three sets of experiments were carried out on this eukaryotic microorganism. These were standard plate-impact experiments, conducted with the aim of assessing the effects of changes in sample concentration on shock response and examining the effects of shock pulse duration on colony growth.

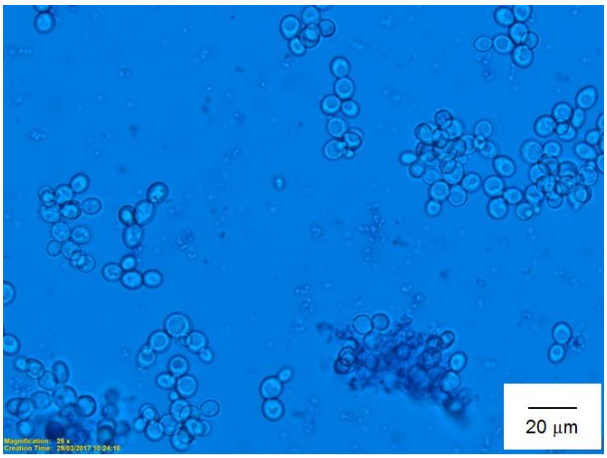

Figure 6.1 *S. cerevisiae* control sample. Individual cells of this organism tend to cluster together, potentially affecting the way in which these cells respond to shock pressures.

6.2 Standard quasi-one-dimensional loading of *S. cerevisiae*

Quasi-planar impacts were carried out on *S. cerevisiae* using the plate-impact technique and the capsule system described in Chapter 3. Pressures for this set of experiments ranged from 0.52-1.78 GPa with impact velocities between 150 and 287 m s^{-1}. The impact velocities for each experiment show steadily decreasing errors with increasing pressure, as shown in Table 6.1. The reason for this was that the shots on the light gas gun were more repeatable at higher pressures due to the use of a higher driving gas pressure and higher resulting velocities. Errors in pressure also decreased with increasing pressure since there was more agreement between the gauge points in the numerical models as the shock wave travelled faster and with more one-dimensionality across the Teflon® liner. An example of modelled shock profiles for each gauge point in a high pressure shot is shown in Figure 6.2.

Table 6.1 Growth of *S. cerevisiae* following shock loading experiments using standard capsule technique with planar Al flyers.

Velocity (m s^{-1})	Pressure (GPa)	Colony forming units (CFU/ml)	Growth (%)
150.00 (±4.1%)	0.52 (+23.1/-25%)	7.8 x 10^6	3.50 (+20.0/-16.4%)
175.12 (± 2.4%)	0.80 (+18.8/-17.5%)	5.8 x 10^6	2.60 (+21.1/-22.0%)
227.58 (± 1.8%)	1.18 (+11/-12.7%)	2.0 x 10^6	0.81 (+9.7/-14.2%)
236.18 (± 1.8%)	1.58 (+6.3/-5.7%)	1.8 x 10^6	0.90 (+9.2/-11.6%)
287.00 (± 1.2%)	1.78 (+7.8/-7.3%)	5.6 x 10^5	0.25 (+9.1/-8.2%)

Colony growth for the *S. cerevisiae* was particularly prolific following the lower pressure shock experiments. It was noted that for the lowest pressure shot on *S. cerevisiae* (0.52 GPa), for example, that colony growth reached up to 3.5%; a trend similar to what was seen previously with the *E. coli* experiments. The highest pressure

reached with the most repeatable results was 1.78 GPa with a colony growth rate of 0.25%. Interestingly, Figure 6.3 shows a largely exponential decline in *S. cerevisiae* colony growth rates; the general pattern shown here is a decrease in colony growth with increasing pressure. There is an exception for the shot at 236.18 m s^{-1} which has a slightly higher growth rate of 0.9% than the slower 227.58 m s^{-1} shot with 0.81% survival. However, the error bars for these results show slight overlap (see the inset in Figure 6.3).

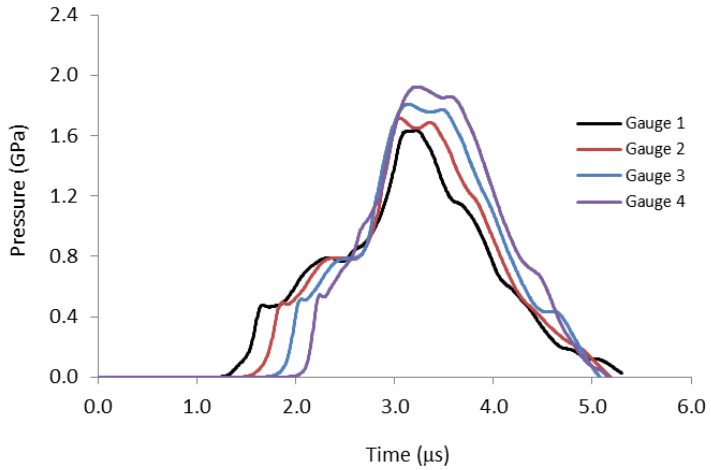

Figure 6.2 Example of pressure profiles from the four different gauge points in a numerical model with an impact velocity of 287 ms^{-1}. The average of these values was calculated to determine a pressure seen within the Teflon® liner during a shock.

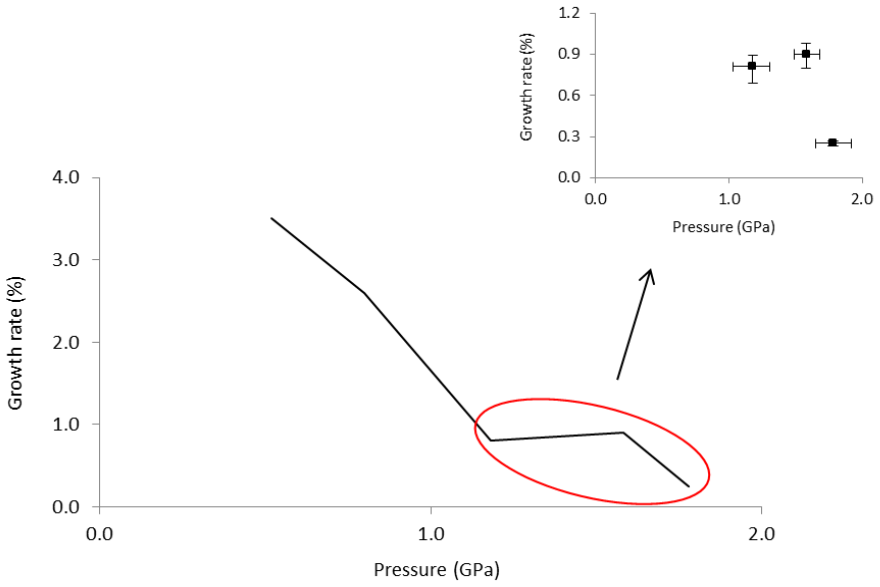

Figure 6.3 Growth rate of *S. cerevisiae* colonies *vs* pressure. While the lower pressure shots present very high growth rates, the higher pressure shots likely offer more realistic results. The growth rates at higher pressures, which fall below 1%, are highlighted and shown separately to the lower pressure results.

There is a sharp decline in growth between the shock pressures 0.8 and 1.18 GPa; colony growth rates were 2.6 and 0.81%, respectively. It is suggested that this may indicate a possible threshold where pressure has a more stringent effect on growth. This suggests involvement of mechanisms either within the cell membrane, or further inside the matrix. This concept was further explored, as detailed in the following sections of this chapter. As with the *E. coli* studied in the previous chapter, the high growth rates of *S. cerevisiae* colonies in the lower pressure regime were found to disagree with those in the current literature.

The average CFU/ml was taken in the case of each of these experiments performed three times each. The lower pressure results presented in Table 6.1 were plotted as they were in keeping with results in the literature regarding trends in yeast cell and spore survival rates. The high concentration of cells used in the stock solutions

was considered to be a contributing factor to the high survival rates at lower pressures. This is especially evident at the shots at 150 and 175.12 m s^{-1} with colony growth rates of 3.5 and 2.6%, respectively. The errors in growth rates noted here were higher at the low end of the pressure scale due to a reduction in repeatability. However, even incorporating the results from these lower pressure shots, there is still a logarithmic reduction in growth rates for the microorganisms. This is shown in Figure 6.4 where there is a clear linear relationship between the logarithm of survival and loading pressure. As discussed previously, this high concentration of cells is proposed to induce overcrowding inside the Teflon® liner and as a result, a 'cushioning' effect on the cells towards the centre of the sample. The inner cells may be provided protection from the damaging effects of the wave front, thereby protecting its morphology, and also potentially protecting the native biochemical reactions taking place within the cell.

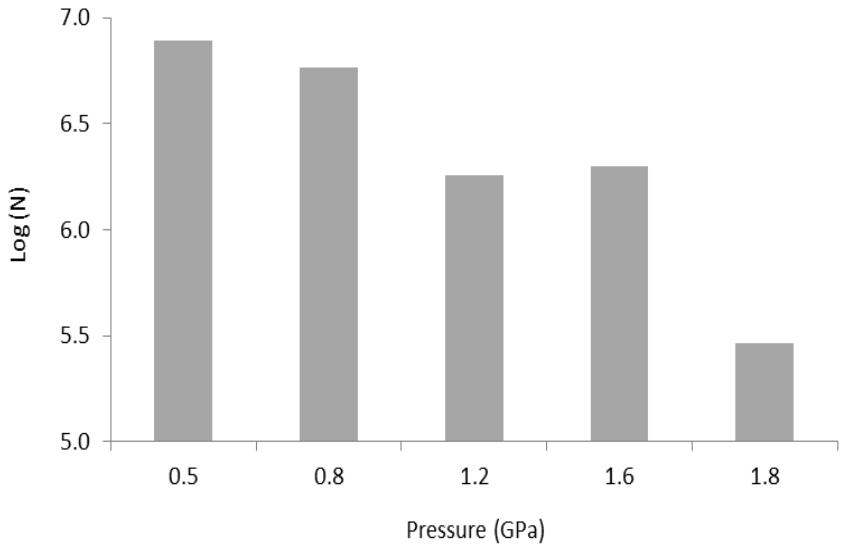

Figure 6.4 Log plot of *S. cerevisiae* colony growth *vs* pressure. There is a general decline in growth with increasing pressure, with growth rates dropping notably between 1.6 and 1.8 GPa.

A similar pattern seen in Figure 6.4 was noted with the *E. coli* in the previous chapter as well. The death of the vast majority of these cells may be attributed to a number of

effects; cell membrane disruption which may include a change in morphology as well as ion channels; equally, it may be a combination of cell membrane disruption and damage to the cell organelles. Each of these potential effects / mechanisms will be discussed in Chapter 8. As a result of the findings from these experiments, further shots on diluted samples, like those performed on *E. coli* in Chapter 5, section 5.5, were carried out as detailed in the following section.

6.3 Effects of varied sample concentration on *S. cerevisiae* growth

S. cerevisiae was found to demonstrate very high colony growth rates at lower pressures that were not entirely believable in the previous section. As discussed, this was attributed again to a potential 'cushioning' effect of a high concentration of cells on those in the centre of a cluster, similar to what was suggested for the bacteria in Chapter 5. In order to assess this hypothesis, diluted samples of *S. cerevisiae* were shock loaded to pressures ranging from 0.49-2.33 GPa and these were compared to the results from the more concentrated samples examined in section 6.2. The pressures and colony growth results are detailed in Table 6.2.

Table 6.2 Growth of dilute samples of *S. cerevisiae* following shock loading experiments using the plate impact technique and the capsule recovery system. *No colony growth.

Velocity (m s^{-1})	Pressure (GPa)	Colony forming units (CFU/ml)	Growth (%)
145.34 (± 2.7%)	0.49 (±24.5%)	4 x 10^6	1.80 (+25.0/-19.2%)
170.07 (±1.6%)	0.70 (+19/-17.5%)	2.6 x10^5	1.50 (+20.4/-17.3%)
287.52 (± 1.3%)	1.80 (+7.8/-6.9%)	6.7 x 10^4	0.03 (+13.4/-12.7%)
290.87 (± 1.5%)	1.81 (+8.3/-7.2%)	4.2 x 10^5	0.19 (+10.0/-15.5%)
310.00* (± 1.2%)	2.33 (±5.2%)	-	-

Cell concentration was 5.3 x 10^3 cells/ml for the undiluted samples. Lower concentrations (10^{-3} of the original stock solution) were prepared for this set of experiments and, after shock loading, were plated on agar nutrient medium using the usual protocol of performing serial dilutions. Growth rates for the diluted samples appeared to be predominantly higher than those seen for the more concentrated samples. This trend is highlighted in Figure 6.5. These results provided further evidence of a possible 'cushioning' results in a decrease in survivability. In keeping with the previous set of experiments, colony growth rates were still found to decrease with an increase in pressure. Figure 6.6 presents the log plot of this data with generally decreasing numbers of colony forming units with increasing pressure.

Growth of colonies from the dilute samples were significantly reduced at lower shock pressures in comparison to the concentrated samples. For example, the lowest pressure for the dilute samples (0.49 GPa) yielded a growth rate of just 1.8%. For the lowest pressure used with the concentrated samples (0.52 GPa) the growth rate was 3.5% as reported in the last section. Figure 6.5 shows that there is no overlap of results for the diluted and undiluted samples, even including the calculated errors, at lower pressures. However, from ~ 1.8 GPa, it appears there could be some overlap between both samples. This is a potentially interesting observation. Essentially, the fact that the results become comparable at higher pressures implies that there may be a particular threshold at which microorganism concentration becomes negligible in terms of overcoming shock pressure. Although mechanisms surrounding the response of a cell to shock pressure in terms of its structural integrity are not yet understood, it is evident from this research that high concentration appears to play a role in the survival and growth of *S. cerevisiae* following shock pressure. Initial results suggest that dilute samples leave cells more exposed to the shock front with little surrounding them to absorb the shock. A number of potential models to explain greater growth and survival with higher concentrations can be inferred from these results; the aforementioned 'cushioning' likely offers the best explanation for this, but details of how this may affect

cell membranes and even internal cellular structures will be considered in the Discussion in Chapter 8.

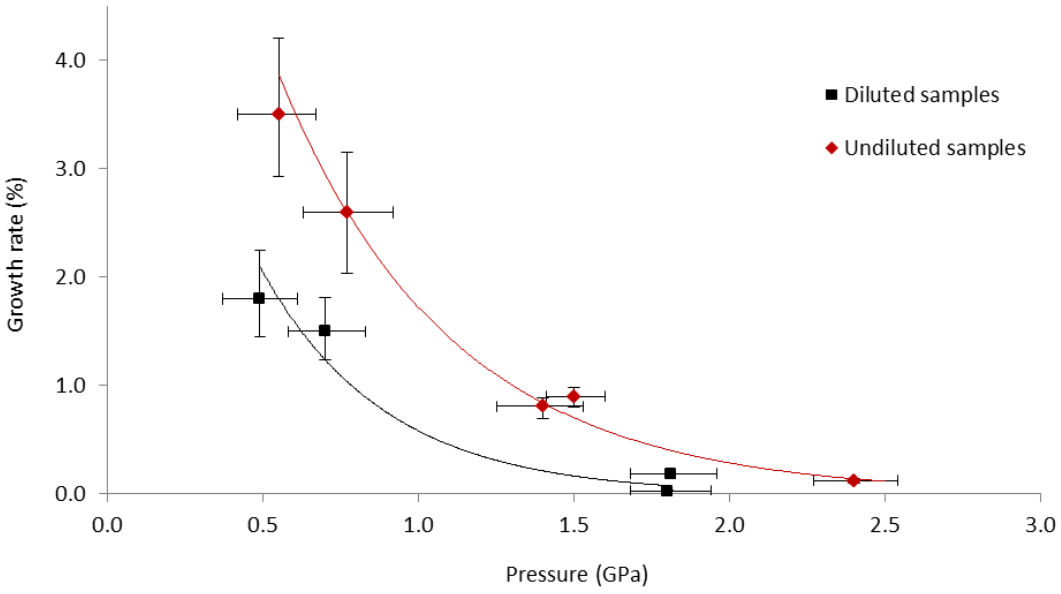

Figure 6.5 Growth rate of dilute and undiluted samples of *S. cerevisiae* colonies *vs* pressure. There is a marked difference in response between these samples of different concentration. The diluted samples show lower growth rates than the samples of original concentration until ~ 1.8 GPa where there appears to be more agreement between both sets of results.

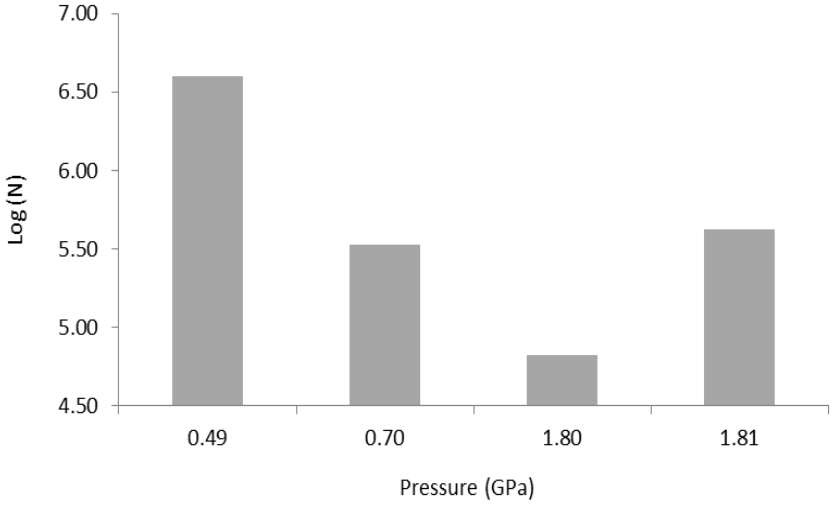

Figure 6.6 Log plot of *S. cerevisiae* colony growth from a dilute stock solution *vs* pressure. Excluding the final value at 1.81 GPa, there is a general decrease in growth with increasing pressure.

6.4 Control of pulse duration on *S. cerevisiae* with 20 mm flyers

The final set of experiments performed on *S. cerevisiae* was the shock loading of the cells with different thicknesses of flyer plates; 5, 15 and 20 mm respectively. As noted in Chapter 5 with the *E. coli*, there was very little difference in pulse duration between the 15 and 20 mm flyers; therefore, only 20 mm flyers were used to produce prolonged shock pulses. Shock pressures for these experiments ranged from 0.52-1.47 GPa with survival rates ranging from 5.6-0.01% as outlined in Table 6.3. The log plot of the average number colony forming units presented in Figure 6.7 is taken only from the four repeatable experiments with perceived more reliable growth rates. Two shots with growth rates that were excessively high in comparison to the remaining results were excluded from this plotted data. These shots were 176.01 and 204 m s^{-1} which showed growth rates of 3.5 and 5.6%, respectively.

Table 6.3 Growth of *S. cerevisiae* following shock loading with 20 mm flyer plates. The colony forming units listed here are average values for three experiments. *The growth rates following these shock velocities were excluded from the plotted data due to their inconsistency with the remaining results. These two experiments were not repeatable.

Velocity (m s^{-1})	Pressure (GPa)	Colony forming units (CFU/ml)	Growth (%)
150.00 (± 2.6%)	0.52 (+23.1/-25.0%)	5.6 x 10^4	0.03 (+19.5/-29.4%)
168.00 (± 2.7%)	0.66 (±19.7%)	5.6 x 10^4	0.03 (+27.7/-16.8%)
176.01 (± 1.6%)*	0.80 (+18.5/-17.0%)	7.8 x 10^6	3.50 (+16.7/-21.4%)
204.00 (± 1.2%)*	1.02 (+13.7/-15.7%)	1.2 x 10^7	5.60 (+18.5/-22.2%)
242.00 (± 1.4%)	1.61 (+9.7/-9.0%)	4.4 x 10^4	0.02 (+13.2/-19.6%)
255.00 (± 1.2%)	1.74 (+5.7/-5.2%)	1.1 x 10^5	0.01 (+11.3/-14.2%)

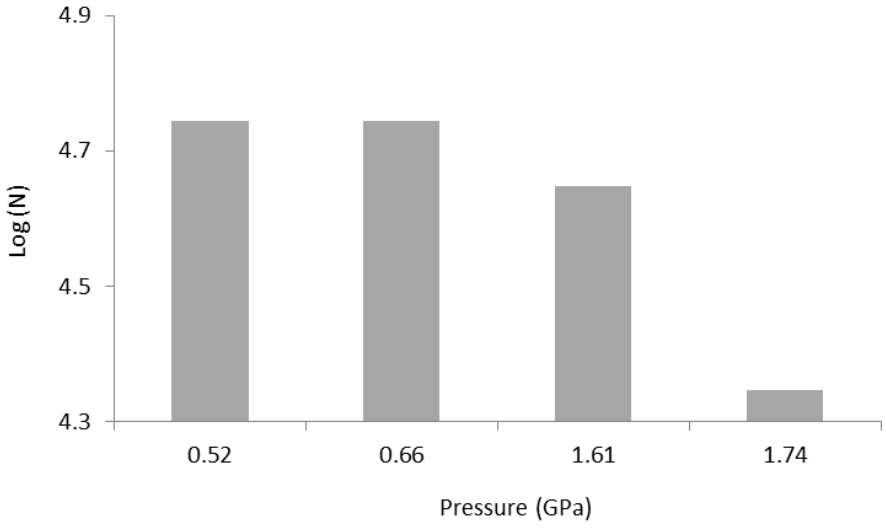

Figure 6.7 Log plot of *S. cerevisiae* colony growth *vs* pressure following shock loading with a 20 mm flyer plate.

To demonstrate the difference between the 5 and 20 mm flyers, modelled shock profiles for low and high velocity shots are compared in Figure 6.8. For the impact velocity of 168 m s^{-1} with the 20 mm flyer, the pulse times for the gauge points 1-4 were 3.73, 4,13, 4.38 and 4.74 μs, respectively, with an average value of 4.25 μs. At the same velocity for the 5 mm, the shock pulse durations were 3.13, 3.38, 3.71 and 4.25 μs with an average value of 3.61 μs. There was a difference of ~ 0.64 μs between both flyers at this pressure (0.66 GPa). However, a much lower survival rate of 0.03% was seen with the 20 mm flyer compared to the much higher rate of 3.5% at just 0.52 GPa using a 5 mm flyer. At the higher velocity of 242 m s^{-1}, for the 20 mm flyer, the shock pulse durations for gauges 1-4 were 3.59, 3.96, 4.37 and 4.79 μs, respectively. The average value was 4.18 μs. The results for the 5 mm flyer were 3.07, 3.37, 3.72 and 4.16 μs, with an average of 3.58 μs. The difference in pulse duration between the two flyers at this velocity was 0.6 μs with a colony growth rate of 0.02% for the 20 mm flyer. At a similar pressure (1.58 GPa) for the 5 mm flyers as mentioned in section 6.2, the growth rate was 0.9%. In this set of experiments, the growth rates were all consistently lower than those seen for the 5 mm flyer shots, with values of well below 1%. This data from the 20 mm flyer shots is plotted below in Figure 6.9.

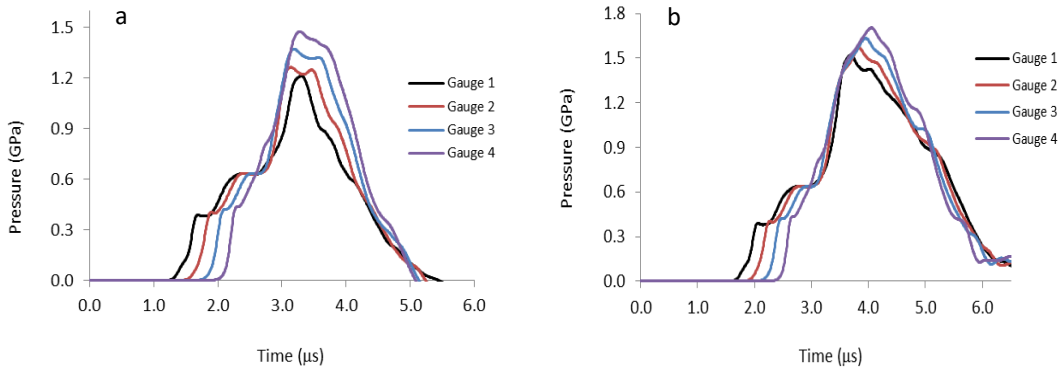

Figure 6.8 Shock pulse profiles for shots at 242 m s^{-1} using the a) 5 mm flyer and b) the 20 mm flyer. A longer pulse time of 4.18 μs was seen for the 20 mm flyer compared to the 3.58 μs pulse of the 5 mm flyer.

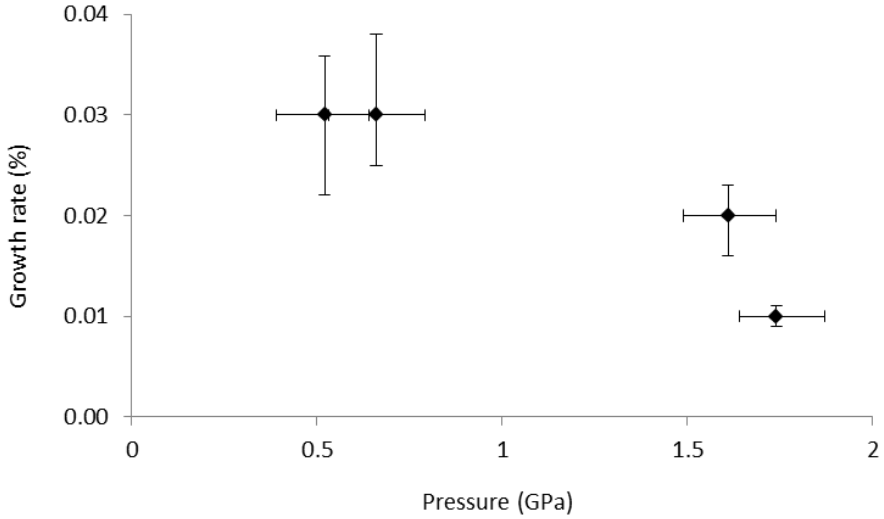

Figure 6.9 Growth rate of *S. cerevisiae vs* pressure following shock loading with a 20 mm flyer plate. While there were larger errors once again at lower pressures, there was less variance between these growth rates than what has been seen from previous experiments.

The use of thicker flyer plates in each experiment increased the shock pulse by a number of microseconds and led to significantly lower survival rates for the longer pulse. Although protein folding and unfolding kinetics are on the second timescale, this

study suggests that perhaps a particular threshold may exist within the microsecond range that affects either internal cellular mechanisms, or the structural integrity of the cell membrane.

The contrast in growth rates between flyers of different thickness demonstrates the importance of the pulse duration and how long a cell may be exposed to a particular pressure before it begins to expire. Since growth of colonies tends to decrease with increasing pressure, it can be deduced that the pressure itself has detrimental effects on chemical processes within the cell or the structure of the cell itself that result in cell death. The fact that with increasing shock pressure the exposure time of the cells to the shock pulse at any given point along the Teflon® liner is decreased is also worthy of note. It is now known that longer loading periods - i.e. through the use of static pressurisation - result in lower survival than what is seen following shock loading. This demonstrates that the length of exposure of *S. cerevisiae* is important when considering the effects of stress on the outer surface of the cell and any damage mechanisms that occur within the cell.

6.5 Summary

The results presented in this chapter demonstrate the relationship between the growth of *S. cerevisiae* colonies and increasing hydrodynamic pressures. The plots of percentage growth *vs* pressure generally show an exponential decline in growth with increasing pressure and this is in agreement with other results in the literature regarding shock pressurisation of yeast samples. Interestingly, significantly more profuse growth was noted at lower pressures in every set of experiments – immediately highlighting the influence of dynamic loading on the survival of *S. cerevisiae*. At particularly low shock pressures, concentrated samples seem to have a positive influence on survival and growth of colonies. While the dilute samples also showed higher growth rates at low

pressures, these results were still lower in comparison to more concentrated samples. For example, at the lowest pressures, a difference of 1.7% was noted between the two concentration types. This may be explained by a ‘cushioning’ effect which may act to protect cells within the centre of a cluster from the most damaging effects of the shock wave. For the final set of experiments, there was a particularly clear correlation between the pulse duration and the growth of yeast cells. The growth rates following the use of 20 mm flyer plates fell well below the values recorded for the 5 mm flyers. This may also be explained by internal or external mechanisms being triggered in response to the shock. These mechanisms to explain how *S. cerevisiae* cells may remain intact and viable following shock compression will be explored further in Chapter 8.

7 Quasi-one-dimensional shock loading of *Artemia salina*

7.1 Introduction

In this chapter, the results of shock loading the multicellular organism *Artemia salina* (brine shrimp) are presented. *Artemia salina* is a parthenogenetic branchiopod crustacean that has long been used in studies as a food source for a number of aquatic organisms [107, 108], as well as for bioassays to test for toxicity in various systems [109, 110]. As an organism, *Artemia salina* is significantly more complex than the unicellular organisms investigated in Chapters 5 and 6. They have shown a tolerance for high pressures, leading into the gigapascal range for static loading. One of the best examples of this is the tardigrade (water bear) of which there are several different species. *Richtersius coronifer* is one such species pictured in Figure 7.1. Certain organisms are capable of surviving extreme pressures as well as radiation exposure in space [111-114]. *Artemia salina* have also proven to be a good organism for such investigations given that they demonstrate good survivability in extreme conditions [114 - 116]. *Artemia* are often used in attempts to indicate toxicity in different systems; however, in a number of reported cases, their viability is based on whether normal motility is observed [116], with no indication of what is happening in terms of their biochemistry. It is currently unclear as to what intercellular mechanisms may be affected, or how the cell structure may sustain itself, or fail, in response to shock compression. In order to help determine this, the influence of the type of pressure loading (dynamic or static) as well as the nature of the shock wave front (one-dimensionality or radial expansion) is examined in this chapter.

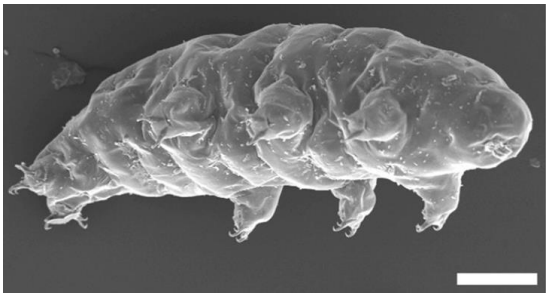

Figure 7.1 Scanning electron micrograph of a live specimen of tardigrade, *Richtersius coronifer* [117].

An example of shock pressurisation of *Artemia* is an experiment carried out by Udagawa and Suzuki (2013). Ultra-high pressure underwater shock waves were created by an imploding detonation of a propane-oxygen mixture and this was used to impact a cylindrical sample holder containing *Artemia* larvae (nauplii) [42] (Figure 7.2). This dynamic loading technique reached pressures of 100 MPa, but was not significant in comparison to static loading tests implemented on these organisms which reached several gigapascal (7.4 GPa) and showed a rate of survival of ~ 80% after 50 hr [42]. It could be said however, that the pressure itself may not have contributed entirely to the death of the organisms. Given the fact that the bodies underwent high levels of deformation, as was observed after the shock, it is possible that a non-uniform shock front may have disrupted their structure.

Figure 7.2 Image taken of an *Artemia* nauplius. The antennae positioned near the head of the larva are used for motility [116].

Gaining an understanding of the *Artemia salina* response to high pressure could prove vital for studies involving organisms living in natural high pressure environments and decoupling the effects of high pressure may be useful when performing these bioassays. A hatching rate of 24-48 hr in optimum conditions for *Artemia* cysts make them ideal for testing in a laboratory environment. *Artemia* are typically ovoviviparous; they are born as free-swimming nauplii. In less favourable environments, embryos are developed oviparously; in cysts that hatch only when conditions are stable. This dormant state in which encysted embryos reside is known as diapause where they experience reduced metabolic activity [107]. Once they are exposed to water they typically exhibit a hatching rate of approximately 90%, with a minimum of ~75% [115], under normal conditions. They are capable of surviving a number of stressors, including salinity and temperature that can vary substantially, with an optimum salt concentration in most *Artemia* species of 60 g L^{-1} and an optimum temperature of 25 °C in laboratory conditions [107]. The temperatures for nauplii viability, however, have a considerable range of 5-40 °C [106]. In addition, cysts have been found to survive even more extreme temperatures [114] along with certain evident enzyme activities that are maintained. For example, protease activity in the cyst shells of *Artemia franciscana* has been detected, although at a reduced rate, following a 15 min exposure to 100 °C [116].

Artemia exposure to high pressures extending into the GPa range has also been investigated in recent years. Quasi-hydrostatic tests carried out on *Artemia salina* cysts in fluorinert medium by Ono *et al*. [116] found hatching rates of 80–90% after exposure of several dozen examples to a pressure of 7.5 GPa for up to 48 hr. In contrast, Udagawa and Suzuki [42] showed that relatively low pressure shock waves with pressures in the range of 25-100 MPa, which were produced by underwater detonations, resulted in cyst hatching rates of < 2.5% after 48 hr observation. The marked difference between these findings seems likely to be related to the nature of the pressure loading; in particular, greater survival at higher pressures suggests that the different timescales over which the pressures were applied when compared with the biochemical or

physiological changes that determine hatching is likely a key mechanism in the observed behaviour.

Artemia salina eggs, or cysts, have also been investigated under stressors such as hydration with changes in metabolic activity [117]. Cysts form when the nauplii enter a reversible state of dormancy known as diapause when conditions are not favourable. Metabolism in *Artemia* cysts have reportedly been restored within 1 hr of being dehydrated at their optimum temperature (25°C) [117]. More than 50 percent of these were found to hatch after 24 hr. Some, however, did not hatch until 72 hr after hydration. It was concluded that dehydration is reversible until 12-18 hr after rehydration. After this time, differentiation of the cells occurs and dehydration becomes irreversible [115].

It is well known that proteins play a key role in system development of organisms and one protein specific to *Artemia* development and cyst stress response is the p26 protein found only in encysting *Artemia* embryos. Miller and McLennan (1988) [115] determined that cysts are more thermotolerant than freshly hatched nauplii [115]. They found that development was proportional to the severity of the stress and it was noted that the time at which stress is applied time during development is very important. Interestingly, a number of proteins present in the larvae are known to be no longer synthesised upon exposure to higher temperatures. However, most proteins within cysts continue to be synthesised when subjected to sub-lethal temperatures for *Artemia*, showing their robustness under extreme conditions [118, 119].

7.2 Shock response of *Artemia salina* cysts

This thesis has focussed on the response of *Artemia salina* to three different shock pressures: 0.78, 0.96 and 1.5 GPa. The conditions for each experiment are explained in Table 7.1. Dried *Artemia salina* cysts were obtained from Sciento® and used for both

cyst and nauplii shock loading experiments. Hatched nauplii were collected by incubating several cysts in a 3% saline solution at 25 °C for 48 hr in a water bath. Sample sizes of 100 cysts were chosen for shock loading at each pressure, while 100 hatched nauplii were examined at the lowest pressure only. These sample sizes were divided into subsets of 20 for the purpose of encapsulating them during the shock as well as to prevent overcrowding within the sealed capsule during shock loading. Similar to what has been discussed for both the bacterial and yeast samples examined in this thesis, the number of cysts and hatched nauplii within the capsule was determined to play an important role in the resulting levels of hatching and survival. To prevent any potential 'cushioning' of *Artemia* cysts or nauplii, a lower sample number was utilised in each experiment. The overall sample size examined at each pressure provided a measure of statistical significance for the hatching and survival rates.

Table 7.1 Breaking and hatching rates of *Artemia salina* cysts observed for each shock pressure after both 24 and 48 hr.

Impact velocity (ms^{-1})	Pressure (GPa)	Cyst breaking frequency (%)		Hatching frequency (%)		Shock peak temperature (K)
		24 hr	48 hr	24 hr	48 hr	
135 (±2.3)	0.78 (+18.4/-17%)	60	75 (± 3)	16	26 (± 3)	314
153 (1.8±)	0.96 (+13.6/14.2%)	59	70 (± 4)	12	23 (± 3)	315
230 (1.3±)	1.50 (+9.1/7.4-)	30	43 (± 3)	4	18 (± 2)	323

The shock loading experimental set-up included the plate-impact technique with the capsule recovery system described previously in Chapter 3. A capsule containing 20 cysts or nauplii was overfilled with 3% saline solution to avoid any cavitation in the sample during the shock. As detailed previously in a study by Hazell *et al.* [120], such

cavitation can lead to death of microbial samples and this occurrence becomes even more likely for a multicellular organism. The larger Al capsule was then filled with 20% ballistic gelatine to attenuate the shock and minimise rarefaction waves that may move back through the sample.

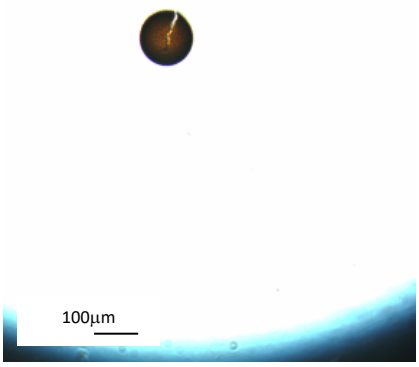

Figure 7.3 Image of an *Artemia salina* cyst at the 'breaking' stage post shock loading at 0.96 GPa.

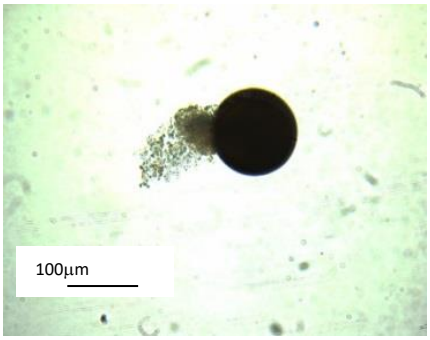

Figure 7.4 Embryo emerging from cyst post shock loading at 0.96 GPa.

Following incubation of the shocked cysts, the hatching rates (i.e., emergence of the embryo from the hatching membrane) were determined after 24 hr and 48 hr in each case (Table 7.1). The 'breaking' stage of the cysts (when the cyst shell begins to crack)

was also recorded to observe the emergence of the embryo from the shell (Figures 7.3 and 7.4). These rates were higher than the hatching rates in each case and this is shown clearly in Figure 7.5. At the lowest pressure reached, 0.78 GPa, a breaking rate of 75 % was attained after 48 hr and 0.96 GPa resulted in a breaking rate of 70 %. The maximum pressure achieved during shock loading was 1.5 GPa and this led to the lowest breaking rate of 43 %. The hatching rates also showed similar decrease (26%, 23% and 18%) with increasing peak pressures. One sample from each different shock pressure was also analysed after 14 days of incubation to search for any further hatched nauplii. However, no additional hatching was observed. Peak temperatures reached during the shock runs were determined through the ANSYS® Autodyn models (Table 4.1). These ranged from 314 K at 0.78 GPa to 323 K at 1.5 GPa.

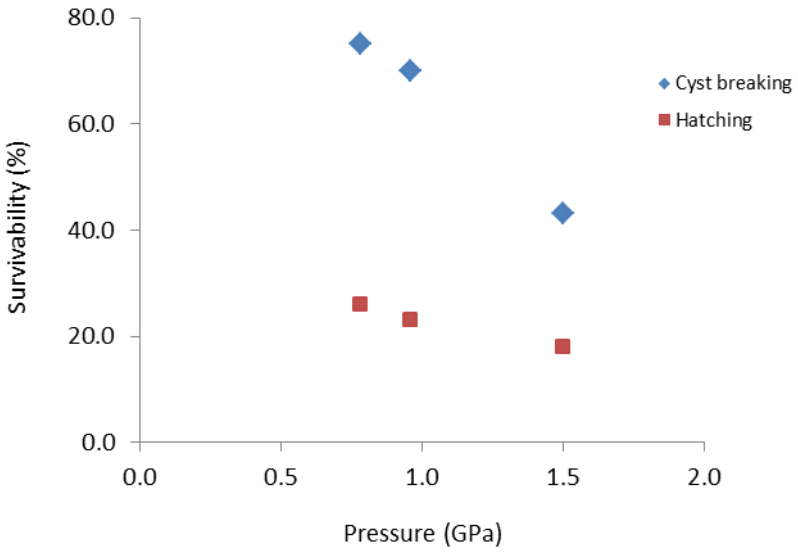

Figure 7.5 Survivability as determined by the breaking of the cyst and the hatching of the nauplii after 48 hr.

In addition, hatched nauplii were studied following shock loading at 0.78 GPa but only at the lowest pressure due to a likely temperature increase of the samples during the

shock. The motility of their antennae was observed for up to 48 hr and 20% of the samples demonstrated motility of their antennae throughout this time, but with a noticeable lack of overall motion compared to nauplii hatched from shock loaded cysts. Many did not appear to have any significant structural damage following shock loading and an example of this can be seen in Figure 7.6. Nauplii that were found to be unmoving but appeared to be structurally intact were left for up to 14 days in order to check for any subsequent movement in their antennae; however there appeared to be no viability after this time.

Figure 7.6 Hatched nauplius after shock loading at 0.78 GPa.

A decrease in both cyst breaking and hatching rates were seen following shock pressures of 0.78 and 0.96 GPa, whereas a much larger effect was observed following shock loading at 1.5 GPa. The nauplii that hatched successfully after shock loading at this pressure appeared to be largely undamaged, although 20% demonstrated impaired motility. The results presented here show that *Artemia* cysts are significantly more sensitive to quasi-one-dimensional shock compression than static loading into the GPa range. Hatching rates here were also much higher than those seen for the aforementioned experiments noted in the literature. This may be attributed to the mechanical response of the cyst shell to shock *vs* static pressurisation in determining the rate of successful hatching, and subsequent properties of the hatched nauplii. However, in order to avoid complications due to heating of the samples during shock

compression, a single series of experiments subjecting hatched nauplii to a pressure of 0.78 GPa were undertaken.

Nauplii were examined through light microscopy, revealed that antenna motion indicated that motility was greatly reduced. In the case of the cyst shells, light microscopy also showed that in some instances, the breaking stage was initiated, but was not completed. This breaking stage can be seen in Figure 7.3. Little damage appeared to have occurred to the external structure of the cysts, even for those that did not hatch after 48 hr. This could indicate that delayed hatching or possible death of the embryos contained inside the cysts might be due to internal biochemical mechanisms controlling their shock response; for example, particular genes being activated in the encysted embryos but not in the hatched nauplii. Some such genes involved in the production of proteins for embryo protection have already been identified, including p26, but it is not yet known how these genes respond to pressure loading.

Understanding the mechanics of the cyst itself and of the membranes of individual cells within the organism is crucial for interpreting its behaviour under both dynamic and static pressures. Given the high tolerance of *Artemia salina* to a simplified quasi-1D shock wave, the likelihood of larger organisms surviving very high pressure impacts – such as planetary asteroid impacts – is greatly increased as well as the probability that individual cells of the organism would show even greater survivability, as has been shown with *E. coli* and *S. cerevisiae* in Chapters 5 and 6.

7.3 Summary

By undertaking a unique set of experiments applying quasi-one-dimensional shock wave pressures in the range of 0.78-1.5 GPa, breaking and hatching rates of *Artemia salina* cysts were found to decrease with increasing pressure, unlike static compression results from the literature that maintained up to 90% hatching rates after exposure to 7.5

GPa for up to 48 hr. The enhanced effect of shock *vs* static pressurization in reducing *Artemia* cyst hatching is in general agreement with previous studies, although the hatching rates found here were significantly greater than those seen following shock from underwater detonation waves. This implied that the nature of the wave front (one-dimensionality *vs* radial expansion) must play an important role in survival and hatching probability of the cysts, certainly by affecting the mechanical stress fields applied to the cyst envelope. It is apparent that shock and static pressurisation also certainly affect the biochemical and biophysical state of the encysted embryo and these effects could be studied by future genomic and proteomics investigations.

8 Discussion

8.1 Introduction

The various plate-impact experiments carried out in this project led to some unexpected results in terms of the response of *E. coli*, *S. cerevisiae* and *Artemia salina*. There was a general pattern seen for all organisms, which was that increased shock pressure inhibited normal functioning. This was presented either as reduced growth rates with respect to the microbes, or reduced cyst hatching and motility for the *Artemia*. These results were not directly referred to as survival, since this is a term difficult to define as cells may appear dead when they are only dormant. The same can be said for the *Artemia* cysts. In this discussion, comparisons will be drawn between the *E. coli* and *S. cerevisiae* growth rates for each type of dynamic loading experiment. Additionally, potential mechanisms for any survival recorded in these experiments are proposed for each organism, such as that depicted in Figure 8.1.

8.2 Quasi-one-dimensional shock loading of microorganisms

Standard plate-impact shots were carried out on *E. coli* and *S. cerevisiae* with 5 mm thick Al flyer plates at pressures ranging from 0.8-1.78 GPa. The growth rates for each organism are shown in Figure 8.2. For both microorganisms, there is a general trend of exponentially decreasing colony growth with increasing pressure. This has been noted in the literature previously for a number of organisms; from *Shewanella oneidensis* cells [32], to spores of bacteria [85] and yeast [37]. A potential pressure threshold between 0.9-1.4 GPa was found for *E. coli* and this was further suggested with the dilution experiments, discussed in section 8.4. This threshold is also in keeping with results by Leighs *et al.*, 2014 [105]. This was noted previously in Figure 5.3. A pressure threshold

for *S. cerevisiae* was not clearly definable, particularly due to the point at 1.58 GPa where colony growth rates seem to deviate from the others in the plot. Additionally, based on the results from the standard plate-impact and dilution experiments, growth rates appear to be higher for *S. cerevisiae* than for *E. coli* in a similar range of pressures, shown in Figure 8.2; this was deduced to be a result of differing cell structures, with the yeast being a eukaryote and having a more complex overall structure than the prokaryotic bacteria. It is plausible that a pressure wave capable of overcoming the shear strength of the cell wall would cause damage not only to the outer structure, but to mechanisms within the cytoplasm of the cell. While it has been previously shown that static pressure loading does influence some genetic pathways [82] in *E. coli*, it is important to first understand how a cell may behave structurally under particular conditions, since damage to the cell envelope may result in changes to the biochemistry of the cell; ion channels which are important for cell signalling could be affected, for example. Section 8.6 discusses a few mechanisms which could be used to explain the results found for *E. coli* and *S. cerevisiae* throughout this project.

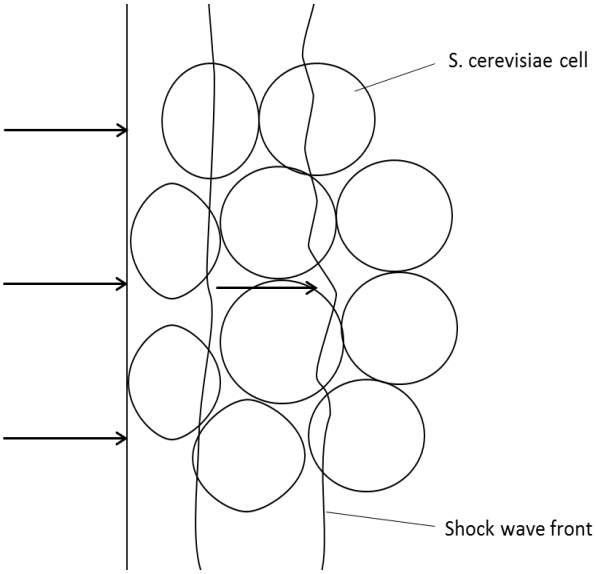

Figure 8.1 Proposed mechanism of a shock wave entering a sample of closely packed *S. cerevisiae* cells. Excluding the quasi-one-dimensionality of waves entering the capsule system, a 1D shock wave may become less one dimensional as it moves the sample, much like it would while traversing an inanimate solid material with tightly packed particles.

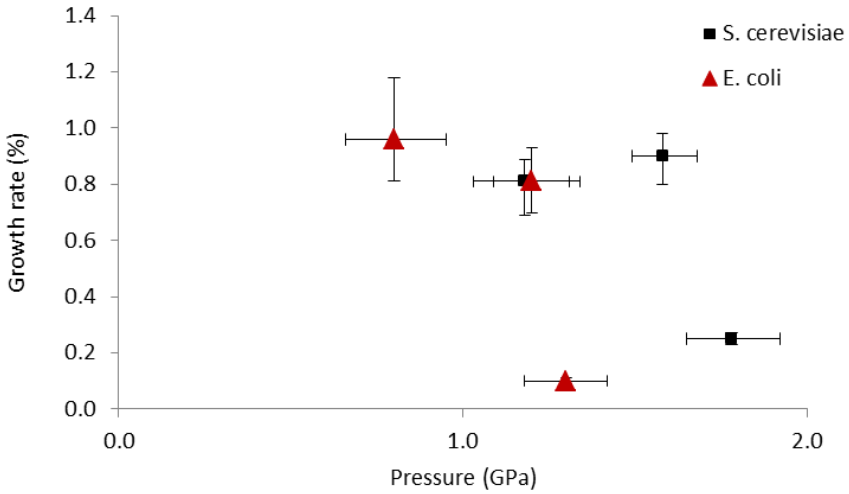

Figure 8.2 Comparison of *E. coli* and *S. cerevisiae* colony growth *vs* pressure. While there is some overlap between them, *S. cerevisiae* appears to be more pressure-resistant at this regime.

Figure 8.2 shows a plot of *E. coli* and *S. cerevisiae* colony growth with respect to pressure. *S. cerevisiae* appears to show greater resistance to quasi-one-dimensional shock loading. One explanation is that although *S. cerevisiae* is larger than *E. coli* and as a eukaryotic organism has an overall more complex structure, it has a tough cell wall that may withstand shock compression better than the elastic cell wall of *E. coli*. The Young's modulus of both organisms is given in Table 8.1.

8.3 Temperature measurements

Studies have shown that *E. coli* can survive temperatures up to 47 °C, but they may also be trained to survive higher temperatures (up to 48.5 °C) [17]. Likewise, *S. cerevisiae* may survive high temperatures up to 45 °C as reported by Salvado *et al*. [121]. As mentioned previously, the study by Casadei *et al*. (2002) found that *E. coli* NCTC 8164 showed higher resistance if cultured at lower temperatures, i.e. 10 °C. As culture temperature was increased, resistance to pressure decreased [122]. These studies demonstrate the robust nature of these unicellular organisms and in this project, both *E. coli* and *S. cerevisiae* were subjected to some of these temperatures

The combination of numerical modelling and the use of nickel temperature gauges showed that the temperatures reached throughout most of the shots carried out during this project were below temperatures recorded to affect the viability of both *E. coli* and *S. cerevisiae*. Although some temperatures reached during the shock experiments are above the temperature for enzyme denaturation, as discussed in Chapter 2, the organisms are not subjected to these elevated temperatures for any great length of time (~ 10 mins). It was postulated that the growth rates of the colonies would not be severely affected. As such, given the one-dimensionality of the shock wave, any effects on colony growth rates would be a direct result of the pressure applied across the sample.

The higher-pressure temperature-control experiments, with the Surfi-Sculpt® and planar stainless steel flyers however did involve some elevated temperatures, the highest of which was 341 K, or 67.85 °C, at 10 GPa. Colony growth was also recorded after this shot, possibly due to the short term of exposure to this temperature. At lower pressures, a more distinct difference was seen between the shock wave front produced by the Surfi-Sculpt® flyers and the planar flyers, as shown in Figure 5.5. Contrast between temperatures at these pressures was very slight, but the samples impacted with the planar flyers, which displayed slightly higher temperatures were still shown to be generally lower than with the Surfi-Sculpt®.

This method highlights a potential new method for loading organisms while controlling temperature to have a better understanding of both the effects of temperature and pressure. It also stands to highlight the potential importance of the shock wave front, a factor that was proven to be of great importance in Chapter 7 with the examination of the *Artemia salina*. Since the temperature changes seen in the *E. coli* sample as a result of these flyers was minimal, there may be an explanation for the growth rates seen, other than temperature thresholds; the higher survival could be attributed to the ramp wave produced by the flyer which reaches peak pressure more gradually. This may have offered the *E. coli* time to adjust to the loading.

Further to the measurement of the peak temperatures occurring in the capsule, the temperatures reached during these experiments were compared to the phase diagram according to Nagayama *et al*. [89], mentioned in Chapter 2. It revealed shock pressures ranging between 0.7 and 3 GPa leads to ice phases occurring in water; thus, this likely occurred in the liquid medium inside the Teflon® liner since PBS was shown to have a very similar EOS to deionised water. However, as shown previously by Sharma [92], these ice phases should not have any notable effect on cell viability. This offered further validation to the experiments carried out during this investigation.

8.4 Effects of concentration on microbial shock response

It has been shown in this thesis that concentration plays an important role in the response of microorganisms to shock loading. Microorganisms are known for growing clustered together in dense populations, as this allows more room for new cells to grow [123]. This means that for any meteoritic bodies that carry microbial life, the existence of dense cell populations on meteoritic bodies is quite likely, which makes this a 'real world' scenario experiment.

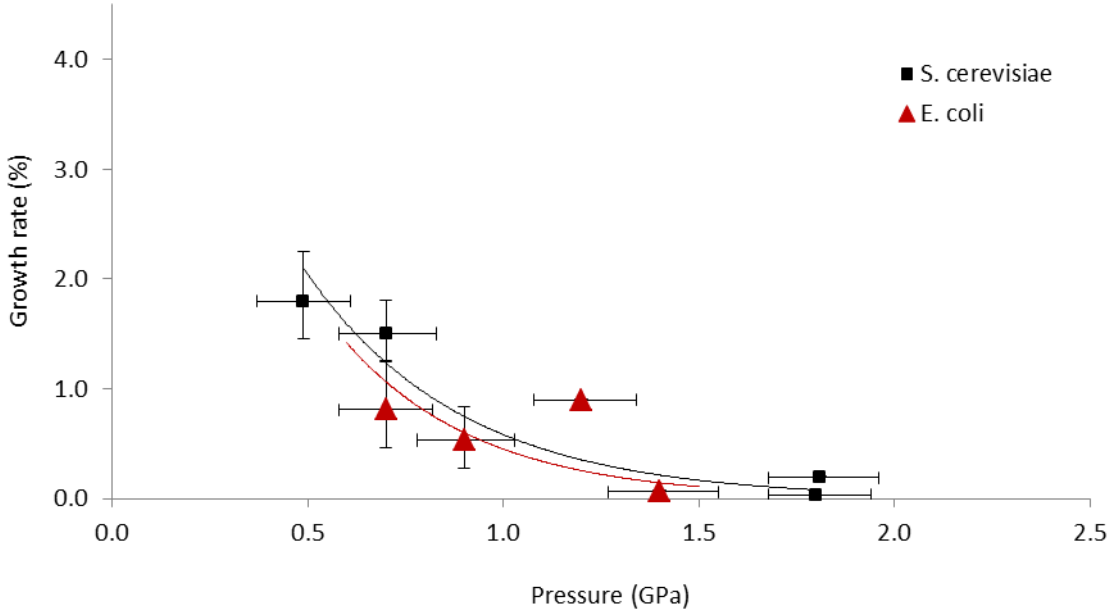

Figure 8.3 Physical properties of *E. coli* and *S. cerevisiae* to determine the maximum concentration of each organism that may fit inside the Teflon® liner.

In an effort to understand the packing of cells inside the Teflon® liner and how many cells may be present in a totally saturated sample, the data in Table 8.1 were compiled. It was also desired to compare the ability of both *E. coli* and *S. cerevisiae* to withstand shock pressures; as a result, the Young's moduli for both microorganisms are also listed in Table 8.1. According to the literature, multiple experiments in which the Young's

modulus of the both *E. coli* and *S. cerevisiae* have been carried out, but with disagreement between the results. *S. cerevisiae* has a higher Young's modulus, indicating that is less likely to recover from any damage inflicted upon it due to shock pressure. This appears to be in disagreement with some of the results presented here, where *S. cerevisiae* shows greater survival than *E. coli*. However, there may be a number of internal mechanisms of the cell which help to abate the effects of the shock. As mentioned previously, it could also indicate that the cell wall is sufficiently 'tough' that it can withstand pressures up to a particular threshold. The greater level of elasticity of the *E. coli* is attributed to the elastic nature of the PG, present in the cell wall [124, 125].

The colony growth results for both organisms after being diluted by 10^{-3} from their stock solutions are much lower than the undiluted samples, with strong evidence pointing towards the higher concentrations protecting cells in the centre of a cluster. It is put forth that cells directly exposed to the wave will be damaged, or killed, while cells further behind them may remain intact and unaffected and hence demonstrate higher growth rates. In contrast, for a dilute sample, each individual cell has more chance of being directly exposed to the wave and any damage that may occur, hence the lower growth rates.

Table 8.1 Physical properties of *E. coli* and *S. cerevisiae*. The purpose of these data was to determine the maximum concentration of each organism that may fit inside the Teflon® liner.

Organism	***E. coli***	***S. cerevisiae***
Shape	Rod	Spherical
Cell size (μm)*	1 x 2	6 (diameter)
Young's modulus	25-150 MPa [124, 125]	107 MPa [20]
Cell volume (μm^3)*	2	113
Max. capacity of Teflon® capsule (cells)	3×10^9	5.3×10^7

8.5 Pulse duration experiments

For experiments involving extended pressure pulses, the maximum pulse length noted for the *E. coli* experiments was 5.29 μs, approximately 2 μs greater than its 5 mm flyer counterpart. *S. cerevisiae* showed a strong response to longer pulse lengths displaying greatly diminished colony growth rates. While it could be argued that the results may be due to the 20 mm flyers having a larger mass than the 5 mm flyers, the same pressures were reached in each set of experiments and *E. coli* was treated in the same way but did not exhibit this strong decline in growth due to the longer pulse. The two are compared in Figure 8.4. In the case of *S. cerevisiae*, the largest difference in pulse duration between the two different flyer types was 0.66 μs and as shown in Chapter 6, section 6.4, there was a dramatic reduction in colony growth rates. These results were consistent and repeatable implying some level of sensitivity to this loading, but in order to more fully understand what is happening to the cells under these conditions an SEM or TEM imaging may prove useful.

Conversely to the results of the *S. cerevisiae* response to the longer pulse, *E. coli* showed much higher survival in comparison to what was seen with the 5 mm flyer. The reasoning behind this was that more cells would be exposed to the longer pulse, thus dispersing energy across a wider range and, much like the effect of high concentration, individual cells would be exposed to less of this energy and be capable of overcoming this pressurisation.

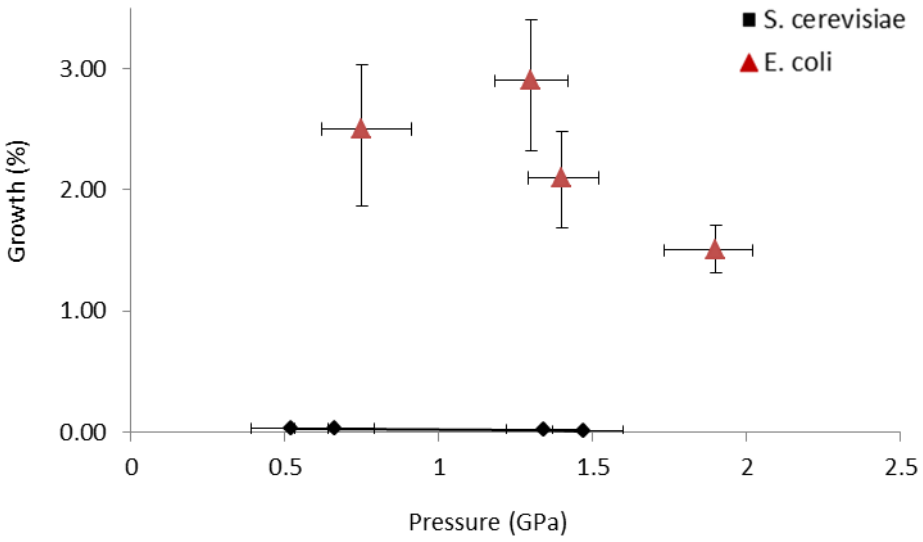

Figure 8.4 Colony growth rates of *E. coli* and *S. cerevisiae* with respect to pressure following dynamic loading with a 20 mm Al flyer plate.

8.6 Potential mechanisms for microbial survival

There are a number of mechanisms already known to be involved in the protection of *E. coli* and *S. cerevisiae* cells, allowing them to overcome natural stressors that exist in their environment. However, some of these are proposed in this section to potentially play a part in cell survival or death during shock loading.

a) Elasticity of the peptidoglycan layer in *E. coli*

The fact that *E. coli* were found to survive very high shock pressures during this project – and in others including, Leighs *et al*. and Hazell *et al*. [106, 120] – supports evidence of an elastic feature within the cell wall, allowing the cell to revert to its original shape after being distorted. This would explain the ability of *E. coli* to withstand shock pressures up to 10 GPa as well as high temperatures associated with it as explored in this thesis. As mentioned in Chapter 1, the single peptidoglycan layer of the cell wall in gram negative bacteria is elastic and this may therefore act as an absorber to shock loading. This implies that it may undergo temporary changes to its native structure, but return to its original form and allow the cell to keep growing. This has already been shown when exposing this organism to hydrostatic pressures. This mechanism is proposed to be involved in the survival of *E. coli*, and likely other gram-negative bacteria cell under shock pressures.

b) Response of the cell membrane to shock compression

The cell membrane for both prokaryotes and eukaryotes consists of a phospholipid bilayer. Additionally, some ion channels in the cell envelope of *E. coli* have been found to be sensitive to pressure [126]. These could be affected by gel phase transitions of the lipid bilayer shown in Figure 8.5. High pressures are known to cause these phase transitions in which the gel phase is essentially a ‘frozen’ phase [127, 128]. Here, permeability is reduced which inhibits ion transfer; this could be an explanation for why certain cell do not survive these high shock pressures.

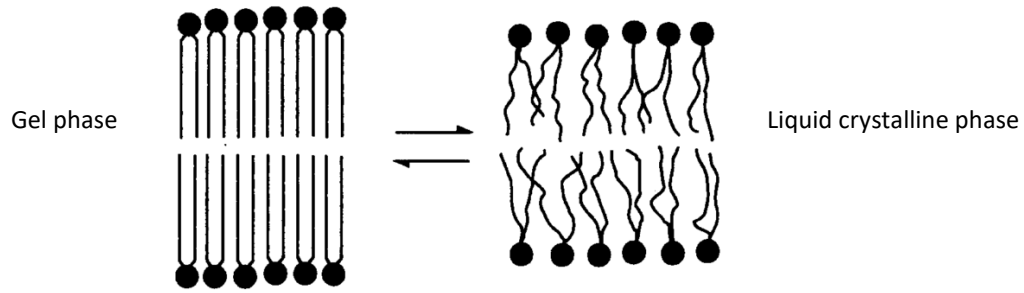

Figure 8.5 The gel phase vs the liquid crystalline phase in the cell membrane [128].

c) ‘Cushioning’ of the cells in a concentrated sample

Based on the results found using dilute sample concentrations for both *E. coli* and *S. cerevisiae*, the aforementioned ‘cushioning’ mechanism for higher growth rates has been suggested. It is presumed that given a higher concentration of cells, damage to an individual cell caused by the shock wave may be reduced as this energy would be dispersed amongst a higher number of cells, resulting in the higher growth rates recorded in this thesis.

8.6 Potential mechanisms of survival of *Artemia salina* larvae and cysts

As mentioned in the previous chapter, the mechanisms that control the survival of *Artemia salina* cysts under various stress conditions are not fully understood. Some proteins are already known to be involved in the response to UV radiation, anoxia and high temperature, but little is known about their response to physical stresses such as high pressure environments. Given the results that were discussed Chapter 7, there were very high survival rates in comparison to the application of multidimensional, uncontrolled shock waves.

Following these results, it may be postulated that there are particular proteins that might be involved in how the cyst shell may withstand pressure into the GPa range. Similarly to the *E. coli* and *S. cerevisiae*, although this was not investigated in this project, it is likely that filling the capsule with cysts, so that there is a high concentration of tightly packed cysts, may affect survival rates. In the same vein as the microorganisms, cysts in the centre of tightly packed cluster may demonstrate higher survival rates, the stress being applied across a larger number of cysts, meaning the strain on a single one is less and not enough to overcome the yield stress of the cyst shell.

There were a number of occurrences where breaking of the cyst shell would take place but there was no hatching of the larva – where the larva, or nauplius, would emerge from the inner hatching embryo. In some instances, the nauplius would partially emerge from the cell; a process that was also described by Trotman *et al.* [129]. In this article, *Artemia* cysts were treated with the crystalline salt potassium cyanide (KCN) which was said to expand the hatching embryo, but not kill the embryo. After this treatment, a partial emergence of the embryo occurred. Hatching was also delayed as a result. Treatment with cycloheximide also caused a delay in hatching and slowed locomotor activity. The behaviours described by these authors were also seen as a result of shock loading in this thesis, implying that similar processes within the cyst shell and the nauplius itself may be affected by both chemical treatment and dynamic pressure loading. In this paper, a suppression of osmosis by KCN between the medium and the hatching embryo was posited to impair the *Artemia* ability to hatch. This was because of the apparent importance of osmosis occurring across the permeable hatching membrane to sufficiently expand and rupture the cyst shell, allowing the embryo to emerge. A lack of osmotic expansion would prevent the embryo from hatching properly. If behaviour is similar under both chemical and mechanical stresses, the same biomolecules are likely to be affected, although this could occur in different ways. The results from the experiments in this project suggest the shock wave could damage the structure of the hatching membrane, affecting its permeability and inhibiting the

exchange of ions between the hatching membrane and surrounding medium. This is useful for future work and better understanding the mechanisms that control *Artemia* hatching and even movement to an extent.

The fact that *Artemia* has been shown to survive such high shock pressures, relative to the other multicellular organisms such as those found in the deep sea, implies that the nature of the shock wave front plays a very important role in the ability of an organism to survive shock pressures. This was proven by the comparison of the work carried out in this thesis and the previous studies involving uncontrolled shock waves.

8.7 Asteroid impact

A range of pressures have been discussed in the literature regarding asteroid impact onto planetary bodies; this includes hypervelocity impactors such as gabbro and ice, which have been calculated to reach pressures of 540 and 506 GPa following impact velocities of 20 and 30 km s^{-1}, respectively [130]. Even the launching of ejecta as a result of asteroid impact has been calculated to reach pressures of ~ 70 GPa [130]. The relevance of the studies carried out in this project to asteroid impact is that a better understanding of the pressures that microorganisms, both eukaryotic and prokaryotic, can withstand has been achieved. Different types of dynamic loading and pulse duration were explored in this thesis while primarily keeping pressure as the main factor affecting colony growth. The same can also be said of *Artemia salina* which was explored under quasi-one-dimensional loading for the first time and have shown that even multicellular organisms can survive shock pressures extending to the GPa range.

Although the highest pressure reached during this project was 10 GPa with the use of Cu capsules, the likelihood that the organisms studied in this thesis may survive asteroid impact would depend on a number of factors; these of course include the peak pressure, high temperature and the length of exposure to this high pressure and

temperature. Additionally, as was shown during this project, their survival may also depend on how high the concentration of the cell population is, since this could potentially offer protection for cells even existing on, or within, meteoritic bodies.

8.8 Summary

The results presented in this thesis demonstrate the robustness of a variety of organisms to shock pressure loading. A number of features of shock response mechanisms were suggested to explain the results seen in *E. coli*, *S. cerevisiae* and *Artemia salina*. The mechanics of the *E. coli* and *S. cerevisiae* cell wall were considered first. The findings in this chapter illustrate the response of each organism to shock pressure loading. When comparing growth rates of yeast and bacteria, the former was generally found to show higher survival rates than the yeast, implying that the cell wall may more robust than that of *E. coli* to offer greater protection against compression.

9 Conclusions

A number of conclusions may be drawn from the results of this thesis. The initial aims were to interrogate the possibility of panspermia by gaining a better understanding of how organisms belonging to different orders of life, and with varying levels of structural complexity, might respond to shock pressures. In order to successfully undergo panspermia, each organism examined throughout this research – *E. coli*, *S. cerevisiae* and *Artemia salina* – has demonstrated some form of unique behaviour (relative to the other organisms studied in this project) as a result of one or more types of quasi-one-dimensional shock loading. This has led to the proposal of two mechanisms – already known to play a role in hydrostatic pressure loading of microorganisms – having some involvement in the growth rates seen in this investigation. The third mechanism was suggested in response to abnormal microbial growth rates in the low pressure regime. In an attempt to explore how a vastly different and more complex organism responds to the same form of dynamic compression, the multicellular organism *Artemia salina* was also investigated.

It was also of interest to this study to explore a method of controlling temperature during shock loading to allow the effects of shock to be explored to higher pressure regimes. The way in which this was carried out was with the use of a novel type of graded areal density flyer plate called Surfi-Sculpt®. In addition to observing the effects on organisms post-shock, it was of great interest to determine what was occurring inside the Teflon® liner during the shock. The use of hydrocode models provided useful information as to the shape of the wave front inside the capsule and, backed by temperature gauge data, gave a good approximation as to the peak temperature experienced by the sample during the shock. In this manner this research has also provided a unique high pressure and strain-rate loading technique for such

microbial / organic systems. Key conclusions for the different organisms considered were as follows:

Unicellular organisms *Escherichia coli* NCTC 10538 and *Saccharomyces cerevisiae* ATCC 18824:

d) The mechanisms for cell death and survival proposed in Chapter 8 were determined to offer viable explanations for the results seen in each set of shock experiments.

e) *E. coli* were shock loaded to 10 GPa using a quasi-one-dimensional shock loading method. Given the controlled nature of these shock experiments, the survival of *E. coli* at this pressure could be attributed to the dynamic loading technique and the quasi-one-dimensional shock wave (where high temperatures were not a factor for lower velocity shots).

f) Although *S. cerevisiae* was not tested to 10 GPa, it showed generally higher growth rates than *E. coli*, which could lead to further investigations into the strength of the cell wall of both of these organisms and exactly what shock conditions they may survive, including high temperature.

The multicellular organism *Artemia salina*:

- *Artemia salina* cysts and nauplii were shock loaded to a maximum pressure of 1.5 GPa, with little to no motility for the nauplii at this pressure, but with hatching still occurring at 18%. This contrasts with static pressure work carried out previously, showing survival and hatching rates of ~ 80%. The current study also yielded higher hatching rates than previous results that utilised multi-dimensional shock wave loading.

- The results highlight the importance of the shape of the shockwave front and the affect it can have on the external structure of an organism.
- Since it is a multicellular organism that would generally be considered incapable of tolerating pressures into the GPa range, the results show that *Artemia salina* is more robust than previously thought. Further investigation into how it responds mechanically to shock compression must still be elucidated. Atomic force microscopy (AFM) and experiments in shock loading *Artemia salina* cysts to higher pressures could provide such information.

Novel method of exploring temperature control during shock compression:

- The use of the Surfi-Sculpt® flyer plates offered a projectile produced using a novel protocol to create adiabatic loading in its target. While there were inherent errors in the design of these flyer plates, they were shown to influence temperature while still meeting shock pressures produced by a planar counterpart. This was proven through control experiments as well as with the experiments on *E. coli*.
- The difference in temperatures produced through the Al and Cu capsules between the Surfi-Sculpt® and planar flyer plates were minimal, though a distinction was clear between the temperatures produced, as well as the type of wave moving through the target at lower pressures.
- At higher pressures of ≤ 3.6 GPa, the difference in temperature between the two flyer types was lessened. Equally, at faster impact velocities, the ramp wave for the Surfi-Sculpt® flyer became less obvious, revealing a shock profile more similar to that of the planar flyer. This could be explained by wavelets coalescing more quickly in the target material with a faster velocity. Since the spikes protruding from the front surface of the Surfi-Sculpt® flyers were quite small and displayed a degree of variance in length across the surface, it is likely

that flyers with larger and more controlled protrusions would exhibit larger differences in temperature and a more obvious ramp wave with respect to the planar flyer.

- This type of flyer also has the potential to allow ice phases that may be produced during shock loading to be explored by keeping temperatures below a certain threshold.
- The flyers may be used to precisely control temperature during shock experiments in the future. However, these would be improved with longer spikes on the surface to encourage more ramped waves.

Panspermia and asteroid impact pressures:

- While the asteroid impact pressures could not be replicated using the equipment available during this investigation, the highest shock pressure reached during these experiments was 10 GPa, to which *E. coli* showed a colony growth rate of 0.09%. If one-dimensional shock pressures reaching the asteroid impact regime could be reached, it is likely that both *E. coli* and *S. cerevisiae* survival, given previous work described in the literature.
- By further investigating microbes in the conditions surrounding asteroid impact, including extremely high temperatures, the investigation of panspermia and the possibility of the origins of life occurring outside of this planet could be furthered.

References

[1] Wang, A., Feldman, W. C., Mellon, M. T. and Zheng, M. (2013) ‘The preservation of subsurface sulfates with mid-to-high degree of hydration in equatorial regions on Mars’, Icarus, 226(1), pp. 980–991. doi: 10.1016/j.icarus.2013.07.020.

[2] Mileikowsky, C., Cucinotta, F., Wilson, J. W., Gladman, B., Horneck, G., Lindegren, L., Melosh, J., Rickman, H., Valtonen, M. and Zheng, J. Q. (2000) ‘Risks threatening viable transfer of microbes between bodies in our solar system’, Planetary and Space Science, 48, pp. 1107–1115. doi: 10.1016/S0032-0633(00)00085-4.

[3] Gladman, B. J., Burns, J. A., Duncan, M., Lee, P. and Levison, H. F. (1996) ‘The exchange of impact ejecta between terrestrial planets’, Science, 271(5254), pp. 1387–1392. doi: 10.1126/science.271.5254.1387.

[4] Mileikowsky, C., Cucinotta, F. A., Wilson, J. W., Gladman, B., Horneck, G., Lindegren, L., Melosh, J., Rickman, H., Valtonen, M. and Zheng, J. Q. (2000) ‘Natural Transfer of Viable Microbes in Space: 1. From Mars to Earth and Earth to Mars’, Icarus, 145(2), pp. 391–427. doi: 10.1006/icar.1999.6317.

[5] Lingam, M. and Loeb, A. (2018) ‘Implications of Captured Interstellar Objects for Panspermia and Extraterrestrial Life’, The Astrophysical Journal, pp. 1–10. arXiv:1801.10254v2.

[6] Melosh, H. J. (1988) ‘The rocky road to panspermia’, Nature, 332(6166), pp. 687–688. Available at: http://dx.doi.org/10.1038/332687a0.

[7] Rankine, W. J. M. (1869) ‘On the Thermodynamic Theory of Waves of Finite Longitudinal Disturbance’, Proceedings of the Royal Society of London, 18, pp. 80–83. Available at: http://www.jstor.org/stable/112718.

[8] Hugoniot, H. (1998) ‘On the Propagation of Motion in Bodies and in Perfect Gases in Particular — I BT’, in Johnson, J. N. and Chéret, R. (eds) Classic Papers in Shock Compression Science. New York, NY: Springer New York, pp. 161–243. doi: 10.1007/978-1-4612-2218-7_7.

[9] Hugoniot, H. (1998) ‘On the Propagation of Motion in Bodies and in Perfect Gases in Particular — II BT’, in Johnson, J. N. and Chéret, R. (eds) Classic Papers in Shock Compression Science. New York, NY: Springer New York, pp. 245–360. doi: 10.1007/978-1-4612-2218-7_8.

[10] Bourne, N. (2013) Materials in Mechanical Extremes: Fundamentals and Applications. New York: Cambridge University Press.

[11] Nellis, W. J. (2006) ‘Dynamic compression of materials: metallization of fluid hydrogen at high pressures’, Reports on Progress in Physics, 69(5), p. 1479. Available at: http://stacks.iop.org/0034-4885/69/i=5/a=R05.

[12] Meyers, M. A. (1994) Dynamic behavior of materials. New York: John Wiley & Sons.

[13] Ahrens, T. J. (1993) ‘Equation of State’, in Asay, J. R. and Shahinpoor, M. (eds) High-Pressure Shock Compression of Solids. 1st edn. New York: Springer-Verlag, pp. 75–113. doi: 10.1007/978-1-4612-0911-9_4.

[14] Miller, S. L. (1953) ‘A production of amino acids under possible primitive earth conditions’, Science, 117(3046), pp. 528–529.

[15] Madigan, M., Martinko, J., Stahl, D. and Clark, D. (2012) Brock Biology of Microorganisms. 13th edn. Benjamin Cummings (Brock Biology of Microorganisms). Available at: https://books.google.co.uk/books?id=RawZTwEACAAJ.

[16] Bennion, B. J. and Daggett, V. (2003) ‘The molecular basis for the chemical denaturation of proteins by urea’, Proceedings of the National Academy of Sciences, 100(9), pp. 5142–5147.

[17] Aertsen, A., Houdt, R. Van, Vanoirbeek, K. and Michiels, C. W. (2004) ‘An SOS response induced by high pressure in *Escherichia coli*’, Journal of Bacteriology, 186(18), pp. 6133–6141. doi: 10.1128/JB.186.18.6133.

[18] Considine, K. M., Kelly, A. L., Fitzgerald, G. F., Hill, C. and Sleator, R. D. (2008) ‘High-pressure processing - Effects on microbial food safety and food quality’, FEMS Microbiology Letters, 281(1), pp. 1–9. doi: 10.1111/j.1574-6968.2008.01084.x.

[19] Price, M. C., Solscheid, C., Burchell, M. J., Josse, L., Adamek, N. and Cole, M. J. (2013) ‘Survival of yeast spores in hypervelocity impact events up to velocities of 7.4kms-1’, Icarus. Elsevier Inc., 222(1), pp. 263–272. doi: 10.1016/j.icarus.2012.10.035.

[20] Pradillon, F., Shillito, B., Chervin, J.-C., Hamel, G. and Gaill, F. (2004) ‘Pressure Vessels for in vivo Studies of Deep-Sea Fauna’, High Pressure Research, 24(772812103), pp. 237–246. doi: 10.1080/08957950410001699818.

[21] Romanowicz, B. and Dziewonski, A. (eds) (2015) Treatise on Geophysics, Volume 1: Deep Earth Seismology. 2nd edn. Amsterdam: Elsevier. Available at: https://books.google.co.uk/books?id=Rg6dBAAAQBAJ&printsec=frontcover&source=gbs_ge_summary_r&cad=0#v=onepage&q=DAC&f=false.

[22] Orlikowski, D., Nguyen, J. H., Patterson, J. R., Minich, R., Martin, L. P. and Holmes, N. C. (2007) ‘New experimental capabilities and theoretical insights of high pressure compression waves’, AIP Conference Proceedings, 955, pp. 1186–1191. doi: 10.1063/1.2832932.

[23] Winter, R. E., Cotton, M., Harris, E. J., Chapman, D. J. and Eakins, D. (2014) ‘A novel graded density impactor’, Journal of Physics: Conference Series, 500(14), p. 142034. doi: 10.1088/1742-6596/500/14/142034.

[24] Taylor, P., Goff, M., Hazell, P. J., Leighs, J. A., Wood, D. and Appleby-Thomas, G. J. (2014) ‘Ramp wave generation using graded areal density ceramic flyers and the plate impact technique’, Journal of Physics: Conference Series, 500(14), p. 142016. doi: 10.1088/1742-6596/500/14/142016.

[25] Winter, R. E., Cotton, M., Harris, E. J., Chapman, D. J. and Eakins, D. (2015) ‘Generation of ramp waves using variable areal density flyers’, Shock Waves. doi: 10.1007/s00193-015-0558-3.

[26] Setchell, R. (1981) ‘Ramp-wave initiation of granular explosives’, Combustion and Flame, 43, pp. 255–264. doi: 10.1016/0010-2180(81)90025-0.

[27] Goff, M., Hazell, P. J., Appleby-Thomas, G. J., Wood, D. C., Stennett, C. and Taylor, P. (2015) ‘Gas gun ramp loading of Kel-F 81 targets using a ceramic graded areal density flyer system’, International Journal of Impact Engineering. Elsevier Ltd, 80, pp. 152–161. doi: 10.1016/j.ijimpeng.2015.02.010.

[28] Nellis, W. J. (2007) ‘Adiabat-reduced isotherms at 100 GPa pressures’, High Pressure Research, 27(4), pp. 393–407. doi: 10.1080/08957950701659734.

[29] Ray, A. and Menon, S. V. G. (2011) ‘Hydrodynamic simulation and thermodynamic characterization of functionally graded material induced isentropic compression: Towards optimum density profile’, Journal of Applied Physics, 110(2). doi: 10.1063/1.3606406.

[30] Boehler, R. and Kennedy, G. C. (1980) ‘Equation of state of sodium chloride up to 32 kbar and 500°C†’, Journal of Physics and Chemistry of Solids. Pergamon, 41(5), pp. 517–523. doi: 10.1016/0022-3697(80)90183-3.

[31] Picard, A., Testemale, D., Wagenknecht, L., Hazael, R. and Daniel, I. (2014) ‘Iron reduction by the deep-sea bacterium *Shewanella profunda* LT13a under subsurface pressure and temperature conditions’, Frontiers in Microbiology, 5(DEC), pp. 1–8. doi: 10.3389/fmicb.2014.00796.

[32] Hazael, R., Foglia, F., Kardzhaliyska, L., Daniel, I., Meersman, F. and McMillan, P. (2014) ‘Laboratory investigation of high pressure survival in *Shewanella oneidensis* MR-1 into the gigapascal pressure range.’, Frontiers in microbiology, 5(November), p. 612. doi: 10.3389/fmicb.2014.00612.

[33] Hazael, R., Meersman, F., Ono, F. and McMillan, P. (2016) ‘Pressure as a Limiting Factor for Life’, Life, 6(3), p. 34. doi: 10.3390/life6030034.

[34] Lawson, A. W. and Tang, T.-Y. (1950) ‘A Diamond Bomb for Obtaining Powder Pictures at High Pressures’, Review of Scientific Instruments, 21(9), pp. 815–817.

[35] Ferraro, J. R. (2012) Vibrational Spectroscopy At High External Pressures: The Diamond Anvil Cell. Orlando: Academic Press, Inc. Available at: https://books.google.co.uk/books?id=qDuYOZGe2MYC&printsec=frontcover&dq=Diamond+anvil+cell&hl=en&sa=X&redir_esc=y#v=onepage&q=Diamond anvil cell&f=false.

[36] M Kuwayama, Y., Hirosea, K., Sata, N. and Ohishic, Y. (2008) ‘Phase relations of iron and iron–nickel alloys up to 300 GPa: Implications for composition and structure of the Earth’s inner core’, Earth and Planetary Science Letters, 273(3–4), pp. 379–385.

[37] Oger, P. M., Daniel, I. and Picard, A. (2006) ‘Development of a low-pressure diamond anvil cell and analytical tools to monitor microbial activities in situ under controlled P and T’, Biochimica et Biophysica Acta - Proteins and Proteomics, 1764(3), pp. 434–442. doi: 10.1016/j.bbapap.2005.11.009.

[38] Davison, L. (2008) Fundamentals of Shock Wave Propagation in Solids. 1st edn. Berlin: Springer-Verlag (Shock Wave and High Pressure Phenomena). Available at: https://books.google.co.uk/books?id=dl4lQUWIRq8C.

[39] Antoun, T., Seaman, L., Curran, D. R., Kanel, G. I., Razorenov, S. V and Utkin, A. V (2006) Spall Fracture. Springer New York (Shock Wave and High Pressure Phenomena). Available at: https://books.google.co.uk/books?id=RdARBwAAQBAJ.

[40] Udagawa, Y. and Suzuki, M. (2015) ‘Effects of each operating condition on the underwater shock waves driven by imploding detonation and microorganism treatment experiments’, Journal of Thermal Science and Technology, 10(1), pp. 1–11. doi: 10.1299/jtst.2015jtst00.

[41] Udagawa, Y. and Suzuki, M. (2013) ‘A Study on Treatment of Microorganisms Using Underwater Shock Waves by Gas Imploding Detonation’, Transactions of the JSME, 79, pp. 2818–2825.

[42] Udagawa, Y. and Suzuki, M. (2013) ‘Effects of Underwater Shock Waves on *Artemia salina* (Basic Study on Microorganisms Treatment Technology Using Underwater Shock Waves)’, Transactions of the Japan Society of Mechanical Engineers, 79(801), pp. 804–808.

[43] Ogden, J. A., Tóth-Kischkat, A. and Schultheiss, R. (2001) ‘Principles of shock wave therapy.’, Clinical Orthopaedics and Related Research, (387), pp. 8–17. doi: 10.1097/00003086-200106000-00003.

[44] Worle, K., Steinbach, P. and Hofstadter, F. (1994) ‘The combined effects of high-energy shock waves and cytostatic drugs or cytokines on human bladder cancer cells’, British Journal of Cancer, 69(1), pp. 58–65. Available at: http://www.ncbi.nlm.nih.gov/entrez/query.fcgi?cmd=Retrieve&db=PubMed&dopt=Citation&list_uids=8286211.

[45] Coleman, A. J. and Saunders, J. E. (1993) ‘A review of the physical properties and biological effects of the high amplitude acoustic fields used in extracorporeal lithotripsy’, Ultrasonics, 31(2), pp. 75–89. doi: 10.1016/0041-624X(93)90037-Z.

[46] Boustie, M., Berthe, L., de Resseguier, T. and Arrigoni, M. (2008) ‘Laser shock waves: fundamentals and applications’, 1st International Symposium on Laser Ultrasonics Proceedings, pp. 1–6. Available at: http://www.ndt.net/article/laser-ut2008/papers/Boustie LU2008.pdf.

[47] Stafe, M., Marcu, A. and Puscas, N. (2014) Pulsed Laser Ablation of Solids: Basics, Theory and Applications. Heidelberg: Springer Science & Business Media.

[48] Paisley, D. L., Luo, S.-N., Greenfield, S. R. and Koskelo, A. C. (2008) ‘Laser-launched flyer plate and confined laser ablation for shock wave loading: validation and

applications.', The Review of Scientific Instruments, 79(2 Pt 1), p. 023902. doi: 10.1063/1.2839399.

[49] Lorenz, K. T., Edwards, M. J., Jankowski, A. F., Pollaine, S. M., Smith, R. F. and Remington, B. A. (2006) 'High pressure, quasi-isentropic compression experiments on the Omega laser', High Energy Density Physics, 2(3–4), pp. 113–125. doi: 10.1016/j.hedp.2006.08.001.

[50] Bourne, N. K. (2003) 'A 50mm bore gas gun for dynamic loading of materials and structures', Measurement science and technology, 14, pp. 273–278.

[51] Kinslow, R. (2012) High-Velocity Impact Phenomena. Elsevier Science. Available at: https://books.google.co.uk/books?id=6xxQGm5lb2wC.

[52] Seiler, F. and Igra, O. (2016) Hypervelocity Launchers. Springer International Publishing (Shock Wave Science and Technology Reference Library). Available at: https://books.google.co.uk/books?id=6zmFCwAAQBAJ.

[53] Chhabildas, L. C., Davison, L. and Horie, Y. (2006) High-Pressure Shock Compression of Solids VIII: The Science and Technology of High-Velocity Impact. Berlin: Springer Berlin Heidelberg (Shock Wave and High Pressure Phenomena). Available at: https://books.google.co.uk/books?id=U1vGYiL13dUC.

[54] Barker, L. M. and Hollenbach, R. E. (1972) 'Laser interferometer for measuring high velocities of any reflecting surface', Journal of Applied Physics, 43(1972), pp. 4669–4675. doi: 10.1063/1.1660986.

[55] Strand, O. T., Goosman, D. R., Martinez, C., Whitworth, T. L. and Kuhlow, W. W. (2005) 'A Novel System for High-Speed Velocimetry Using Heterodyne Techniques', Proceedings of SPIE - The International Society for Optical Engineering, 5580, pp. 593–599.

[56] Barker, L. M. (2008) ‘VISAR vs PDV’, Valynvisar.Com, (1), pp. 1–7. Available at: http://valynvisar.com/VISAR_vs_PDVLynn_M.pdf.

[57] Strand, O. T., Berzins, L. V, Goosman, D. R., Kuhlow, W. W., Sargis, P. D. and Whitworth, T. L. (2005) ‘Velocitimetry using heterodyne techniques’, SPIE Proceedings, 5580, pp. 593–599. doi: 10.1117/12.567579.

[58] Briggs, M. E., Hill, L., Hull, L. and Shinas, M. (2010) ‘Applications and Principles of Photon Doppler Velocimetry for Explosives Testing’, Proceedings of the14th International Detonation Symposium, 836(7106), pp. 1–12.

[59] Dolan, D. H. (2011) ‘Time-resolved diagnostics: Measurements of behaviour at high strain-rates’, in Time-resolved velocimetry in dynamic compression research: VISAR versus PDV (HetV). London: Imperial College London.

[60] Martins, Z., Price, M. C., Goldman, N., Sephton, M. a and Burchell, M. J. (2013) ‘Shock synthesis of amino acids from impacting cometary and icy planet surface analogues’, Nature Geoscience. Nature Publishing Group, 6(September), pp. 1045–1049. doi: 10.1038/ngeo1930.

[61] Bray, V. J., Collins, G. S., Morgan, J. V., Melosh, H. J. and Schenk, P. M. (2014) ‘Hydrocode simulation of ganymede and europa cratering trends - how thick is europa’s crust?’, Icarus. Elsevier Inc., 231, pp. 394–406. doi: 10.1016/j.icarus.2013.12.009.

[62] Benson, D. J. (1992) ‘Computational methods in Lagrangian and Eulerian hydrocodes’, Computer Methods in Applied Mechanics and Engineering, 99(2–3), pp. 235–394. doi: 10.1016/0045-7825(92)90042-I.

[63] Liu, G. R. and Liu, M. B. (2003) Smoothed Particle Hydrodynamics: A Meshfree Particle Method. World Scientific. Available at: https://books.google.co.uk/books?id=_cwFMmEQvZQC.

[64] Zukas, J. (2004) Introduction to Hydrocodes. Elsevier Science (Studies in Applied Mechanics). Available at: https://books.google.co.uk/books?id=qEisMAqkut0C.

[65] Melosh, H. J. (1984) 'Impact ejection, spallation, and the origin of meteorites', Icarus, 59, pp. 234–260. doi: 10.1016/0019-1035(84)90026-5.

[66] Ahrens, T. J. and O'Keefe, J. D. (1978) 'Energy and mass distributions of impact ejecta blankets on the moon and Mercury', in Lunar and Planetary Science Conference, 9th Houston, Texas. New York: Pergamon Press, Inc., pp. 3787–3802. doi: 10.1007/s13398-014-0173-7.2.

[67] Bridgman, P. W. (1914) 'The coagulation of albumen by pressure', J Biol Chem, 19, pp. 511–512. Available at: http://www.researchgate.net/profile/Alaa_Omar4/publication/258309726__/links/00b49527c04e1b3fb6000000.pdf (Accessed: 7 April 2015).

[68] Meersman, F. and McMillan, P. F. (2014) 'High hydrostatic pressure: a probing tool and a necessary parameter in biophysical chemistry.', Chemical communications (Cambridge, England), 50, pp. 766–75. doi: 10.1039/c3cc45844j.

[69] Meersman, F., Daniel, I., Bartlett, D. H., Winter, R., Hazael, R. and McMillan, P. F. (2013) 'High-Pressure Biochemistry and Biophysics', Reviews in Mineralogy and Geochemistry, 75(Kamekura 1998), pp. 607–648. doi: 10.2138/rmg.2013.75.19.

[70] Creighton, T. E. (1990) 'Protein folding.', Biochemical Journal, 270, pp. 1–16.

[71] Remmele, R. L., McMillan, P. and Bieber, A (1990) 'Raman spectroscopic studies of hen egg-white lysozyme at high temperatures and pressures.', Journal of protein chemistry, 9(4), pp. 475–486.

[72] Jane B. Reece, Lisa A. Urry, Michael L. Cain, Steven A. Wasserman, Peter V. Minorsky, R. B. J. (2011) Campbell Biology. 9th edition. Boston: Benjamin Cummings.

[73] Martin, W. F., Sousa, F. and Lane, N. (2014) ‘Energy at life’s origin’, Science, 344, pp. 1092–1093. doi: 10.1111/soru.12033.11.

[74] Johnstone, R. A. W. and Rose, M. E. (1996) Mass Spectrometry for Chemists and Biochemists. 2nd edn. Cambridge: Cambridge University Press. Available at: https://books.google.co.uk/books?id=k8o6E1BvVZEC&dq=mass+spectrometry,+LC-MS&source=gbs_navlinks_s.

[75] de Hoffmann, E. and Stroobant, V. (2007) Mass Spectrometry: Principles and Applications. 3rd edn. West Sussex: Wiley & Sons.

[76] Macko, S. A., Uhle, M. E., Engel, M. H. and Andrusevich, V. (1997) ‘Stable Nitrogen Isotope Analysis of Amino Acid Enantiomers by Gas Chromatography/Combustion/Isotope Ratio Mass Spectrometry’, Analytical Chemistry, 69, pp. 926–929.

[77] Wysocki, V. H., Resing, K. A., Zhang, Q. and Cheng, G. (2005) ‘Mass spectrometry of peptides and proteins’, Methods, 35(3 SPEC.ISS.), pp. 211–222. doi: 10.1016/j.ymeth.2004.08.013.

[78] Zea, L., Larsen, M., Estante, F., Qvortrup, K., Moeller, R., Dias de Oliveira, S., Stodieck, L. and Klaus, D. (2017) ‘Phenotypic Changes Exhibited by *E. coli* Cultured in Space’, Frontiers in Microbiology, 8(August), pp. 1–12. doi: 10.3389/fmicb.2017.01598.

[79] Marra, A., Asundi, J., Bartilson, M., Lawson, S., Fang, F., Christine, J., Wiesner, C., Brigham, D., Schneider, W. P. and Hromockyj, A. E. (2002) ‘Differential fluorescence induction analysis of *Streptococcus pneumoniae* identifies genes involved in pathogenesis.’, Infect. Immun., 70(3), pp. 1422–33. doi: 10.1128/IAI.70.3.1422.

[80] Erill, I., Campoy, S. and Barbé, J. (2007) ‘Aeons of distress: An evolutionary perspective on the bacterial SOS response’, FEMS Microbiology Reviews, 31(6), pp. 637–656. doi: 10.1111/j.1574-6976.2007.00082.x.

[81] Aertsen, A., Vanoirbeek, K., Spiegeleer, P. De, Sermon, J., Hauben, K., Farewell, A., Michiels, C. W. and Nystro, T. (2004) 'Heat Shock Protein-Mediated Resistance to High Hydrostatic Pressure in *Escherichia coli*', Applied and Environmental Microbiology, 70(5), pp. 2660–2666. doi: 10.1128/AEM.70.5.2660.

[82] Aertsen, A. and Michiels, C. W. (2005) 'Mrr instigates the SOS response after high pressure stress in *Escherichia coli*', Molecular Microbiology, 58(5), pp. 1381–1391. doi: 10.1111/j.1365-2958.2005.04903.x.

[83] Hauben, K. J., Bartlett, D. H., Soontjens, C. C., Cornelis, K., Wuytack, E. Y. and Michiels, C. W. (1997) '*Escherichia coli* mutants resistant to inactivation by high hydrostatic pressure.', Applied and environmental microbiology, 63(3), pp. 945–950.

[84] Horneck, G., Rettberg, P., Reitz, G., Wehner, J., Eschweiler, U., Strauch, K., Panitz, C., Starke, V. and Baumstark-Khan, C. (2001) 'Protection of bacterial spores in space, a contribution to the discussion on Panspermia', Origins of Life and Evolution of the Biosphere, 31(6), pp. 527–547. doi: 10.1023/A:1012746130771.

[85] Burchell, M. J., Mann, J. R. and Bunch, A. W. (2004) 'Survival of bacteria and spores under extreme shock pressures', Monthly Notices of the Royal Astronomical Society, 352, pp. 1273–1278. doi: 10.1111/j.1365-2966.2004.08015.x.

[86] Leighs, J. A., Hazell, P. J. and Appleby-Thomas, G. J. (2012) 'The effect of shock loading on the survival of plant seeds', Icarus. Academic Press, 220(1), pp. 23–28. doi: 10.1016/j.icarus.2012.04.015.

[87] Ahmadi, H., Mollazade, K., Khorshidi, J., Mohtasebi, S. S. and Rajabipour, A. (2009) 'Some Physical and Mechanical Properties of Fennel Seed (Foeniculum vulgare)', Journal of Agriculture Science, 1(1), pp. 66–75.

[88] Herák, D., Kabutey, A., Sedláček, A. and Gurdil, G. (2012) 'Mechanical behaviour of several layers of selected plant seeds under compression loading', Research in Agricultural Engineering, 58(1), pp. 24–29.

[89] Hazael, R., Fitzmaurice, B., Foglia, F., Appleby-Thomas, G. J. and McMillan, P. F. (2017) 'Bacterial survival following shock compression in the GigaPascal range', Icarus, 293, pp. 1–7.

[90] Nagayama, K., Mori, Y., Shimada, K. and Nakahara, M. (2002) 'Shock Hugoniot compression curve for water up to 1 GPa by using a compressed gas gun', Journal of Applied Physics, 91(1), pp. 476–482. doi: 10.1063/1.1421630.

[91] Dolan, D. H. and Gupta, Y. M. (2003) 'Time-dependent freezing of water under dynamic compression', Chemical Physics Letters, 374(5–6), pp. 608–612. doi: 10.1016/S0009-2614(03)00777-2.

[92] Sharma, A. (2002) 'Microbial Activity at Gigapascal Pressures', Science, 295(5559), pp. 1514–1516. doi: 10.1126/science.1068018.

[93] Luscher, C., Balasa, A., Fröhling, A., Ananta, E. and Knorr, D. (2004) 'Effect of high-pressure-induced ice I-to-ice III phase transitions on inactivation of *Listeria innocua* in frozen suspension', Applied and Environmental Microbiology, 70(7), pp. 4021–4029. doi: 10.1128/AEM.70.7.4021-4029.2004.

[94] Crovisier, J. and Bockelée-Morvan, D. (1999) 'Remote Observations of the Composition of Cometary Volatiles', Space Science Reviews, 90(1), pp. 19–32. doi: 10.1023/A:1005217224240.

[95] Ehrenfreund, P. and Charnley, S. B. (2000) 'Organic Molecules in the Interstellar Medium, Comets, and Meteorites: A Voyage from Dark Clouds to the Early Earth', Annual Review of Astronomy and Astrophysics, 38, pp. 427–483.

[96] Bockelée-Morvan, D., Lis, D. C., Wink, J. E., Despois, D., Crovisier, J., Bachiller, R., Benford, D. J., Biver, N., Colom, P., Davies, J. K., Gérard, E., Germain, B., Houde, M., Mehringer, D., Moreno, R., Paubert, G., Phillips, T. G. and Rauer, H. (2000) 'New molecules found in comet C / 1995 O1 (Hale-Bopp) Investigating the link between cometary and interstellar material', Astronomy and Astrophysics, 353, pp. 1101–1114.

[97] Baldwin, W. W. and Wegener, W. S. (1986) ‘Kinetics of gram-negative bacterial-cell elongation as measured by using the large rod lineola-longa’, Journal of Bacteriology, 166(2), pp. 435–438.

[98] Rojas, E., Theriot, J. a and Huang, K. C. (2014) ‘Response of *Escherichia coli* growth rate to osmotic shock.’, Proceedings of the National Academy of Sciences of the United States of America, 111(21), pp. 7807–12. doi: 10.1073/pnas.1402591111.

[99] Leighs, J. A., Appleby-Thomas, G. J., Stennett, C., Hameed, A., Wilgeroth, J. M. and Hazell, P. J. (2012) ‘A sealed capsule system for biological and liquid shock-recovery experiments’, Review of Scientific Instruments, 83(11), p. 115113. doi: 10.1063/1.4767901.

[100] Barsis, E., Williams, E. and Skoog, C. (1970) ‘Piezoresistivity coefficients in manganin’, Journal of applied physics, 41(13), pp. 5155–5162.

[101] Rosenberg, Z., Yaziv, D. and Partom, Y. (1980) ‘Calibration of foil-like manganin gauges in planar shock wave experiments’, Journal of Applied Physics, 51(7), pp. 3702–3705. doi: 10.1063/1.328155.

[102] ‘Bondable Resistance Temperature Sensors and Associated Circuitry TN-506-3’ (2010).

[103] Fitzmaurice, B. C., Appleby-Thomas, G. J., Painter, J. D., Ono, F., McMillan, P. F., Hazael, R. and Meersman, F. (2017) ‘Tolerance of *Artemia* to static and shock pressure loading’, Journal of Physics: Conference Series, 950(4). doi: 10.1088/1742-6596/950/4/042002.

[104] Tham, C. Y. (2005) ‘Reinforced concrete perforation and penetration simulation using AUTODYN-3D’, 41, pp. 1401–1410. doi: 10.1016/j.finel.2004.08.003.

[105] Rosenberg, Z. and Partom, Y. (1981) ‘Temperature measurement of shock-loaded polymethylmethacrylate with in-material nickel gauges’, Journal of Applied Physics, 52(10), pp. 6133–6136. doi: 10.1063/1.328510.

[106] Leighs, J. A., Appleby-Thomas, G. J., Wood, D. C., Goff, M. J., Hameed, A. and Hazell, P. J. (2014) ‘The bactericidal effect of shock waves’, Journal of Physics: Conference Series, 500(18), p. 182026. doi: 10.1088/1742-6596/500/18/182026.

[107] Gajardo, G. M. and Beardmore, J. A. (2012) ‘The brine shrimp *Artemia*: Adapted to critical life conditions’, Frontiers in Physiology, 3, pp. 1–8. doi: 10.3389/fphys.2012.00185.

[108] Grabner, M., Wieser, W. and Lackner, R. (1981) ‘The suitability of frozen and freeze-dried zooplankton as food for fish larvae: A biochemical test program’, Aquaculture, 26(1–2), pp. 85–94.

[109] Milhem, M. M., Al-Hiyasat, A. S. and Darmani, H. (2008) ‘Toxicity testing of restorative dental materials using brine shrimp larvae (*Artemia salina*).’, Journal of applied oral science: revista FOB, 16(4), pp. 297–301. doi: 10.1590/S1678-77572008000400013.

[110] Caldwell, G. S., Bentley, M. G. and Olive, P. J. W. (2003) ‘The use of a brine shrimp (*Artemia salina*) bioassay to assess the toxicity of diatom extracts and short chain aldehydes’, Toxicon, 42, pp. 301–306. doi: 10.1016/S0041-0101(03)00147-8.

[111] Beltrán-Pardo, E., Jönsson, K. I., Wojcik, A., Haghdoost, S., Harms-Ringdahl, M., Bermúdez-Cruz, R. M. and Bernal Villegas, J. E. (2013) ‘Effects of Ionizing Radiation on Embryos of the Tardigrade *Milnesium* cf. *tardigradum* at Different Stages of Development’, PLoS ONE, 8(9), pp. 1–6. doi: 10.1371/journal.pone.0072098.

[112] Jönsson, K. I., Rabbow, E., Schill, R. O., Harms-Ringdahl, M. and Rettberg, P. (2008) ‘Tardigrades survive exposure to space in low Earth orbit’, Current Biology, 18(17), pp. 729–731. doi: 10.1016/j.cub.2008.06.048.

[113] Price, M. C., Burchell, M. J. and Cole, M. J. (2011) 'Survival of the *tardigrade hypsibius dujardini* during hypervelocity impact events up to 3.23 km s-1.', 7(2), p. 651. Available at: http://dx.doi.org/10.1016/j.cryobiol.2015.12.003.

[114] Liu, Y.-L., Zhao, Y., Dai, Z.-M., Chen, H.-M. and Yang, W.-J. (2009) 'Formation of diapause cyst shell in brine shrimp, *Artemia parthenogenetica*, and its resistance role in environmental stresses', Journal of Biological Chemistry, 284(25), pp. 16931–16938. doi: 10.1074/jbc.M109.004051.

[115] Miller, D. and McLennan, A. G. (1988) 'The heat shock response of the cryptobiotic brine shrimp *Artemia*—I. A comparison of the thermotolerance of cysts and larvae', Journal of Thermal Biology, 13(3), pp. 119–123.

[116] Ono, F., Minami, K., Saigusa, M., Matshushima, Y., Mori, Y., Takarabe, K., Saini, N. L. and Yamashita, M. (2010) 'Life of *Artemia* under very high pressure', Journal of Chemistry and Physics of Solids, 71(8), pp. 1127–1130.

[117] Guidetti, R., Rizzo, A. M., Altiero, T. and Rebecchi, L. (2012) 'What can we learn from the toughest animals of the Earth? Water bears (tardigrades) as multicellular model organisms in order to perform scientific preparations for lunar exploration', Planetary and Space Science. Elsevier, 74(1), pp. 97–102. doi: 10.1016/j.pss.2012.05.021.

[118] Stabili, L., Miglietta, A. M. and Belmonte, G. (1999) 'Lysozyme-like and trypsin-like activities in the cysts of *Artemia franciscana* Kellog, 1906: Is there a passive immunity in a resting stage?', Journal of Experimental Marine Biology and Ecology, 237(2), pp. 291–303. doi: 10.1016/S0022-0981(99)00007-6.

[119] Morris, J. E. (1971) 'Hydration, its reversibility, and the beginning of development in the brine shrimp, *Artemia salina*', Comparative Biochemistry and Physiology Part A Physiology, 39(4), pp. 843–857.

[120] Hazell, P. J., Beveridge, C., Groves, K. and Appleby-Thomas, G. (2010) 'The shock compression of microorganism-loaded broths and emulsions: Experiments and simulations', International Journal of Impact Engineering. Elsevier Ltd, 37(4), pp. 433–440. doi: 10.1016/j.ijimpeng.2009.08.007.

[121] Salvadó, Z., Arroyo-López, F. N., Guillamón, J. M., Salazar, G., Querol, A. and Barrio, E. (2011) 'Temperature adaptation Markedly Determines evolution within the genus *Saccharomyces*', Applied and Environmental Microbiology, 77(7), pp. 2292–2302. doi: 10.1128/AEM.01861-10.

[122] Casadei, M., Mañas, P., Niven, G., Needs, E. and Mackey, B. M. (2002) 'Role of Membrane Fluidity in Pressure Resistance of *Escherichia coli* NCTC 8164', Applied and environmental microbiology, 68(12), pp. 5965–5972. doi: 10.1128/AEM.68.12.5965.

[123] Ranjard, L. and Richaume, A. (2001) 'Quantitative and qualitative microscale distribution of bacteria in soil', Research in Microbiology, 152(8), pp. 707–716. doi: 10.1016/S0923-2508(01)01251-7.

[124] Yao, X., Jericho, M., Pink, D. and Beveridge, T. (1999) 'Thickness and Elasticity of Gram-Negative Murein Sacculi Measured by Atomic Force Microscopy', Journal of Bacteriology, 181(22), pp. 6865–6875.

[125] Tuson, H. H., Auer, G. K., Renner, L. D., Hasebe, M., Salick, M., Crone, W. C., Gopinathan, A., Huang, K. C. and Weibel, D. B. (2013) 'Measuring the stiffness of bacterial cells from growth rates in hydrogels of tunable elasticity', 84(5), pp. 874–891. doi: 10.1111/j.1365-2958.2012.08063.x.Measuring.

[126] Martinac, B., Buechner, M., Delcour, A. H., Adler, J. and Kung, C. (1987) 'Pressure-sensitive ion channel in *Escherichia coli*', Proceedings of the National Academy of Sciences, 84(8), pp. 2297–2301. doi: 10.1073/pnas.84.8.2297.

[127] Lai, K., Wang, B., Zhang, Y. and Zhang, Y. (2012) ‘High pressure effect on phase transition behavior of lipid bilayers’, Physical Chemistry Chemical Physics, 14(16), p. 5744. doi: 10.1039/c2cp24140d.

[128] Eze, M. O. (1991) ‘Phase Transitions in Phospholipid bilayers: Lateral Phase Separations Play Vital Roles in Biomembranes’, Biochemical Education, 19(4), pp. 204–208.

[129] Trotman, C. N. A., Mansfield, B. C. and Tate, W. P. (1980) ‘Inhibition of emergence, hatching, and protein biosynthesis in embryonic *Artemia salina*’, Developmental Biology, 80(1), pp. 167–174. doi: 10.1016/0012-1606(80)90506-0.

[130] Willis, M. J., Ahrens, T. J., Bertani, L. E. and Nash, C. Z. (2006) ‘Bugbuster-survivability of living bacteria upon shock compression’, Earth and Planetary Science Letters, 247(3–4), pp. 185–196. doi: 10.1016/j.epsl.2006.03.054.

Appendices

Appendix A Temperature profiles

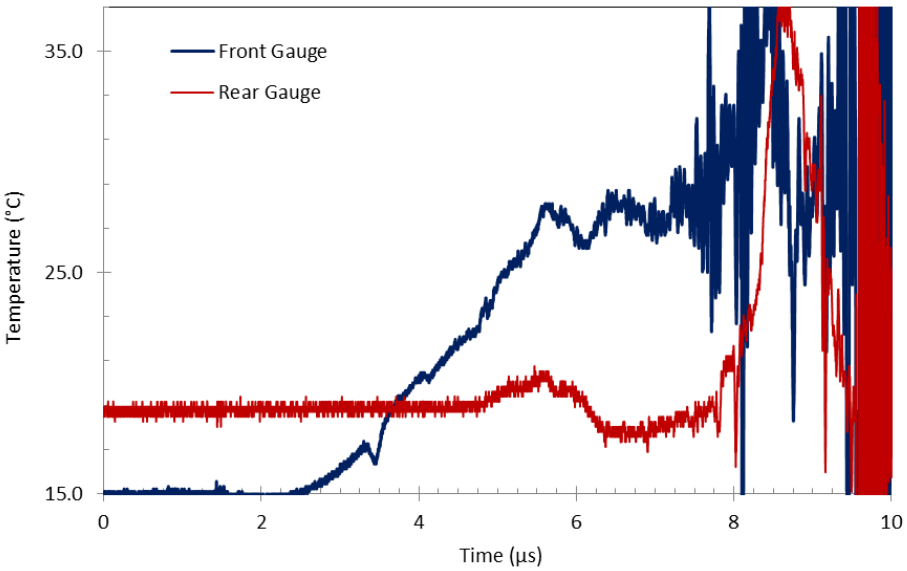

Figure A.1 Temperature profile for shot carried out at 190.91 m s^{-1}. Note that the starting temperature is equivalent to room temperature at the time of calibration. Calibration of the nickel gauges tended to cause slight heating of the gauges, hence the higher starting temperature of 18.7 °C for the rear gauge.

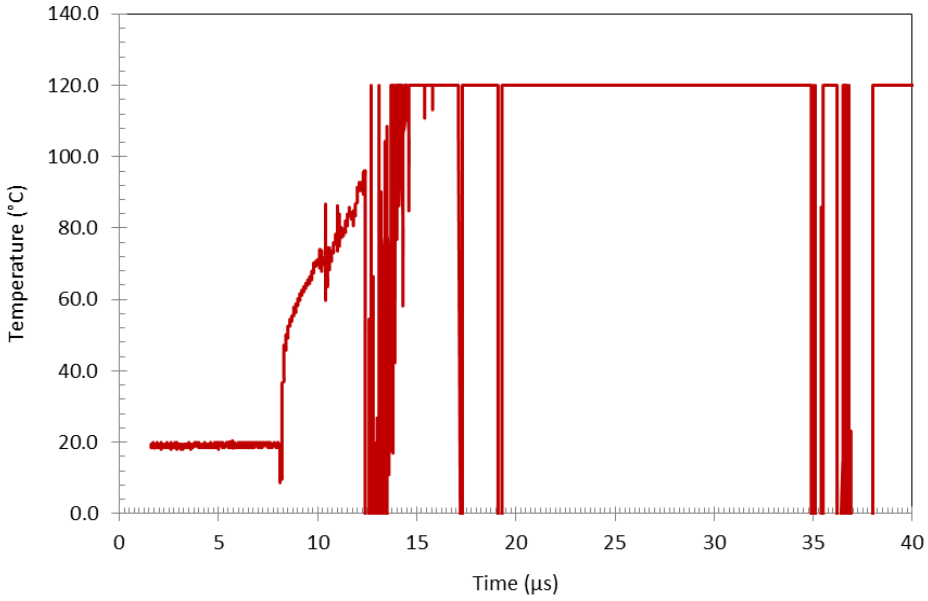

Figure A.2 Temperature profile for shot carried out at 463.39 m s^{-1}. This was the first shot carried out with a temperature gauge with just one gauge attached to a 10 mm Cu buffer plate.

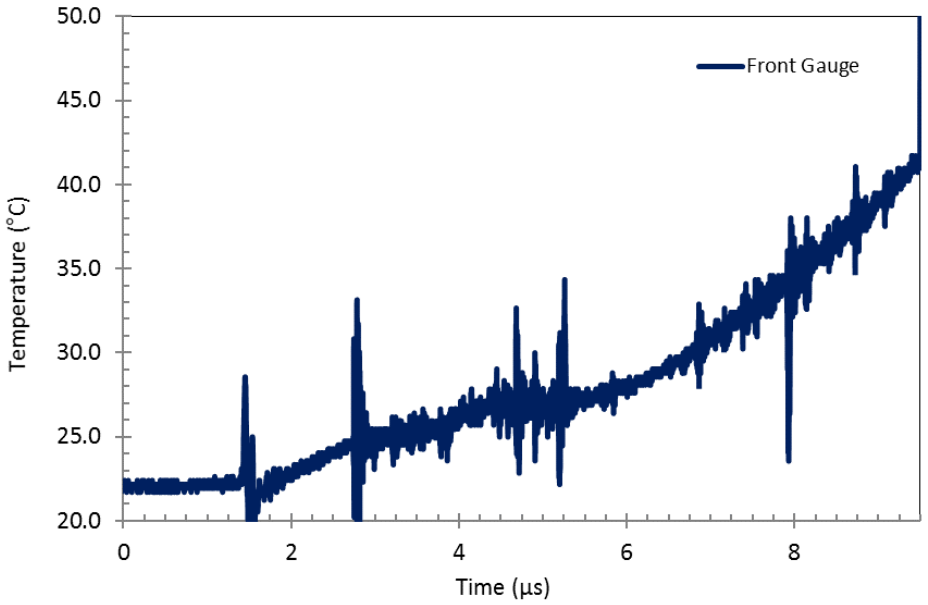

Figure A.3 Temperature profile for shot carried out at 403.55 m s^{-1}. This was the second test shot but it incorporated two nickel gauges on a 10 mm Cu target. The rear gauge failed before any trace was recorded, possibly due to interference from rarefaction waves from the free surface of the back plate of the target.

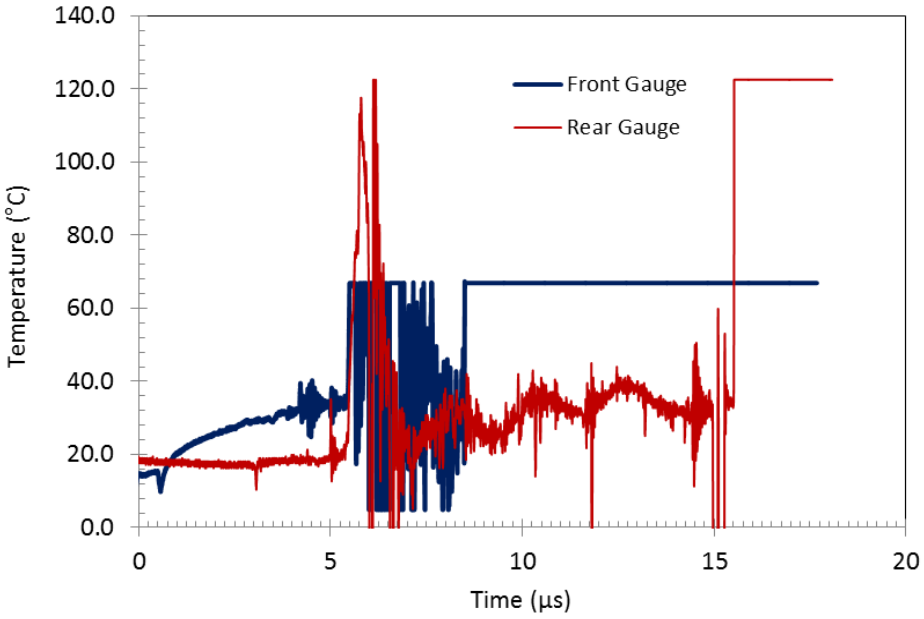

Figure A.4 Temperature profile for shot carried out at 266.09 m s^{-1}. An initial rise for the rear gauge was seen before it failed. It was then deemed necessary to use larger backing to prevent this and allow time for the temperature to reach equilibrium.

Appendix B Publications related to this thesis

B.1 Icarus – Bacterial survival following shock compression in the GigaPascal range

Icarus 293 (2017) 1–7

Contents lists available at ScienceDirect

Icarus

journal homepage: www.elsevier.com/locate/icarus

Bacterial survival following shock compression in the GigaPascal range

Rachael Hazael[a,c,*], Brianna C. Fitzmaurice[b], Fabrizia Foglia[a,d], Gareth J. Appleby-Thomas[b], Paul F McMillan[a]

[a] Christopher Ingold Laboratories, Department of Chemistry, University College London, London WC1H 0AJ, UK
[b] Centre for Defence Engineering, Cranfield University, Defence Academy of the United Kingdom, Shrivenham, SN6 8LA, UK
[c] Department of Earth Sciences, University College London, London WC1E 6BT
[d] Department of Chemical Engineering, Imperial College London, London SW7 2AZ, UK

ARTICLE INFO

Article history:
Received 6 June 2016
Revised 10 February 2017
Accepted 31 March 2017
Available online 2 April 2017

Keywords:
Impact process
Astrobiology
Earth
Experimental techniques

ABSTRACT

The possibility that life can exist within previously unconsidered habitats is causing us to expand our understanding of potential planetary biospheres. Significant populations of living organisms have been identified at depths extending up to several km below the Earth's surface; whereas laboratory experiments have shown that microbial species can survive following exposure to GigaPascal (GPa) pressures. Understanding the degree to which simple organisms such as microbes survive such extreme pressurization under static compression conditions is being actively investigated. The survival of bacteria under dynamic shock compression is also of interest. Such studies are being partly driven to test the hypothesis of potential transport of biological organisms between planetary systems. Shock compression is also of interest for the potential modification and sterilization of foodstuffs and agricultural products. Here we report the survival of *Shewanella oneidensis* bacteria exposed to dynamic (shock) compression. The samples examined included: (a) a "wild type" (WT) strain and (b) a "pressure adapted" (PA) population obtained by culturing survivors from static compression experiments to 750 MPa. Following exposure to peak shock pressures of 1.5 and 2.5 GPa the proportion of survivors was established as the number of colony forming units (CFU) present after recovery to ambient conditions. The data were compared with previous results in which the same bacterial samples were exposed to static pressurization to the same pressures, for 15 minutes each. The results indicate that shock compression leads to survival of a significantly greater proportion of both WT and PA organisms. The significantly shorter duration of the pressure pulse during the shock experiments (2–3 μs) likely contributes to the increased survival of the microbial species. One reason for this can involve the crossover from deformable to rigid solid-like mechanical relaxational behavior that occurs for bacterial cell walls on the order of seconds in the time-dependent strain rate.

1. Introduction

Life on Earth is traditionally considered to occupy a relatively narrow range of pressure (P-) and temperature (T-) conditions at or near the surface of our planet. However, sampling expeditions have demonstrated that life can exist under deep subsurface conditions, extending to several km below the oceanic and continental crust (Daly et al., 2016; Huber 2015; Inagaki et al., 2015; Anderson et al., 2013, Borgonie et al., 2011, Colwell and D'Hondt, 2013, Meersman et al., 2013; Picard and Daniel, 2013, Oger and Jebbar, 2010; Ono et al., 2010). It has also been suggested that the origins of life might lie at depth, associated with submarine volcanic activity (Lane and Martin, 2012). Laboratory studies have also demonstrated that microbes can survive even more extreme pressures extending to within the GigaPascal (GPa) range (Hazael et al., 2014; Kish et al., 2012; Griffin et al., 2012; Vanlint et al., 2011; Sharma et al., 2002), raising the possibility that organisms might exist within the deep interiors of colder planetary systems (Hazael et al., 2016; Vance et al., 2016). In addition to their relevance for Earth and planetary biology, studies of the survival of organisms have been conducted for the food industries, where the techniques of "Pascalization" *vs* "Pasteurization" can be applied to remove unwanted pathogens while maintaining color, texture, flavor and nutritional value (Demazeau and Rivalain, 2011).

Most investigations of microbial survival under extreme high pressure conditions have been conducted using static compression techniques, where the microbes are typically exposed to the pressure stress on timescales ranging from minutes to hours. However,

* Corresponding author.
E-mail addresses: rachael.hazael@ucl.ac.uk, r.hazael@ucl.ac.uk (R. Hazael), p.f.mcmillan@ucl.ac.uk (P.F. McMillan).

http://dx.doi.org/10.1016/j.icarus.2017.03.031
0019-1035/

other studies have focused on dynamic shock compression, where the pressure is applied as a pulse rising to a peak value on a much shorter timescale, on the order of tens of nanoseconds (ns), and is maintained within the sample for a few microseconds (μs), for example. Such studies are relevant to the possibility that organisms might have been transported between planetary bodies, giving rise to the potential phenomenon of "panspermia" (Melosh, 1988). That hypothesis presupposes that bacteria or other primitive life forms could survive the extreme environments of space trapped inside cometary or meteoritic bodies and then be delivered intact to the early Earth during an impact event (Howard et al., 2013; Paulino-Lima et al., 2010; Fajardo-Cavazos et al., 2009; Willis et al., 2006). Several pioneering studies have now investigated the survival of living microorganisms during the transient high-P,T conditions encountered during shock compression (Gruzielanek et al., 2010; Hazell et al., 2010; Horneck et al., 2008; Burchell et al., 2004; Burchell et al., 2001). These experiments have been conducted using light gas guns (Burchell et al., 1999) on various broths, spores and bacterial organisms to achieve peak pressures between 1–8 GPa (Price et al., 2013; Hazell et al., 2010; Hazell et al., 2009; Burchell et al., 2004; Burchell et al., 2001). Reported proportions of surviving colony-forming units (CFU) have been remarkably high (Fajardo-Cavazos et al., 2009), with survivors recorded following exposure to peak shock pressures as high as 78 GPa (Burchell et al., 2004).

Here we report results of the effects of dynamic shock compression on the survival of samples of *Shewanella oneidensis* following exposure to peak pressures of 1.5 and 2.5 GPa, using a target assembly designed to facilitate recovery of the bacterial cells, and also to maintain the temperatures developed during the shock compression as low as possible. The experiments were carried out using a light gas gun apparatus at the Shrivenham campus of Cranfield University, U.K., using bacterial strains developed at University College London (UCL). Previously we had investigated colony formation among survivor populations of this organism following static pressurization to pressures extending up to 2.5 GPa using a piston cylinder apparatus at UCL (Hazael et al., 2014). In our initial experiments in that work, colonies of bacteria were raised directly to the target pressure, retained at that value for 15 minutes, and then returned to ambient conditions for examination of the survival statistics. In further series of runs, bacteria were sequentially exposed to successively higher pressures, in pressure increments of 250 MPa. The survivors from each compression experiment were cultured and used to provide feedstock for the subsequent treatments at progressively higher pressures, resulting in increased survival rates for the "pressure adapted" (PA) or more pressure resistant members of the population. A similar protocol had been previously described in our work on *E. coli* by Vanlint et al. (2011). For the present shock compression study, we compared survival results for wild type (WT) and PA examples of *S. oneidensis,* shocked to peak pressures of 1.5 and 2.5 GPa. The PA samples had been developed from survivors that had previously been compressed to 750 MPa, following prior culturing of survivor populations at 250 and 500 MPa (Hazael et al., 2014). In this way we could directly compare the survival rates obtained in the shock compression study with the previous static compression results, for both WT and PA bacterial samples. The results provide new information about the bacterial response to dynamic *vs* static compression.

2. Materials and methods

Shewanella oneidensis MR-1 (CIP 106,686) was purchased from the Collection Institut Pasteur (Paris, France) (Venkateswaran et al., 1999) and samples were rehydrated in 200 µl of Luria-Bertani Miller (LB) medium. From this stock, 50 µl was used for a liquid culture in 10 ml of LB broth grown at 30 °C and 180 rpm, and two separate plate spreads of 50 µl provided stock solutions. For each experiment a 10 ml starter culture was inoculated either from plate or liquid stock. The bacteria were harvested in stationary phase at a concentration of 1×10^8 cells/ml. For each experiment a 1 ml aliquot of the starter culture was washed three times with phosphate buffered saline (PBS) solution adjusted to pH 7.2 to remove damaged and dead cells. The cells were then re-suspended in PBS for the experiments. These samples constituted the "wild type" (WT) specimens used in both the static and shock compression experiments.

For the static compression experiments described previously (Hazael et al., 2014), a Teflon® capsule was loaded with 6 µl of the bacterial suspension. An aliquot of this solution was plated to serve as a control sample. All microbiological preparations and sample handling were carried out under aseptic conditions. Compression experiments were carried out in a stepwise manner in a piston cylinder device, to reach final pressures of 1.5 and 2.5 GPa as reported in the previous publication (Hazael et al., 2014). Those results are quoted here to provide comparison points with the present shock compression data. In order to prepare "pressure adapted" (PA) samples for the shock compression runs, bacterial samples were exposed to static high pressures in 250 MPa steps up to 750 MPa, with survivors from each intermediate step recovered and cultured before being exposed to the next highest pressure. This generated the PA strain of *S. oneidensis* bacteria used in the shock compression runs (Hazael et al., 2014).

For shock experiments, the bacterial samples were contained within a Teflon® lined capsule placed inside a specially designed target assembly in order to carry out low velocity shock loading and recovery experiments (Leighs et al., 2012) (Fig. 1). The introduction of a Teflon® sleeve reduced pressure and temperature hotspots and aided uniform pressure wave generation within the sample. The shock studies were carried out using a 5 m length, 50 mm bore single stage gas gun to accelerate 5 mm thick Al flyer plates, with the final velocity measured just prior to impact. Measured impact velocities were 273 and 360 m/s leading to peak pressures of 1.5 and 2.5 GPa, respectively. While we were able to control the capsule system and the mass of our projectile, the fact that we relied on a release of gas to drive a piston into the projectile meant there could be some variation in impact velocity. Despite these slight variations in velocity, the overall effect on pressure was deemed negligible, according to results obtained using the hydrocode models. These peak pressures were calculated using ANSYS® Autodyn® (Autodyn 2012; Robertson et al., 1994), using the compressibility factor for pure water (45.8×10^{-11} Pa^{-1}) to model the compressional behavior of the bacterial suspensions (Table 1; Fig. 2). The validity of this assumption was tested by two impact experiments where the rear free surface of (a) water and (b) bacterial solution contained within identical capsules was monitored *via* heterodyne velocimetry (Het-V). This powerful technique uses Doppler shifted light reflected from the moving end of the target during the shock experiment to determine the particle velocity (u_P) as a function of the progress of the shock wave through the sample (Strand et al., 2006) (Fig 1). The Het-V traces for the bacterial suspension and pure H_2O were indistinguishable, indicating that our use of the water compressibility factor gives reliable results for the pressure and temperature profiles simulated using ANSYS® Autodyn® codes during the dynamic compression runs.

The designed target configuration led to a complex ramped loading path lying between the principal Hugoniot and the isentrope, yielding final state temperatures of 322 and 328 K, for samples shocked to 1.5 and 2.5 GPa respectively, determined by the simulations (Fig. 2; Table 1). We tested our simulation models against the plate impact studies of pure H_2O by Nagayama et al. (2002), using the target configurations and material parameters

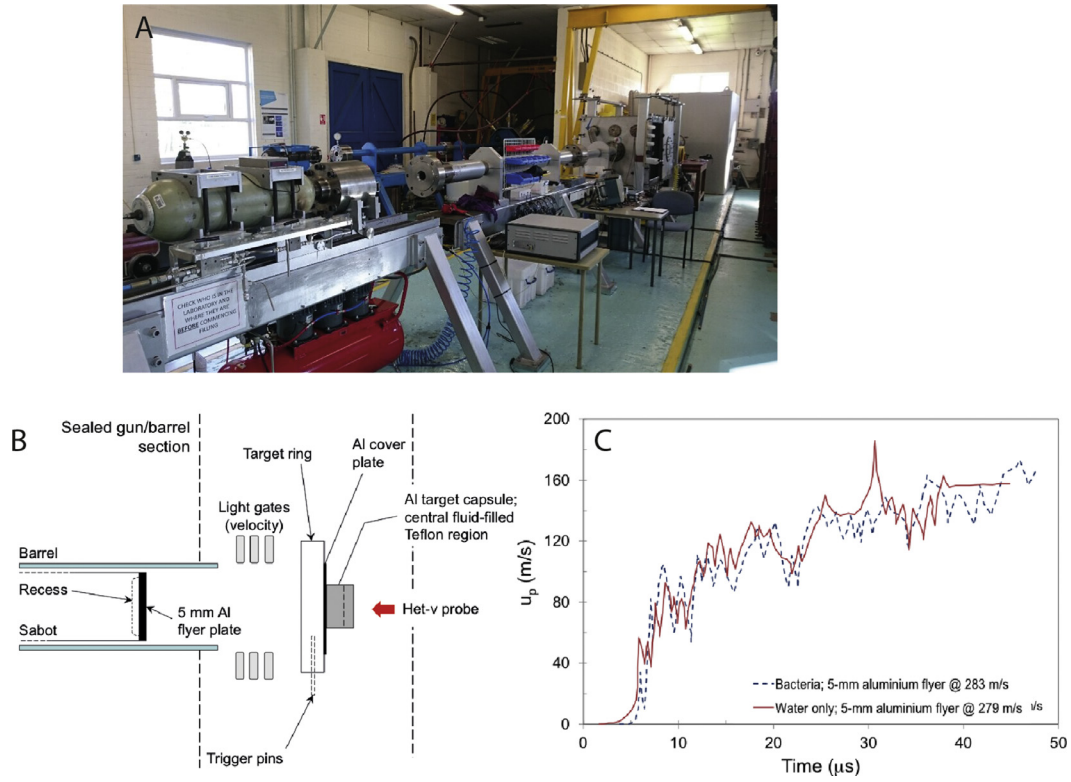

Fig. 1. Experimental details for the shock experiments. A. Photograph of the single stage gas gun and shock laboratory at Cranfield University. The sample target and recovery chamber is shown at the far end of the laboratory. The recovery chamber is packed with rags to ensure a "soft landing" for the target capsule containing the sample following the shock experiment. B. A schematic drawing of the target and flyer plate assembly used in these shock studies. Material parameters for the various components and used in ANSYS® Autodyn® simulations are provided in Table 1. C. Het-V traces comparing the evolution of the particle velocity, u_P *vs* time, for pure H_2O with that of a bacterial suspension. Both were impacted at 280 m/s to achieve a peak shock pressure of 1.5 GPa. The two systems show identical behavior with u_p asymptotically approaching a plateau near 150 m/s after approximately 25–30 μs.

Table 1
Materials and material properties used in the ANSYS® Autodyn® simulations. Impact velocities used were 273 and 360 ms^{-1} and achieved pressures of 1.5 and 2.5 GPa, respectively. Al 6061-T6 refers to an Al alloy with the highest tensile strength of the 6061 series of at least 290 MPa. [1]Taken from the Los Alamos Scientific Laboratory, Selected Hugoniots. LA-4167-MS, May 1969.

Material	Material properties					
	Density (g cm^{-3})	Strength model	Gruneisen coefficient	Thermal conductivity (J m^{-1} K^{-1} s^{-1})	Specific heat capacity (J kg^{-1} K^{-1})	Equation of State
Al 6061-T6	2.703	Steinberg-Guinan	1.97	247	885	Steinberg (1991)
Water	1.0	N/A	0.28	0.609	4.181×10^3	Nagayama et al. (2002)
Rubber	1.439	N/A	1.39	0.19	1.05×10^3	LA-4167-MS, 19,69[1]
Teflon	2.16	von Mises	0.9	0.25	1.05×10^3	Matuska (1984)

reported by these authors. Both results were in excellent agreement (with standard errors $\leq 5\%$) leading to a high level of confidence in our modelling procedures. The low temperatures developed during the shock experiments meant that thermal resistance of the bacteria was not an issue.

3. Results

Shock compression studies were carried out for WT and PA bacterial populations to peak pressures of 1.5 and 2.5 GPa. The results are compared in Fig. 3 and Table 2.

Our data clearly show that significantly larger numbers of survivors leading to colony forming units (CFU/ml) are recovered following shock compression compared with static pressurization to the same pressures for both WT and PA samples (Fig. 3). The difference in behavior is particularly striking for the 2.5 GPa experiments. At 2.5 GPa there were no recorded survivors for the WT static compression experiment (Hazael et al., 2014). This is in direct contrast to the dynamic compression study where we now observe approximately 3×10^4 CFU/ml survivors for the same WT sample. At 1.5 GPa, slightly more than 10^3 CFU/ml survivors are recorded for the static experiment, but dynamic shock compression leads to approximately 3×10^5 CFU/ml viable survivors to be recovered. For the PA population, both static and dynamic shock compression to 1.5 GPa leads to similar survival statistics with $5–7 \times 10^5$ CFU/ml recorded following both types of pressurization experiment. However, at 2.5 GPa, static compression resulted in only $\sim 10^4$ CFU/ml survival, whereas dynamic compression yielded $> 10^6$ CFU/ml among the survivor population (Fig. 3, Table 2).

4. Discussion

The survival rate found here for *S. oneidensis* subjected to shock compression at 2.5 GPa peak pressure is lower, by 1–2

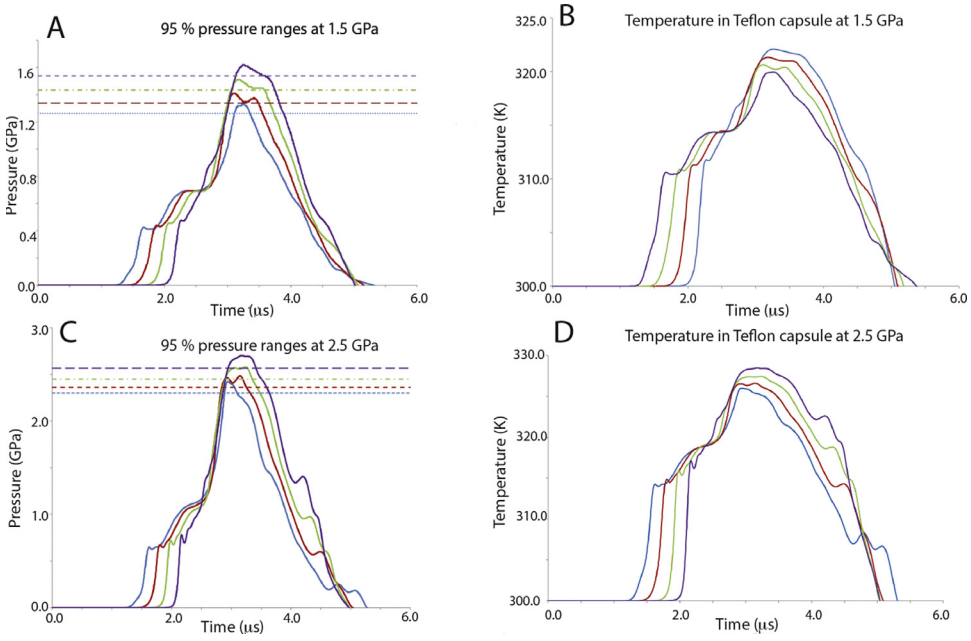

Fig. 2. Results of modelling experiments carried out to determine pressure and temperature conditions developed as a function of time during shock compression at 273 and 360 m/s using ANSYS® Autodyn® simulations. A. Calculated pressures developed within the sample as a function of time for a peak impact pressure of 1.5 GPa; B. Calculated temperatures developed within the sample at an impact pressure of 1.5 GPa; C. Calculated pressure-time trace for a shock with peak impact pressure of 2.5 GPa; D. Calculated T profile for an impact pressure of 2.5 GPa. Different coloured lines refer to different P,T profiles at different gauge points within the simulations, selected to estimate the range of P,T conditions developed at various points throughout the sample volume, and thus provide an estimate of the range of values that are expected to exist at various stages during the shock compression event.

Table 2
Results of bacterial survival expressed as the number of colony-forming units log (N) (as CFU/ml of suspended solution). All initial bacterial populations were 1×10^8 CFU/ml. [1]For the 1.5 GPa peak shock impacts a velocity matching technique was used to ensure identical peak pressures for both runs. For the 2.5 GPa shock runs, the flyer velocities varied slightly between different experiments.

	Static Compression			Shock Compression			
Sample	Pressure GPa	Survival CFU (N)	Log N (Average)	Peak Impact Pressure (GPa)	Flyer Velocity (ms^{-1})	Survival/ CFU (N)	Log (N)
WT Static	1.5	1.30, 1.32, 1.32×10^3	3.1				
WT Static	2.5	0, 0, 0	0				
PA Static	1.5	5, 6, 3×10^5	5.6				
PA Static	2.5	8,4,3 $\times 10^4$	4.1				
WT Shock				1.5 (+10.4/−9.4%)	273[1] (±1.7%)	3.14×10^5	5.4
WT vShock				2.5 (+6.1/−4.9%)	360 (±2.8%)	3.83×10^4	4.5
PA Shock Run 1				1.5 (+10.4/−9.4%)	273[1] (±1.7%)	6.6×10^5	5.8
PA Shock Run 2				1.5 (+10.4/−9.4%)	273[1] (±1.7%)	7.24×10^5	5.6
PA Shock Run 1				2.5 (+6.1/−4.9%)	354 (±1.7%)	1.93×10^6	6.2
PA Shock Run 2				2.5 (+6.1/−4.9%)	363 (±2.2%)	4.61×10^6	6.6

orders of magnitude, than that reported previously for a range of other organisms (Fajardo-Cavazos et al., 2009; Horneck et al., 2008; Burchell et al., 2004). However, several of those experiments used sporulating organisms, that can exhibit enhanced survival rates following exposure to applied mechanical stress (Fajardo-Cavazos et al., 2009; Horneck et al., 2008; Burchell et al., 2004). Burchell et al. (2004) examined an active sample of *Bacillus subtilis* as well as the non sporulating organism *Rhodococcus erythropolis,* and found greater survival rates for both samples than those found here for similar peak shock pressures. However, these authors noted that their experimental protocol might have produced uncertainties in the determined survival rates of up to 1–2 orders of magnitude, that could bring the 3 GPa data for *R. erythropolis* into general agreement with our present result for *S. oneidensis* at 2.5 GPa.

A main feature of our results reported here is that the PA population that had been cultured from survivors following previous exposure to progressively higher static pressures were more resistant than the WT species to dynamic compression, to higher peak shock pressures. That mimics the result found previously in our static pressurization experiments (Hazael et al., 2014), but the survival rates are considerably enhanced in the dynamic compression runs (Fig. 3, Table 2). In particular, bacterial survival following compression to 2.5 GPa is significantly greater in the shock experiments than found previously in static compression runs at the same pressure. We can examine some of the possible effects that could result in this markedly different behavior.

The different biochemical and microbiological factors affecting bacterial survival at high pressure are not yet understood (Meersman et al., 2013; Aertsen et al., 2004). Recent studies have suggested that the demise of microbes within the lower pressure range (up to 700–800 MPa) relevant to static compression protocols used in commercial Pascalization processes is related to formation, migration and expulsion of protein aggregates formed

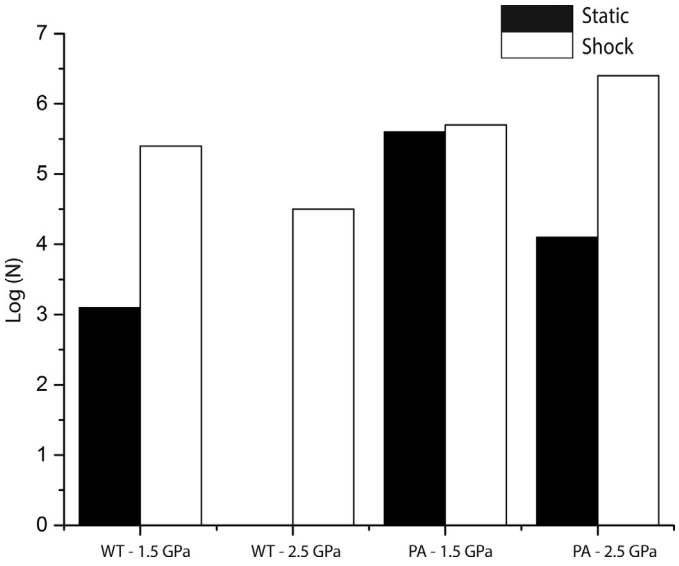

Fig. 3. Bar chart showing bacterial survival on a logarithmic scale (log (N)) with N as the number of colony forming units (CFU) per ml. These were established following recovery to ambient pressure relative to the initial concentrations (10^8 CFU/ml) for wild type (WT) and pressure adapted (PA) samples of *Shewanella oneidensis* following static (Hazael et al., 2014) *vs.* shock compression experiments (longer *vs.* shorted timescales). Note that no WT survivors could be cultured following static compression to 2.5 GPa (Hazael et al., 2014), although $\sim 3 \times 10^4$ CFU were counted following incubation of survivors following shock compression of the same WT sample to this peak pressure.

within the cells (Govers and Aertsen, 2015). However, the survival mechanisms that apply to bacteria exposed to pressures extending into the GPa range have not yet been examined in detail.

As a next step to begin to understand the differential effects of static *vs* shock pressurization on the bacterial survival, we should take account of the markedly different timescales of the static *vs* dynamic compression experiments, in relation to the mechanical and viscoelastic relaxation properties of the bacterial cell envelope. Understanding the mechanical behavior and time-dependent deformation behavior of living cells subjected to mechanical loading is becoming an important area in soft matter biophysics, with implications for medical and nanomaterials research (Bonakdar et al., 2016; Vadillo-Rodriguez and Dutcher, 2011, Fabry et al., 2001; Thwaites et al., 1991). Most living cells show a viscoelastic deformation response that follows a power law in time (Bonakdar et al., 2016; Fabry et al., 2001). Dynamic mechanical relaxation experiments and simulations carried out for bacteria indicate that the viscoelastic behaviour of the cell envelope passes from exhibiting a relaxed ("rubbery") response upon slower application of the mechanical stress to more solid-like ("glassy") behavior by increasing the speed of the applied stress, at a timescale of about ~1 s. During our dynamic compression experiments a planar shock wave was launched into the aqueous suspension medium with a peak pressure developing and persisting over a timescale of 2–3 μs (Fig. 2). That indicates that the cell walls of the *S. oneidensis* bacteria studied in our shock experiments should not deform elastically during passage of the shock wave, but instead behaved as a more rigid envelope. In that case, the biomolecular apparatus and fluids internal to the cells would not have experienced any significant effects due to compression, although protein complexes and other biomolecules located in the outer part of the membrane or external to the cell wall would be directly exposed to the shock compression conditions, and might be expected to have altered structures and functionality. On the other hand, the external cell wall could experience rupture due to the applied stress exceeding the fracture tolerance limit. Experiments have indicated that the tensile strength of bacteria is approximately 300 MPa with a Young's modulus on the order of 13 GPa (Thwaites et al., 1991). We note that the PA populations appear to have altered characteristics, including the external shape and size of the bacteria (R. Hazael, P.F McMillan et al, in prep). Those changes could indicate that the process of selection among the WT population implied by the progressive pressurization-resuscitation-culturing steps carried out as part of our static compression protocols to achieve the PA samples studied here might have an altered outer envelope structure, with enhanced pressure-resistant mechanical properties.

We must also examine the possible effects of crystallization to form ice crystals within the aqueous suspension medium or inside the bacteria themselves that might damage the cell walls and result in non-viability. In addition, the crystallization phase boundaries in the system might be altered by the presence of dissolved salts, that might also change the ionic strength as crystals of pure H_2O appear. The H_2O phase diagram shows that the high pressure crystalline phases ice VI followed by ice VII become stabilized at 1.5 and 2.5 GPa, respectively, at temperatures within the 310–330 K range achieved here. Dynamic compression experiments along the principal Hugoniot show that the P,T path lies close to the ice crystallization boundary (Nagayama et al., 2002). In our studies, the compression followed a complex dynamic loading path between the Hugoniot and isentrope, leading to lower temperatures achieved at 1.5 and 2.5 GPa peak pressures. The formation of crystalline ice phases from liquid H_2O is typically considered to be a slow process during shock events, however ramp compression studies have indicated a much faster nucleation rate as the loading conditions approach the isentrope (Dolan et al., 2007). It is possible if not likely that crystals of ice VI and/or ice VII nucleated within the aqueous suspension medium. In our static compression experiments, no WT survivors were recorded at 2.5 GPa that lies within the ice VII phase field at room temperature, whereas $\sim 1.3 \times 10^3$ survivors (a approximately 0.001% survival rate) were observed at 1.5 GPa, where ice VI would have been present during the high pressure run (Hazael et al., 2014). However, the PA specimen exhibited 10^4–10^6 CFU/ml survivors following compression to both pressures, making it unlikely that physical damage to the bacterial cell walls could have limited survival, unless the PA samples had presented a strategy to resist mechanical rupture. During a static compression study carried out to 1.4 GPa in a diamond anvil cell, the aqueous medium surrounding the microbes was observed to solidify into ice VI. However, apparently intact bacteria continued to remain visible inside fluid inclusions as well as along grain boundaries between the crystals, and metabolic activity continued to be recorded (Sharma et al., 2002). In our piston cylinder compression studies, by 2.5 GPa no viable members of the WT population exhibited colony-forming behavior, however, a substantial number of survivors from the PA populations could be recovered and cultured at ambient pressure. The shock experiments showed a significantly increased survival rate for both WT and PA bacteria at 2.5 GPa compared with the static compression results; however, static and dynamic pressurization appeared to show comparable survival rates for the PA sample exposed at 1.5 GPa. This complex series of observations leads us to suggest that H_2O crystallization can not be the main effect causing the survival or demise of bacteria following exposure to high pressures in the GPa range.

Although we have established that WT bacteria are more sensitive to shock than are the specialized survivors within PA populations, it is not known why this occurs, or what the upper limits of bacterial survival might be following a dynamic compression event. That is likely to be set by the intrinsic mechanical resistance of the cell envelope to applied stress over a short timescale. Establishing those mechanical parameters should then help determine the ultimate survival of microbes and other organisms following a shock impact event.

The impact properties of meteorites on Earth, Martian and lunar surfaces are well known. Typical speeds of impactors are expected to lie in the range of km s^{-1} with peak impact pressures estimated to be on the order of several GPa (Beck et al., 2005), dependent upon the target material and the dimensions of the impacting body. The shock wave propagation velocities inside the impactor should remain on the order of μs or faster, so that any included organisms within the bolide (or impacted body) could exhibit a similar "glassy" cellular response to the applied dynamic stress conditions. The resistance of the cell envelope to maintain its integrity would then limit microbial survival. If the temperatures developed during a bolide impact event were to remain sufficiently low (El Goresy et al., 2001), then survival of bacteria in a live as well as a dormant state could be considered as a realistic possibility.

4. Conclusions

From our data we have shown that bacterial survival following shock compression is greatly increased over that found following static compression. Specifically, shock experiments at 2.5 GPa, for which no survival can be recorded for WT samples exposed to static pressurization, exhibit some survival following shock compression. The greatest number of survivors is recorded for PA species following shock *vs* static pressurization. These results shed new light on the survival mechanisms for microbes exposed to different dynamic *vs* static pressurization conditions, as well as demonstrating the potential survival of viable species following bolide impact events and transport between planetary systems.

5. Acknowledgments

RH, FF and PFM acknowledge support from the Leverhulme Trust (RPG-350), NERC and the Deep Life program of the Deep Carbon Observatory (Sloan Foundation). GAT and BCF thank Mr Andrew Roberts and Dr David Wood for their assistance in carrying out the shock experiments. The authors also thank Paul J Hazell and James A Leighs for initial discussions and advice in designing the shock experiments. We thank the anonymous reviewers for their extensive and helpful comments.

References

ANSYS® Autodyn® (2012) 12.1. Materials Library.
Aertsen, A., Van Houdt, R., Vanoirbeek, K., Michiels, C.W., 2004. An SOS response induced by high pressure in. *Escherichia coli*. J. Bacteriol. 186, 6133–6141.
Anderson, R.E., Braxelton, W.J., Baross, J.A., 2013. The deep viriosphere: assessing the viral impact on microbial community dynamics in the deep subsurface. Rev. Miner. Geochem. 75, 649–675.
Beck, P., Gillet, P., El Goresy, A., Mostefaoui, S., 2005. Timescales of shock processes in chondritic and martian meteorites. Nature 435, 1071–1074.
Bonakdar, N., Gerum, R., Kuhn, M., Sporrer, M., Lippert, A., Schneider, W., Aifantis, K.E., Fabry, B., 2016. Mechanical plasticity of cells. Nature Lett. 15, 1090–1095.
Borgonie, G., Garcia-Moyano, A., Litthauer, D., Bert, W., Bester, A., van Heerden, E., Moller, C., Erasmus, M., Onstott, T.C., 2011. Nematoda from the terrestrial deep subsurface of South Africa. Nature 474, 79–82.
Burchell, M., Cole, M., McDonnell, J., Zarnecki, J., 1999. Hypervelocity impact studies using the 2 MV Van de Graaff accelerator and two-stage light gas gun of the University of Kent at Canterbury. Meas. Sci. Technol. 10, 41.
Burchell, M.J., Mann, J., Bunch, A.W., Brand, P.F.B., 2001. Survivability of Bacteria in hypervelocity impact. Icarus 547, 545–547.
Burchell, M.J., Mann, J.R., Bunch, A.W., 2004. Survival of bacteria and spores under extreme shock pressures. Mon. Not. R. Astron. Soc. 1278, 1273–1278.
Colwell, F.S., D'Hondt, S., 2013. Nature and extent of the deep biosphere. Rev. Miner. Geochem. 75, 547–574.
Daly, R.A, Borton, M.A, Wilkins, M.J, Hoyt, D.W, Kountz, D.J, Wolfe, R.A, Welch, S.A, Marcus, D.N, Trexler, R.V, MacRae, J.D, Krzychi, J.A, Cole, D.R, Mouser, P.J., Wrighton, K.C., 2016. Microbial metabolisms in a 2.5 km deep ecosystem cerated by hydraulic fracturing in shales. Nat. Microbiol. 1, 16146.
Demazeau, G., Rivalain, N., 2011. The development of high hydrostatic pressure processes as an alternative to other pathogen reduction methods. J. Appl. Microbiol. 110, 1359–1369.
Dolan, D.H., Knudson, M.D., Hall, C.A., Deeney, C., 2007. A metastable limit for compressed liquid water. Nat. Phys. 3, 339–342.
El Goresy, A., Chen, M., Gillet, P., Dubrovinsky, L., Graup, G., Ahuja, R., 2001. A natural shock-induced dense polymorph of rutile with α-PbO_2 structure in the suevite from the Ries crater in Germany. Earth. Planet. Sci. Lett. 192, 485–495.
Faby, B., Maksym, G.N., Butler, J.P., Glogauer, M., Navajas, D., Fredberg, J.J, 2001. Phys. Rev. Lett. 87 148102–1.
Fajardo-Cavazos, P., Langenhorst, F., Melosh, H.J., Nicholson, W.L., 2009. Bacterial spores in granite survive hypervelocity launch by spallation: Implications for lithopanspermia. Astrobiol 9, 647–657.
Govers, S.K., Aertsen, A., 2015. Impact of high hydrostatic pressure processing on individual cellular resuscitation times and protein aggregates in. Escherichia coli. Int. J. Food Microbiol. 213, 17–23.
Griffin, P.L., Kish, A., Steele, A., Hemley, R.J., 2012. Differential high pressure survival in stationary-phase *Escherichia coli* MG1655. High Press. Res. 31, 325–333.
Gruzielanek, S., Zhai, Y., Winter, R., 2010. Unraveling the pressure effect on nucleation processes of amyloidogenic proteins. Chem. Phys. Chem. 11, 2016–2020.
Hazael, R., Meersman, F., Ono, F., McMillan, P.F, 2016. Pressure as a limiting factor for life. Life 6. doi:10.3390/life6030034.
Hazael, R., Foglia, F., Kardzhaliyska, L., Daniel, I., Meersman, F., McMillan, P., 2014. Laboratory investigation of high pressure survival in *Shewanella oneidensis* MR-1 into the Gigapascal pressure range. Front. Microbiol. 5, 612. doi:10.3389/fmicb.2014.00612.
Hazell, P.J., Beveridge, C., Groves, K., Appleby-Thomas, G., 2010. The shock compression of microorganism-loaded broths and emulsions: Experiments and simulations. Int. J. Impact Eng. 37, 433–440.
Hazell, P.J., Beveridge, C., Groves, K., Stennett, C., Elert, M., Furnish, M.D., Anderson, W.W., Proud, W.G., Butler, W.T., 2009. Shock compression and recovery of microorganism-loaded broths and an emulsion. In: AIP Conference Proceedings, pp. 1395–1398.
Horneck, G., Stöffler, D., Ott, S., Hornemann, U., Cockell, C.S., Moeller, R., Meyer, C., de Vera, J.-P., Fritz, J., Schade, S., Artemieva, N.A., 2008. Microbial rock inhabitants survive hypervelocity impacts on Mars-like host planets: First phase of lithopanspermia experimentally tested. Astrobiol 8, 17–44.
Howard, K.T., Bailey, M.J., Berhanu, D., Bland, P.A., Cressey, G., Howard, L.E., Jeynes, C., Matthewman, R., Martins, Z., Sephton, M.A., Stolojan, V., Verchovsky, S., 2013. Biomass preservation in impact melt ejecta. Nat. Geosci. 6, 1018–1022.
Huber, J.A., 2015. Making methane down deep. Science 349, 376–377.
Inagaki, F., Hinrichs, K.-U., Kubo, Y., Bowles, M.W., Heuer, V.B., Hong, W.-L., Hoshino, T., Ijiri, A., Imachi, H., Ito, M., et al., 2015. Exploring deep microbial life in coal-bearing sediment down to ~2.5 km below the ocean floor. Science 349, 420–424.
Kish, A., Griffin, P.L., Rogers, K.L., Fogel, M.L., Hemley, R.J., Steele, A., 2012. High–pressure tolerance in *Halobacterium salinarum* NRC-1 and other non-piezophilic prokaryotes. Extremophiles 16, 355–361.
Lane, N., Martin, W.F., 2012. The origin of membrane bioenergetics. Cell 151, 1406–1416.
Leighs, J.A., Appleby-Thomas, G.J., Stennett, C., Hameed, A., Wilgeroth, J.M., Hazell, P.J., 2012. A sealed capsule system for biological and liquid shock-recovery experiments. Rev. Sci. Instr. 83 m115113.
Matuska, D.A., 1984. HULL Users Manual. AFATL-TR-84–59.
Meersman, F., Daniel, I.D., Bartlett, D.H., Winter, R., Hazael, R., McMillan, P.F, 2013. High pressure biochemistry and biophysics. Rev. Mineral. Geochem. 75, 607–648.
Melosh, H.J., 1988. The rocky road to panspermia. Nature 332, 687–688.
Nagayama, K., Mori, Y., Shimada, K., Nakahara, M., 2002. Shock Hugoniot compression curve for water up to 1 GPa by using a compressed gas gun. J. App. Phys. 91, 476–482.
Oger, P.P., Jebbar, M., 2010. The many ways of coping with pressure. Res. Microbiol. 161, 799–809.
Ono, F., Minami, K., Saigusa, M., Matsushima, Y., Mori, Y., Takarabe, K., Saini, N.L., Yamashita, M., 2010. Life of Artemia under very high pressure. J. Phys. Chem. Solids. 71, 1127–1130.
Paulino-Lima, I.G., Pilling, S., Janot-Pacheco, E., de Brito, A.N., Barbosa, J.A.R.G., Leitão, A.C., Lage, C.d.A.S., 2010. Laboratory simulation of interplanetary ultraviolet radiation (broad spectrum) and its effects on *Deinococcus radiodurans*. Planet. Space Sci. 58, 1180–1187.
Picard, A., Daniel, I., 2013. Pressure as an environmental parameter for microbial life — A review. Biophys. Chem. 183, 30–41.
Price, M.C., Solscheid, C., Burchell, M.J., Josse, L., Adamek, N., Cole, M.J., 2013. Survival of yeast spores in hypervelocity impact events up to velocities of 7.4 km s^{-1}. Icarus 222, 263–272.
Robertson, N., Hayhurst, C., Fairlie, G., 1994. Numerical simulation of impact and fast transient phenomena using AUTODYN™- 2D and 3D. Nucl. Eng. Design. 50, 235–241.
Sharma, A., Scott, J.H., Cody, G.D., Fogel, M.L., Hazen, R.M., Hemley, R.J., Huntress, W.T., 2002. Microbial activity at gigapascal pressures. Science 295, 1514–1516.
Steinberg, D., 1991. Equation of State and Strength Properties of Selected Materials. Lawrence Livermore National Laboratory Report UCRL-MA.
Strand, O.T., Goosman, D.R., Martinez, C., Whitworth, T.L., Kuhlow, W.W., 2006. Compact system for high-speed velocimetry using heterodyne techniques. Rev. Sci. Instr. 77, 083108.
Thwaites, J.J., Surana, U.C., Jones, A.M., 1991. Mechanical properties of Bacillus subtilis cell walls: effects of ions and lysozyme. J. Bacteriol. 173, 204–210.

Vadillo-Rodriguez, V., Dutcher, J.R., 2011. Viscoelasticity of the bacterial cell envelope. Soft Matter. 7, 4101–4110.
Vance, S.D, Hand, K.P., Pappalardo, T., 2016. Geophysical controls of chemical disequalibria in Europa. Geophys. Res. Lett. 43, 4871–4879.
Vanlint, D., Mitchell, R., Bailey, E., Meersman, F., McMillan, P.F., Michiels, C.W., Aertsen, A., 2011. Rapid acquisition of Gigapascal-high-pressure resistance by Escherichia coli. Mbio 2 (1) e00130–10.
Venkateswaran, K., Moser, D.P., Dollhopf, M.E., Lies, D.P., Saffarini, D.A., MacGregor, B.J., Ringelberg, D.B., White, D.C., Nishijima, M., Sano, H., Burghardt, J., Stackebrandt, E., Nealson, K.H., 1999. Polyphasic taxonomy of the genus Shewanella and description of *Shewanella oneidensis* sp. nov. Int. J. Sys. Evol. Microbiol. 49, 705–724.
Willis, M.J., Ahrens, T.J., Bertani, L.E., Nash, C.Z., 2006. Bugbuster, survivability of living bacteria upon shock compression. Earth Planet. Sci. Lett. 247, 185–196.

B.2 Journal of Physics: Conference Series – Tolerance of *Artemia* to static and shock pressure

Tolerance of *Artemia* to static and shock pressure loading

IOP Conf. Series: Journal of Physics: Conf. Series **950** (2017) 042002 doi:10.1088/1742-6596/950/4/042002

Tolerance of *Artemia* to static and shock pressure loading

B C Fitzmaurice[1], G J Appleby-Thomas[1], J D Painter[1], F Ono[2], P F McMillan[2], R Hazael[2] and F Meersman[2]

[1]Cranfield Defence and Security, Cranfield University, Shrivenham, Swindon, SN6 8LA, United Kingdom
[2]Department of Chemistry, University College London, 20 Gordon Street, London WC1H 0AJ, United Kingdom

E-mail: b.fitzmaurice@cranfield.ac.uk

Abstract. Hydrostatic and hydrodynamic pressure loading has been applied to unicellular organisms for a number of years due to interest from food technology and extremophile communities. There is also an emerging interest in the response of multicellular organisms to high pressure conditions. *Artemia salina* is one such organism. Previous experiments have shown a marked difference in the hatching rate of these organisms after exposure to different magnitudes of pressure, with hydrostatic tests showing hatching rates at pressures up to several GPa, compared to dynamic loading that resulted in comparatively low survival rates at lower pressure magnitudes. In order to begin to investigate the origin of this difference, the work presented here has focussed on the response of *Artemia salina* to (quasi) one-dimensional shock loading. Such experiments were carried out using the plate-impact technique in order to create a planar shock front. *Artemia* cysts were investigated in this manner along with freshly hatched larvae (nauplii). The nauplii and cysts were observed post-shock using optical microscopy to detect motility or hatching, respectively. Hatching rates of 18% were recorded at pressures reaching 1.5 GPa, as determined with the aid of numerical models. Subjecting *Artemia* to quasi-one-dimensional shock loading offers a way to more thoroughly explore the shock pressure ranges these organisms can survive.

1. Introduction

Artemia salina, commonly known as brine shrimp, is a parthenogenetic branchiopod crustacean that has long been used in studies of a number of aquatic organisms as a food source [1, 2] as well as for bioassays to test for toxicity in various systems [3, 4]. A hatching rate of 24-48 hr in optimum conditions for *Artemia* cysts make them ideal for testing in a laboratory environment. *Artemia* are typically ovoviviparous; they are born as free-swimming nauplii. In less favorable environments, embryos are developed oviparously; in cysts that wait to hatch until conditions are stable. This dormant state in which encysted embryos reside is known as diapause where they experience reduced metabolic activity [1]. Once they are exposed to water they typically exhibit a hatching rate of approximately 90%, with a minimum of ~75% [5], under normal conditions They are capable of surviving a number of stressors, including salinity and temperature that can vary substantially, with an optimum salt concentration in most *Artemia* species of 60 gL^{-1} and an optimum temperature of 25 °C in laboratory conditions [1]. The temperatures for nauplii viability, however, have a rather considerable range of 5-40 °C [1]. In addition, cysts have been found to remain viable at even more extreme temperatures [6] along with certain evident enzyme activities that are maintained. For

example, protease activity in the cyst shells of *Artemia franciscana* has been detected, although at a reduced rate, following a 15 min exposure to 100 °C [7].

Artemia exposure to high pressures extending into the multi GPa range has also been investigated more recently. Quasi-hydrostatic tests carried out on *Artemia salina* cysts in fluorinert medium by Ono *et al.* [8] found hatching rates of 80–90% after exposure of several dozen examples to a pressure of 7.5 GPa for up to 48 hr. In contrast, Udagawa and Suzuki [9] showed that shock waves with a pressures in the range of 25-100 MPa produced by underwater detonations resulted in cyst hatching rates of < 2.5% after 48 hr observation [9]. The marked difference between these findings could be related to the nature of the pressure loading, along with the different timescales over which the pressures were applied when compared with the biochemical or physiological changes that determine hatching.

The study presented here focuses on the response of *Artemia salina* nauplii and cysts to quasi-one-dimensional shock pressures. This is in keeping with similar work carried out on *Escherichia coli* [10] in order to analyse the effects of shock pressure on biological systems without the effects of a multi-dimensional wave front. Both hydrostatic and hydrodynamic pressure investigations have been carried out over a number of years to ascertain the survivability of single- to multicellular organisms following pressurisation to several hundred MPa or into the multi-GPa range. The results are of interest to fields ranging from food and agricultural products sterilisation and preservation, deep subsurface biology and exobiology through to panspermia and the origins of life [11, 12].

2. Experimental method

The response of *Artemia salina* was tested at three different shock pressures; 0.78, 0.96 and 1.5 GPa. Dried *Artemia salina* cysts were obtained from Sciento® and used for both cyst and nauplii shock loading experiments. Hatched nauplii were attained by immersing several cysts in a 3% saline solution at 25 °C for 48 hr in a water bath. Sample sizes of 100 cysts were chosen for shock loading at each pressure, while 100 hatched nauplii were examined at the lowest pressure only. These sample sizes were divided into subsets of 20 for the purpose of encapsulating them during the shock. Multiple experiments with reduced sample sizes prevented overcrowding within the sealed capsule used during shock pressure loading. Comparing the results from different runs also provided a measure of statistical significance.

The shock loading experimental set-up, outlined in figure 1, included the plate-impact technique with aluminium flyer plates carried out on a 50 mm bore single stage gas gun for quasi-one-dimensionally loading the *Artemia* samples. The sample capsule assembly was described previously [13]. A capsule containing 20 cysts or nauplii was filled to overflowing with 3% saline solution to avoid any cavitation in the sample during the shock. The cavity in the larger Al capsule was then filled with 20% ballistic gelatin to attenuate the shock and minimise rarefaction waves that may move back through the sample.

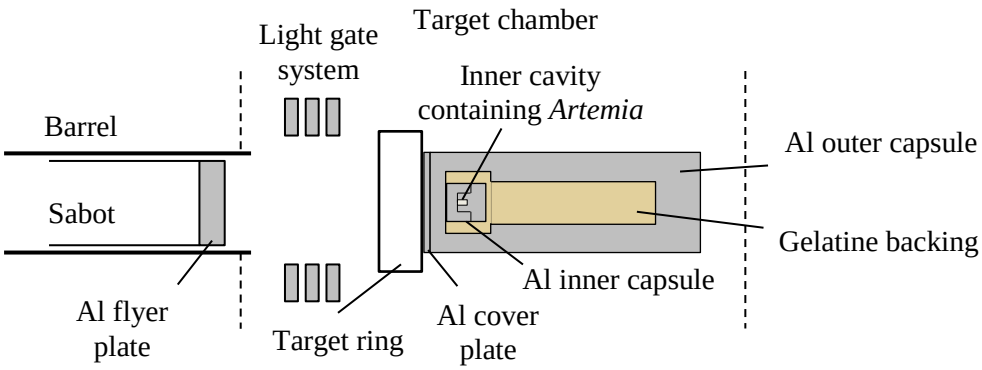

Figure 1. Experimental set-up with the Al capsule and Teflon system in the target chamber of the 50 mm bore gas gun.

In place of pressure gauges, peak shock pressures attained for each sample of cysts and nauplii were evaluated using previously validated numerical models [13]. Our estimates were based on a Lagrangian model of the capsule system implemented within ANSYS® Autodyn. The materials properties used were as listed by Leighs *et al*. [13] and followed the same set-up as used during the shock loading experiments. In order to validate the models the initial shock pressure for one experiment at both the lowest and highest impact velocities were measured using manganin pressure gauges. Subsequent comparison indicated that the pressures derived from the numerical simulations were reliable (figure 2). Fluctuations appearing in the stress-time trace for the experimental data were attributed to wave reflections occurring within the lid of the outer capsule.

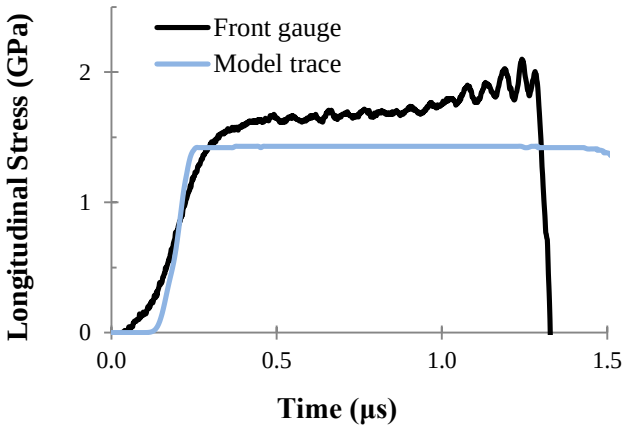

Figure 2. Shock traces from experimental data and numerical model for highest pressure with 230 ms^{-1} impact velocity.

In order to maintain *Artemia* under anaerobic conditions, it was ensured that the nauplii and cysts remained sealed inside their capsules for < 2 hr for each experiment. Control samples were encapsulated for the same period of time. The samples were immediately examined post-shock using light microscopy to search for any visible external damage to the cysts and nauplii. They were then studied after 24 and 48 hr to determine hatching rates and observe motility of the nauplii.

3. Results

Following incubation of the shocked cysts, the hatching rates (i.e., emergence of the embryo from the hatching membrane) were determined after 24 hr and 48 hr in each case (table 1, figure 2). The 'breaking' stage of the cysts was also recorded to observe the emergence of the embryo from the shell (figures 3 and 4). These rates were systematically higher than the hatching rates in each case. At the lowest pressure reached, 0.78 GPa, a breaking rate of 75 % was attained after 48 hr, while applying a pressure of 0.96 GPa resulted in a breaking rate of 70 %. The maximum pressure achieved during shock loading was 1.5 GPa and this led to the lowest breaking rate of 43 %. The hatching rates also showed similar decrease (26, 23 and 18%) with increasing peak pressures. One sample from each different shock pressure was also analysed after 14 days of incubation to search for any further hatched nauplii. However, no additional hatching was observed. Peak temperatures attained during the shock runs were determined through the numerical models (table 1). These ranged from 41^{o}C at 0.78 GPa to 50^{o}C at 1.5 GPa.

Table 1. Breaking and hatching rates of *Artemia salina* cysts observed for each shock pressure after both 24 and 48 hr

Impact velocity (ms^{-1})	Pressure (GPa)	Cyst breaking frequency (%)		Hatching frequency (%)		Shock peak temperature (°C)
		24 hr	48 hr	24 hr	48 hr	
135	0.78	60	75 (± 3)	16	26 (± 3)	41
153	0.96	59	70 (± 4)	12	23 (± 3)	42
230	1.5	30	43 (± 3)	4	18 (± 2)	50

In addition, hatched nauplii were studied following shock loading at 0.78 GPa but only at the lowest pressure due to the temperature increase of the samples during the shock. The motility of their antennae was analysed after shock and observed after 24 and 48 hr for 1 min each. 20% demonstrated motility of their antennae throughout this time, but with a noticeable lack of overall motion compared to nauplii hatched from shock loaded cysts. Many did not appear to have any significant structural damage post shock, as illustrated by figure 5. Nauplii that were found to be unmoving but appeared to be structurally intact were left for up to 14 days in order to check for any subsequent movement of their antennae; however, none was observed in any case.

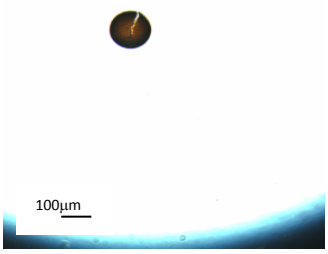

Figure 3. Breaking cyst after shock loading at 0.96 GPa.

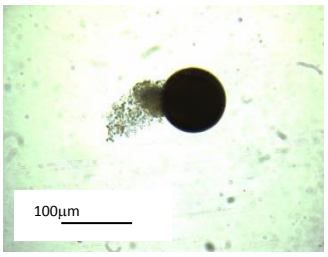

Figure 4. Emerging embryo from cyst after shock loading at 0.96 GPa.

Figure 5. Hatched nauplius after shock loading at 0.78 GPa.

4. Discussion

Exposure of *Artemia* cysts to shock pressures of 0.78 and 0.96 GPa caused a decrease in both cyst breaking and hatching rates, whereas a much larger effect was observed following 1.5 GPa shock. While the nauplii that hatched successfully following 1.5 GPa exposure appeared to be largely undamaged, a small number demonstrated impaired motility. Our results confirm the observation that *Artemia* cysts appear to be significantly more sensitive to quasi-one-dimensional shock compression than static pressurisation into the multi-GPa range. Our experiments resulted in considerably greater hatching rates than had been observed in previous shock experiments, carried out at substantially lower peak shock pressures. However, the previous work used non-planar wave fronts that could have played a role in the reduced hatching success. More studies will be required to elucidate the relative roles played by biochemical changes and the mechanical response of the cyst coating to shock *vs* static pressurisation in determining the rate of successful hatching, and subsequent properties of the hatched nauplii. In order to avoid complications due to heating of the samples during shock compression, we only carried out a single series of experiments subjecting hatched nauplii to 0.78 GPa pressure. Studies of antenna motion indicated that motility was considerably reduced.

In the case of the cyst shells, visible light microscopy showed that in some instances, the breaking stage was initiated, but was not completed (figure 3). Little damage appeared to have occurred to the external structure of the cysts, even for those that did not hatch after 48 hr. This could indicate that delayed hatching or possible death of the embryos contained inside the cysts might be due to some internal biochemical mechanism controlling their shock response, such as particular genes being activated in the encysted embryos but not in the hatched nauplii. Some such genes involved in the production of proteins for embryo protection have already been identified, including p26, but it is not yet known how these genes respond to pressure loading. It is clear that future work lies with studying the internal mechanisms that govern *Artemia salina* response to shock as well as static pressure.

5. Conclusions

By applying quasi-one-dimensional shock wave pressures in the range of 0.78-1.5 GPa, breaking and hatching rates of *Artemia salina* cysts were found to decrease with increasing pressure, unlike static compression results that maintained 80-90% hatching rates after exposure to 7.5 GPa for up to 48 hr. The enhanced effect of shock *vs* static pressurization in reducing *Artemia* cyst hatching is in general agreement with previous studies, although the hatching rates found here were significantly greater than those seen following shock from underwater detonation waves. This implied that the nature of the wave front must play an important role in survival and hatching probability of the cysts, certainly by affecting the mechanical stress fields applied to the cyst envelope. It is apparent that shock and static pressurisation also certainly affect the biochemical and biophysical state of the encysted embryo and these effects could be studied by future genomic and proteomics investigations.

Acknowledgements

The authors would like to thank Mr Andrew Roberts and Dr David Wood for their invaluable assistance in carrying out these experiments. Contributions of PFM and RH were supported by grant RPG-350 from the Leverhulme Trust.

References

[1] Gajardo G M and Beardmore J A 2012 *Front. Physiol.* **3** 1
[2] Grabner M, Wieser, W and Lackner R 1981 *Aquaculture* **26** (1–2) 85
[3] Milhem M M, Al-Hiyasat A S and Darmani H 2008 *J. Appl. Oral Sci.* **16** (4) 297
[4] Caldwell G S, Bentley M G and Olive P J W 2003 *Toxicon*. **42** (3) 301
[5] Liu Y-L, Zhao Y, Dai Z-M, Chen H-M and Yang W-J 2009 *J. Biol. Chem.* **284** (25) 16931

[6] Miller D and McLennan A G 1988 *J. Therm. Biol.***13** (3) 119
[7] Stabili L, Miglietta A M and Belmonte G 1999 *J. Exp. Mar. Bio. Ecol.* **237** (2) 291
[8] Ono F, Minami K, Saigusa M, Matsushima Y, Mori Y, Takarabe K, Saini N L and Yamashita M 2010 *J. Chem. Phys. Solids* **71** (8) 1127
[9] Udagawa Y and Suzuki M 2013 *Trans. Japan Soc. Mech. Eng. Part B* **79** (801) 804
[10] Leighs J A, Appleby-Thomas G J, Wood D C, Goff M J, Hameed A and Hazell P J 2014 *J. Phys. Conf. Ser.* **500** (18) 182026
[11] Dasgupta R 2013 *Rev. Mineral. Geochem.*, **75** (1) 183
[12] Rios A C 2015 *PNAS* **112** (3) 643
[13] Leighs J A, Appleby-Thomas G J, Stennett C, Hameed A, Wilgeroth J M and Hazell P J 2012 *Rev. Sci. Instrum.* **83** (11) 115113

B.3 AIP Conference Proceedings – On the shock response of Escherichia coli to high rates of deformation

On the response of Escherichia coli to high rates of deformation

B. C. Fitzmaurice, J. D. Painter, G. J. Appleby-Thomas, D. C. Wood, R. Hazael, and P. F. McMillan

Citation: AIP Conference Proceedings **1793**, 140002 (2017); doi: 10.1063/1.4971722
View online: https://doi.org/10.1063/1.4971722
View Table of Contents: http://aip.scitation.org/toc/apc/1793/1
Published by the American Institute of Physics

On the response of *Escherichia coli* to high rates of deformation

B. C. Fitzmaurice[1, a)], J. D. Painter[1], G. J. Appleby-Thomas[1], D. C. Wood[1], R. Hazael[2] and P. F. McMillan[2]

[1] *Cranfield Defence and Security, Cranfield University, Shrivenham, Swindon, SN6 8LA, United Kingdom.*
[2] *Department of Chemistry, University College London, 20 Gordon Street, London WC1H 0AJ, United Kingdom*.

[a)] Corresponding author: b.fitzmaurice@cranfield.ac.uk

Abstract. While a large body of work exists on the low strain-rate loading of biological systems such as bacteria, there is a paucity of information on the response of such organisms at high rates of deformation. Here, the response of a readily accessible strain of bacteria, *Escherichia coli* (*E. coli*), has been examined under shock loading conditions. Although previous studies have shown greatly reduced growth in shock conditions up to several GPa, relationships between loading conditions and bacterial response have yet to be fully elucidated. Initial results of a more rigorous investigation into the 1D shock loading response of *E. coli* are presented here, expectantly leading to a more comprehensive view of its behaviour when exposed to high pressures. Comparison has been drawn to provide insight into the importance of the nature of the loading regime to the survival of these biological systems.

INTRODUCTION

There are a number of reasons for studying the effects of high pressures on organisms and biological materials and, in line with the focus of this study, especially shock pressures. From the sterilisation of foods by pressure loading bacteria to gaining a better understanding of the types of micro-organisms that survive in extreme environments, there has been a surge in research on the high pressures on a variety of organisms. More specifically, and within the scope of this paper, there have been a number of investigations into how micro-organisms might fare in the face of panspermia (the possible transfer of life and its building blocks through space) and equally, the extinction of life that can be caused by such an occurrence. In order to survive transfer through space, an organism must be capable of surviving the pressures and temperatures involved in their ejection into space and exposure to other risks such as UV radiation [1, 2].

There is evidence to support the resilience of at least small percentages of some microbial life under extremely high pressures and temperatures. In fact, recent evidence of amino acid formation upon impact of an ice mixture found on comets [3] has led to more questions about not only whole cells surviving asteroid impact pressures, but also individual cellular components. Pressures that are associated with asteroid impact are in the range of 1-100 GPa. It was also shown by Melosh (1984) [4] that upon asteroid impact onto a planetary body, small ejecta (between 1 and 5% of the mass of the original impactor) can result and manage to escape actual shock pressures. This could potentially mean even greater rates of survival for micro-organisms exposed to these impact events.

More evidence has been gathered in support of the concept of panspermia and lithopanspermia (the transfer of life through space via rocks) with examinations of the survival rates of bacteria, including *Escherichia coli* and spores of *Bacillus subtilis*, on the surface of rocks undergoing dynamic impact [5, 6]. Dynamic pressure loading of *B. subtilis* cells by Burchell *et al*. [7] even showed survival rates of 10^{-7} at pressures of close to 100 GPa; within the region of pressures faced by rock ejection into space and asteroid impact. A more complex eukaryotic organism,

Shock Compression of Condensed Matter - 2015
AIP Conf. Proc. 1793, 140002-1–140002-5; doi: 10.1063/1.4971722
Published by AIP Publishing. 978-0-7354-1457-0/$30.00

Saccharomyces cerevisiae (baker's yeast), was also investigated in a similar manner by Price *et al*. [8] and found to have a survival rate of ~10^{-4} at a peak pressure of ~43 GPa.

While shock loading of micro-organisms has become more extensive, the area of interest here is in quasi-one dimensional loading of these biomaterials. Loading regimes likely play a part in micro-organism survival rates, evidence for which has been seen from contrasting *E. coli* survival rates between particular past studies [5, 9]. However, this paper aims to provide additional data to previous work on the one-dimensional shock loading of *E. coli* by Leighs *et al*. [10] and may contribute to further understanding of what the nature of the loading regime does to bacterial survival before eventually examining what mechanisms may be affected within the cell.

EXPERIMENTAL TECHNIQUE

The shock loading experimental set-up, outlined in Fig. 1, included the plate-impact technique carried out on a 50 mm bore single stage gas gun for quasi-one-dimensionally loading the bacteria samples. *E. coli* NCTC 10538, a genetically modified lab-safe strain of this bacterium, was used in this investigation. Lysophilised (freeze-dried) pellets of the bacteria were rehydrated and incubated overnight at 37°C for 18 hours (based on previous measurements of their growth curve to encourage maximum production of colonies) [10]. The incubated *E. coli* broth was then introduced to the aluminium capsule system [11] shown in Fig. 1, within a Teflon® (PTFE) liner which held 6 μl of broth.

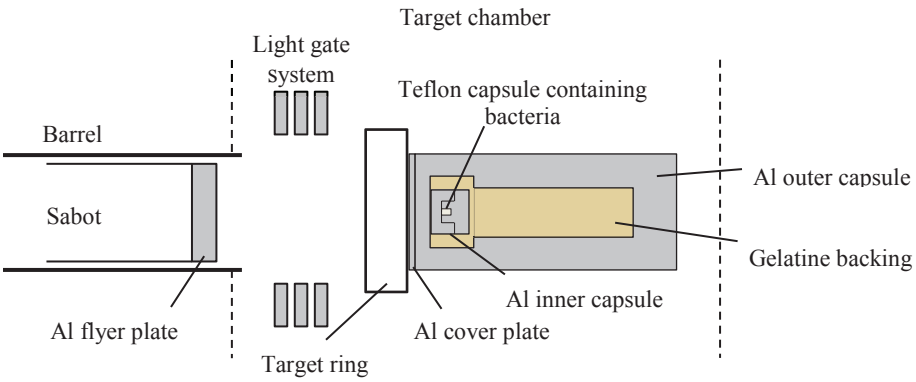

FIGURE 1. Experimental set-up with the Al capsule and Teflon system in the target chamber of the 50 mm bore gas gun.

The purpose of the Teflon liner was to ensure a quasi-one-dimensional shock wave for as long as possible through the sample and to attenuate the shock to prevent any excess ringing and reduce the effects of rarefaction. The liner was overfilled to avoid cavitation in the bacterial broth during the shock. The cavity in the larger Al capsule was filled with 20% ballistic gelatin to also attenuate the shock and reduce rarefaction. In place of pressure gauges to measure pressure during the shock loading event, peak shock pressures reached for each bacterial sample were measured using a Lagrangian model employed via ANSYS Autodyn®.

After shock loading, the bacterial broth was plated on an agar nutrient medium and incubated for 18 hours. The process was repeated for the control samples which consisted of un-shocked *E. coli* from the original broth. After incubation, the *E. coli* colonies were counted and survival rates calculated according to population measured in colony forming units (CFU) per millilitre.

RESULTS AND DISCUSSION

Shock profiles from the hydrocode models provided the mean peak pressures reached for the three shock loading experiments carried out in this investigation, which are listed in Table 1. Error in the pressure measurements was considerably reduced by validation of the models by previous Heterodyne velocimetry experiments to calculate real shock pressures [10]. A representative depiction of the modeled Teflon liner and the points at which pressures were

measured during simulation is shown in Fig. 2. Four peak pressures were obtained for each experiment in order to obtain the mean peak pressure experienced by the bacteria within the capsule. An example of the modelled shock profiles for one experiment is displayed in Fig. 3.

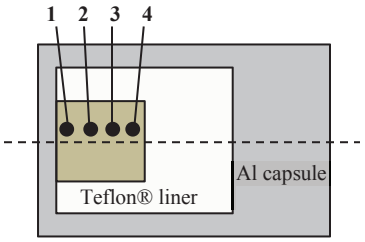

FIGURE 2. Teflon® liner (4 mm x 4 mm) filled with bacterial broth. Dashed line depicts the axial symmetry used in the hydrocode models. Gauges in the models are labelled 1-4.

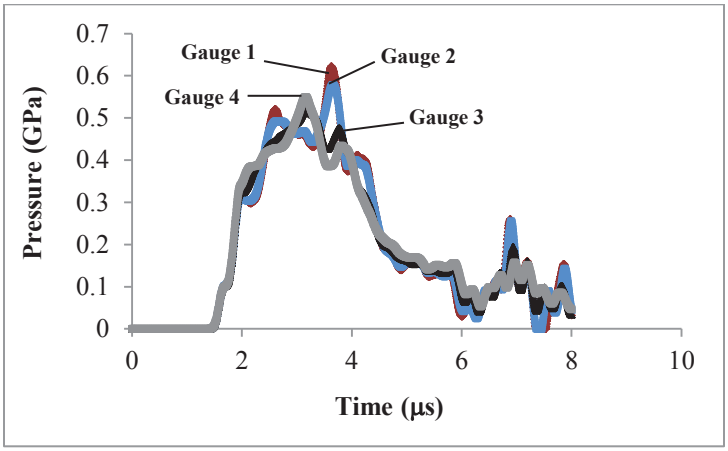

FIGURE 3. Shock profile from ANSYS Autodyn® model showing the peak pressures from four different gauges within the bacterial broth. The mean of these pressures was taken as the final peak pressure (in this case 0.55 GPa).

TABLE 1. Impact velocity, peak pressure and percentage survival for each shot on E. coli NCTC 10538; comparison between data from this study with previous data (Leighs *et al*. 2014).

Study	Velocity (ms^{-1})	Pressure (GPa)	% Survival
Present data	152	0.55	6
Present data	233	1.2	1
Present data	247	1.3	0.08
Leighs et al., 2014	181	0.78	0.52
Leighs et al., 2014	223	1.1	0.6
Leighs et al., 2014	265	1.5	0.01
Leighs et al., 2014	298	1.88	0.03

Upon calculating the population of *E. coli* colonies, survival rates were determined and plotted alongside the preceding data (Table 1, Fig. 4). Results by Leighs *et al*. [10] revealed relatively low rates of survival and showed slightly more sensitivity to shock pressures in the 1 GPa range compared to those found in this study. The two data points from the present investigation that were plotted above 1 GPa compare relatively closely with the previous data, although the rates of survival show some variance between the two studies, despite being carried out within the same pressure regime. The most significant variance is the 6% survival rate observed at 0.55 GPa, although this rate of survival is debatable since the next highest pressure obtained by Leighs *et al*. [10] was 0.78 GPa with a survival rate of 0.52%. Further work into quasi-one-dimensionally shock loading *E. coli* at these pressures would help to verify these data and possibly reduce scatter while confirming where survival increases at the lower end of this scale. However, the apparent exponential decrease in survival with pressure increase in the present data does match up with previous work on *E. coli* and other types of bacteria [5, 7], while demonstrating that the nature of the loading regime likely effects survival. It is also clear from both investigations that there is a drop in magnitude of survival within the 1–1.5 GPa range.

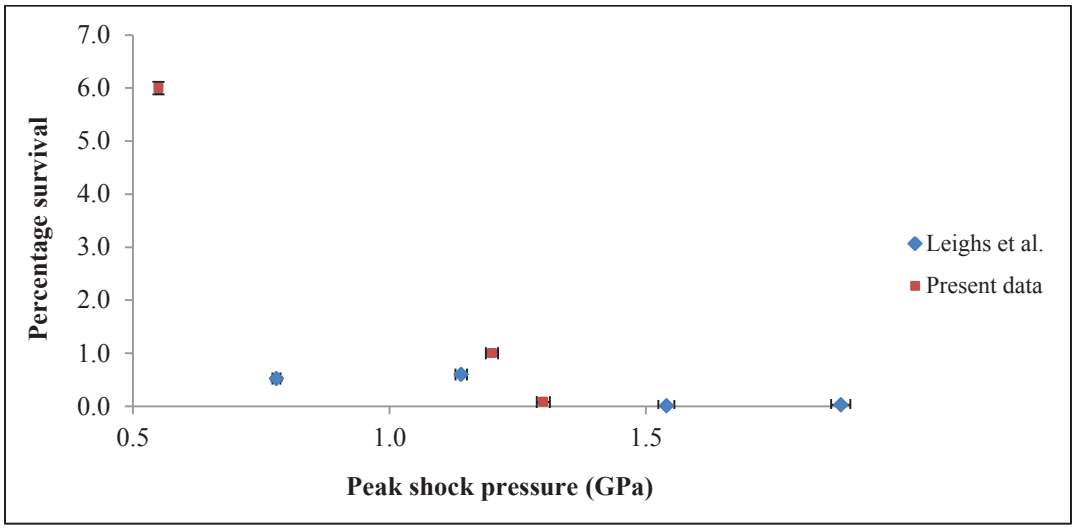

FIGURE 4. Comparison of percentage survival rates of *E. coli* found during the present study and previously by Leighs *et al*. (2014) within the 1 GPa range.

CONCLUSIONS

In an attempt to provide a more detailed view of the behavior of *E. coli* NCTC 10538 under shock loading conditions this study has provided new data to be considered with the previous work carried out on this bacterium. This was achieved by varying pressures to observe where the *E. coli* fit on the survival-pressure curve. Pressures in this investigation ranged from 0.55 GPa to 1.3 GPa with a possible exponential decline in survival rates from 6% to 0.08%. The discrepancies found between the current and previous set of experiments may be noteworthy, although with the current focus on a relatively small range of pressures it remains to be seen whether scatter in the data would be as significant on a larger scale. Ultimately, it would be of interest to continue shock loading at both higher and lower velocities to get a better sense of *E. coli* survival rates over a wider range of pressures. This would also be in the interest of panspermia which sees a pressure range of 1-100 GPa. While attempting to reach quasi-one-dimensional shock pressures at low MPa would be arguably more challenging, to observe differences in survival rates on a broader scale would be of importance for future in-depth studies of cellular mechanisms governing these responses. Further investigation would aim to see how particular cellular components and the biochemistry of *the E. coli* cell are affected in order to understand the effects of shock loading at a more fundamental level.

ACKNOWLEDGMENTS

The authors would like to thank Mr. Andrew Roberts for his invaluable help and technical advice during the experimental process.

REFERENCES

[1] C. Mileikowsky, F. A. Cucinotta, J. W. Wilson, B. Gladman, G. Horneck, L. Lindegren, J. Melosh, H. Rickman, M. Valtonen and J. Q. Zheng. Planet Space Sci. **48**, 1107–15 (2000).

[2] G. Horneck, P. Rettberg, G. Reitz, J. Wehner, U. Eschweiler, K. Strauch , C. Panitz, V. Starke and C. Baumstark-Khan. Orig Life Evol Biosph. **31**, 527–47 (2001).

[3] Z. Martins, M. C. Price, N. Goldman , M. A. Sephton, M. J. Burchell. Nat Geosci. **6**, 1045–9 (2013).

[4] H. J. Melosh. Icarus. **59**, 234–60 (1984).

[5] M. J. Willis, T. J. Ahrens, L. E. Bertani, C. Z. Nash. Earth Planet Sci Lett. **247**, 185–96 (2006).

[6] P. Fajardo-Cavazos, F. Langenhorst, H. J. Melosh, W. L. Nicholson. Astrobiology. **9**, 647–57 (2009).

[7] M. J. Burchell, J. R. Mann, A. W. Bunch. Mon Not R Astron Soc. **352**, 1273–8 (2004).

[8] M. C. Price, C. Solscheid, M. J. Burchell, L. Josse, N. Adamek, M. J. Cole. Icarus. **222**, 263–72 (2013).

[9] P. J. Hazell, C. Beveridge, K. Groves, G. Appleby-Thomas. Int J Impact Eng. **37**, 433–40 (2010).

[10] J. A. Leighs, G. J. Appleby-Thomas, D. C. Wood, M. J. Goff, A. Hameed, P. J. Hazell. J Phys Conf Ser. **500**, 182026 (2014).

[11] J. A. Leighs, G. J. Appleby-Thomas, C. Stennett, A. Hameed , J. M. Wilgeroth, P. J. Hazell. Rev Sci Instrum. **83**, 115113 (2012).

B.4 AIP Conference Proceedings – On a novel graded areal density solution to facilitate ramp wave generation in plate-impact studies

On a novel graded areal density solution to facilitate ramp wave generation in plate-impact studies

J. D. Painter, B. C. Fitzmaurice, M. Goff, G. J. Appleby-Thomas, D. C. Wood, and T. Pinto

Citation: AIP Conference Proceedings **1793**, 060017 (2017); doi: 10.1063/1.4971573
View online: https://doi.org/10.1063/1.4971573
View Table of Contents: http://aip.scitation.org/toc/apc/1793/1
Published by the American Institute of Physics

On a novel graded areal density solution to facilitate ramp wave generation in plate-impact studies

J. D. Painter[1, b)], B. C. Fitzmaurice[1, a)], M. Goff[2], G. J. Appleby-Thomas[1], D. C. Wood[1], and T. Pinto[3]

[1]*Cranfield Defence and Security, Cranfield University, Shrivenham, Swindon, SN6 8LA, United Kingdom*
[2]*AWE, Aldermaston, Reading, RG7 4PR, United Kingdom*
[3]*TWI Ltd., Granta Park, Great Abington, Cambridge CB21 6AL, United Kingdom*

[a)] Corresponding author: b.fitzmaurice@cranfield.ac.uk
[b)] j.d.painter@cranfield.ac.uk

Abstract. Building on a substantial body of work on functionally graded materials in the literature, it has been previously shown that the use of graded areal density impactors, in conjunction with buffer materials, allows generation of ramp-wave loading profiles in impacted targets. Such off-principle-Hugoniot loading paths are of particular interest where control of one or more state variables (e.g. temperature) is desirable during the loading event. Previous attempts to produce suitable graded areal density impactors have focused on rapid prototyping techniques such as 3D printing. While suitable for small-scale production of impactors, such technologies are relatively immature. Instead, here a novel approach to creating graded areal density structures -- TWI Ltd.'s novel surface modification process, Surfi-Sculpt®, with a nominal surface spike distribution of 1.5 per mm^2, has been employed to produce the required impactors. Initial experimental results are presented highlighting the potential of this experimental approach; further, these results -- combined with basic hydrocode simulations -- are used to postulate idealised structures which would allow useful loading paths such as the Adiabat to be readily accessed.

INTRODUCTION

The generation of ramp waves has been of interest for several decades, but has become even more prevalent in recent literature given its usefulness in areas of research including explosive detonation, equations-of-state and quasi-isentropic processes. A number of techniques have been used to apply these ramp waves across various media, including lasers and magnetic flux, but as with the present study, gas guns are also frequently used in ramp wave production [1, 2, 3, and 4]. Waves of this nature can be produced through a number of different avenues, from layered impactors with shock impedance gradients [5] to contemporary graded areal density flyer plates, or functionally graded material (FGM) impactors. These impactors have a varying density across the structure; a low density at the initial point of contact with the target material, gradually increasing with the depth of the impactor.

The use of ramp waves in explosives has led to numerous studies on their generation in various target materials, including granular explosives [6] and Kel-F 81(PCTFE) [7]. Furthermore, there has been a keen interest to quantify the dissipation of energy in these quasi-isentropic processes in recent years [1, 8] and to provide additional means to investigate material properties supplementary to those obtained from shock waves. It should be noted that although quasi-isentropic loading features shock-ramps [9], in this paper, they are referred to as ramps simply for comparison with traditional shock profiles. Markedly, this approach also offers insight into equations-of-state, particularly thermal equations-of-state [8], of materials in a shock pressure magnitude but with relatively low temperature. It facilitates observation of each stage of compression of a material, as opposed to a 'jump' to shock states that are observed with shock loading paths. In addition, the low temperature regime may prove useful for other types of temperature-sensitive targets, such as biological materials.

Shock Compression of Condensed Matter - 2015
AIP Conf. Proc. 1793, 060017-1–060017-5; doi: 10.1063/1.4971573
Published by AIP Publishing. 978-0-7354-1457-0/$30.00

Methods implemented to produce these ramped waves have recently included the 3D printing of metallic and ceramic flyer plates with graded areal density [3, 7]. Various additive manufacturing techniques have been used to produce such flyer plates, including Selective Laser Melting (SLM) and Toll Ceramic Stereolithography (CSL) [3, 4, 5]. Here, the ramp wave profiles of a new type of stainless steel 316 graded areal density flyer plate (produced via the Surfi-Sculpt® method by TWI Ltd.) were examined. This Surfi-Sculpt technology involves the use of electronic beams to displace material and effectively create a textured surface across a medium [10, 11]. Two Surfi-Sculpt flyer plates, each with different surface spike lengths, were manufactured for these experiments. Additionally, just as Ray and Menon (2011) [8] analysed the isentrope in a simulated dynamic impact event using a series of FGM flyer plates with varying densities, the use of the Surfi-Sculpt flyer plates could provide the opportunity to explore the reversible Adiabat along with hydrocode models, and thus, the quasi-isentropic nature of this type of loading event.

TECHNIQUE

Experimental procedure

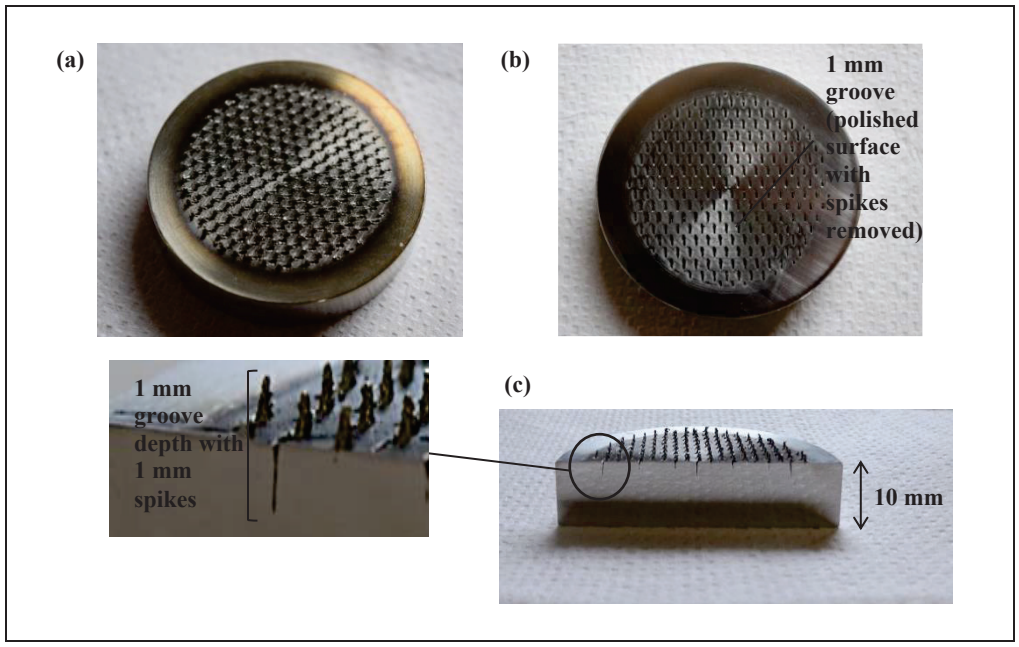

FIGURE 1. Surfi-Sculpt flyer plate with 1 mm spikes (a); polished surface of flyer plate (b); transverse section through flyer plate revealing groove depth in the surface (c).

For the purposes of this study, each Surfi-Sculpt flyer (Fig. 1) was manufactured with surface spikes of, nominally, 1 mm or 1.5 mm (errors of ± 0.3 mm and ± 0.2 mm, respectively). Each type was sectioned and polished in order to characterise these features. Consisting of a solid steel 316 base with a diameter of 48 mm and thickness of 10 mm, the flyers were found to display grooves ~ 1 or 1.5 mm in length (and depth) along the surface where material was displaced to form the protruding spikes. The grooves corresponded to the spike length in each case.

The plate-impact technique was used during this investigation, illustrated in Fig. 2, to allow for a quasi-one-dimensional loading path with an analogous 2 mm stainless steel 316 buffer plate as the target. The set-up incorporated a single manganin pressure gauge mounted on the rear surface of the buffer plate in order to record the wave profile. Each shot was carried out on the 50 mm bore single stage gas gun at Cranfield University [12] at a velocity of 500 m s^{-1}. The control used in this experiment was a planar stainless steel 316 flyer plate, also with a 10 mm thickness (< ±5 μm).

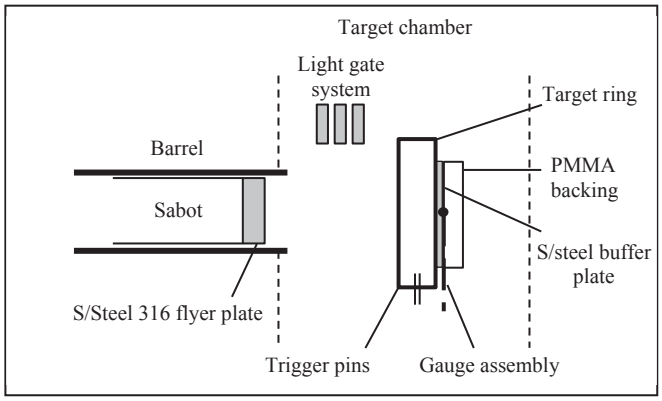

FIGURE 2. Experimental set-up for the plate impact technique. Surfi-Sculpt flyers were positioned so that the spikes were and the wells were facing downward.

Hydrocode modelling

In order to demonstrate the difference in temperature increase between the Surfi-Sculpt flyers and planar flyer, SPH hydrocode simulations via ANSYS® Autodyn [13] were employed, the material properties of which are outlined in Table 1. Gauges were set at various depths within the modelled target to obtain mean pressure and temperature values after impact with each flyer type.

TABLE 1. Material properties of stainless steel used in ANSYS® Autodyn models. Starting temperature was 300 K.

Strength model	**Density ($g\ cm^{-3}$)**	**Gruneisen coefficient**	**Thermal conductivity ($J\ m^{-1}\ K^{-1}\ s^{-1}$)**	**Specific heat capacity ($J\ kg^{-1}\ K^{-1}$)**
Steinberg-Guinan	2.703	1.97	247	8.85×10^2
N/A	1.0	0.28	0.609	4.18×10^3
N/A	1.439	1.39	0.19	1.05×10^3
von Mises	2.16	0.9	0.25	1.05×10^3
Piecewise JC	7.86	1.67	N/A	4.23×10^2

RESULTS

The ramp and shock profiles, from the Surfi-Sculpt and planar flyers, respectively, indicated different loading paths resulting in very similar plateaus (Fig. 3). While variation between the Surfi-Sculpt flyers of each spike length was virtually undetectable, the potential use of these Surfi-Sculpt flyers in dynamic impact experiments was validated by the fact that an equal pressure was reached by both graded areal density and planar flyers. Notably, there was a time delay in the peak pressures reached during the shock; the rise time for the Surfi-Sculpt flyer traces was 1.11 μs, contrasting to a more instantaneous rise, 0.27 μs, for the planar flyer. The pressure plateaued at 9.7 GPa in each case. The fact that no significant difference was apparent between the traces for the 1 and 1.5 mm spikes was likely due to some variation in spike length across the surface of these flyers. It was anticipated that a more obvious ramp would be seen in the 1.5 mm spike Surfi-Sculpt trace, but with a reduction in error of spike length, and particularly with an increase in spike length, a difference would likely be seen in these shock traces and in the temperature-time profile.

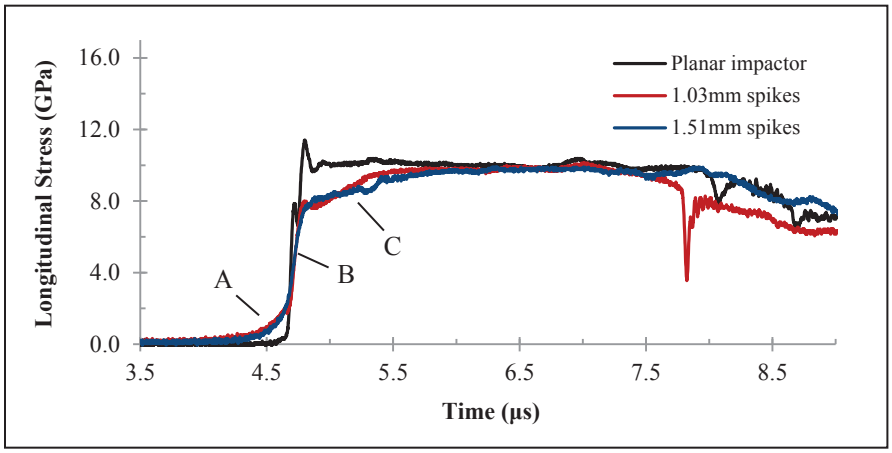

FIGURE 3. Shock profile for the graded areal density flyers (with 1.03 mm and 1.51 mm spikes) and the planar stainless steel 316 flyer. Peak pressure reached was 9.7 GPa. The spikes gradually puncture through the target material while an increasing density simultaneously moves into the target, hence initial shock followed by ramping (A); planar surface of the impactor material reaches the target, stress begins to rise more promptly (B); the material has fully compressed and slowly reaches peak stress (C).

The shock traces obtained from the hydrocode models revealed pressures which agreed with the experimental data within 5% [Fig. 4 (a)]. Based on this agreement, temperatures during the loading events for the planar and 1.5 mm spike Surfi-Sculpt flyers were measured through the models [Fig. 4 (b)]. Maximum temperature for the planar flyer was found to be ~ 340 K, while the Surfi-Sculpt trace peaked at ~ 330 K. Gauges in the models showed a maximum error in temperature of 3%. With the use of the graded areal density flyer plates, the process saw a more gradual increase in temperature within the system, comparably lower than the rate of temperature change during the planar flyer experiments. This variance in temperature was evidence for the potential applicability of impactors of graded density to research concerning temperature sensitive targets.

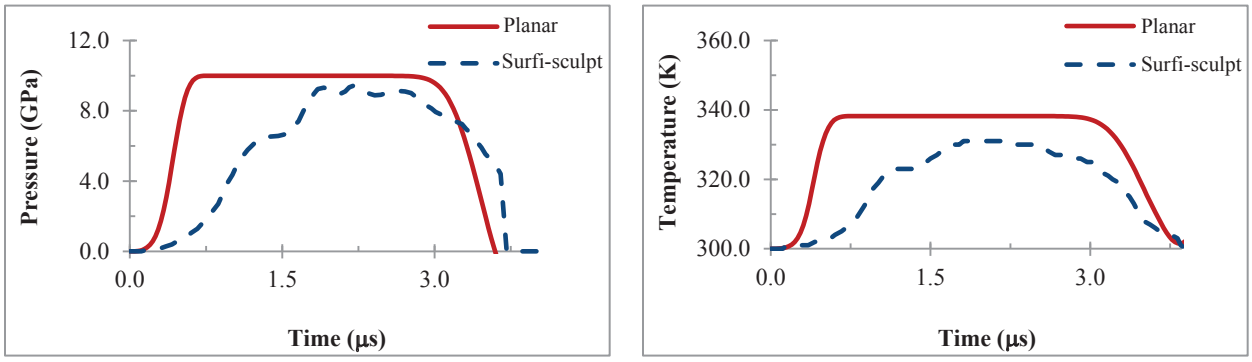

FIGURE 4. Predicted pressure curves for planar (red solid curve) and Surfi-Sculpt (blue dashed curve) flyers from hydrocode simulation (a). Temperature profiles comparing the planar and Surfi-Sculpt peak temperatures reached during hydrocode simulation of the impact event (b).

CONCLUSION

The results presented here suggest that flyer plates produced through the novel Surfi-Sculpt technique may be suitable for future dynamic impact work. Given the change in temperature observed between this new flyer type and traditional planar flyers of the same material, it can be said that the application of these graded areal density impactors to studies in which temperature increase must be minimised becomes a greater possibility. These studies could potentially involve materials that range from explosives to those that are biological in nature. Future work

would then require validation of Surfi-Sculpt flyers at even higher velocities to see the effects on temperature at these elevated pressures. Additionally, investigation of flyers with spikes of greater length could show more significant ramp features than those that have been demonstrated in this study. Nevertheless, the concept of graded areal density flyer plates constructed via the Surfi-Sculpt method has proven to be effective in ramp wave generation. The experiments here showed that relatively controlled ramp waves may be produced through an efficient and readily available method. Consequently, they may assist in further studies of off-Hugoniot processes, including those that are quasi-isentropic, and allow control of state variables during impact events, particularly temperature.

ACKNOWLEDGMENTS

The authors would like to thank Mr. Andrew Roberts and Mr. Adrian Mustey for their technical assistance throughout this study.

REFERENCES

[1] D. Orlikowski, J. H. Nguyen, J. R. Patterson , R. Minich, L. P. Martin and N. C. Holmes. AIP Conf Proc. **955**, 1186–91 (2007).

[2] R. E. Winter, M. Cotton , E. J. Harris, D. J. Chapman and D. Eakins. J Phys Conf Ser. **500**, 142034 (2014).

[3] P. Taylor, M. Goff, P. J. Hazell, J. Leighs, D. Wood, G. J. Appleby-Thomas. J Phys Conf Ser. **500**, 142016 (2014).

[4] R. E. Winter, M. Cotton , E. J. Harris, D. J. Chapman and D. Eakins. Shock Waves. 10.1007/s00193-015-0558-3 (2015).

[5] L. M. Barker, in *Shock waves in condensed matter-1983*, edited by J. R. Asay, R. A. Graham and G. K. Straub, (Elsevier Science, New York, 1984), pp. 217-224.

[6] R. Setchell. Combust Flame. **43**, 255–64 (1981).

[7] M. Goff , P. J. Hazell, G. J. Appleby-Thomas, D. C. Wood, C. Stennett and P. Taylor. Int J Impact Eng . **80**, 152–61 (2015).

[8] A. Ray and S. V. G. Menon. J Appl Phys. **110**, 024905 (2011).

[9] W. J. Nellis, High Pressure Res. **27**, 393-407 (2007).

[10] A. L. Buxton and B. G. I. Dance. (2005), available at: http://www.twi-global.com/technical-knowledge/published-papers/surfi-sculpt-revolutionary-surface-processing-with-an-electron-beam-august-2005/.

[11] T-S. Jun, S. Y. Zhang, G. Appleby-Thomas, P. S. Grant and A. M. Korsunsky, *Proceedings of the Denver X-Ray Conference on Applications of X-ray Analysis*, Denver, 2009 (JCPDS-International Centre for Diffraction Data, Denver, 2009), 1097-0002, pp. 519-528.

[12] N. Bourne. Meas Sci Technol. **14**, 273-8 (2003).

[13] ANSYS Autodyn version 15.0 Materials Library (2014).